THE INVESTIGATION OF THE CAUSE AND SEVERITY OF CORROSION AT THE PORT OF DOVER

Kieran Scobbie

School of Physical Sciences

University of Kent

Thesis Submitted For The Degree Of Research Masters In Chemistry At The University Of Kent

Supervised By Dr A. Berko and Dr M. Alfredsson

2017-2018

Declaration

I hereby declare that this thesis is my own work and effort, that it has not been submitted by me or anyone else in support of an application for a degree or qualification at the University of Kent or at any other university. Where other sources have been used, they have been acknowledged.

Signed: Kieran Scobbie

Date: 13/09/2018

Acknowledgements

I would like to acknowledge my supervisors who without their guidance and training, would have made this project a near impossible task. I would also like to thank Kane Disbury who was my Port of Dover contact, he has been brilliant with looking after me around the port.

I would also like to thank my office 114, for the brilliant people who have been looking after me on the University side of this project. With a special mention to Sally Pang, who has gone out of her way to show me how things where run around the university and had helped whenever I have asked for it without question.

To all of the people I have met during this project, my experience in England has been nothing short of incredible and welcoming. Thank you….

Abstract

This thesis is an investigation into the origins and severity of corrosion caused to the elevated road at the Port of Dover. The research in this thesis is comprised of collecting and analyzing samples, taken uniformly across the bridge as well as providing a recommendation of an adequate protection system based on the results.

The first stage of the project was a visual inspection of the bridge, completed in October 2017. Based on the observations it was concluded that the original (old) part of the bridge showed a higher degree of corrosion than the more recent (younger) part of the bridge. It was also concluded that the Port of Dover itself is affected by parameters of both industrial as well as marine environments, classifying the Port of Dover as a C5 corrosive environment.

There was two occasions of sample collecting, one on the 4th of December 2017 and the second sample collection on the 12th of June 2018. Collected from the old and new parts of the bridge respectively. The sample where stored in a controlled environment until characterized by visual inspection (Scanning Electron Microscopy; SEM), pH, conductivity, X-ray Diffraction (XRD), Electron Dispersive X-ray Fluorescence (EDX) and Raman spectroscopy. From these analyses, the severity, corrosion rates and products could be determined.

The results obtained from the samples characterize the corrosion products to have high levels of iron-based compounds from the steel of the structure. In addition, heavy metal compounds and carbon-based compounds forming black particulates originating from the fuel emissions of heavy traffic could be observed in a majority of the samples. The type and quantity of anions observed in the samples varied across the bridge, proposing that the samples collected in areas exposed to sea spray (elevated and open sites) demonstrated higher levels of chlorine. While sites under the bridge with poor circulation showed higher amounts of sulphates and nitrates from the diesel emission.

The severity of corrosion on the elevated road is not showing signs of structural failure at the present, however, there is corrosion occurring all over the bridge particularly around the bolts where the current paint system has worn off. The most common types if corrosion identified across the bridge are crevice and uniform corrosion.

Carbon-based particulates originating from the diesel emission in the area are a major cause to the observed corrosion types and rates. The particulates create a thin film across the bridge adsorbing other airborne compounds, which contribute to the chemical reaction rates of the corrosion products. Hence, reducing the formation of the carbon(soot) thin films will improve the lifetime of the corrosion protection system. Washing the bridge regularly, is advised to prevent the build-up of the particulates, and that the steel construction of the elevated road is carefully washed and prepared appropriately prior to the addition of the new coating system. The coating system proposed, based on the work in the thesis, is a zinc epoxy/polyurethane paint system.

Table of Contents

Table of Figures

Table of Tables

Table of Equations

Chapter 1:Introduction

Corrosion is an expensive problem for everyone. It is estimated that 3.1% of the worlds GDP is allocated for corrosion maintenance every year [1]. Corrosion process when the right conditions and as a result, it is heavily affected by the conditions around the corroding material. Many different factors affect corrosion though they are mainly environmental, this means environmental conditions play a major role in the rate and type of corrosion a material may undergo. Atmospheric pollution, acid rain, greenhouse gases, depletion of the ozone layer all affect the rate of the corrosion process. This has led to proposals of international legislation to repair and prevent the damage caused by corrosion. Corrosion is one of the observed devastations that pollution is causing to the environment, this decay is difficult to stop but it can be slowed down. An effective method for the prevention or slowing of this process, is to have a system that provides protection in the form of a barrier to these factors and monitor it continuously.

A properly installed system would perform more efficiently, for a longer duration without maintenance and would also reduce the pollution in the environment. As environmental conditions affect the speed of degradation, the type of material and protective coating should be modified in the necessary way to reduce this process [2].

This thesis details the investigation carried out on the elevated bridge in the Port of Dover, in order to determine the causes and types of corrosion present on the structure. It reviews previous research done on corrosion and coating materials, the chemistry of the corrosion that is happening to the bridge, by analyzing the corrosion products and attempting to form a direct correlation between these products and the environmental conditions down at the port. A map detailing the corrosion types, their severity and the environmental factors affecting the different areas of the bride will be produced.

In conclusion, this thesis will provide recommendations on the types of coatings that would be best employed to prevent anymore corrosion occurring on the elevated bridge.

The Project – Port of Dover

The Port of Dover is an industrial Port, one of the world's largest and is the UK's leading link to the rest of Europe. In the 1990's the port was handling 19.4 million passengers, 3.3million cars, 7.5 million freight vehicles, 14 million tons of cargo and over 66,000 shipping movements. All within the space of 243 hectares of water and 140 hectares of land [3]. This is a large amount of traffic travelling through the port and the numbers will only have increased since the 1990's. The pollution from the heavy traffic and natural environment of the Port gives rise to a corrosive environment. This has resulted in recently new section of the bridge showing signs of faster corrosion than expected. The investigation into the corrosion process was sponsored by the Port of Dover with the aim of identifying a solution to the corrosion associated with the elevated bridge.

As part of this investigation, samples were taken from both the old and new parts of the elevated bridge in the Port. The samples were analyzed using several analytical techniques, including Scanning Electron Microscope/Electron Dispersion X-Ray (SEM/EDX), Raman Spectroscopy and X-Ray Diffraction (XRD). Air monitoring was carried out in order to find a correlation between the corrosion products found along the bridge and the air quality of those areas. pH and conductivity of the samples were also recorded, it was expected that lower pH would correlate with more acidic corrosion products and vice versa with basic corrosion products. The pH, corrosion products and environmental analysis should provide a correlated overview of the bridge and what is affecting the corrosion process in the different areas of the bridge. Details of procedure, analysis and discussion of results will be discussed later in this thesis.

1.1:Project Objectives

In co-operation with the Port of Dover authorities a series of objectives where agreed upon that the was to be delivered at the end of the project:

- The causes of corrosion
- The severity of corrosion
- The types of corrosion
- The corrosion products
- An environmental analysis

Lastly, a paint system recommendation to then apply to the elevated road to protect it from the corrosive environment, as well as any other methods that could be implemented to protect the structure. The milestones that where discussed and confirmed with the Port in order to meet the project objectives were as follows:

- Milestone 1: Training on analytical equipment, SEM/EDX, Raman and XRD.
- Milestone 2: Begin mapping the elevated road.
- Milestone 3: Sample collection from the first sample sites.
- Milestone 4: Characterization and analysis of samples from the first sample collection and produce a midterm report for the Port of Dover.
- Milestone 5: The second set of sample collection.
- Milestone 6: Analysis of the environment.
- Milestone 7: Research of coating systems and the most appropriate according to the corrosivity of the environment.
- Milestone 8: After analysis and interpretation of the samples, after research of protection systems and viable paint systems for protection of the elevated bridge. A report and presentation were to be made to the Port of Dover presenting the results and recommendations.
- Milestone 9: Finishing the master's thesis and presenting them with a copy for future reference.

This thesis will meet the final requirements for the project agreed with the Port of Dover to a standard where it can be used for reference in future decisions with corrosion problems at the Port.

1.2:Site Analysis

The Port of Dover has a lot of vehicular traffic going through it every day as mentioned in the introduction, in such a small area this creates a concentrated area of corrosive agents [3]. The elevated bridge is situated in a highly polluted part of this environment, part of the bridge is directly on top of the filter road to each ferry outlet allowing for all the pollution to be deposited on the underside of the bridge. The elevated bridge is also the main way to exit the Port from leaving the ferry, sometimes there is a lot of traffic causing congestion allowing for any exhaust fluids to drip down the side of the bridge. As can be seen in **figure 1** below the bridge goes over the input road to the ferries, the security gates and a car park. The vehicles coming from the ferries filter onto the elevated road via the ramps.

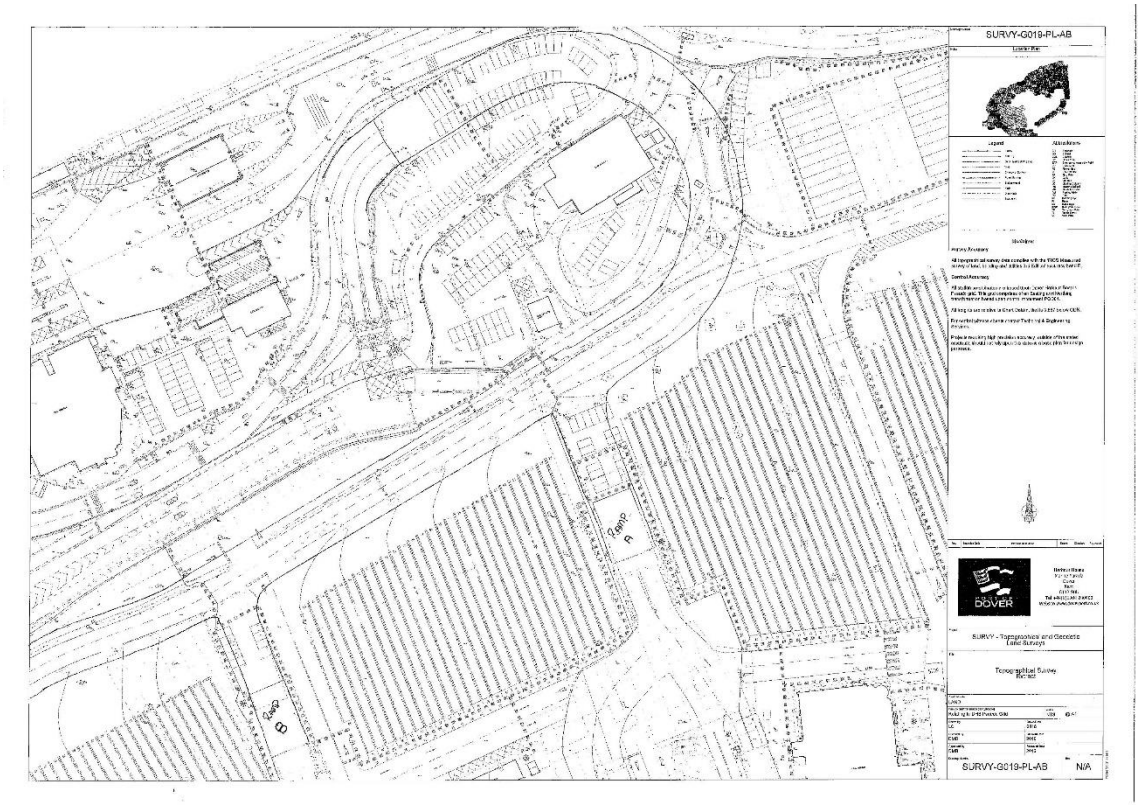

Figure 1. Schematic of the Port of Dover including the elevated road.

The humidity of the Port is higher than 40% which is the level required for corrosion to take place [61]. There may be other compounds involved, from the cliffs, oil/lubricants that have run off from vehicles and other elements from unburned hydrocarbons. Including chlorine from the sea and the sulfur oxides coming from vehicle pollution, the Port meets the requirements to be classified a marine/industrial corrosive environment [29].

1.3:Corrosion

For a material to corrode it must have access to oxygen and water, a common example is the corrosion of steel which contains iron. In the corrosion process iron is transferred into rust, which is an iron oxide. As this process is taking place in the thin film, other corrosive impurities in the air are adsorbed, this is referred to as atmospheric corrosion, the most commonly studied type of corrosion. This is an electrochemical process that occurs through surface wetting, a thin layer film forms on the surface of the material and allows for electrolytes to adsorb onto the surface of the metal. Due to the thin film, the process is easily influenced by temperature, humidity, precipitation, type of alloy and air pollutants. There is an anodic and cathodic process that happens like a battery, where there is a redox reaction in the thin film. The iron in the metal is anodic and is oxidized meaning that the iron loses electrons as shown below in **Equation 1**.

$$Fe \rightarrow Fe^{2+} + 2e^{-}$$

Equation 1. Oxidization of iron, the anodic part of the reaction.

This process then reacts with the product of the cathodic reaction, the reduction of water into hydroxide ions as shown below in **Equation 2**.

$$O_2 + 2H_2O + 4e^{-} \rightarrow 4OH^{-}$$

Equation 2. Reduction of water into hydroxide ions, the cathodic part of the reaction.

The total reaction will give the corrosion product iron hydroxide(rust), which is shown below in **Equation 3**, the full redox reaction.

$$2Fe + O_2 + 2H_2O \rightarrow 2FeOOH$$

Equation 3. Full redox reaction of the anodic and cathodic parts of the electrochemical process for iron degradation.

The iron was the target material in this example with the water being the electrolyte in the presence of oxygen from the atmosphere to form a rust product iron hydroxide [4,5].

Corrosion is a process that affects most materials but mainly metals, ceramic and polymers. The driving force behind the corrosion is due to the change in a systems Gibb's energy. A material is continuing to undergo chemical reactions until it transformed into the energetically most favorable state under the environmental conditions present. Again, iron metal is used as an example. Under the correct conditions iron metal will be oxidized to iron oxide (Fe_2O_3), where iron is in oxidation state 3. Reducing the pH of the environment, Fe(III) is less stable which transforms into Fe(II) leading to the formation of other oxide compounds such as Fe_3O_4[6,7].

1.4:Types of Corrosion

As seen in the reaction scheme for corrosion above, corrosion can be thought of as an electrochemical process. This is the main mechanism for the corrosion process. The reaction presented in **Equation 3** above has assumed no outside interference from other chemical compounds. Another assumption is that the anodic and cathodic reactions are happening over the total surface of the metal but are not occurring simultaneously in the same place. Because of this assumption it is viewed as having no macroscopic pockets of concentration differences in the electrolyte across the surface of the metal and that the metal itself is homogenous.

All these assumptions lead to a uniform attack on the metal surface, referred to as uniform corrosion. This is, however, one of many different types of corrosion that can occur. The other types of corrosion deviate from the previously mentioned "uniform" corrosion. There are several parameters that can occur and change the type of corrosion, some of these are:

- The design of the metal surface
- The combination the environment interacting with the metal
- How clean/rough the surface of the metal is
- Other deterioration mechanism
- Metal/alloy composition
- Acid material synthesis.

These differences will change the direction and appearance of the attack, each type of corrosion has its own visual characteristics. Due to this the type of corrosion can usually be identified via visual inspection and, if necessary aided by a magnifying glass. Each type of corrosion has different causes, so a visual inspection is important when it comes to determining the cause of corrosion/failure of the metal structure [8][9]. On this basis the following corrosion types can be identified:

1. Uniform (general) corrosion
2. Galvanic (two-metal) corrosion
3. Thermogalvanic corrosion
4. Crevice corrosion
5. Pitting corrosion
6. Selective attack (de-alloying)
7. Intergranular corrosion

8. Erosion corrosion
9. Cavitation corrosion
10. Fretting corrosion
11. Stress corrosion cracking
12. Corrosion fatigue

These are all the different types of corrosion that can be distinguished due to visual features. **Figure 2** below provides a simple illustration for these types of corrosion [8].

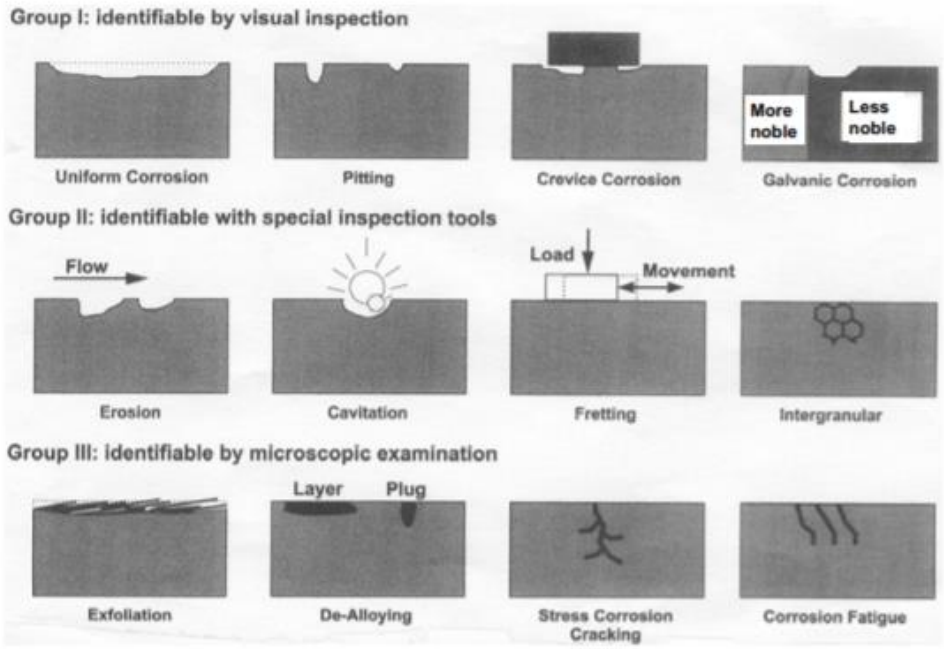

Figure 2. The different types of corrosion [8].

1.4.1:Uniform corrosion

Uniform corrosion as the name suggests is a corrosion type that occurs over the entire surface of the material at a slow and often predictable pace [10]. Uniform corrosion is essentially the basic definition of localized corrosion as it is only occurring on the surface of the metal. Ideal uniform corrosion occurs when there is an equal flux of metal ions from the surface of the material and cathodic ions from the reactants, interacting on the surface of the material. The anodic and cathodic sites are sufficiently small and uniformly distributed such that there will not be failure due to a localization of the anodic reaction site.

This failure usually occurs when there is any kind of physical irregularity with the metal surface. This can involve, grain boundaries, crystal imperfections (dislocation and surface steps), different phases and rough surfaces from; scratches, machining and grinding. Any physical change down to the atomic level can make some areas behave differently electrochemically, some being more anodic when under aqueous conditions. These changes are usually very small, macroscopic, making the corrosion appear to be uniform corrosion. Effective uniform corrosion can also occur when the diffusion through the corrosion products is the rate determining step [11][12].

1.4.2:Galvanic corrosion

Galvanic corrosion occurs when two different metals are physically touching in an oxidizing medium. This is one of the most common types of corrosion and it can be found anywhere in a corrosive environment, where there are two different conducting metals touching. This type of corrosion results in a fast degradation of the metals but, as the potential of the two metals are different it means that one metal will consume the other. The galvanic corrosion of one metal can result in the corrosion protection of another metal, due to this, sacrificial metals are heavily used in industry to protect steel structures.

In galvanic corrosion, two dissimilar conducting metals are exposed to an electrolyte, where a current called the galvanic current flows from one metal to the other. At the anode, electrons will be created by an oxidation process:

$$Me \rightarrow Me^{n+} + ne^{-}$$

Equation 4. Anodic reaction.

This means that the anodic member is consumed. The reaction is directly related to the current by Faraday's law. Under coupling conditions another type of corrosion is taking place simultaneously to the anodic member of the two metals. The difference between the galvanic corrosion and the other type of corrosion is called the difference effect, which is either positive or negative. In this case the galvanic protection protects the cathodic member of the two metals and is known as being "cathodically protected" [13][14].

Thermodynamically this process can occur spontaneously. The change in Gibbs (ΔG) free energy for the corrosion reaction predicts if the reaction is spontaneous: if it is spontaneous $\Delta G < 0$. The change in free energy can be calculated from measuring cell potential, E. The work done can be delivered by an electrochemical cell in a given state with $nF\ E$, which is equivalent to Gibbs free energy [90].

$$\Delta G = -nF\ E$$

Equation 5. Gibbs free energy [90].

Where n, is the number of moles of electrons, F is Faradays constant (96,485 C/mol) and E is the cell potential (in volts) for a cell in a given state [90].

1.4.3:Thermogalvanic corrosion

Thermogalvanic corrosion results from a macrocouple, which is formed when two pieces of the same metal are in a corrosive medium and have different temperatures. One of the pieces of metal in this case will form the anode and corrode. The extent of the corrosion depends on the potential difference between the hot and cold pieces of metal, the electrical conductivity of the corrosive medium, the distance between he pieces of metal and the overvoltage's of the anode and cathode process [15]. The best method of prevention for this type of corrosion is to cool the metal and bring it to a uniform temperature [10].

1.4.4:Crevice corrosion

Crevice corrosion is a common type of localized corrosion that can be found in crevices or at shielded surfaces where a stagnant solution is present. This is a common type of corrosion that can cause structural failure, as it occurs with alloys that usually have excellent corrosion resistance like stainless steel and corrosion is not always immediately visible. Crevices make a sheltered chemical environment which is different from the normally exposed surface of a structure and as a result can increase the rate and severity of corrosion. The environment keeps moisture trapped, adsorbs pollutants from the atmosphere, concentrates corrosion products and diffuses oxygen. Most cases of crevice corrosion occur in near-neutral pH environments in which dissolved oxygen is the cathode reactant.

The crevices in which this type of corrosion occurs are formed by:

1. The geometry of the structure
2. Contact of metal with non-metallic solids
3. Deposits of sand, dirt or permeable corrosion product on the metal surface (referred to as a deposit attack).

With any kind of corrosion, energy is required for the process to occur. The reacting components go from a higher energy state to a lower energy state, This releases energy that allows the corrosion reaction to take place. In dry conditions the diffused oxygen reacts, forming oxides with the metal. By forming a metal oxide layer the reaction acts as a barrier for oxygen diffusion. Forming a protective layer, halting the corrosion process, this will last if this layer is intact and is not removed or cracked [17].

When moisture is trapped in a crevice and is the cause of the corrosion, it is referred to as filiform corrosion. This is another type of crevice corrosion that essentially involves the trapping of moisture between the surface of the metal and a non-metal material. There are specific cases that involve magnesium containing alloys and this type of crevice corrosion. An example involves the imperfect chemical conversion coating treatments using salts. Such salts include cerium, vanadium, zirconium, tin or manganese to protect alloys containing magnesium [16].

1.4.5:Pitting corrosion

Pitting corrosion is a type of localized corrosion, where the material loss is characterized by penetrations occurring the in the surface of the metal. This type of corrosion can be identified with the naked eye as there will be blemishes on the metal [18].

Pitting corrosion will only occur in the presence of aggressive anionic species, and most commonly chloride ions, although they are not always the cause. The severity of the pitting tends to vary with the logarithmic of the chloride concentration. Chloride is an anion of a strong acid and many metal cations exhibit great solubility in chloride ions. As a result, the presence of oxidizing agents in a chloride containing environments is extremely detrimental to steel structures, and further enhances localized corrosion [19].

1.4.6:Selective attack – De-alloying corrosion

Dealloying is a corrosion process which targets and removes one constituent from the alloy leaving an altered structure. The most commonly seen example of dealloying is from copper base alloys, such as copper-zinc and copper aluminum alloys. These attacks result in severe structural loss from the alloy as it removes a key constituent. The mechanism for this corrosion is relatively well understood, where the targeted metal undergoes an anodic reaction, similar to the way steel corrodes with the oxidation of iron, removing the metal from the structure or alloy [20][21].

1.4.7:Intergranular corrosion

Intergranular corrosion is also localized corrosion occurring at the microstructure level, specifically the grain boundary region of the alloy, and is electrochemically different from the rest of the alloy's microstructure. Corrosion can occur when there is heterogeneity such as, a change in the grain boundary structure. An example is in aluminum-copper alloys, if Al_2Cu particles are precipitated at the grain boundary it leaves the adjacent solid solution anodic and then more prone to corrosion. In aluminum-magnesium alloys the opposite occurs, Mg_2Al_3 is less noble than the adjacent solid solution. This corrosion can be avoided, if the correct manufacturing and heat treatment is applied.

Exfoliation corrosion is a type of corrosion that results from intergranular corrosion. Caused by serious intergranular corrosion resulting in sheets of the metal to come away parallel to the alloy. Exfoliation is characterized by the lifting of the layer of uncorroded metal, which are swelling away from the alloy, due to the corrosion products produced by the intergranular corrosion. This type of corrosion is usually observed around rivets and bolt holes where the end of the grain boundaries are exposed [22].

1.4.8:Erosion corrosion

Erosion corrosion is a gradual wearing of a metal surface due to a combination of both corrosion and abrasion from a water stream running over the area. The greater the velocity, the greater the corrosion of the metal. An example is that water moving in pipes will contain air bubbles and solid matter, particulates, like sand. This can string the protective oxide films on the surface of the metal, which then allows for the corrosion of the metal to take place [23].

1.4.9:Cavitation corrosion

The cavitation process is defined as the formation of the vapor phase from a liquid due to change in temperature at a constant ambient temperature. There are a lot of variables such as the change in temperature, turbulence and velocity but, the change of liquid to vapor remains the same. When the bubbles enter a region of high pressure or low temperature they burst, producing a jet of liquid with enough force to erode metal. Despite being a low energy event, it is a very localized type of corrosion [24].

1.4.10:Fretting corrosion

Fretting corrosion is a result of small cyclic movements between two materials caused by cyclic loading. The reason this is called fretting corrosion instead of just fretting, is because the fretting allows for electrochemical imbalances to occur, allowing for corrosion to take place and increase the damage done. The other contribution of damage is rubbing between tow materials. This type of corrosion most commonly occurs to joints and bolts.

Essentially, a piece of metal clamped will rub, not causing visible damage but at the macroscopic level the damage is severe enough to cause cracks between the two materials. The frictional heat generated form the rubbing allows for subsequent welding to take place between the two metals, which breaks apart during rubbing cycles. Oxidization promotes this process which is why it is named fretting corrosion instead of just fretting [25].

1.4.11:Stress cracking corrosion

This type of corrosion is quite rare but when it does occur it can be devastating structurally, occurring with very little metal loss. There are three basic mechanisms from this type of corrosion the first being active path dissolution.

Active path dissolution is very similar to intergranular corrosion where there is a gap in the grain boundaries and some loss of metal from the alloy creating an electrochemical imbalance. There have also been cases of no imbalance and instead a form of crevice corrosion has occurred in the alloy. When stress is applied however, it opens the grain boundary more allowing for easier corrosion product diffusion making the crack more dangerous and susceptible to corrosion.

The second mechanism is called hydrogen embrittlement. This is a case where hydrogen diffuses into the alloy, getting in-between all the big metal atoms. Hydrogen goes for areas that are under a lot of high triaxial tensile stress where the metal structure is dilated. Attracted to high stress areas hydrogen aids in the fracturing of the metal and causing metal embrittlement. In the most extreme cases this can be a fast process up to 1mm/s.

Lastly, the third mechanism is film induced cleavage. If a normally ductile material is coated in a brittle film, then a crack initiated in that film due to stress can be propagated into the ductile material before being arrested by ductile blunting. Some materials may reseal after such tensile stress but, if they cannot then that allows for further corrosion to occur [26].

1.4.12:Corrosion fatigue

Corrosion fatigue is the process where the corrosion has weakened - “fatigued”- the structure and with a combination of other factors such as stress and bending, the structure can fail. An example would be off-shore flowlines where gas and oil companies prefer to use low alloyed steel. As a result, pitting corrosion is common, together with stress coming from thermal transients and bending due wave motion, the structure can fail with these pipelines giving rise to corrosion fatigue [27].

1.4.13:Summary

In the case of this project for the Port of Dover, the types of corrosion that are relevant are:

- Uniform corrosion
- Crevice corrosion
- Pitting corrosion
- Selective attack – Dealloying corrosion
- And intergranular corrosion

Uniform corrosion is the most basic type of corrosion, so this expected to be encountered. Crevice corrosion likely due to the structure of the bridge and the pollution from the continuous traffic flow at the site providing atmospheric pollutants that aid corrosion and covering the bridge in carbon particulates. Pitting corrosion can also occur because of the chlorine ions coming from the sea salt. Dealloying as the bridge is made of a steel alloy so there is bound to be some leaching of metal from the alloy. Lastly intergranular corrosion is a very common type of corrosion and it opens up the coating and metal to more corrosion types.

1.5:Environmental Conditions Affecting Corrosion

The Port of Dover is an industrial port with a lot of traffic passing through. This makes it a marine and industrial environment with heavy atmospheric pollution from transport associated by their activities [3]. For a marine-industrial environment the loss of metals, for example, iron, zinc, aluminum and copper have been attributed to the following factors:

- The relative humidity (if it's less than 40% the corrosion will not take place) [61]
- Wetting time
- Amount of chloride
- Presence of SO_x and NO_x in the atmosphere

High corrosion rates in industrial areas have been linked to high concentration of SO_2 while, for marine environments it is the chloride content [28]. At the Port of Dover there will also be the NO_x from diesel engines, resulting in the synthesis of nitric acid which contributes to a more acidic environment [89]. However, when it comes to categorizing the type of environment whether it is urban, rural, marine or industrial, there are three main parameters used: the time of wetness (TOW); sulfur compounds based of sulfur dioxide (SO_2), and airborne salinity contamination (Cl^-). These parameters are defined as τ for TOW, P for sulfur dioxide (SO_2) and S for salinity (Cl^-). Based on the measurements of these parameters a classification can be assigned.

TOW	$h\,yr^{-1}$	SO_2	$\mu g\,m^{-3}$	$mg\,m^{-2}\,d^{-1}$	Cl	$mg\,m^{-2}\,d^{-1}$
τ_1	≤10	P_0	≤12	≤10	S_0	≤3
τ_2	10–250	P_1	12–40	10–35	S_1	3–60
τ_3	250–2500	P_2	40–90	35–80	S_2	60–300
τ_4	2500–5500	P_3	90–250	80–200	S_3	300–1500
τ_5	>5500					

Table 1. Classification of TOW, sulfur compounds using SO_2 and salinity contamination (Cl^-) [29].

Using the properties in **Table 1**, provides standards that allows for different look-up tables for metals, iron, copper, aluminum, zinc, leading to a classification system of corrosivity based on the environment. These classes denoting corrosion are given as C1-C5.

Corrosivity	Category	Carbon steel ($\mu m\ yr^{-1}$)	Zinc ($\mu m\ yr^{-1}$)	Copper ($\mu m\ yr^{-1}$)	Aluminum ($g\ m^{-2}\ yr^{-1}$)
Very low	C1	≤1.3	≤0.1	≤0.1	Negligible
Low	C2	1.3–25	0.1–0.7	0.1–0.6	≤0.6
Medium	C3	25–50	0.7–2.1	0.6–1.3	0.6–2
High	C4	50–80	2.1–4.2	1.3–2.8	2–5
Very high	C5	80–200	4.2–8.4	2.8–5.6	5–10

Table 2. Corrosivity categories based on the corrosion rates of iron, zinc, copper and aluminum [29].

As an example, the lowest rating (C1) is an indoor area with no pollution and low humidity, the highest rating (C5) is a marine/industrial environment with a lot of atmospheric pollution. This is the system from the ISO 9223 "International Organization for Standardization" [29]. The system can be fully used to evaluate environmental stress on corrosion. The selection of anticorrosion measures or estimations of service life according to the provisions of the international standards. Selective accelerated corrosion tests are used to verify the proposal of anticorrosion measures for given environments. When these tests are compared to the expected corrosivity of the atmosphere in the exposure conditions, they prove to not be similar. This is expected because accelerated corrosion tests do not correlate with corrosion stress in the conditions of a real environment [29].

1.6:Coatings

Before a decision is made on the type of protective coatings that can be used to prevent or slow down the corrosion in steel structures, there must be an evaluation of the environment that the structure is in and how this affects the types and rate of corrosion. There are classifications for how corrosive an environment is and depending on location and pollution, recommendations can be made on what the steel should be coated in [30].

As stated before, The Port of Dover is an industrial Port, one of the world's largest and is the UK's leading link to the rest of Europe. In the 1990's the port was handling 19.4 million passengers, 3.3million cars, 7.5 million freight vehicles, 14 million tons of cargo and over 66,000 shipping movements. All within the space of 243 hectares of water and 140 hectares of land [3]. This port is in a marine environment with heavy industrial pollution from all the traffic that goes through it. It is in a small area with a high concentration of pollution and this, can be visually seen on the bridge in black particulates and other stains on the metal surface.

In terms of exterior environments, the Port of Dover is the highest on the corrosivity scale as it is both an industrial and marine environment [31]. The Port of Dover fits a C5 classification, wcih according to the official description is, "the most corrosive atmospheric conditions that may occur locally at western coasts or at particularly polluted industrial and urban areas" [36]. According to the International Organisation for Standardisation, with their document on: "Paints and varnishes – Corrosion protection of steel structures by protective paint systems – Part 2: Classification of environments" EN ISO 12944-2, C5 is the highest corrosivity factor and is in an aggressive environment for pollution with continuous condensation [37].

Having established how corrosive the environment is purely from it being an industrial port the next phase will be to pick the appropriate coating that will be effective in preventing the corrosion for as long as possible in such a difficult environment.

Coatings are made up of many different parts, a primer, sealer/under coat, intermediate coat and finishing coat. The national physical laboratory has an example of a protective paint system that helps display an example, the build-up of a coating system (see **Figure 3**).

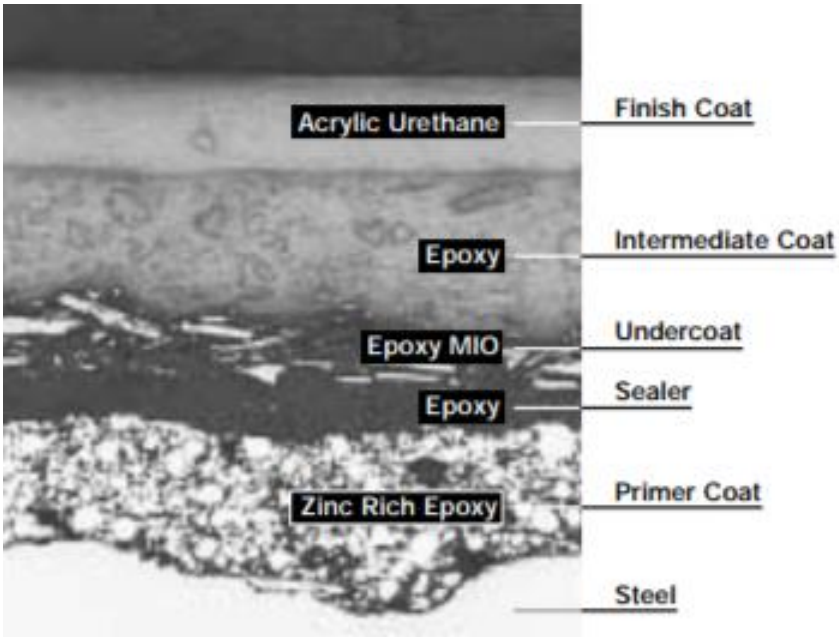

Figure 3. Protective coating system [32].

1.6.1:Hot Dip Galvanising and Surface Preparation

The technique of "hot dip galvanising" along with a coating of paint is what is used for high corrosive environments [8]. This technique is a cost-effective way of protecting steel structures and has been in use since 1850 when it took off as an industry in protecting steel structures [34][38].

Before going into this technique, the steel must be prepared for it, this is known as surface preparation of the steel, an important step in the coating process. Most instances of coating failure are usually down to poor or incorrect surface preparation, this is itself a quality control as the zinc will not react with the unclean areas of the steel after coming out of the zinc bath.

There are three steps to surface coating: degreasing, acid pickling and fluxing.

1.6.1.1:Degreasing: is either a hot alkali solution, mild acidic bath, or biological cleaning bath to remove organic contaminants such as dirt, paint markings, grease, and oil from the steel surface. Degreasing baths cannot remove epoxies, vinyl's, asphalt, or welding slag; thus, these materials must be removed by grit-blasting, sand-blasting, or other mechanical means before the steel is sent to the galvanizer. This process is to remove dirt and contaminants on the metal.

1.6.1.2:Acid pickling: is a dilute solution of hot sulfuric acid or ambient temperature hydrochloric acid, which removes mill scale and iron oxides (rust) from the steel surface. As an alternative to or in conjunction with pickling, this step can also be accomplished using abrasive cleaning, air blasting sand, metallic shot, or grit onto the steel. This process is to remove any present rust on the metal.

1.6.1.3:Fluxing: the final surface preparation step in the galvanizing process serves two purposes. Firstly, removing any remaining oxides and secondly deposits a protective layer onto the steel to prevent any further oxides from forming on the surface prior to galvanizing.

The flux process can be applied any one of two ways, wet or dry. In the dry galvanising process, the steel is dipped into a solution of zinc ammonium chloride. The steel is then dried before being dipped in molten zinc. In the wet galvanising process a layer of zinc ammonium chloride is floated on top of the molten zinc so that the metal is fluxed as it is dipped into the molten zinc [34][38].

In the galvanising step the metal structure is completely immersed in 98% molten Zinc. The bath temperature is maintained at 449ºC, Items immersed in the bath are kept there until they themselves reach the bath temperature. The Zinc then reacts with the iron on the steel surface to form an intermetallic alloy of Iron and Zinc [34][38][39][40][41].

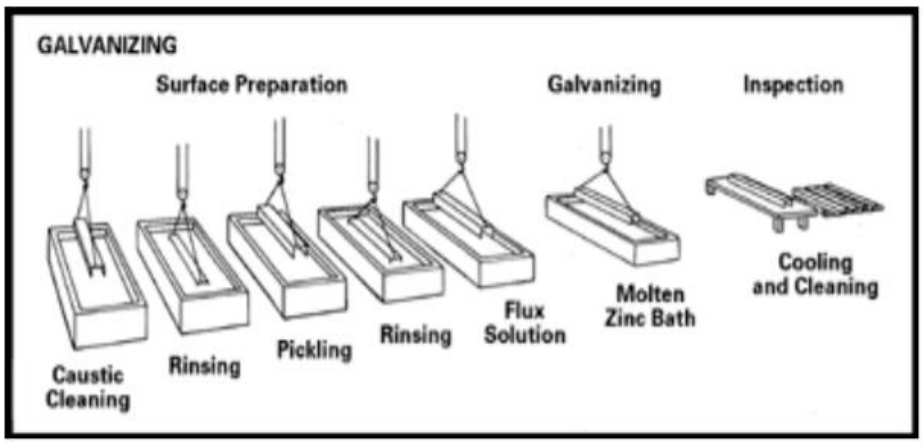

Figure 4. Schematic picture of the galvanising process [40].

1.6.2:Thermally Spraying

Thermally sprayed coatings have been in use for many years to coat steel structures in a molten metal that will protect it from corrosion in aggressive environments [37]. The thermal spray process itself can be split into two groups, combustion and electrical.

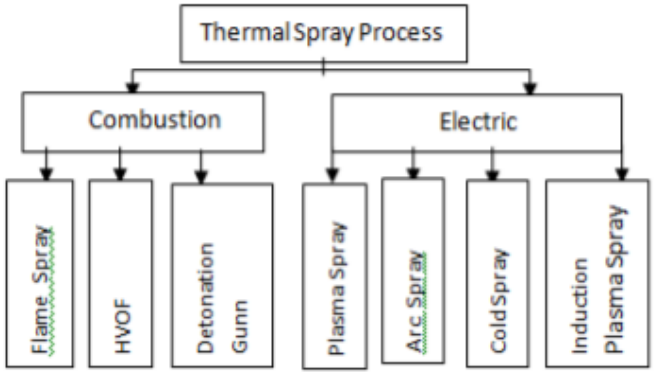

Figure 5. Schematic picture of the thermal spray process [45].

Currently thermal (wire arc) spray is the preferred method based on cost and maintenance for coating application. The cost comparison of both methods for this technique can be seen illustrated below in **Figure 6**.

Characteristic	Flame spraying	Arc spraying
Liquefaction of zinc, kg/h	18	35
Energy costs for liquefying zinc, $/h	≈28	≈25
Effective use, min/h	40	40
Effective use, kg/h	12	23
Energy costs, $/m² ($/kg equals $/m² at 100 µm zinc thickness)	2.33	0.11
Spraying speed, m²/h for 100 µm zinc	12	23
Wage costs, $/m² at 60 $/h	4.17	2.17
Total costs, $/m²	6.50	2.28

Figure 6. Cost comparison of combustion and electrical methods for the thermal spraying technique [45].

Thermal arc spray technology involves four main components: the spray gun used to receive the wire and shoot melted material onto the substrate (steel), air compressor, which is used to accelerate the melted material out of the spray gun, blasting pot, which is used for garnet space when blasting preparation is performed and lastly the thermal arc spray machine, which is used to supply current to the wire so that the arc can be created.

The arc itself is used to heat up the material that is to be melted, this material will come in the form of a wire feeding into the arc before being accelerated out of the spray gun on to the target metal. An example of the spray gun can be seen in **Figure 7** below.

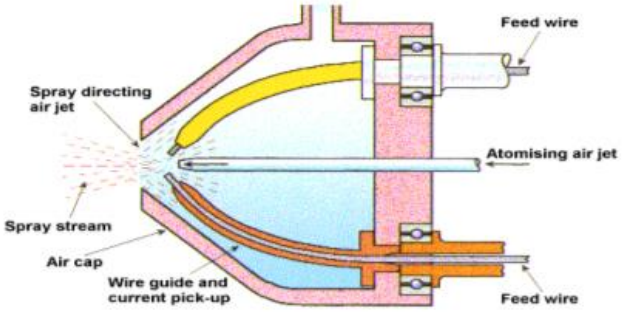

Figure 7. Arc thermal spraying process [45].

Naturally, before any coating can be applied to a substrate, the surface must be cleaned so that no under-coat corrosion occurs [31][45]. For this technique the surface of the substrate is usually blasted with "compressed air abrasive blasting". A method that is effective for cleaning at the mill-scale level and preparing the surface for good adhesion of the thermally applied coating. The cleaning is to make sure that the surface has no contaminants on it and is completely free from any impurities [45].

For bridges both thermal spraying and hot dip galvanisation techniques are popular in applying the primer of the coating to the steel structure. This is usually as bridges have a Zinc-rich primer as well as a multi-layered paint system [46].

1.6.3:Metal Primers

The primer is the last line of defence when it comes to protecting the metal itself and should, therefore, be chemically compatible with both the metal surface and the rest of the paint system. For example, zinc and aluminium are commonly used primers in highly corrosive environments protecting steel structures. This because iron (Fe) has a higher electronegativity potential than zinc (Zn) and aluminium (Al) – leading to the latter sacrifice themselves by providing a higher electronic potential, hence protecting the steel. This is the main reason that they are both used as primers [30][31][32][33].

Out of these two metals, zinc is still the most preferred as a primer for steel structure in corrosive environments. As well as it being a sacrificial metal for steel it also forms dense and, adherent corrosion by-products making the rate of corrosion a lot slower than if it was the steel itself corroding (anywhere between 10-100 times slower depending on the environment). The zinc corrosion products develop naturally on the surface into something known as zinc patina [33][34].

Zinc patina begins when zinc metal corrodes and forms both zinc oxide and zinc hydroxide, which then later reacts with carbon dioxide into zinc carbonate which is not water soluble.

This means that it will not wash away in the rain or snow and is adherent to the surface of the zinc metal. Zinc carbonate will corrode very slowly and has a grey colour to it protecting the pure zinc metal underneath. The corrosion protection of zinc depends heavily on this layer being formed [34]. It is important to not that, while paint will easily adhere to the surface of pure zinc and zinc carbonate it will not adhere to zinc oxide or zinc hydroxide [44]. This is known as a metallic primer. The lifetime of the sacrificial metal is down to the thickness of the coating [35].

1.6.4:Paint systems

There are different types of paint systems. The one shown in **Figure 3** is an epoxy/urethane paint system. Other paint systems include air drying paints. An example would be an alkyd. These materials will dry by absorbing oxygen from the atmosphere giving a very low film thickness. The alkyd paints usually are very limited in their solvent resistance and have poor chemical resistance [31].

Another type of primer relies heavily on the high adhesion and chemical properties of the binding agent and usually two-steps of epoxy coating are applied in this method. These primers rely on a very thoroughly cleaned surface to prevent any under-rusting causing mechanical breaks, zinc phosphate is an example of a preferred corrosion inhibiting pigment is used in this method as part of the primer formulation.

Other chemical resistant paints are usually acrylated rubber and vinyls. These materials harden through solvent evaporation into a thin film. There is no oxidative process involved in the forming of the film. These can be applied as moderately thick films; however, retention of the solvent can be a problem when a greater thickness is applied. The film is relatively soft and has relatively poor solvent resistance but good chemical resistance. **Table 3** shows how effective the different compounds are at corrosion resistance.

Two- component resistance systems often involve epoxy and urethane. These two compounds are usually referred to as the base and the curing agent. As soon as both compounds are mixed a chemical reaction will begin, so they must be applied in a certain amount of time otherwise they will become inert. The polymerisation continues after the paint has been applied and after the solvent has evaporated to form a strong crosslinked film that is very hard and has good solvent and chemical resistance [31][51].

	Cost	Tolerance of poor surface preparation	Chemical resistance	Solvent resistance	Over-coatability after ageing	Other comments
Bituminous	Low	Good	Moderate	Poor	Good with coatings of same type	Limited to black and dark colours Thermoplastic
Alkyds	Low–medium	Moderate	Poor	Poor–moderate	Good	Good decorative properties
Acrylated-rubber	Medium	Poor	Good	Poor	Good	High-build films remain soft and are
Vinyl	High	Poor	Good	Poor	Good	susceptible to 'sticking'
Epoxy	Medium–high	V. poor	V. good	Good	Poor	Very susceptible to chalking in UV
Urethane	High	V. poor	V. good	Good	Poor	Can be more decorative than epoxies
Inorganic or organic silicate	High	V. poor	Moderate	Good	Moderate	May require special surface preparation

Table 3. Main generic types of paint and their properties [51].

1.6.5:Pre-Fabrication Paint Primers

Pre-fabricated paint primers are referred to as blast primers, as they are usually applied to the steel just after an abrasive blasting cleaning process, designed to prevent any corrosion from occurring before painting. They can be classified under the 4 main types of primer applied.

1. Etch primers: are based on polyvinyl butyral resin and reinforced with phenolic resin to increase water resistance. They can be supplied in a single pack or two pack formats, with the two-pack format being the better for corrosion resistance.
2. Epoxy primers: include epoxy resin and usually polyamide or polyamine curing agents. Pigmented with inhibitive and non-inhibitive pigments. zinc phosphate is the most commonly used and give the best protection out of the group.
3. Zinc epoxy primer: these can be categorised into zinc rich and reduced zinc types. Zinc rich epoxy primers produce films that contain 80% zinc powder and reduced zinc, which can be as low as 55%. When exposed to a marine or industrial environment, an aggressive environment, the zinc produces insoluble corrosion produces that must be removed before overcoating. During weld all zinc epoxy primer will produce zinc oxide which is toxic.
4. Zinc silicate primers: are very similar to the zinc epoxy primers, giving the same level of protection. They also suffer the same drawbacks as zinc salts, and zinc oxide formation during welding. However, they are more expensive to use as well as less convenient than zinc/epoxy primers [31][51].

1.6.6:The Duplex System: Sealer/Undercoat and Intermediate coat

Sealing is a good thing to have done to a primer as it will fill all the natural holes/pores of the metal, making the primer completely sealed from oxygen and water [42]. Usually sealers will have a low viscosity allowing good penetration through the metal. Materials such as vinyl, phenolic, acrylic, epoxy and polyurethane formulations. The sealer coat must not be too thick otherwise a glass like surface will occur and this will give adhesion problems when applying the first coat of paint. For the thermal spraying technique sealing should always be the second process to prevent corrosion as in some cases – if stored in a damp place – can adopt the appearance of a dark corrosion substrate on the metal [35][47].

As seen in **Figure 3** epoxy is a commonly used sealing agent. This sealer fills in the pores of the metal primer and creates an inert barrier between the outside atmosphere and the metal. In a polymer metal interface, the epoxy metal-oxide system the hydrogen bonding is key. The epoxide will have weak bonding with pure metal but with metal oxide the hydrogen bonds make it a much more viable sealer. Pure epoxy resin seals the holes in the zinc primer. On top of this epoxy layer is the intermediate layer of epoxy and micaceous iron. This is a compound with strong bonding due to hydrogen bonding. The structure of epoxy and urethane can be seen below in **Figure 8** [31][48][49].

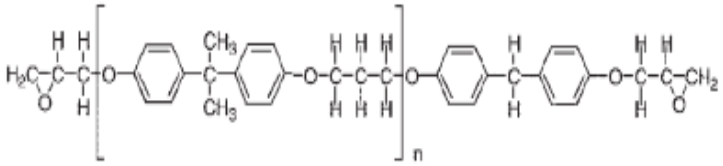

(a)

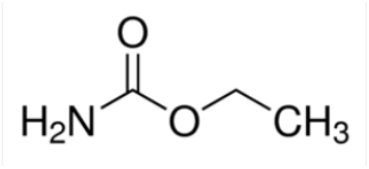

(b)

Figure 8. The structures of epoxy resin(a) and urethane(b) [49].

A duplex system is essentially two corrosion protection systems used together. This is a system that paints over galvanised steel giving another layer of protection before the sacrificial metal is eroded. The second technique thermal spraying is then used in conjunction with galvanising to form a protective barrier in the form of a paint system over the sacrificial metal. With systems like this maintenance is very simple, if the galvanised steel has not been reached and corroded then there is a simple top-up of the paint coating used to protect the galvanised steel [50].

1.6.7:The Top coat

Looking at polyurethane as a topcoat to go with the example coating as seen in **Figure 3** [31]. This is also a very relevant topcoat to look at as it is part of the two-pack paint coating along with epoxy resin to provide the best protection [51][53]. As the Port of Dover is a highly polluted marine environment this is the currently recommended paint system. Polyurethane is a heat reflection top coat with good tensile strength, tear strength and abrasion resistance properties. This means much less coating weight, low temperature flexibility, fair gas permeability, good handling properties, and good weatherability and ozone resistance properties. However, pure polyurethane when exposed to a highly aggressive environment, UV radiation, thermal exposure and oxidative atmosphere it will degrade. Some antiaging agents are therefore, usually added to the polymer [54]. An example being nano zinc oxide which is used to increase stability against UV radiation [55].

This is because polyurethane when it degrades it is due to short wavelength UV rays from the sun, with the life time being limited by the weathering of the polymer. This reduces the physical properties of polymers, breaking bonds in the polymer chain causing the formation of free radicals [56][57]. Polyurethane is an excellent top coat in an anti-corrosion coating, due to its many properties and when mixed with other compounds good UV resistance can be achieved, protecting the rest of the coating underneath. Together with epoxy resin it is classified as the most protective coating available [53].

1.7:Alloys

Coating are not the only protection against corrosion, the metal alloy itself can be made corrosion resistant. The selecting of corrosion resistant alloys for any kind of structure must take into account a lot of factors, including how the alloy would work in the intended environment to avoid mistakes of application [58]. For example, an alloy might not retain the same properties at different temperatures, and other drastic environmental changes such as the change in sulfur concentration. This has a massive impact on the possibility of stress cracking corrosion (SCC), which can be fatal to the structure [59].

One of the reasons why coatings are not the only form of protection is for example; for bridges the alloy used in the construction of the bridge can be made corrosion resistant. In the case of the most aggressive environment, C5, a duplex alloy can be used which does not require a coating. A duplex stainless-steel alloy is an alloy that has a mixed microstructure where it contains roughly equal proportions of ferrite and austenite (steel with various microstructures). These kinds of alloys have a range of grades with varying corrosion resistance properties, depending on their alloy content. There is even the term "super-duplex", which refers to the higher end alloys with greater varied elemental composition, used for high performance duplex stainless steel. With its high chromium content, super duplex steel has brilliant resistance to acids, acid chlorides, caustic solutions and in other environments; often replacing nickel-based alloys and nickel super-austenitic steels. The chemical composition of chromium, nickel and molybdenum helps to improve the corrosion of intergranular and pitting corrosion. Addition of nitrogen helps with structural hardening following the interstitial solid solution mechanism, raising the yield strength and ultimate strength values without sacrificing the toughness of the alloy.
Additionally, the two-phase microstructure gives higher resistance to pitting and stress cracking corrosion when compared to stainless steels [60,61].

UNS Number Duplex Grades	Type[b]	C	Mn	P	S	Si	Cr	Ni	Mo	N	Cu	Other
S31200	...	0.030	2.00	0.045	0.030	1.00	24.0-26.0	5.5-6.5	1.20-2.00	0.14-0.20	...	...
S31260	...	0.03	1.00	0.030	0.030	0.75	24.0-26.0	5.5-7.5	2.5-3.5	0.10-0.20	0.20-0.80	W0.10-0.20
S31803	...	0.030	2.00	0.030	0.020	1.00	21.0-23.0	4.5-6.5	2.5-3.5	0.08-0.20	...	
S32001	...	0.030	4.0-6.0	0.040	0.030	1.00	22.0-23.0	1.00-3.00	0.60	0.05-0.17	1.00	
S32205	2205	0.030	2.00	0.030	0.020	1.00	19.5-21.5	4.5-6.5	3.0-3.5	0.14-0.20	...	
S32304	2304	0.030	2.50	0.040	0.030	1.00	21.5-24.5	3.0-5.5	0.05-0.60	0.05-0.20	0.05-0.60	
S32520	...	0.030	1.50	0.035	0.020	0.80	24.0-26.0	5.5-8.0	3.0-4.0	0.20-0.35	0.50-2.00	
S32550	255	0.04	1.50	0.040	0.030	1.00	24.0-27.0	4.5-6.5	2.9-3.9	0.10-0.25	1.5-2.5	
S32750	2507	0.030	1.20	0.035	0.020	0.80	24.0-26.0	6.0-8.0	3.0-5.0	0.24-0.32	0.50	
S32760	...	0.030	1.00	0.030	0.010	1.00	24.0-26.0	6.0-8.0	3.0-4.0	0.20-0.30	0.50-1.00	c
S32900	329 d	0.06	1.00	0.040	0.030	0.75	23.0-28.0	2.5-5.0	1.0-2.0	...	...	
S32950	...	0.03	2.00	0.035								

Table 4. List of duplex stainless-steel grades as covered in the ASTM (American Society for Testing and Materials) [61].

Table 4 shows what elements are present in the duplex stainless-steel grades [61]. This information will be used to identify where some corrosion products are coming from in the analysis of the elevated bridge at the Port of Dover.

1.7.1:Solid Solution Hardening and Strength

Simple solution hardening is the process of mixing one metal with another, this is done during casting when the metals are in liquid phase. For example, for electrical wiring copper is the main constituent, the solvent, any other additional elements are called solutes. There is a limit to how much solute can be added to the solvent, this is known as the solubility limit. This limit can be increased with the use of temperature and then frozen into place when cooled. Heat treatment of a metal alloy is important for the percentage of elements in alloy.

There are two types of solid solutions the first being substitutional solutions. In this case the solute atoms replace some atoms in the solvent material, this interrupts dislocations in the crystal lattice. Making the mixed material stronger, requiring more stress and energy to move atoms around the crystal lattice.

The second type of solid solution are called interstitial solutions. In this case the solute atoms are small enough to fit into spaces in between the solvent atoms in the crystal lattice, these are referred to as intestices.
This has the same effect as the substitutional solution, where the solute stops the dislocation of atoms in the crystal lattice, providing more strength to the structure, which would require more energy to break and move atoms [62].

To summaries a "super-duplex" system with the addition of chromium, molybdenum, nickel and nitrogen, would provide excellent protection against corrosion. A two-phase micro-structured alloy, as mentioned previously, increases the resistance to pitting and stress cracking corrosion. An alloy with these attributes and the recommended coating system would be enough for a C5 corrosive environment.

Chapter 2:Method

2.1:Analytical Techniques

2.1.1:Scanning Electron Microscope and Energy Dispersive X-ray (SEM/EDX)

This combination of Scanning Electron Microscope and Energy Dispersive X-rays (SEM/EDX) have, in this thesis been used to determine the elemental composition of the corrosion products as well as morphologies of the analyzed corrosion products. The aim is to determine the overall damage mechanism, its specific form, and origin of corrosion, which lead to failure of the structure.

Scanning Electron Microscope (SEM) uses secondary and backscattered electron detectors. SEM utilizes an electron beam which bombards the sample under a vacuum, the main type of signals that are given off and detected are backscattered and secondary electrons. These generate a grayscale image up to very high magnifications(nanoscale). In depth visual inspection has been used to aid in characterizing the type and severity of corrosion in the many samples.

In combination with elemental analysis, using Energy Dispersive X-ray (EDX). The elemental make-up of the samples can be determined, this information can be used to find the corrosion products that are present. The identification of the original chemical composition of the metal, with the environmental pollutants present can be used to aid the investigation of the corrosion process [63][64].

According to the Rutherford-Bohr model electrons orbit a positive nucleus and the number of electrons is equal to that of the number of protons in the atom. With increasing atomic number (Z) orbital states are occupied by electrons in order of minimum energy. The electrons closest to the nucleus are more tightly bounds, the orbital energy is determined by the quantum number (n). The shell closest to the nucleus is (n=1) known as the K shell, the L shell (n=2), the M shell (n=3) etc. **Figure 9** illustrates the positioning of these shells in the atom.

When the sample is hit with the electron beam, it hits an electron in position 1, which is ejected, leaving behind an electron hole. This represents an excited state which is unstable, instead an electron in position 2 will drop down to position 1. This will generate a more energetically stable state. Resulting in a photon being given off in the form of a characteristic X-ray. An excellent example of this is as shown below in **Figure 9**.

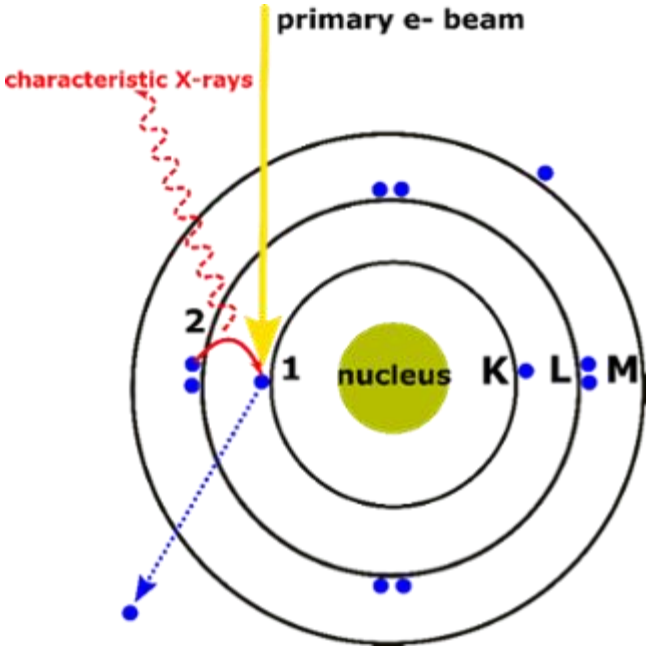

Figure 9. X-ray generation process, the electron beam hits an electron at position 1. Leaving behind a hole that electron at position 2 moves down to fill, generating element specific x-ray [84].

The intensity of these X-rays are categorized by using the subscript of alpha (α) and beta (β) with alpha being the more intense peak, as beta represents forbidden transition as seen in **Figure 10** below. The energy of the X-ray is measured in electron volts (eV). The energies of interest being in-between 1-10keV range [85].

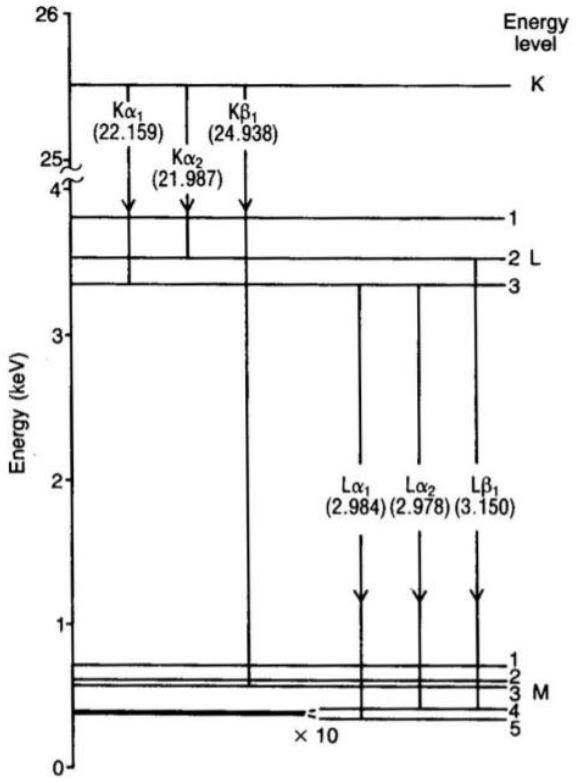

Figure 10. Energy level diagram for silver (Ag) showing the transmission lines for K and L [85].

Figure 10 is an example of an energy level diagram for silver (Ag) showing the energy levels and the shells. For each element there is a unique energy that is given off for each shell, this is used to identify unknown elements in a sample. An example of an EDX spectrum is shown in **Figure 11** [85].

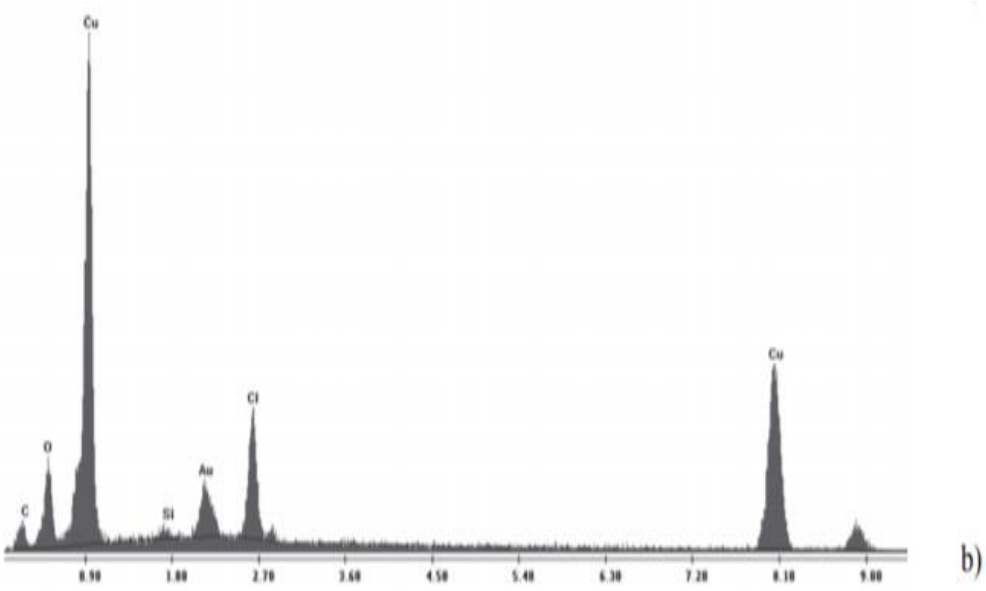

Figure 11. An example of an EDX spectrum [63].

Figure 11 an example of an EDX spectrum. The X-ray given off has a unique energy for every element, allowing for elemental analysis of the sample [65].

2.1.2:X-ray Diffraction (XRD)

X-Ray Diffraction (XRD) is a powerful technique, which is used to identify the chemical compounds. In this project XRD has been used to identify corrosion products in the samples. This is a non-destructive technique that identifies phases in a solid which can be used to characterize a sample with long-range order. In this case the samples originate from the elevated bridge. The most common type of XRD is powder diffraction. Every compound has a unique diffraction pattern and with the use of a database can be compared to known diffraction patterns, allowing for the identification compounds in unknown samples [86].

The unique diffraction pattern is explained by Bragg's law, which states that when a beam of X-rays hits parallel planes of atoms in a crystal there is a particular angle that will allow for the reflection of the incident X-ray beam. In powder XRD this angle is measured as 2θ. Bragg determined that the process of diffraction was due to lattice planes within the crystal. Each plane acted as a semi-transparent mirror where the bombarding X-ray would be reflected and any X-ray that made it through a plane would be reflected from subsequent planes.
Braggs law states that when diffraction occurs, when the following equation is met:

$$n\lambda = 2dsin\theta$$

Equation 6. Braggs law [70].

Where the wavelengths of the incident rays (λ), the angle between the incident/reflected crystal plane (θ), the distance between he crystal planes (d) and (n) which is an integer. The most significant point of Bragg's law is the constructive interference which occurs when the path difference of the travelling waves matches the integral multiplication of the wave length, otherwise known as being in the same phase.

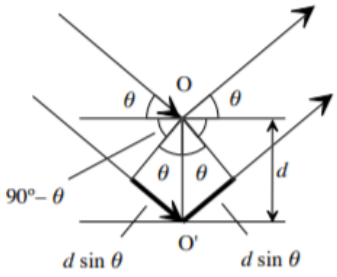

Figure 12. Braggs Law, a representation of path difference with $dsin\theta$ [70].

The waves can be either destructive or constructive which produces the diffraction pattern detected by XRD. Bragg's law calculates the wavelength of waves from the scattered X-rays that hit the atoms in the lattice. The wavelength can tell the atomic distances in a molecule [70].

For the experimental setup of an X-ray diffractor meter there are two main components the x-ray source and the detector. The source will be a metal and a filament inside an evacuated tube, the filament emits the electron beam, which is accelerated towards the metal. The beam will knock core electrons out of their shells allowing for transition to occur from higher shells, filling the holes and giving off X-rays as the electrons drop down in energy. This characteristic X-ray radiation is then used to list the samples. The X-rays when hitting the sample will interact with the compounds according to Bragg's law (**Equation 6**), generating the unique diffraction pattern which can be detected and compared with compounds in the database.

There are a lot of variables involved during the process of corrosion product formation, these are: temperature, pH, pressure and dissolved gases can all affect what types of compounds are formed. This analytical technique can be used to "back track" the corrosion process and identify the cause of the corrosion [66-70][86].

2.1.3:Raman

Raman is advantageous in the use of analyzing corrosion products as the technique itself requires little to no sample preparation and is quick to obtain spectra of the active groups in the composition. As opposed to XRD, samples analyzed with Raman do not require crystalline structures and will therefore, also give information about disordered products. Including amorphous materials, such as, the pantry system and carbon-based corrosion products.

When the light – electromagnetic radiation- passes through a transparent medium it scatters. The visible wavelength of small fractions of light scattered by molecules are different from the incident beam and these "shifts" depend on the chemical composition of the molecules that caused the scattering. This is also known as Rayleigh scattering (elastic scattering). Raman scattering (inelastic scattering), are when a change in polarization has occurred in the system. With this radiation different chemical bonds will interact, making it a good technique for identifying different functional groups. Raman spectroscopy is a good technique for the studying of metallic surfaces, containing coatings and corrosion products as they are both organic and disordered. Raman analysis is not only a non-destructive technique but also the spectra is not affected by the presence of water [71-74].

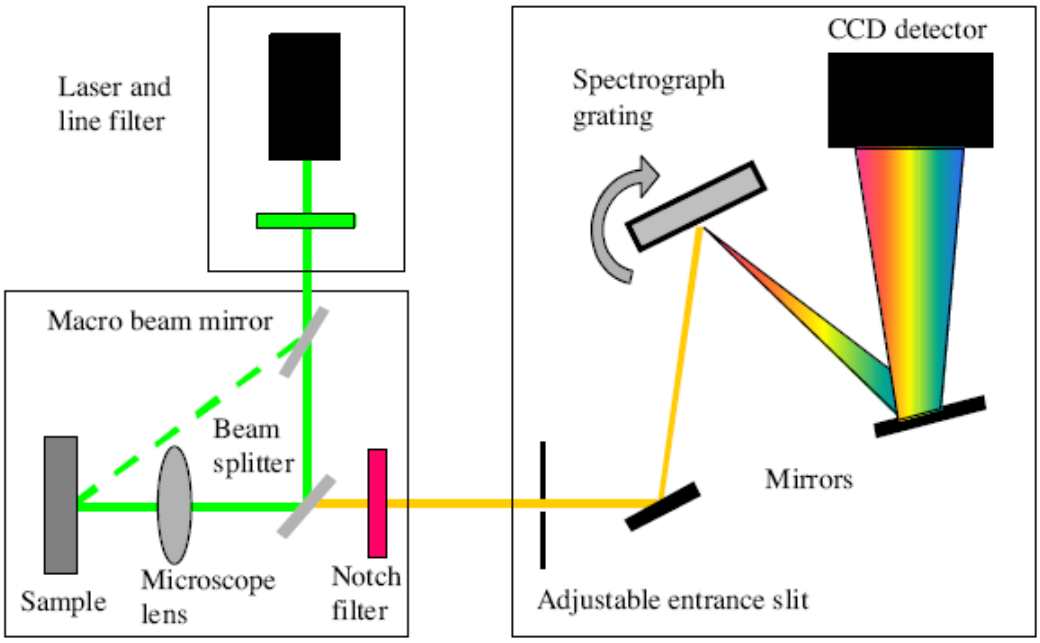

Figure 13. Schematic picture of a Raman spectrometer [87].

As seen in **Figure 13** the Raman spectrometer uses a laser or monochromatic light to excite the electron in the functional group. The light will then scatter from passing through a beam splitter which will filter out the incident light from the laser allowing for only the scattered light to pass through. The notch filter removes all scattering other than Raman scattered light from the reflected beam. This is mainly Rayleigh scattering and the spectrograph is for selecting the favorable wavelength that is being measured [88]. In this project the red laser was used at a wavelength of 633nm.

2.2:Experimental

The sample collection was undertaken at two separate collection times. Prior to sample collection a visual investigation was carried out in October 2017. At this occasion the bridge was photographed and areas of concerns where identified for further sample collection.

The first collection was on the 4th of December 2017, lasting a day. The weather conditions on the day where showing high humidity and heavy precipitation. Temperatures at the site where around 4°C.

The second sample collection was undertaken on 11th June 2018 which also lasted for a day. The weather at the time was a dry but hot 24°C.
There is heavy precipitation at the Port of Dover, coming from vehicles and the sea spray, with constant wind exposure from the north east to the west. This creates a tunnel like effect along the elevated bridge.

All samples where from different sites along the steel bridge, which is used to funnel the traffic between the ferry terminals and the main road network outside of the port as seen in **Figure 14**.

2.2.1:Sample Collection of the Old Part of the Bridge

The first sample collection was from the old part of the bridge, metal was visibly peeling off the structure. The weather condition where dry and cold. The areas sampled from where decided based on where the mobile elevating work platform (MEWP) could access, and what the Port of Dover authorities could close off without disturbing the continuous traffic. Taking access restrictions and all relative information into due consideration, five areas where identified for sampling. In order to not scratch the samples a plastic ice scraper was used to peel of the rust. Pictures where taken of the sample sites with three samples taken from each sample site, each sample was sealed in an airtight plastic bag and labelled according to the sample site and what area within that site the sample came from (area A,B,C). The personal protective equipment (PPE) involved was steel toe capped boots, a hard hat, laboratory gloves and a safety harness.
The handheld Raman machine was also brought along on the sampling day but failed after the third analysis.

2.2.2:Sample Collection of the New Part of the Bridge

The second set of samples were collected from the new part from the new part of the bridge. There was a lot of discoloring, but the rust was not as severe at the old part of the bridge and it was difficult to obtain enough for analysis. The weather was a hot summers day. The sampling was carried out using a mobile elevating work platform (MEWP), in areas that the Port of Dover authorities could close off temporarily. Three areas where sampled, two sample sites where identified in each area. Three samples were taken from each sample site using a camera for visual analysis. An ice scraper was, again used to collect the physical sample and air tight plastic bags with labels were used to catalogue and store each sample. The PPE involved was steel toe capped boots, a hard hat, laboratory gloves and a safety harness.

2.2.3:Sample Preparation for XRD Analysis

The machine used for analysis was the Rigaku Miniflex 6^{th} generation XRD. The sample preparation was as follows: a sample holder was cleaned using water and ethanol; a thin layer of vaseline was then applied to the sample holder in order to keep the powdered sample from dispersing in the machine; in order to get a powdered sample a small quantity of sample was taken and crushed into a powdered form using a mortar and pedestal and placed in the sample holder. The measuring time was 11 hours at a steadily rising temperature from 20-80^{o}C at an angle of 2θ.

2.2.4:Sample Preparation for Raman Analysis

The machine used for analysis of the samples was the Horibu Jobin Yuan model. There was no sample preparation for Raman analysis however, an aluminum stub was used in order to reduce fluorescence. The stub was cleaned with acetone before and after use. The measuring time was 10mins per sample, using the red laser at wavelength nm with a count intensity of 40000 between Raman shift of 0-2000cm^{-1}.

2.2.5:Sample Preparation for SEM Analysis

The SEM/EDX machine used was the Hitachi S3700N Scanning Electron Microscope. Sample preparation required powdering and drying of the samples before mounting the samples. Carbon sticky pads where used with aluminum 15mm stubs to measure the initial samples. however, this method shows carbon as always being present in the samples due to the sticker. Silver paint was then used instead of carbon sticky pads with the silver being discounted from the SEM analysis. The measuring time was 12minutes with 36 points of analysis in a grid fashion for elemental analysis using the EDX. With a magnifying resolution on the SEM at x46 for visual analysis.

2.2.6:Sample Preparation for pH and Conductivity Analysis

Plastic sample bottles where used with Milli-q (ultra-pure) water in order to get the pH and conductivity of the samples, using Hanna pH and conductivity meters. A piece of sample is added to the solution and left overnight before being tested with a pH meter and conductivity meter.

Chapter 3:Results

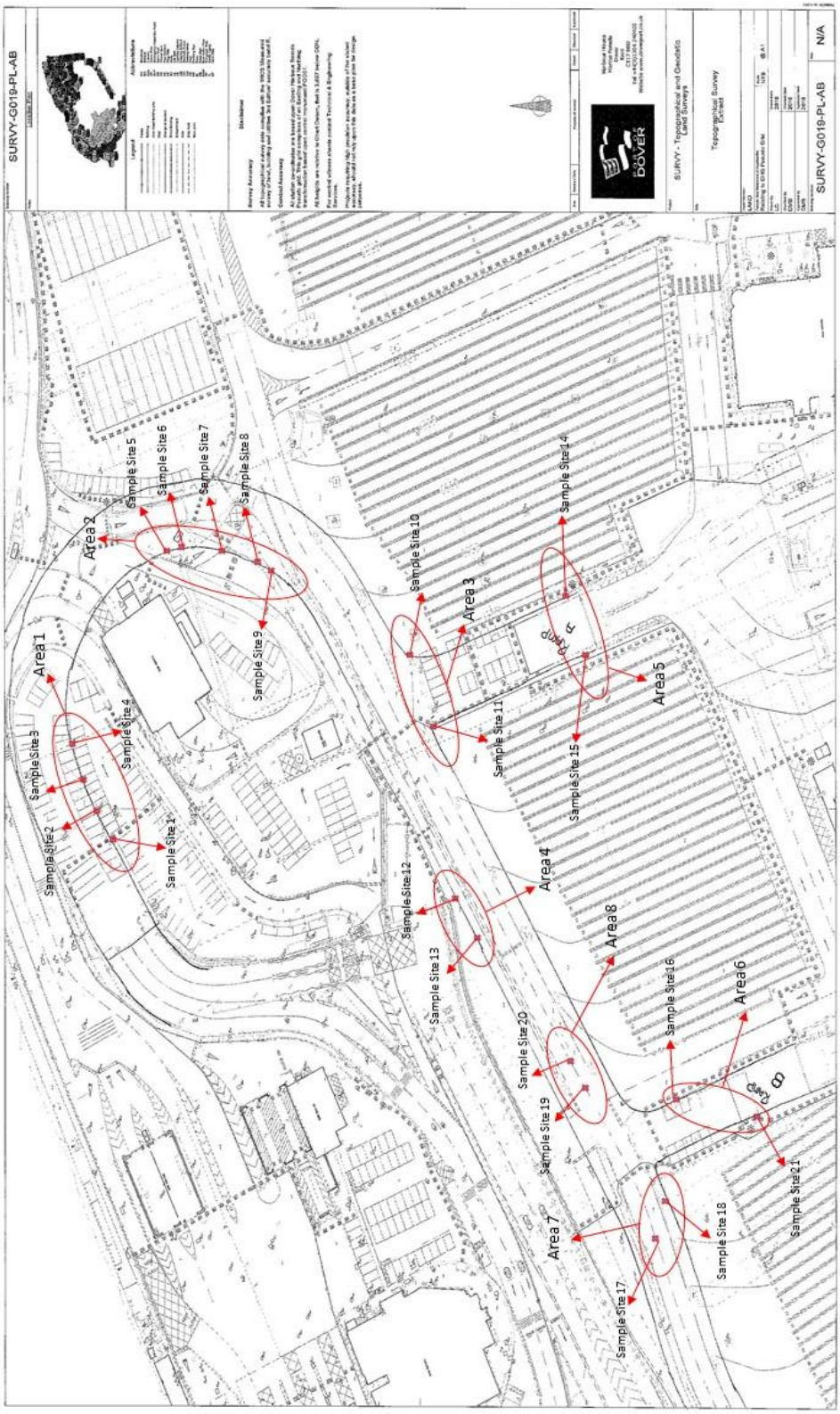

Figure 14. All the sample sites and sample areas on the elevated bridge.

3.1:Area 1

3.1.1:Sample Site 1

The initial visual inspection of sample site one shows a very clear discolouration of the paint layer, with raise lumps underneath the paint. After sampling heavy discolouring was observed under the metal. **Figure 15** below shows before and after sampling.

Figure 15. Sample site 1, A is before sampling and B is after sampling.

The extent of corrosion is not graded as severe but, it is obvious that corrosion has taken place. At this site the paint layer is still visible. Hence corrosion appears to have taken place beneath the coating itself. This type of corrosion is referred to as, under-rusting, when the corrosion takes place between the paint and the metal.

The types of corrosion identified are filiform and uniform corrosion. Filiform due to the bumps underneath the coating and uniform as when the coating is removed the corrosion is evenly spread on the steel underneath.

Appendix 1 shows the severity of the corrosion on the bridge. This section shows the analysis of the various samples. The results are introduced area by area as shown in the map presented in **Figure 14**.

Scanning Electron Microscope (SEM)

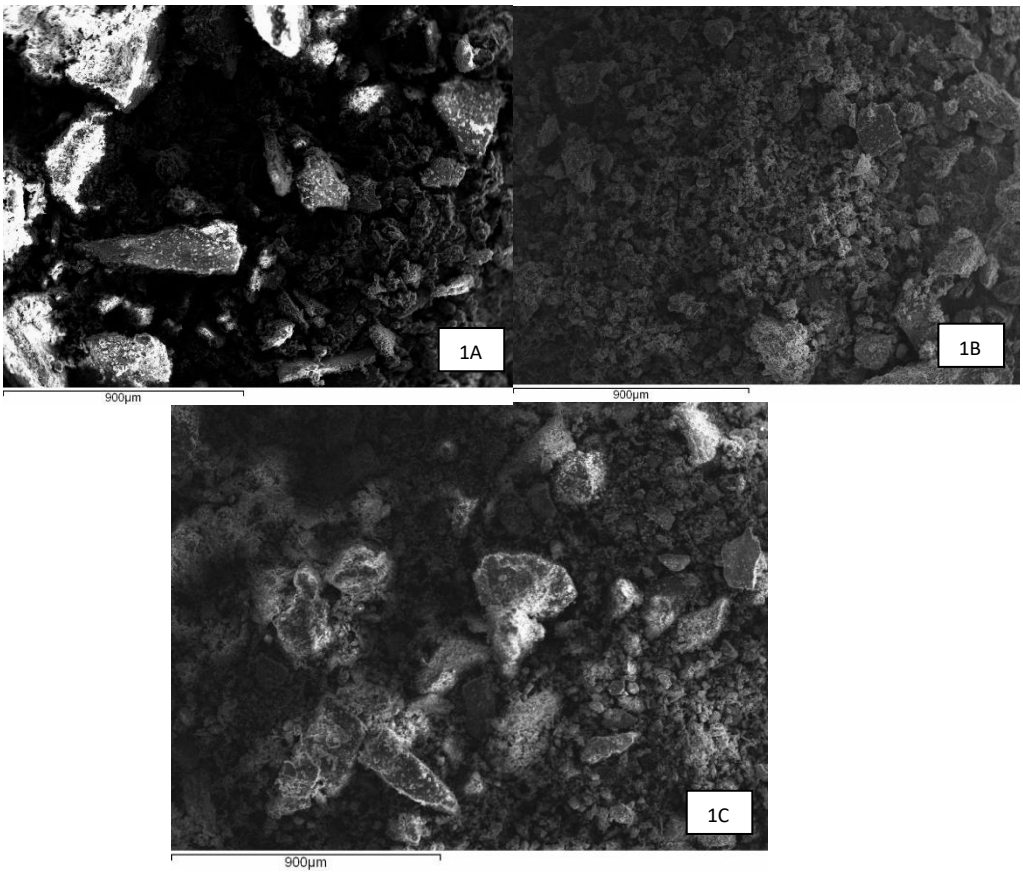

Figure 16. SEM images of samples 1A, 1B and 1C.

The SEM images can be seen in **Figure 16**, the EDX analysis determined that the samples contained the following elements; chlorine, carbon, calcium, titanium, iron, sodium, zinc, silicon, sulfur, magnesium, barium, potassium and manganese. Only samples 1A and 1C contained phosphorus and cerium, sample 1B was the only sample to contain aluminium at this sample site.

Raman

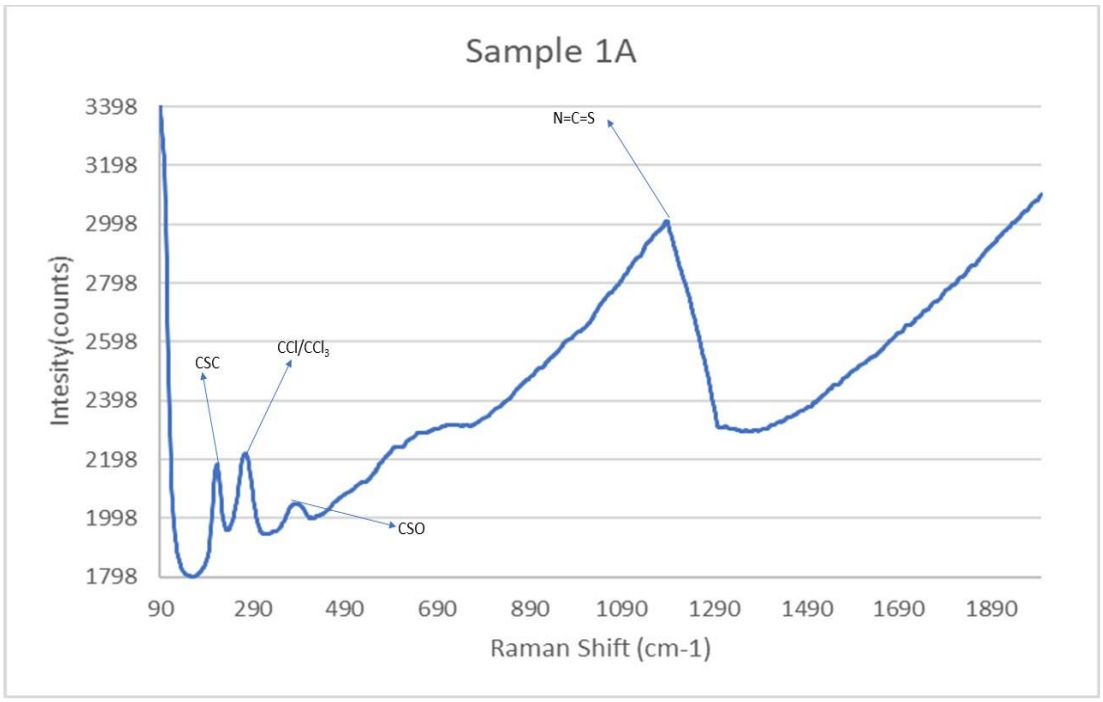
Sample 1A
Intesity(counts)
3398
3198
2998
2798
2598
2398
2198
1998
1798
N=C=S
CSC
CCl/CCl3
CSO
90
290
490
690
890
1090
1290
1490
1690
1890
Raman Shift (cm-1)

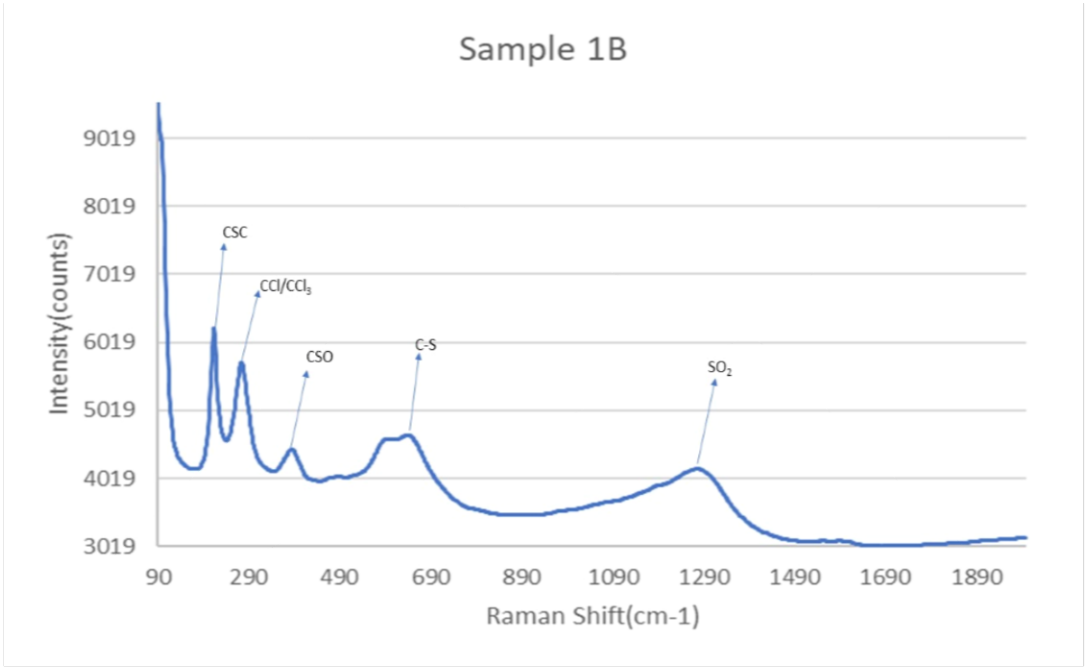
Sample 1B
Intensity(counts)
9019
8019
7019
6019
5019
4019
3019
CSC
CCl/CCl3
CSO
C-S
SO2
90
290
490
690
890
1090
1290
1490
1690
1890
Raman Shift(cm-1)

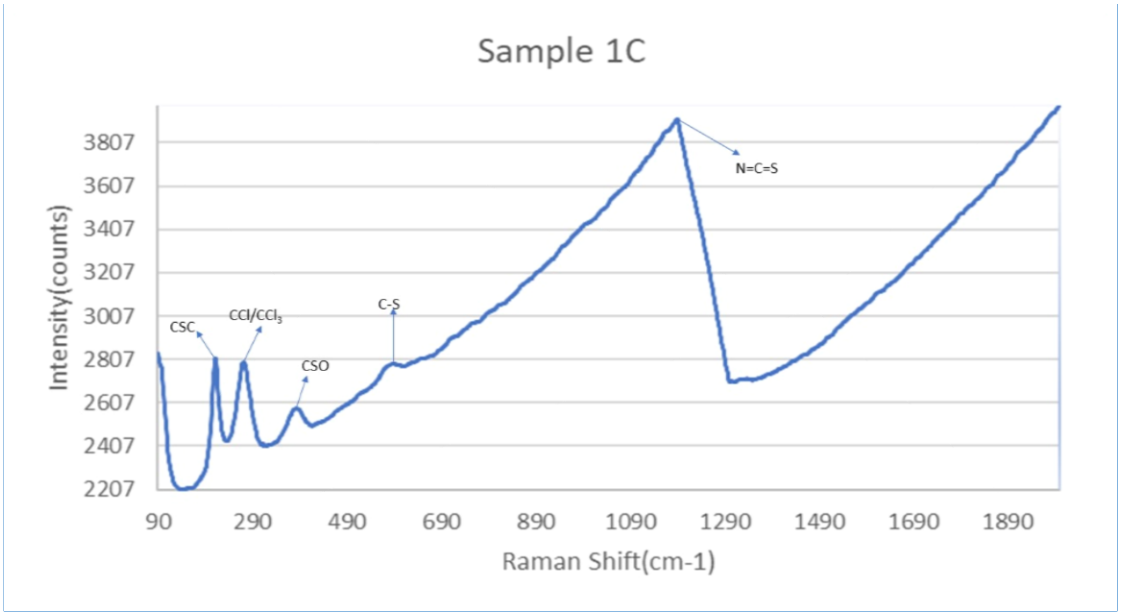

Figure 17. The Raman analysis for samples 1A, 1B and 1C.

By analysing the Raman spectrums as seen in **Figure 17** it was found that sample site 1 contains organic compounds that have mainly carbon and sulfur present. The samples taken from sample site 1 have very similar peaks at 215cm^{-1}(CSC), 270cm^{-1}(CCl/CCl_3) and 380cm^{-1}(CSO) -carbon with sulfur, chlorine and sulphate compounds. Unfortunately, due to fluorescence samples 1A and 1B are difficult to distinguish but there is a peak later at ~1200cm^{-1} which is characteristic for isothiocyanates(N=C=S). There is a shoulder in sample 1A which might be the peak observed in samples 1B and 1C at ~600cm^{-1}(C-S). This can either be aliphatic sulfides and disulphates or covalent sulphates and sulphonic acids(anhydrous). However, seeing as both sulfides and sulphates are present in the sample, they are both overlapping, being represented by the peak at ~600cm^{-1}.

Having identified these organic compounds it was also established that in the EDX and Raman analysis both sulfur and chlorine compounds are present. These are both known for being corrosive elements. These show that carbon particulates are being deposited onto the underside of the bridge from vehicles' fuel (mainly diesel), forming these organic compounds on the surface of the metal. This is adsorbing more of these corrosive elements and forming corrosive organic compounds that are lightly corrosive.

pH and Conductivity

Sample Site	Sample	pH	Conductivity(μS)
1	A	6.31	172
	B	6.77	35
	C	4.3	132

Table 5. Table of the pH and conductivity values for samples obtained from sample site 1.

The pH shows that sample site 1C is quite acidic with a pH of 4.3. The conductivity values show that there are indeed electrochemical reactions occurring, there is more conductivity in samples 1A and 1C suggesting a lush content of cations and anions in the corrosion products.

X-Ray Diffraction (XRD)

Sample 1A	Sample 1B	Sample 1C
Iron Oxide	Iron Oxide	Iron Oxide
Iron Sulfate	Iron Carbonate	Iron Phosphide
Iron Carbonate	Iron Silicate	Iron Phosphate
Iron Phosphide	Potassium Nitrite	Iron Carbide
Potassium Cyanide	Potassium Nitrate	Potassium Carbon Oxide
Potassium Nitrate	Sodium Sulfate	Potassium Nitrate
Potassium Sulfate	Sodium Sulfide	Phosphorus Oxide
Sodium Chlorate	Calcium Silicide	Sodium Phosphate
Sodium Sulfate	Calcium Carbide	Sodium Sulfate
Sodium Nitrate	Calcium Carbonate	Magnesium Silicate
Calcium Carbonate	Calcium Chlorate	Calcium Sulfate
Calcium Silicate	Calcium Silicate	Calcium Carbonate
Silicon Oxide	Silicon Oxide	Calcium Chlorite
Zinc Phosphate	Zinc Sulfate	Calcium Silicate
Zinc Sulfate	Aluminum Sulfide	Zinc Cyanide
Titanium Oxide	Aluminum Oxide	Titanium Oxide
Manganese Oxide	Manganese Carbonate	Titanium Nitride
Molybdenum Carbide	Manganese Silicate	Manganese Oxide
Barium Sulfate	Barium Sulfate	Barium Chloride
Barium Sulfide	Barium Carbonate	Cerium Silicide

Table 6. Compounds identified for each sample by the XRD.

The steel corrosion products are coloured red in **Table 6**, where the iron in the alloy has corroded by reacting with sulfur, carbon, phosphorus and silicon compounds. The most typical product is iron oxide where iron reacts with water and oxygen to return to its original iron oxide state.

The compounds listed in blue fonts are salts made from basic and acidic compounds reacting with each other, the zinc salts are made from the primer (purple fonts) used in the coating for the steel. Salt forms an ion bridge, which increases the conductivity of the solution and in turn increasing the rate of corrosion. The brown and green coloured compounds are also metals that are part of the alloy that the bridge is made up from. Silicon and calcium carbonate come from the Dover cliffs and has been deposited on the bridge where it has reacted with other compounds during the electrochemical reaction.

Barium and cerium are heavy elements and are used in oils and as catalysts in fuels, these have probably run down from the top of bridge in humid environmental conditions and have been trapped in the thin film reacting with other compounds.

There are a lot of sulfur, nitrate and chloride salts present at sample site 1. This increases conductivity and the corrosion rate of the bridge.

3.1.2:Sample Site 2

Sample site 2 is in area 1 which is directly above the car park as seen in **Figure 14**.

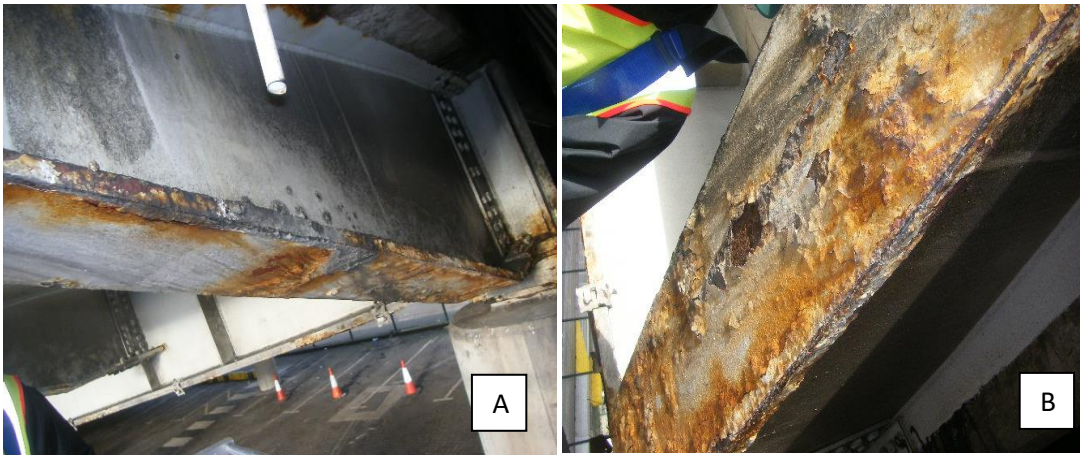

Figure 18. Before(A) and after(B) sampling of sample site 2.

The corrosion here is not very severe (in **Figure 18**) but there is visible corrosion, which has occurred beneath the coating. In both **Figure 18A** and **B** the paint is peeling away from the steel. The types of corrosion visually observed are filiform, due to the raised lumps, uniform corrosion underneath the coating of the steel and exfoliation, which occurs parallel to the surface and along grain boundaries. Exfoliation forces the metal away from the metal in thin sheets.

Scanning Electron Microscope (SEM)

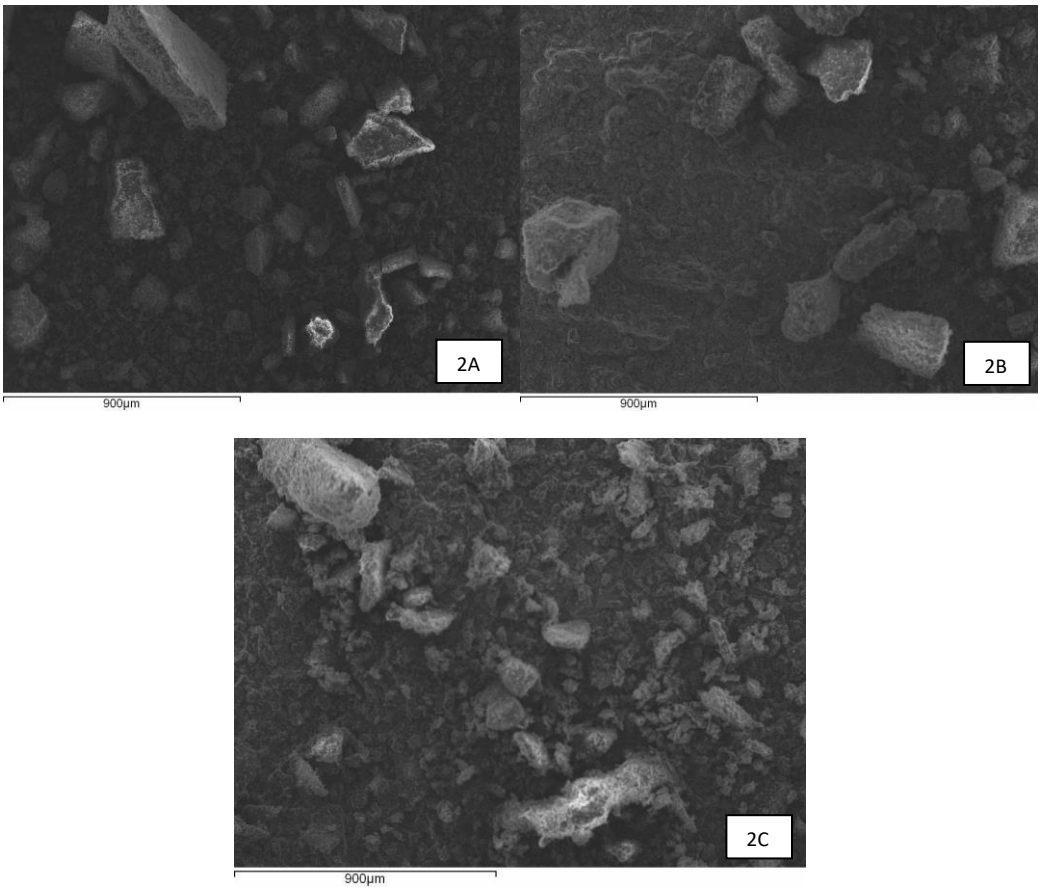

Figure 19. SEM images of sample 2A,2B and 2C.

Figure 19 shows the SEM images for the sample site 2. The following elements were detected using EDX: chlorine, cerium, iron, sulfur, zinc, aluminium, titanium, magnesium, calcium, carbon, potassium, silicon and sodium. Samples 2A and 2B also contain phosphorus, samples 2B and 2C also contain barium, molybdenum and manganese.

Raman

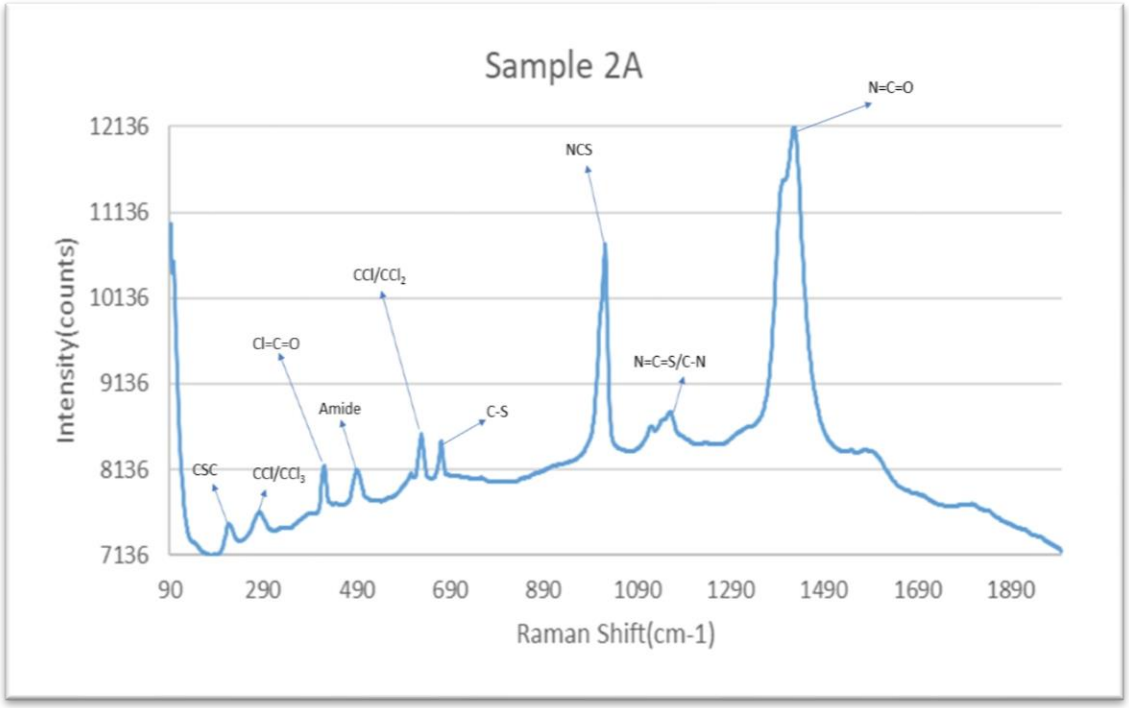
Sample 2A
Intensity(counts)
12136
11136
10136
9136
8136
7136
90
290
490
690
890
1090
1290
1490
1690
1890
Raman Shift(cm-1)
CSC
CCl/CCl3
Cl=C=O
CCl/CCl2
Amide
C-S
NCS
N=C=S/C-N
N=C=O

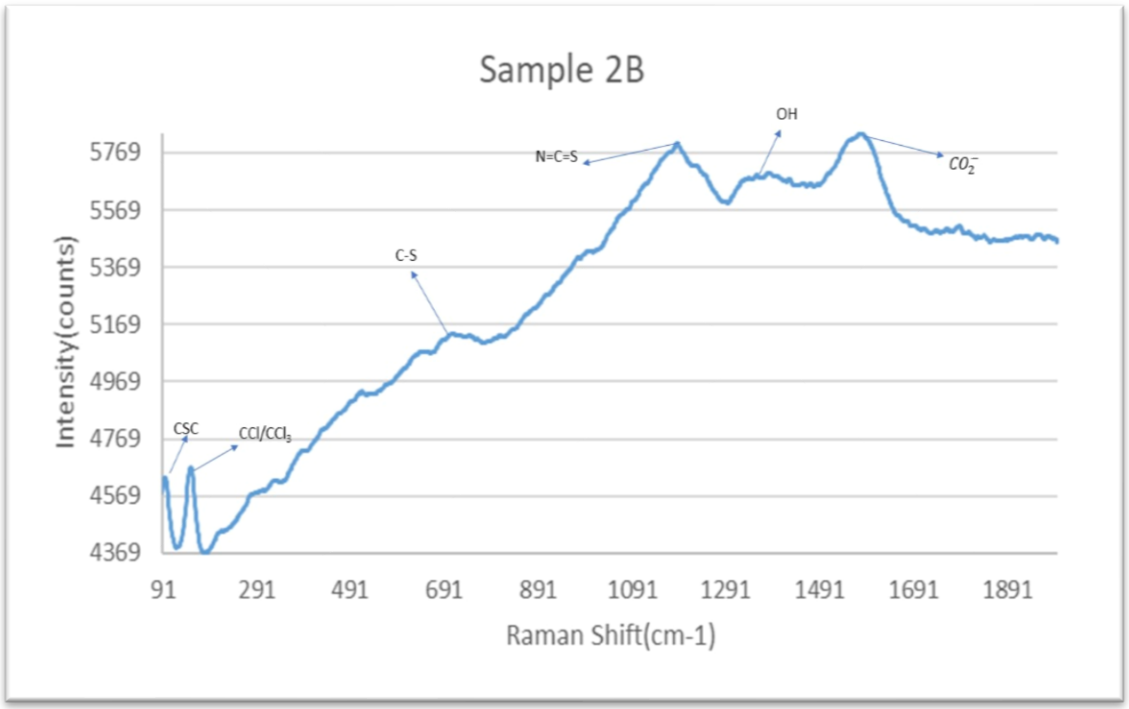
Sample 2B
Intensity(counts)
5769
5569
5369
5169
4969
4769
4569
4369
91
291
491
691
891
1091
1291
1491
1691
1891
Raman Shift(cm-1)
CSC
CCl/CCl3
C-S
N=C=S
OH
CO2-

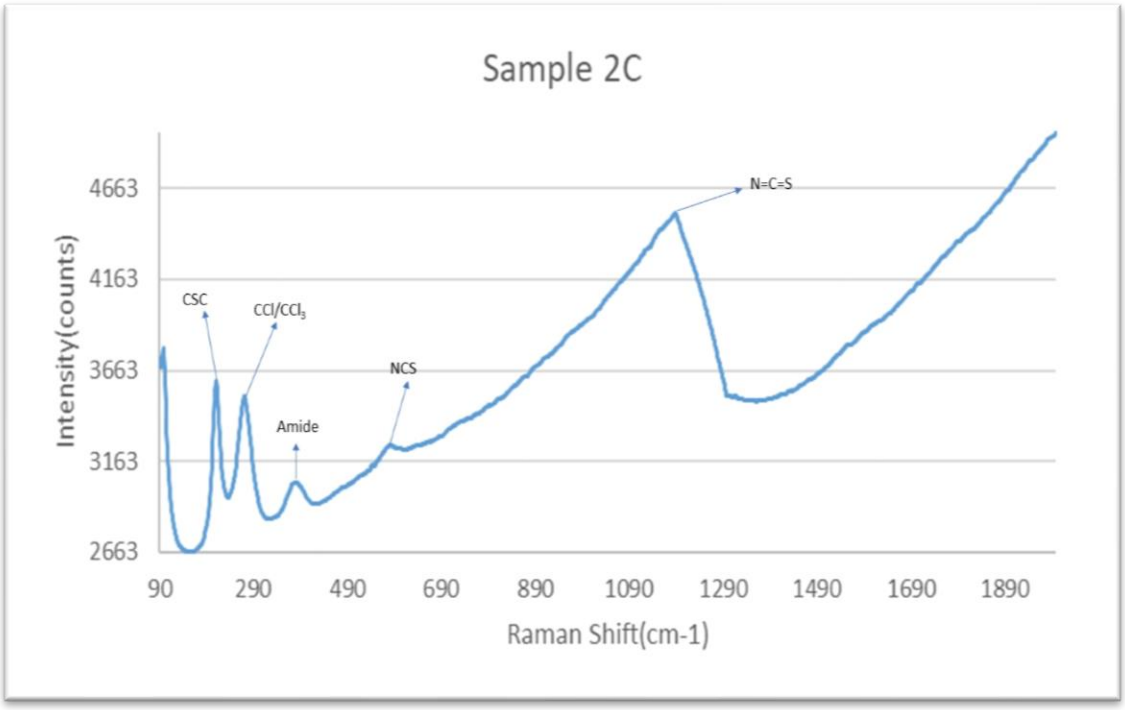

Figure 20. Raman analysis of samples from sample site 2.

All the Raman spectra for the samples taken at sample site 2 are as shown in **Figure 20**. The samples are different from each other. There are only a few similarities at ~210cm^{-1} and ~275cm^{-1} characterised by carbon sulfur and carbon chloride compounds in samples 2A and C. The exception being sample 2B.

Sample 2A has the most defined spectrum out of the three samples, all the organic compounds identified contain carbon. These compounds are: saturated aliphatic acid chlorides (Cl=C=O) at 420cm^{-1}, primary thioamides at 491cm^{-1}, saturated aliphatic acid chlorides (CCl/CCl$_2$) at 628cm^{-1}, mono and disulphonyl chlorides (C-S) at 671cm^{-1}, alkyl isothiocyanates (NCS) at 1022cm^{-1}. At ~1161cm^{-1} there is a broad peak, hence isothiocyanates(N=C=S) and aliphatic amines (C-N) could be present. Lastly, at 1426cm^{-1} there are thiocyanates (N=C=O).

Sample 2B is very similar with the difference of having phenols (OH) present at 1342cm^{-1} and aromatic acid salts (CO_2^-) at 1581cm^{-1}. The differences in Sample 2C form the rest of the samples are amides at 380cm^{-1} and tertiary thioamides (NCS) at 582cm^{-1}.

The carbon along with the nitrogen and sulfur originates from car exhausts in the form of carbon particulates, sulphoxides SO_x and nitroxides NO_x. The chlorine is coming from the sea spray and together with the pollution from the vehicles, is forming acidic compounds in a carbon rich layer on the underside of the bridge.

pH and Conductivity

Sample Site	Sample	pH	Conductivity(μS)
2	A	4.61	41
	B	6.2	60
	C	5.57	87

Table 7. pH and conductivity of samples taken from sample site 2.

This sample site all shows low pH in the range between 5 and 6 as illustrated in **Table 7**. This correlates with the acid chlorides detected by the Raman spectroscopy. The conductivity is low compared to sample site 1. Correlating with the observation that the rate of corrosion is slower in sample site 2 than sample site 1.

X-Ray Diffraction (XRD)

Sample 2A	Sample 2B	Sample 2C
Iron Oxide	Iron Oxide	Iron Oxide
Iron Carbonate	Iron Carbonate	Iron Silicate
Iron Carbide	Iron Sulfate	Potassium Oxide
Potassium Sulfate	Potassium Chlorate	Potassium Nitrate
Potassium Nitrate	Sodium Chlorate	Sodium Molybdenum Chloride
Sodium Phosphide	Sodium Silicate	Magnesium Carbonate
Sodium Oxide	Sodium Nitrate	Calcium Magnesium Carbonate
Sodium Silicate	Sodium Sulfate	Silicon Oxide
Magnesium Carbonate	Sodium Oxide	Silicon Carbide
Magnesium Silicate	Magnesium Carbide	Silicon Nitride
Calcium Sulfate	Calcium Carbide	Zinc Oxide
Calcium Carbonate	Calcium Carbonate	Aluminum Sulfide
Silicon Oxide	Silicon Oxide	Aluminum Phosphate
Zinc Oxide	Zinc Silicate	Aluminum Phosphate
Zinc Phosphide	Manganese Oxide	Manganese Oxide
Titanium Sulfide	Manganese Carbonate	Molybdenum Carbide
Titanium Nitride	Molybdenum Oxide	Titanium Oxide
Titanium Oxide	Titanium Oxide	Barium Chloride
Titanium Silicide	Barium Chloride	Barium Calcium Nitrate
Cerium Carbide	Cerium Sulfide	Barium Oxide

Table 8. Compounds Identified by the XRD for each sample in sample site 2.

Following the colour coding system in **Table 8**, red is iron corrosion products, blue is salts, purple is zinc corrosion products, brown is corrosion products to do with aluminium and titanium metals, green is for the compounds that are from the steel alloy, the black compounds are minerals, heavy element and organic compounds. All the samples contain iron corrosion products providing evidence that the steel itself is degrading. There are a lot of salts in samples 2A and 2B but much less in sample 2C. The origin of these salts are from the sea spray, and atmospheric pollution will result in the deposits of these salts.

There are a lot of mineral and catalyst compounds with heavy elements. These reactants will have originated from cars fumes and the cliffs of Dover. The primer, zinc has not formed any zinc salts in any of these samples, which decreases some deposition when compared to sample 1. This may be an explanation for why the conductivity difference between the two sites is so different.

There are, however, a lot more alloy compounds, aluminium, titanium, molybdenum, manganese and the presence of phosphorus is another difference between sample sites 1 and 2.

3.1.3:Sample Site 3

Sample site 3 is in area 1 which is directly above the car park as seen in **Figure 14.**

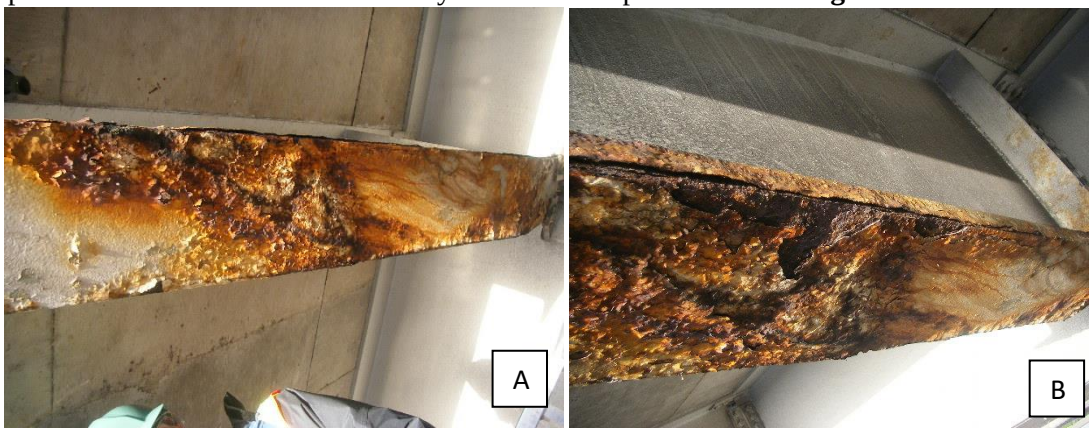

Figure 21. Before(A) and after(B) sampling of sample site 3.

The corrosion on this beam is more severe than that of the last two sample sites from this area. The discolouration of the beam is corrosion caused by deposited pollution that has eaten away the coating as seen in picture A above. There is very clear exfoliation, filiform and intergranular corrosion in **Figure 21A**, **Figure 21B** show that the coating has failed resulting in uniform corrosion on the steel beneath which is a brittle dark red colour. The loss of metal can be seen more noticeably, visually when compared to the other two sample sites in this sampling area.

Scanning Electron Microscope (SEM)

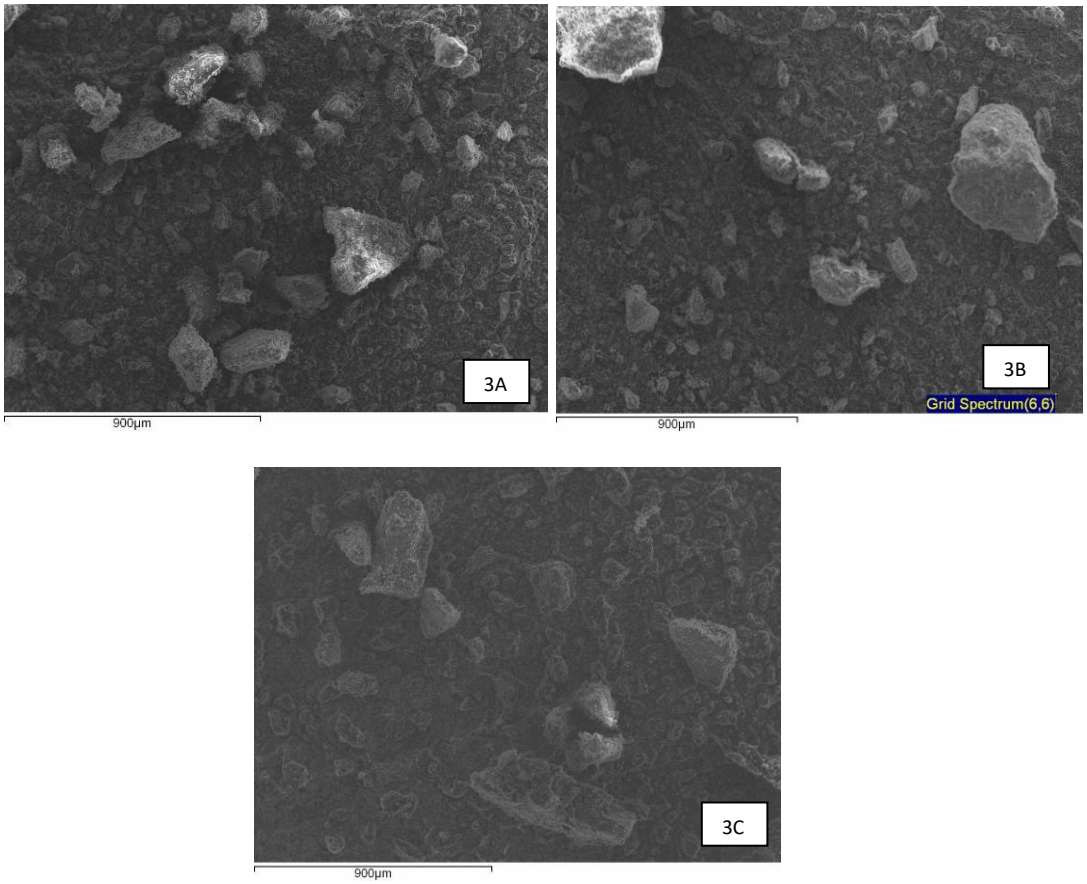

Figure 22.SEM of samples taken from sample site 3.

The analysis from the SEM/EDX as shown in **Figure 22** above contained the following elements: silicon, carbon, sulfur, chlorine, iron, barium, titanium, calcium, magnesium, manganese and zinc. Sample 3A additionally contained aluminium, potassium, phosphorus, sodium, bromine and cerium. Sample 3B also contained molybdenum, phosphorus, sodium, tellurium and aluminium. Sample 3C additionally contained cerium.

Raman

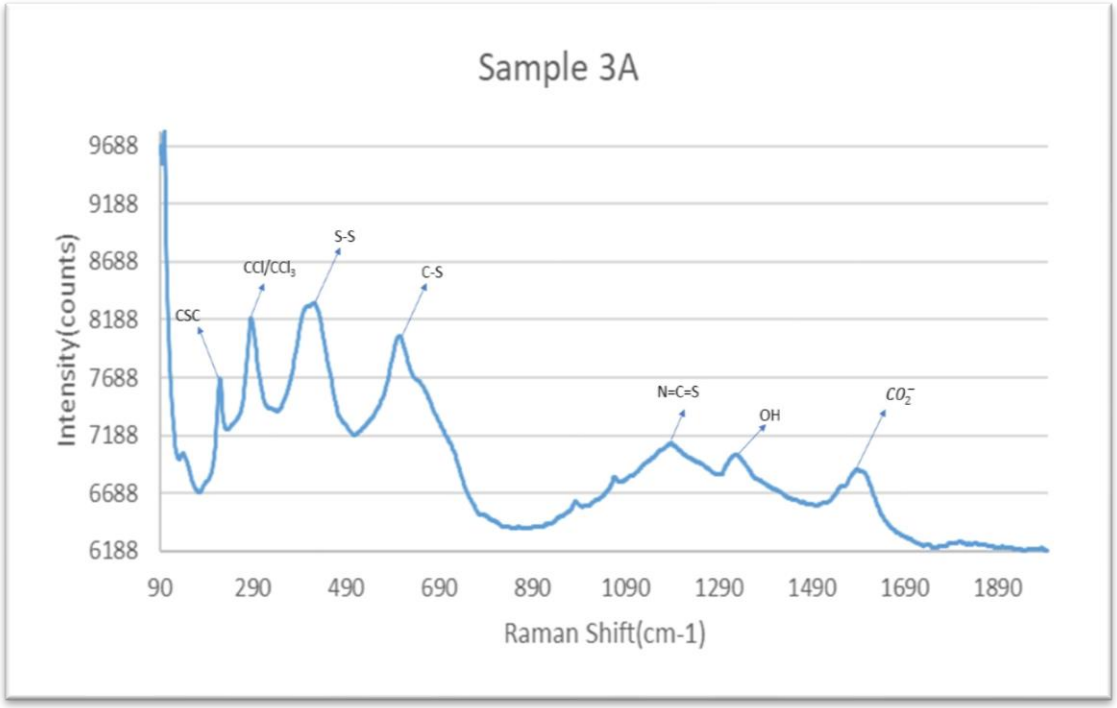
Sample 3A
Intensity(counts)
9688
9188
8688
8188
7688
7188
6688
6188
CSC
CCl/CCl3
S-S
C-S
N=C=S
OH
CO2-
90
290
490
690
890
1090
1290
1490
1690
1890
Raman Shift(cm-1)

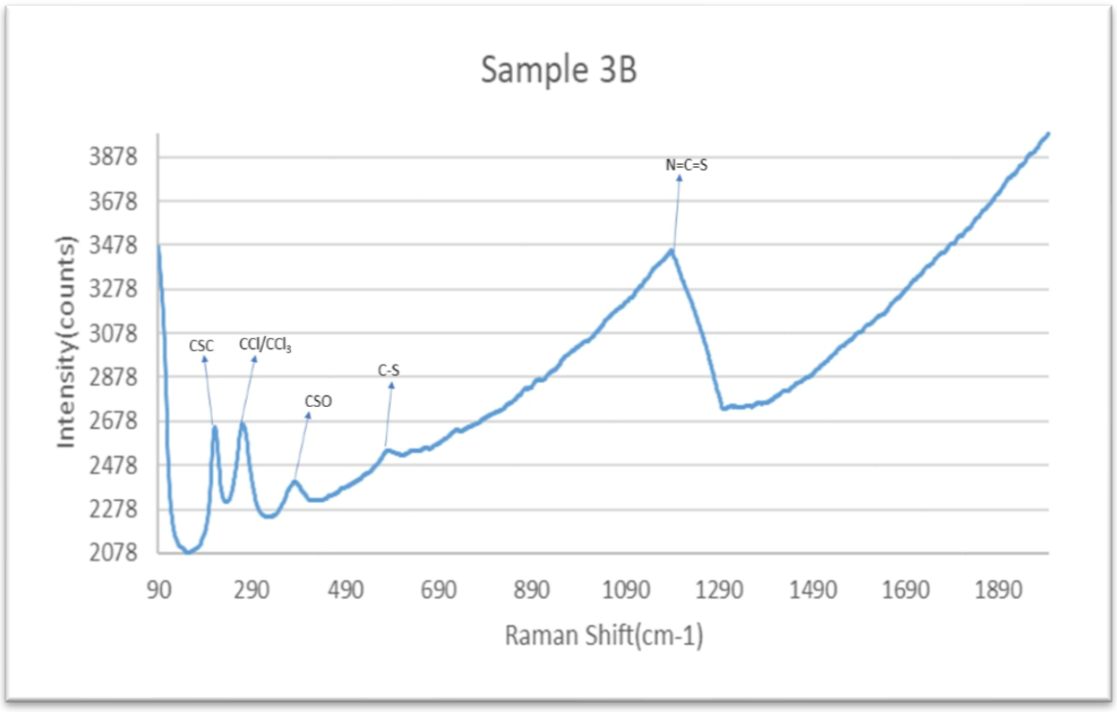
Sample 3B
Intensity(counts)
3878
3678
3478
3278
3078
2878
2678
2478
2278
2078
CSC
CCl/CCl3
CSO
C-S
N=C=S
90
290
490
690
890
1090
1290
1490
1690
1890
Raman Shift(cm-1)

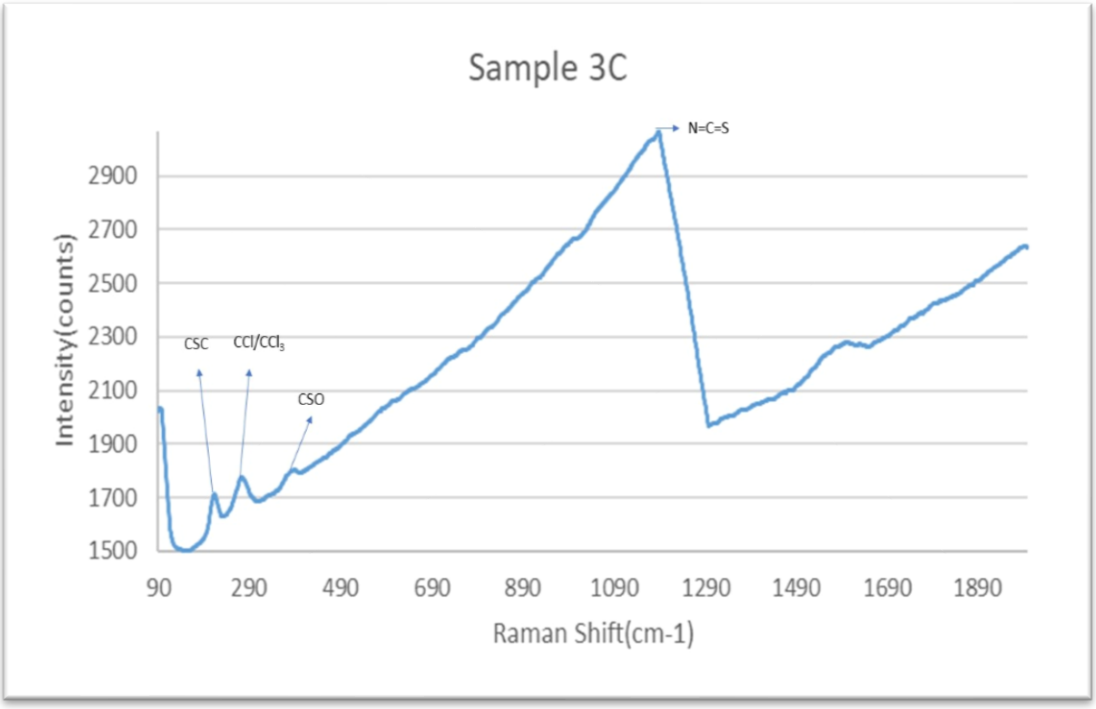

Figure 23. Raman analysis of samples from sample site 3.

Raman spectrums in **Figure 23**, similarly to the other sample sites showed peaks attributing to CSC's and CCl/CCl_3 are common compounds, samples 3B and 3C also have sulphoxides(CSO) at ~380cm^{-1}. At a ~400cm^{-1} sample 3A had a larger, almost double peak hence the aliphatic disulfides (S-S) interpretation. The raman shift ~600cm^{-1} was identified as aliphatic sulfides and disulfides (C-S) for samples 3A and 3B. All the samples at ~1180cm^{-1} contain isothiocyantes (N=C=S). Sample 3A then contains another two additional peaks, at 1325cm^{-1} phenols (OH) and at 1580cm^{-1}aromatic acid salts (CO_2^-).

There are a lot of carbon, sulfur and nitrogen compounds, coming from the oxides that are produced by car fumes being deposited onto the bridge. The phenols (OH) in sample 3A are most probably being made in the thin film as a by-product, from the electrochemical process of water being turned into hydroxide ions.

pH and Conductivity

Sample Site	Sample	pH	Conductivity(μS)
3	A	4.85	136
	B	6.11	95
	C	6.3	44

Table 9. The pH and conductivity of samples taken from sample site 3.

The pH is acidic in sample site 3 as shown in **Table 9**, along with a high conductivity from sample 3A. The conductivity of sample site 3 is higher than sample site 2 but lower than sample site 1. The rate of corrosion is therefore proposed to be in-between sample sites 1 and 2. However, the high levels of carbon, nitrogen and sulfur compounds in this site are evidence of severe corrosion.

X-Ray Diffraction (XRD)

Sample 3A	Sample 3B	Sample 3C
Iron Carbide	Iron Oxide	Iron Carbide
Iron Phosphate	Iron Sulfide	Iron Carbonate
Potassium Oxide	Iron Carbide	Iron Sulfide
Potassium Nitrate	Sodium Chlorite	Sulfur Oxide
Sodium Chlorite	Sodium Chlorate	Calcium Silicate
Sodium Sulfate	Magnesium Silicate	Calcium Carbonate
Magnesium Silicate	Magnesium Carbonate	Silicon Oxide
Calcium Silicide	Magnesium Nitride	Silicon Sulfide
Calcium Carbonate	Calcium Silicate	Zinc Silicate
Calcium Sulfate	Silicon Oxide	Zinc Sulfide
Silicon Oxide	Zinc Phosphate	Manganese Oxide
Zinc Phosphate	Zinc Sulfide	Manganese Silicide
Aluminum Oxide	Aluminum Oxide	Manganese Carbide
Manganese Oxide	Manganese Phosphate	Titanium Nitride
Titanium Oxide	Molybdenum Oxide	Titanium Oxide
Barium Bromate	Molybdenum Silicide	Barium Titanium Oxide
Barium Phosphate	Titanium Oxide	Barium Silicide
Barium Carbonate	Barium Chloride	Barium Oxide
Barium Sulfate	Barium Sulfate	Barium Sulfate
Barium Iron Oxide	Tellurium Molybdenum Oxide	Cerium Iron Nitride

Table 10. XRD of the samples taken from sample site 3.

All the samples contain corrosion products of steel (listed in red font). However, it is only sample 3A showing iron oxide which is linked to rust. Instead these samples are associated with the

formation of iron carbides, which might originate from carbon particles from diesel exhausts. This shows the steel structures are undergoing degradation, as seen in **Table 10**. There a lot less salts than the other two sample sites and as can be seen from the pH and conductivity table above in table 5, the less salts present the lower the conductivity which in turn means the slower the rate of corrosion.

There are, however, more alloy compounds in the samples from sample site 3 indications of more heavy elements, originating from catalysts and car fumes. This is supported by a high level of iron carbides.

3.1.4:Sample Site 4

Sample site 4 is located above the car park in sample area 1 as shown in **Figure 14**.

Figure 24. Before(A) sampling and after (B, C) sampling of sample site 4.

The areas more visible stained on this sample site show what is in the car park and what is outside the car park. Clear discolouration on the cross section of the beam going all the way across it. Picture A shows that the visible corrosion is not very severe before sampling but, the bolts are visibly worse off than the rest of the cross section. The type of corrosion that can be seen here is intergranular corrosion causing that cracked look in the coating which is peeling away from the beam in pictures A and B. Intergranular corrosion will also have caused the coating on the bolts to come loose. Underneath the coating there is obvious uniform corrosion of the steel underneath.

Scanning Electron Microscope (SEM)

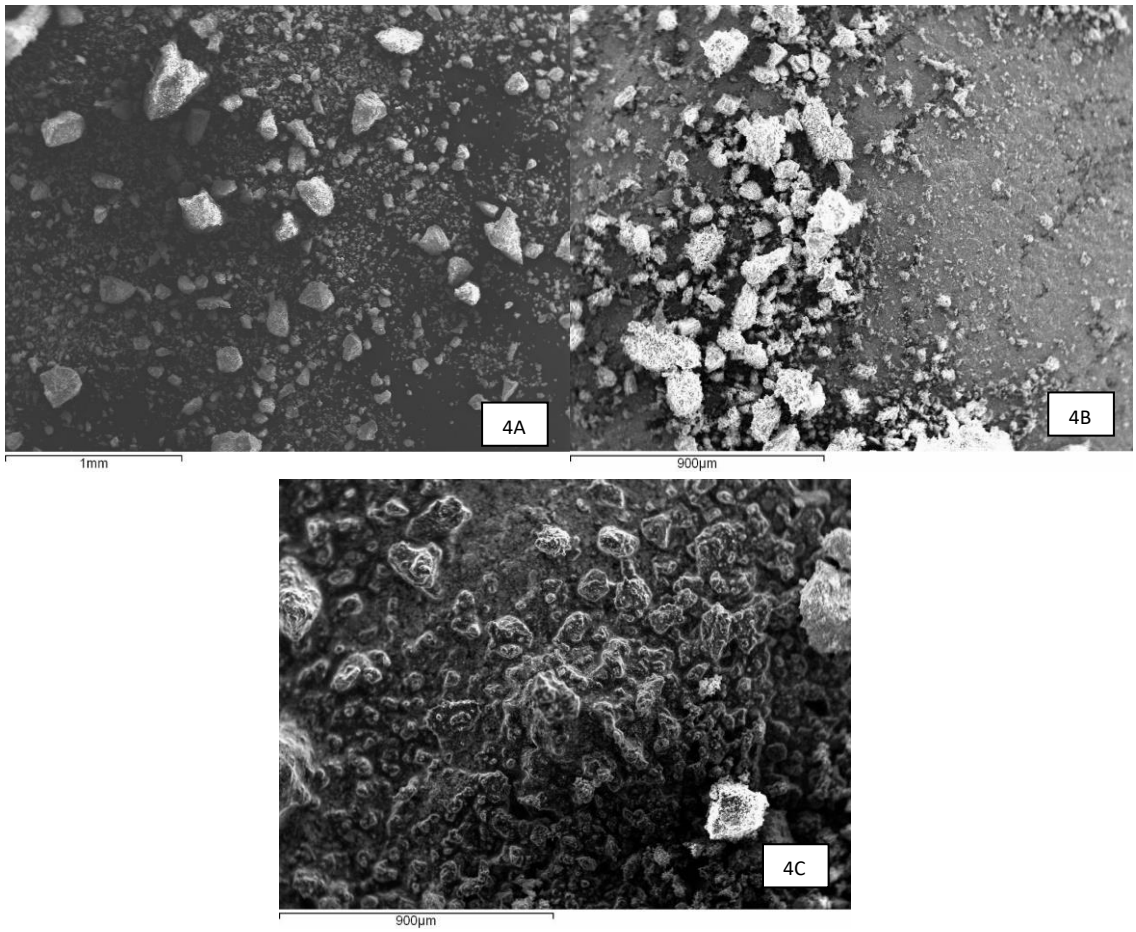

Figure 25. SEM analysis of samples from sample site 4.

The following elements were detected by the SEM/EDX seen in **Figure 25** for sample site 4: carbon, zinc, chlorine, titanium, iron, magnesium, silicon, sulfur, calcium and sodium. Sample 4A also contained manganese, aluminium and potassium. Sample 4B additionally contained, aluminium, copper, arsenic, barium, lead and phosphorus. Sample 4C also contained, cerium, barium, phosphorus, manganese and potassium.

Raman

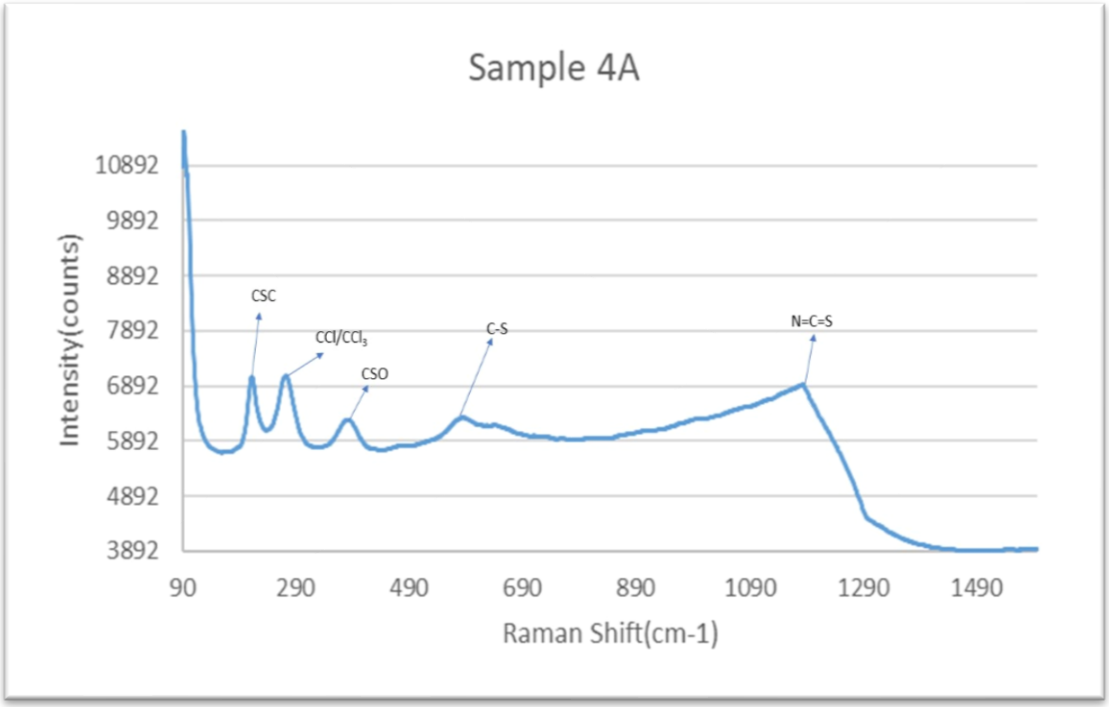
Sample 4A
Intensity(counts)
10892
9892
8892
7892
6892
5892
4892
3892
CSC
CCl/CCl3
CSO
C-S
N=C=S
90
290
490
690
890
1090
1290
1490
Raman Shift(cm-1)

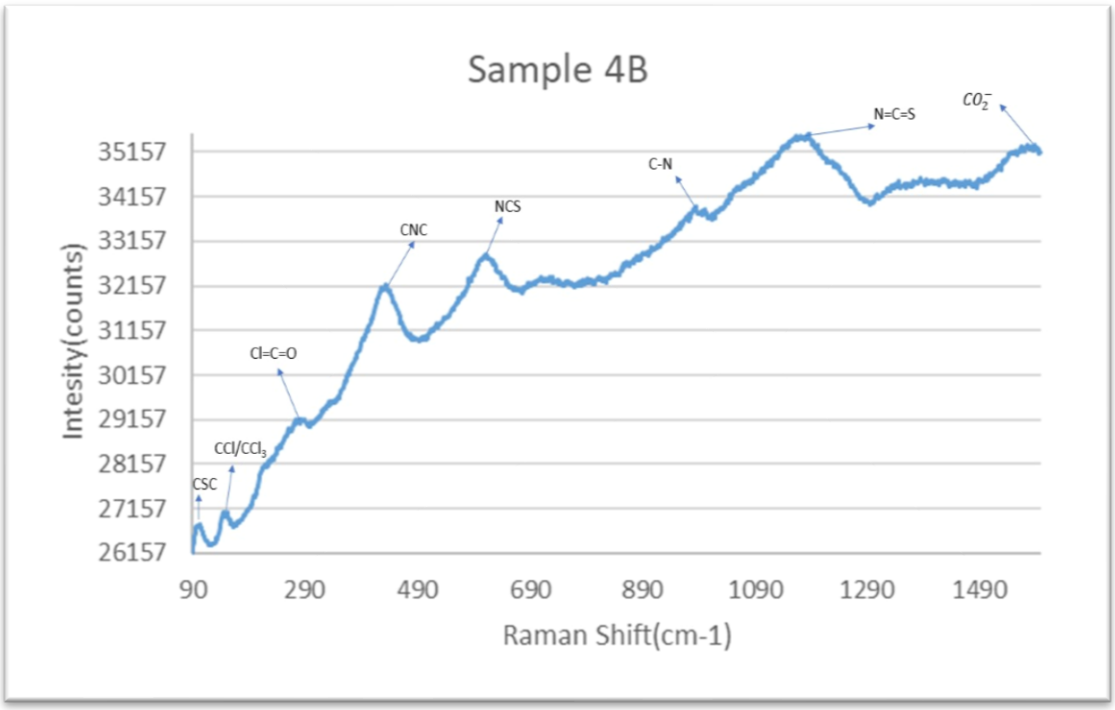
Sample 4B
Intesity(counts)
35157
34157
33157
32157
31157
30157
29157
28157
27157
26157
CSC
CCl/CCl3
Cl=C=O
CNC
NCS
C-N
N=C=S
CO2-
90
290
490
690
890
1090
1290
1490
Raman Shift(cm-1)

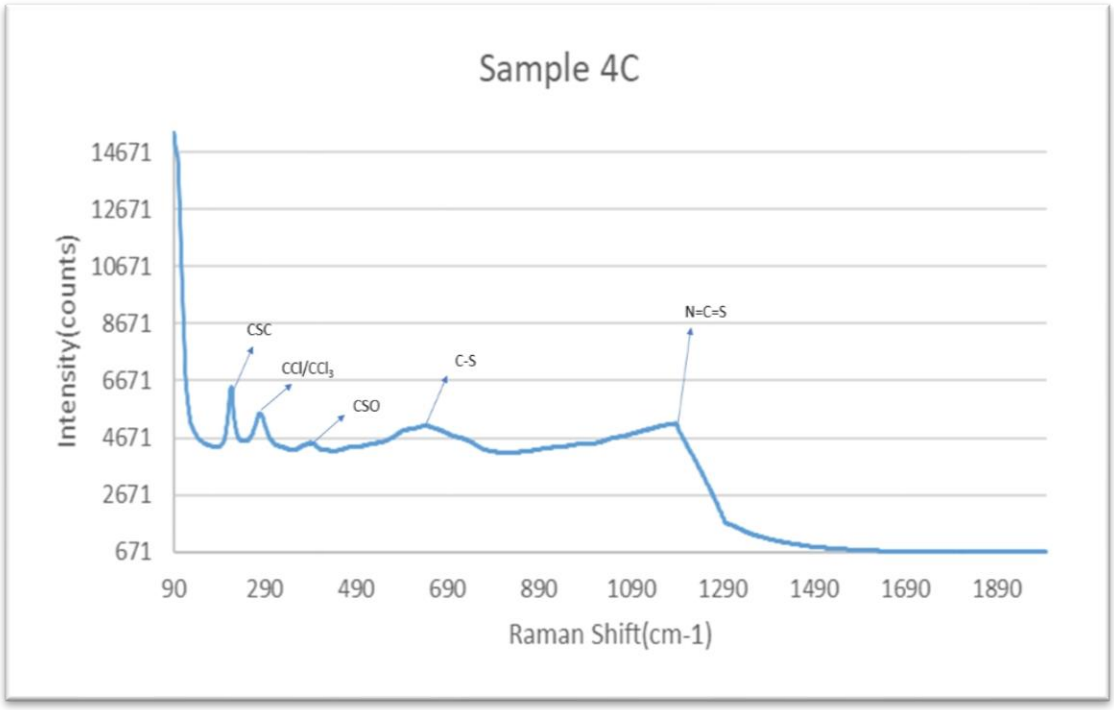

Figure 26. Raman analysis of samples taken from sample site 4.

Raman spectrum shown in **Figure 26** suggests sample 4A and Sample 4C have essentially the same spectrum with isothiocyanates(N=C=S), carbon sulfur and carbon chloride compounds. Sample 4B has a very different spectrum, the spectrum itself is showing a lot of noise and interference. This is the reason that the lower peaks have still been interpreted as CSC and CCl/CCl_3. Raman shift ~280cm^{-1} is a shoulder of a peak and is not very defined, identifying it as a saturated aliphatic acid chloride (Cl=C=O). The clear peak at 434cm^{-1} was identified as secondary aliphatic amines (CNC), at 610cm^{-1} tertiary thioamides (NCS), at 940cm^{-1} saturated primary and secondary nitro compounds (C-N). Lastly at 1185cm^{-1} and 1597cm^{-1} there are the familiar peaks of Isothiocyanates (N=C=S) and aromatic acid salts (CO_2^-) respectively.

No major changes from the other sample sites in terms of the compounds identified. The combination of sea spray, minerals from the cliffs and atmospheric pollution from car fumes has contributed to the compounds identified.

pH and Conductivity

Sample Site	Sample	pH	Conductivity(μS)
4	A	5.75	294
	B	5.52	406
	C	5.5	156

Table 11. Table of pH and conductivity of samples taken from sample site 4.

The pH in all samples are about pH5.5, as seen in **Table 11**. The conductivity is higher in this sample site than the others. The rate of corrosion in this sample site is expected to be higher than any other sample site in this area. Sample 4B has a much higher conductivity suggesting there are more conductive elements present.

X-Ray Diffraction (XRD)

Sample 4A	Sample 4B	Sample 4C
Iron Oxide	Iron Oxide	Iron Oxide
Sodium Iron Oxide	Iron Carbide	Iron Silicate
Sodium Calcium Sulfate	Sodium Nitrate	Potassium Sulfate
Calcium Titanium Oxide	Magnesium Carbonate	Potassium Nitrite
Calcium Aluminum Oxide	Calcium Carbonate	Potassium Sulfide
Calcium Aluminum Oxide Sulfate	Calcium Nitride	Sodium Sulfate
Calcium Iron Oxide	Calcium Phosphate	Magnesium Carbide
Silicon Oxide	Calcium Silicate	Magnesium Silicate
Zinc Silicate	Calcium Carbide	Calcium Chloride
Zinc Sulfate	Silicon Carbide	Calcium Carbonate
Zinc Oxide Sulfate	Zinc Oxide	Calcium Phosphate
Zinc Oxide	Aluminum Sulfide	Calcium Sulfate
Aluminum Silicate	Copper Sulfide	Calcium Sulfate
Manganese Oxide	Titanium Oxide	Silicon Oxide
Manganese Oxide	Lead Sulfite	Zinc Phosphate
	Lead Arsenate	Zinc Sulfate
	Arsenic	Manganese Silicate
	Barium Silicate	Titanium Sulfide
		Titanium Oxide

Table 12. XRD analysis of samples taken from sample site 4.

All the samples from sample site 4 contain iron oxides, providing evidence that corrosion of the steel structure is taking place and that the coating is no longer working as a protective barrier. There is more zinc salts in sample site 4 compared to the other sample sites in area 1.

Sample 4A has a similar Raman spectrum to the other sites in area 1 containing carbon, sulfur and nitrogen organic compounds. This sample also has the second highest conductivity out of all the samples in area 1, possibly due to the zinc products as seen in the XRD **Table 12**.

Sample 4B has the highest conductivity of all the samples in area 1. This sample is associated with heavier elements such as lead, arsenic, barium with the addition of copper. Sample 4C despite having the most salts have the lowest conductivity and the most alloy corrosion products.

Sample 4B contains some toxic heavy elements such as, arsenic and lead compounds. The origins of both these elements is unknown but, might originate from fuels and paint protectors.

3.2:Area 2

3.2.1:Sample Site 5

Sample site 5 is located above the workshop side of the security gate in area 2 as shown in **Figure 14**.

Figure 27. Before(A) sampling and after(B) sampling of sample site 5.

The types of corrosion that can be observed at sample site 5 is filiform, intergranular (exfoliation) and underneath the coating which is visible in **Figure 27** A some uniform corrosion of the steel. Sample site 5 does not have any severe corrosion but is still discoloured with the coating peeling away very easily from the metal. This suggests that just like the other sample sites so far, under-coating corrosion has taken place.

Scanning Electron Microscope (SEM)

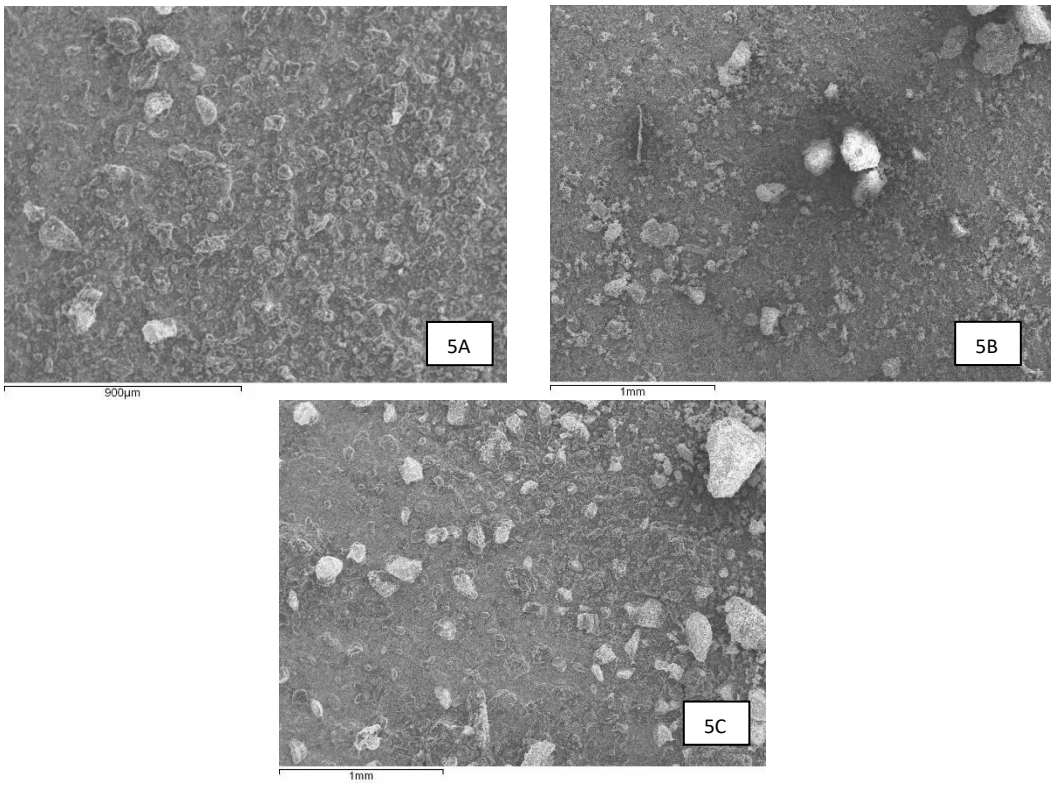

Figure 28. SEM analysis of the samples from sample site 5.

The following elements were detected using the SEM/EDX (**Figure 28**), for all the samples from sample site 5; carbon, magnesium, silicon, chlorine, calcium, sodium, iron, zinc, sulfur and titanium. Sample 5A also contained phosphorus, molybdenum and manganese. Sample 5B additionally had copper, phosphorus and cerium. Sample 5C only had one other element present, which was cerium.

Raman

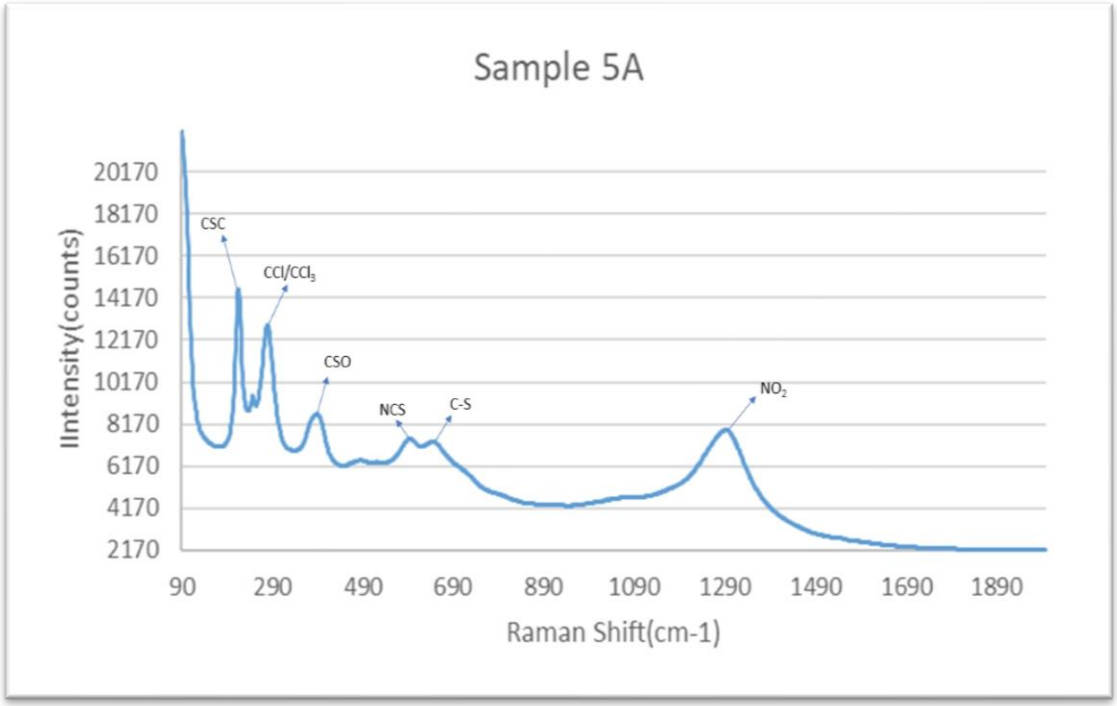
Sample 5A
Intensity(counts)
20170
18170
16170
14170
12170
10170
8170
6170
4170
2170
CSC
CCl/CCl3
CSO
NCS
C-S
NO2
90
290
490
690
890
1090
1290
1490
1690
1890
Raman Shift(cm-1)

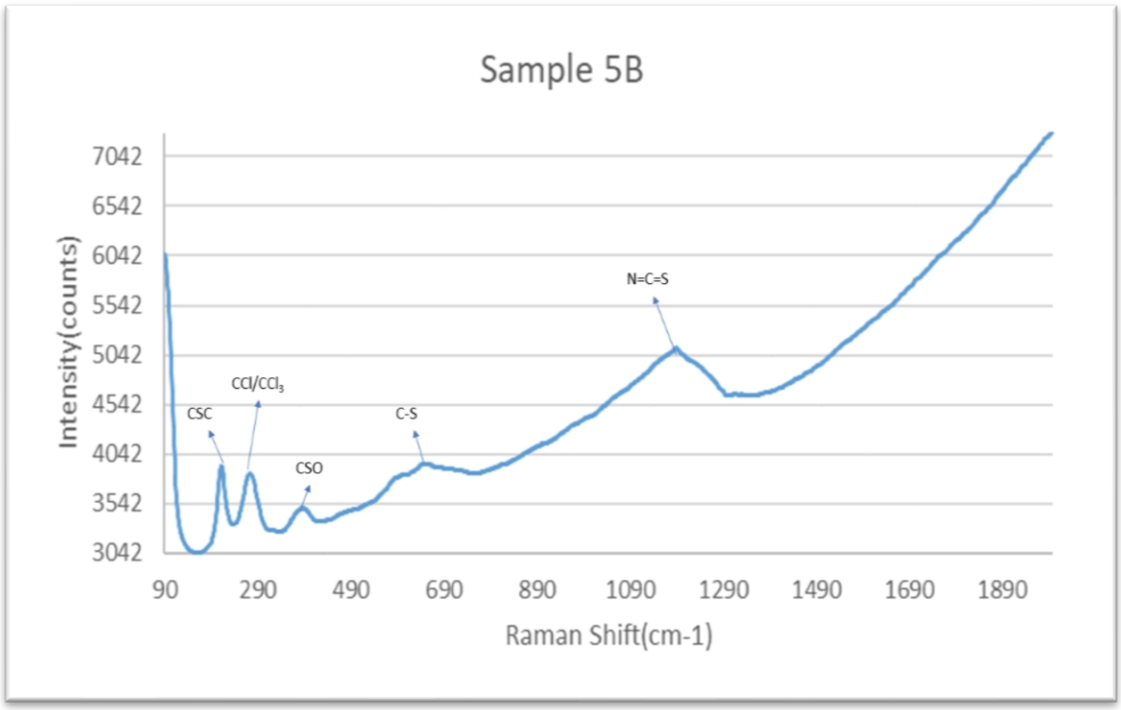
Sample 5B
Intensity(counts)
7042
6542
6042
5542
5042
4542
4042
3542
3042
CSC
CCl/CCl3
CSO
C-S
N=C=S
90
290
490
690
890
1090
1290
1490
1690
1890
Raman Shift(cm-1)

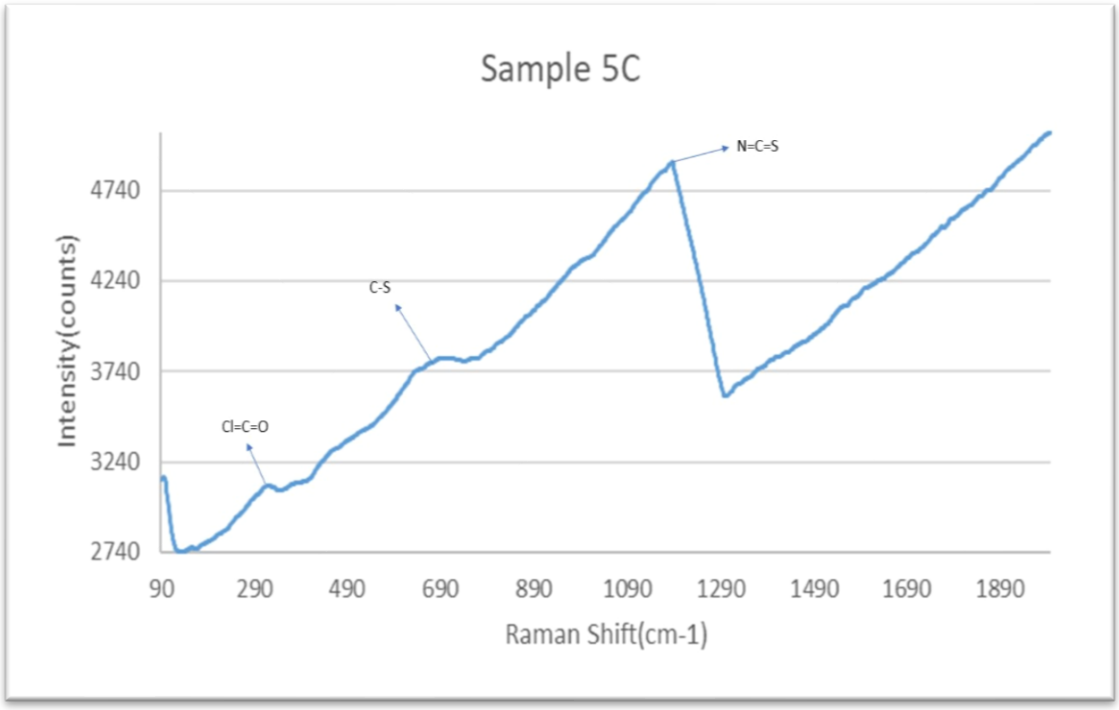

Figure 29. Raman analysis of samples from sample site 5.

The spectrum for samples 5A and 5B is very similar, unfortunately for sample 5C there is a lot of fluorescence interference and only three peaks could be roughly identified as seen in **Figure 29**. Sample 5A contains the same compounds as mentioned for the samples in area 1, the difference being that sample 5A also contains secondary thioamides (NCS) at ~596cm^{-1}. This sample also contains nitroamines (NO_2) at ~1294cm^{-1}. Sample 5C has saturated aliphatic chlorides (Cl=C=O) at 325cm^{-1}, aliphatic sulfides and disulfides (C-S) at 671cm^{-1} and isothiocyanates at 1188cm^{-1}.

There is no large difference from the other Raman spectra observed on the bridge so far. The only new identification is sample 5A at 1294cm^{-1}, nitroamines (NO_2).

pH and Conductivity

Sample Site	Sample	pH	Conductivity(µS)
5	A	5.94	75
	B	6.29	92
	C	6.01	366

Table 13. The pH and conductivity for samples from sample site 5.

Sample site 5 is acidic as shown in **Table 13**, but, has very poor conductivity in the first two samples. Sample 5C instead has the highest conductivity. This suggests that the large bare strip of metal as seen above in **Figure 27**, picture B is undergoing a high rate of corrosion when compared to the rest of sample site 5.

X-Ray Diffraction (XRD)

Sample 5A	Sample 5B	Sample 5C
Iron Sulfate	Iron Oxide Hydroxide	Iron Oxide
Iron Phosphate	Iron Oxide	Iron Silicate
Iron Molybdenum Carbide	Iron Sulfide	Iron Sulfide
Sulfur Nitride	Sodium Oxalate	Iron Silicon Carbide
Sodium Chlorate Hydrate	Magnesium Iron Silicate	Sodium Zinc Silicate
Sodium Carbonate	Magnesium Nitride	Sodium Sulfate
Calcium Phosphate	Magnesium Silicate	Magnesium Silicate
Calcium Nitrate	Calcium Oxide	Magnesium Oxide
Calcium Silicide	Calcium Chloride Hydrate	Calcium Magnesium
Zinc Sulfate	Silicon Oxide	Calcium Sulfate
Zinc Hydroxide	Silicon Phosphide	Calcium Carbide
Manganese Oxide	Zinc Sulfate	Silicon Carbide
Molybdenum Oxide	Zinc Carbonate	Silicon Carbide
Titanium Oxide	Zinc Oxide	Zinc Hydride
Hydrazine Sulfate	Titanium Oxide	Zinc Chloride Hydrazine
Glutamic acid	Titanium Sulfide	Zinc Sulfate
L-Aspartic acid	Copper Phosphate	Zinc Oxide
Aniline hydrochloride	Cerium Carbide	Titanium Oxide
Heptadecylcyclohexane	Ammonium Chlorate	Cerium Carbide
Octachlorodibenzofuran		Ammonium Nitrate

Table 14. XRD analysis of the samples from sample site 5.

All the samples form sample site 5 have a lot of iron corrosion products, with a small number of salts (**Table 14**). There are a lot of zinc corrosion products present in all samples, with only sample 5A containing molybdenum and manganese corrosion products, which will have come from the steel alloy.

There is no aluminium present but there is at least one corrosion product of titanium, which will have come from the steel alloy. Samples 5B and C contain heavier elements (cerium), with sample B having a copper corrosion product. Both samples though have ammonium compounds, sample 5B contains ammonium chlorate, which is when ammonia and chlorine react usually from ammonia neutralising an acid chloride, sample 5C contains the salt ammonium nitrate which is formed when ammonia neutralises a nitric acid.

These two corrosion products give a lot of evidence as to why sample site 5 is acidic. Sample 5A contains a plethora of new compounds: hydrazine sulphate is a salt which formed by the reaction of sulfuric acid and hydrazine (NH_2NH_2), glutamic acid is made up of two carboxyl groups and an amino group, aspartic acid also contains a carboxyl group with the difference being it has the addition of a carbonyl group.

Aniline hydrochloride is essentially a benzene ring and an amine chloride group, heptadecylcyclohexane is a long chain compounds with a carbonyl ring at the end, octachlorodibenzofuran is a series of carbons arranged in a ring like structure containing chlorine functional groups [80].

There is a lot of chlorine present and acids that are producing these corrosion products, some of these corrosion products a most carbon based.

The observation of the many organic compounds indicates that the carbon particulates are adsorbing corrosive compounds and reaction with them on the surface of the metal.

3.2.2:Sample Site 6

Sample site is located very close to sample site 5 as shown in **Figure 14**.

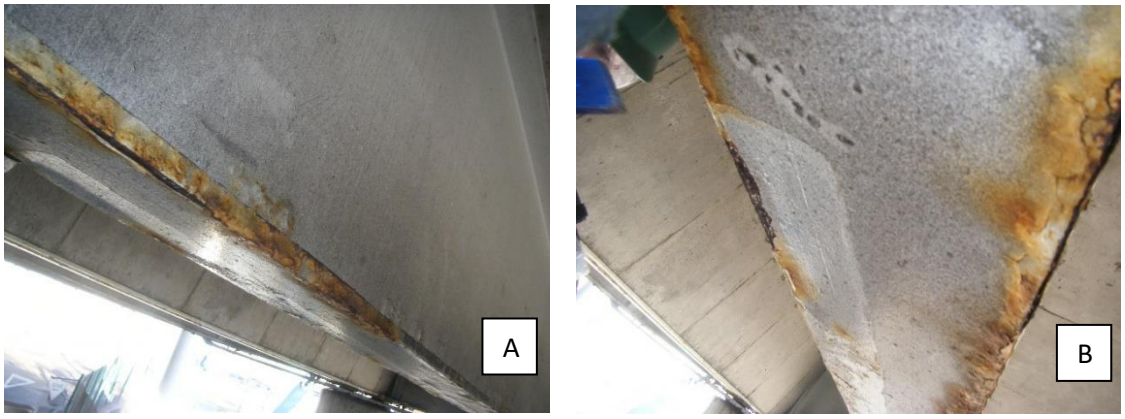

Figure 30. Before(A) and after(B) sampling of sample site 6.

Sample site 6 does not have severe corrosion, from what can be seen in picture A and B in **Figure 30** the coating is still mostly intact. There is a fair amount of staining on the sides of the beam, which has probably come from car fumes. The types of corrosion that can be seen here is mainly intergranular corrosion where the edges of the beam have been corroded firstly, eating the primer from beneath the rest of the coating on the beam. This can be seen in picture B where there is exposed metal that has clearly been corroded, uniform corrosion.

Scanning Electron Microscope (SEM)

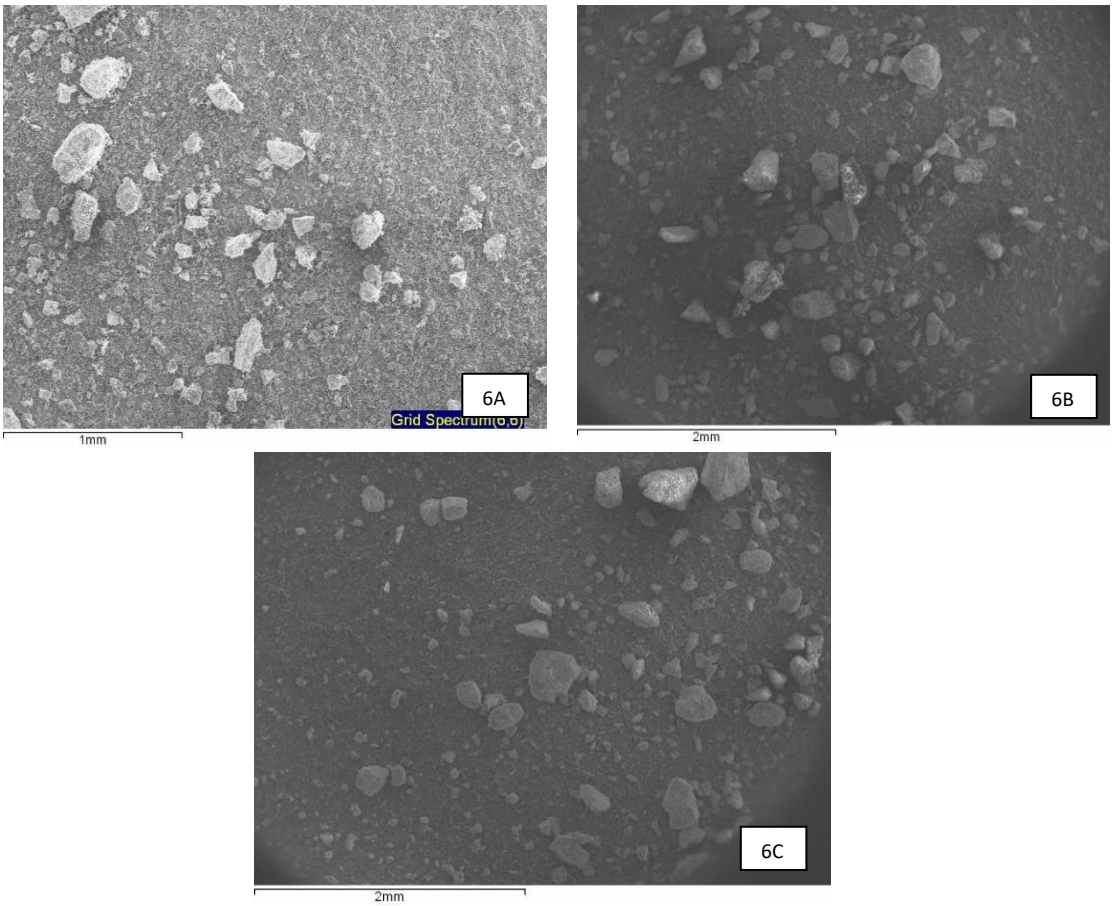

Figure 31. SEM analysis of sample site 6.

Figure 31 shows the SEM images for sample site 6. The following elements were detected in all the samples for sample site 6: carbon, magnesium, chlorine, zinc, iron, calcium, titanium, sulfur, sodium, silicon. Sample 6A also contains phosphorus, potassium and aluminium. Sample 6B additionally contains aluminium and manganese. Sample 6C also contains aluminium, barium and manganese.

Raman

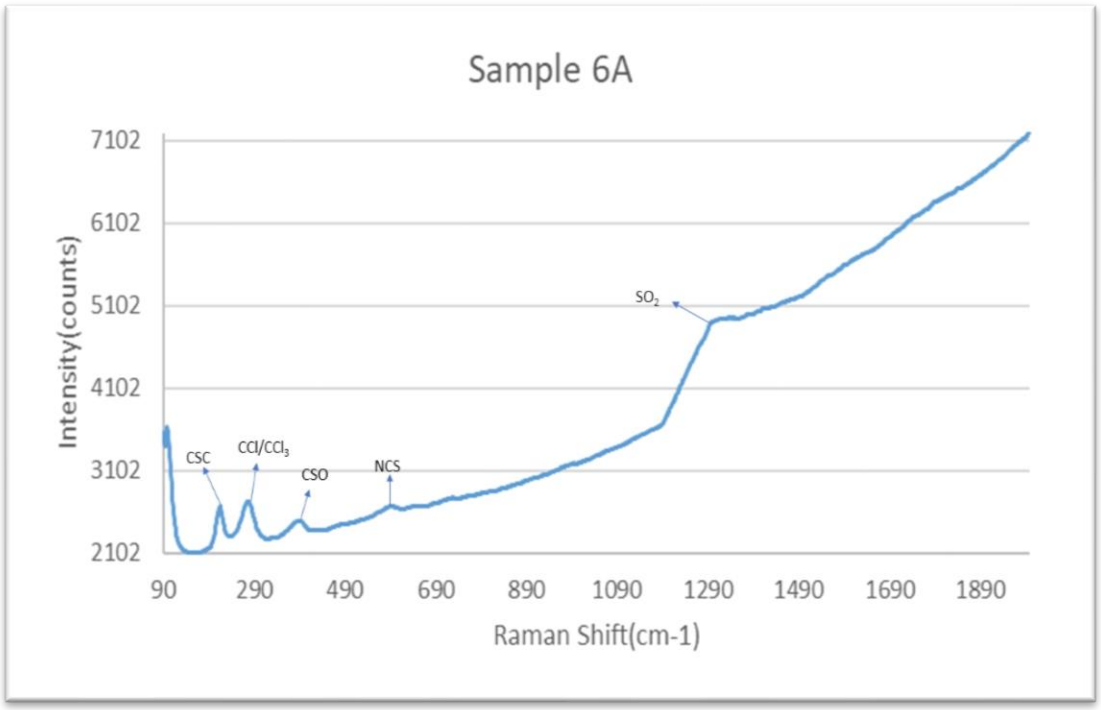
Sample 6A
Intensity(counts)
7102
6102
5102
4102
3102
2102
CSC
CCl/CCl3
CSO
NCS
SO2
90
290
490
690
890
1090
1290
1490
1690
1890
Raman Shift(cm-1)

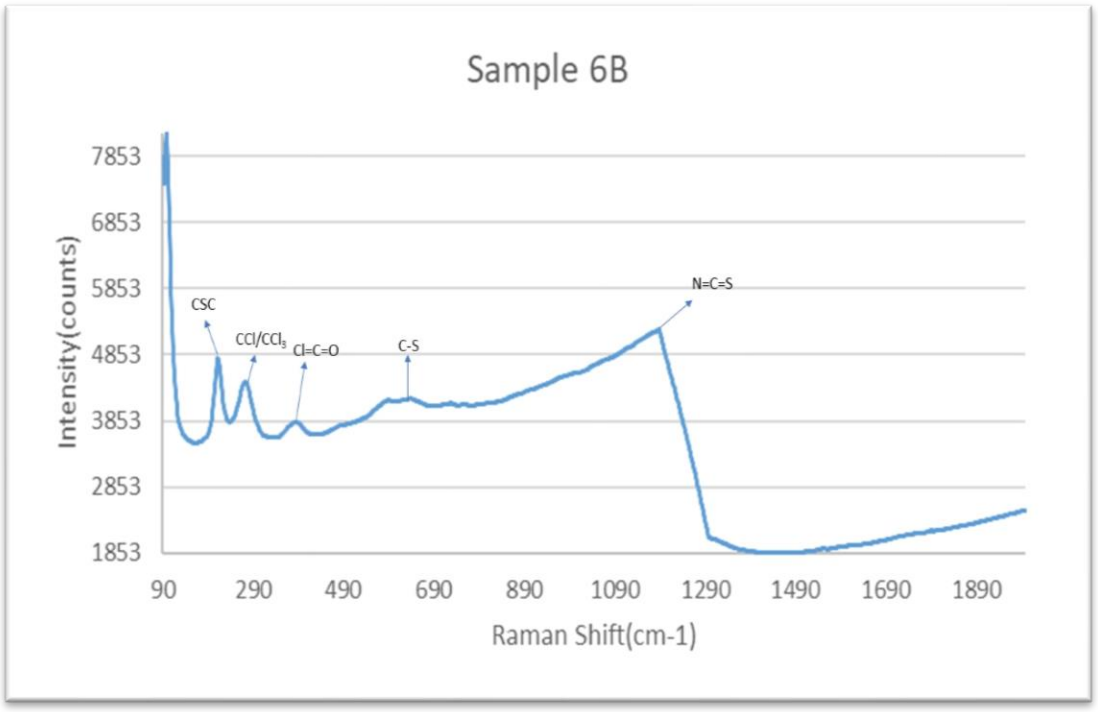
Sample 6B
Intensity(counts)
7853
6853
5853
4853
3853
2853
1853
CSC
CCl/CCl3
Cl=C=O
C-S
N=C=S
90
290
490
690
890
1090
1290
1490
1690
1890
Raman Shift(cm-1)

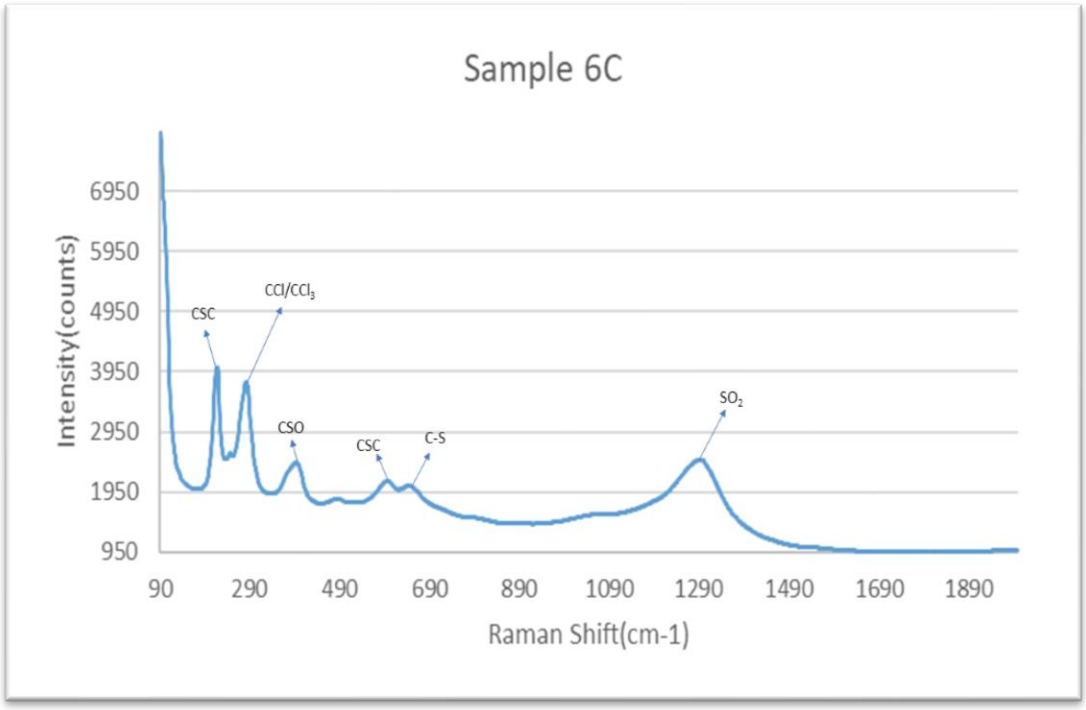

Figure 32. Raman analysis of sample from sample site 6.

Raman spectrum in **Figure 32** shows that sample site 6 contains sulfur and chloride compounds. Sample 6A and C are similar with the differences being that sample 6C has thiocyanates (CSC) at ~550cm^{-1} and aliphatic sulfides and disulfides (C-S) at ~670cm^{-1}. Compared to sample 6A having secondary thioamides (NCS) at 584cm^{-1}. The differences between sample 6B and the other sample is the aliphatic acid chloride (Cl=C=O) at ~380cm^{-1} and isothiocyanates (N=C=S) at ~1188cm^{-1}. Samples 6A and C have methyl sulphones(SO_2) at ~1290cm^{-1}.

The different compounds identified when compared to the other sample site are the additional thiocyanates (CSC) and the methyl sulphones(SO_2), additional evidence of sulfur and nitryl compounds.

pH and Conductivity

Sample Site	Sample	pH	Conductivity(μS)
6	A	8.93	213
	B	7.61	266
	C	8.45	323

Table 15. The pH and conductivity of the samples from sample site 6.

As seen in **Table 15** sample site 6 has an overall basic pH which differs from sample site 5 that is acidic in area 2. Sample site 6 also has a much higher conductivity than the other sample site, this is probably because of the formation of salts. There are a lot of sulfur and chloride compounds identified in the Raman above and if there are a lot of basic compounds then there will be more salts formed.

X-Ray Diffraction (XRD)

Sample 6A	Sample 6B	Sample 6C
Iron Oxide	Iron Oxide	Sulfur Oxide
Iron Oxide Hydroxide	Iron Sulfate	Sodium Iron Oxide
Iron Phosphate	Sodium Oxalate	Sodium Carbonate
Iron Silicate	Sodium Sulfide	Sodium Sulfate
Potassium Oxide	Magnesium Sulfate	Magnesium Iron Silicate
Potassium Nitrate	Magnesium Silicate	Magnesium Nitride
Potassium Cyanide	Magnesium Silicide	Calcium Carbonate
Sulfur Oxide	Zinc Sulfate	Silicon Oxide
Sodium Sulfate	Zinc Carbonate	Zinc Oxide
Calcium Sulfate	Aluminum Hydroxide	Aluminum Magnesium
Calcium Carbonate	Aluminum Oxide	Manganese Oxide
Silicon Oxide	Aluminum Manganese	Manganese Silicate
Zinc Hydroxide	Manganese Oxide	Titanium Oxide
Zinc Sulfate	Manganese Carbide	Barium Silicate
Zinc Oxide	Manganese Sulfide	Barium Chloride
Aluminum Oxide	Titanium Oxide	Barium Titanium Oxide
Titanium Oxide	Hydrogen Sulfate	Barium Carbonate
Ammonium Nitrate	Aminodiacetic acid	Ammonium Chlorate
Ammonium Chloride	Methanol eicosahydrate	Ammonium Thiocyanate

Table 16. XRD analysis of samples form sample site 6.

As seen in **Table 16** samples 6A and B both contain iron corrosion products, which have come from the metal but, sample 6C does not have these corrosion products without the addition of another element. There are not that many salts in each of the samples but there is a lot of corrosion product from other metals that are part of the steel alloy, aluminium, titanium and manganese.

Sample 6A and 6C have ammonium compounds, which means that the acidic corrosion environment is being neutralised by basic compounds. Sample 6C contains a lot of barium which has reacted with the metal, minerals from the cliffs and chlorine from the sea. Sample 6B's interesting compounds that are different from the other samples are; hydrogen sulphate, which is an ion of sulfuric acid, aminodiacetic acid is another acid that has been made in the thin film, and methanol eicosahydrate, which is an alcohol.

Sample site 6 has very little in terms of minerals compared to the other sites so far and less salts. This site has more nitrogen-based groups and metal corrosion products.

3.2.3:Sample Site 7

Sample site 7 is located directly above the security gate separating the workshop from the main road, as seen in **Figure 14**.

Figure 33. Before(A) and after(B) sampling at sample site 7.

The corrosion at this sample site is not severe, even though it might look like it. It is just decolourised and stained as seen in **Figure 33**. The types of corrosion that can be seen from both pictures is: filiform, intergranular and uniform. This sample site does, however, look as if cracking corrosion has taken place from the stress applied to the bridge or a change in the structure of the steel. The change in the structure is if it is cooled and heated shrinking and enlarging the metal. The cracks are raised and therefore the type of carrion has been concluded to be filiform as that gets underneath the coating and eats away the metal, which can be clearly seen in picture B. This sample site like others has been stained around where the corrosion has occurred.

Scanning Electron Microscope (SEM)

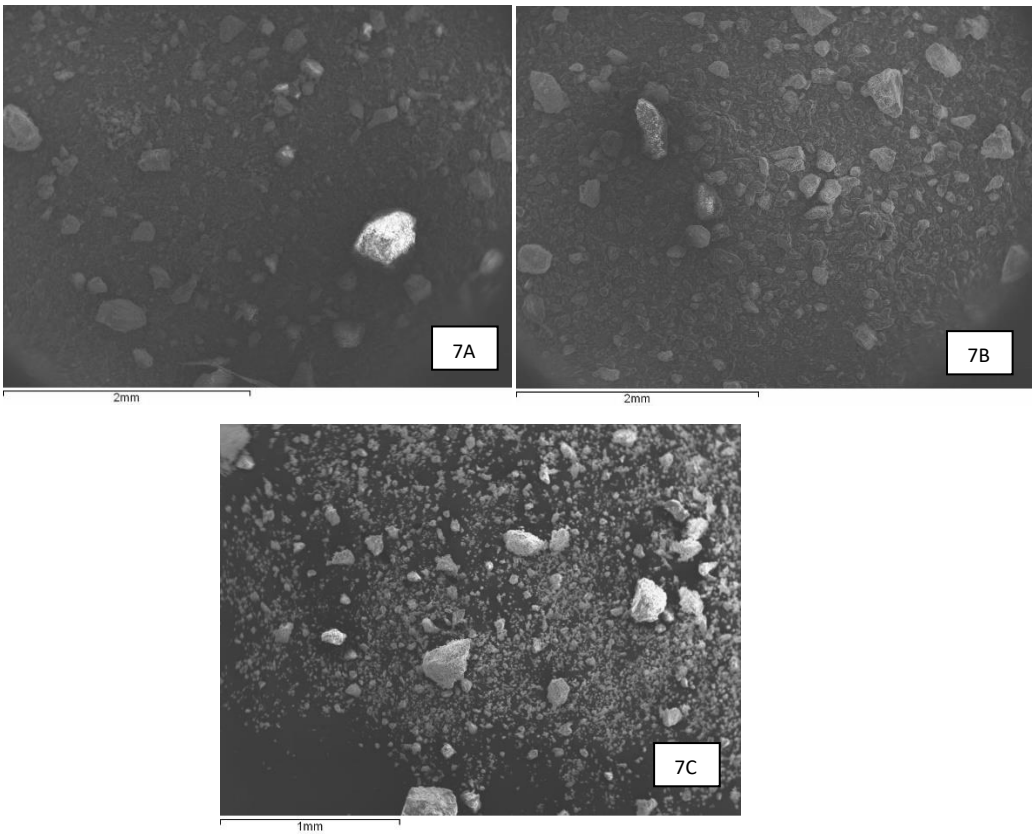

Figure 34. SEM analysis of sample site 7.

Figure 34 shows the SEM images for sample site 7. The EDX detected the following elements in all the samples: carbon, silicon, chlorine, manganese, calcium, sulfur, titanium, iron, zinc, sodium and magnesium, Sample 7A also contained cerium, barium, potassium, phosphorus and aluminium. Sample 7B additionally contained barium and bromine while sample 7C also contained aluminium and potassium.

Raman

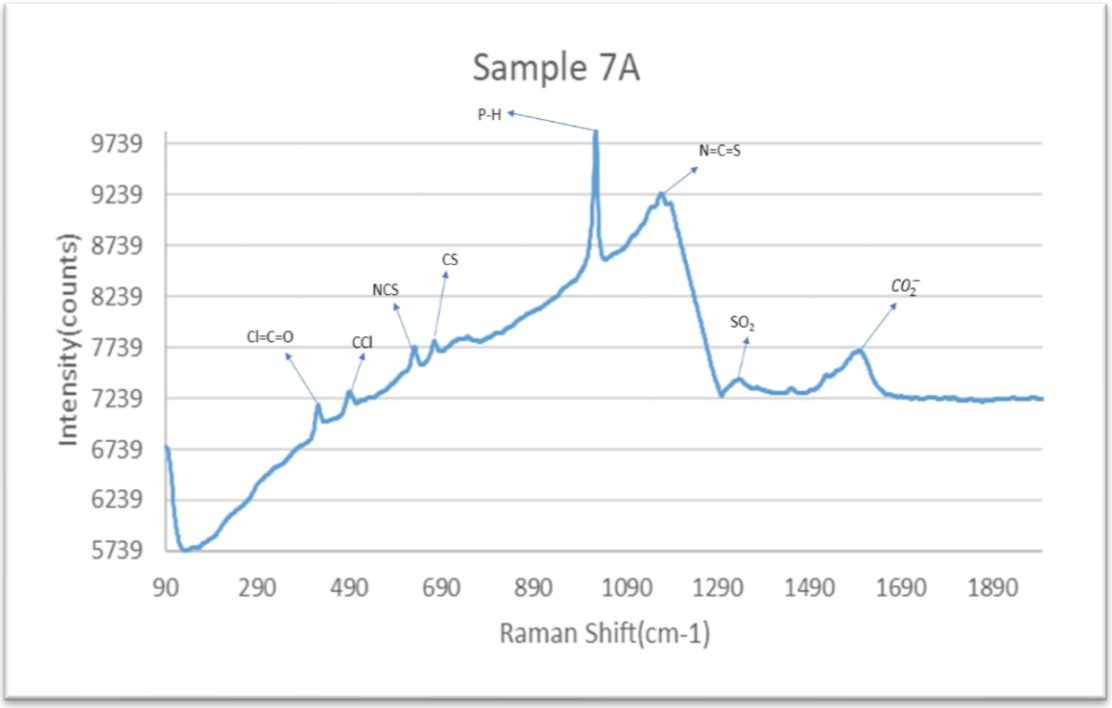
Sample 7A
P-H
N=C=S
CS
NCS
Cl=C=O
CCl
SO2
CO2-
Intensity(counts)
9739
9239
8739
8239
7739
7239
6739
6239
5739
90
290
490
690
890
1090
1290
1490
1690
1890
Raman Shift(cm-1)

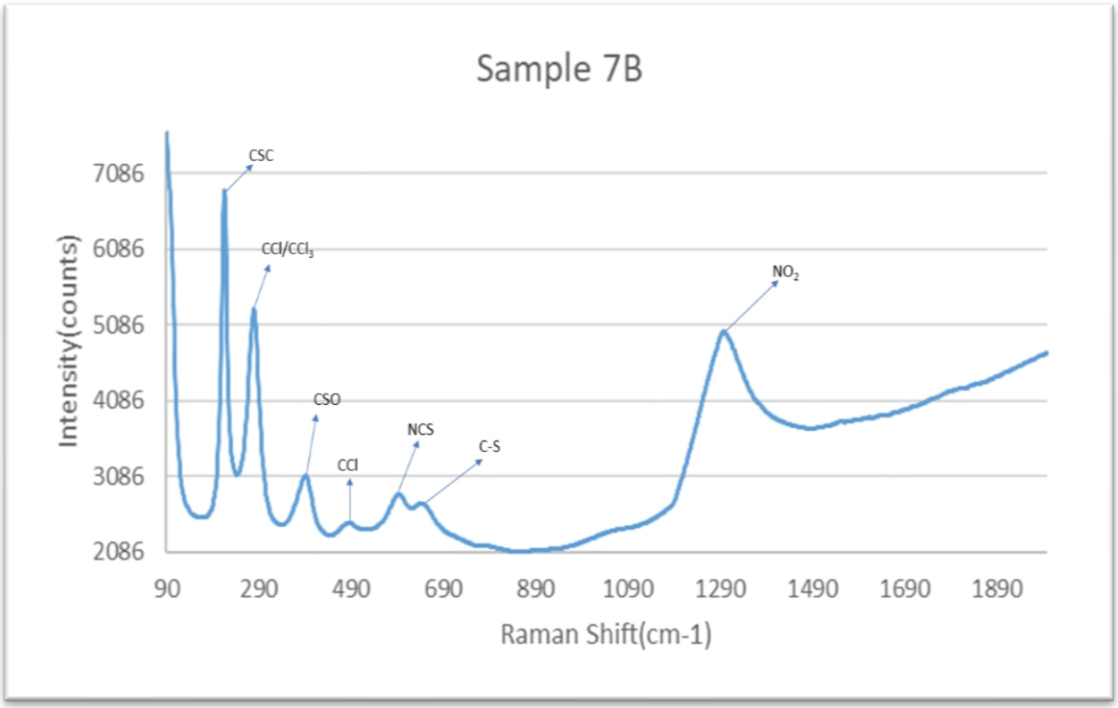
Sample 7B
CSC
CCl/CCl3
NO2
CSO
NCS
C-S
CCl
Intensity(counts)
7086
6086
5086
4086
3086
2086
90
290
490
690
890
1090
1290
1490
1690
1890
Raman Shift(cm-1)

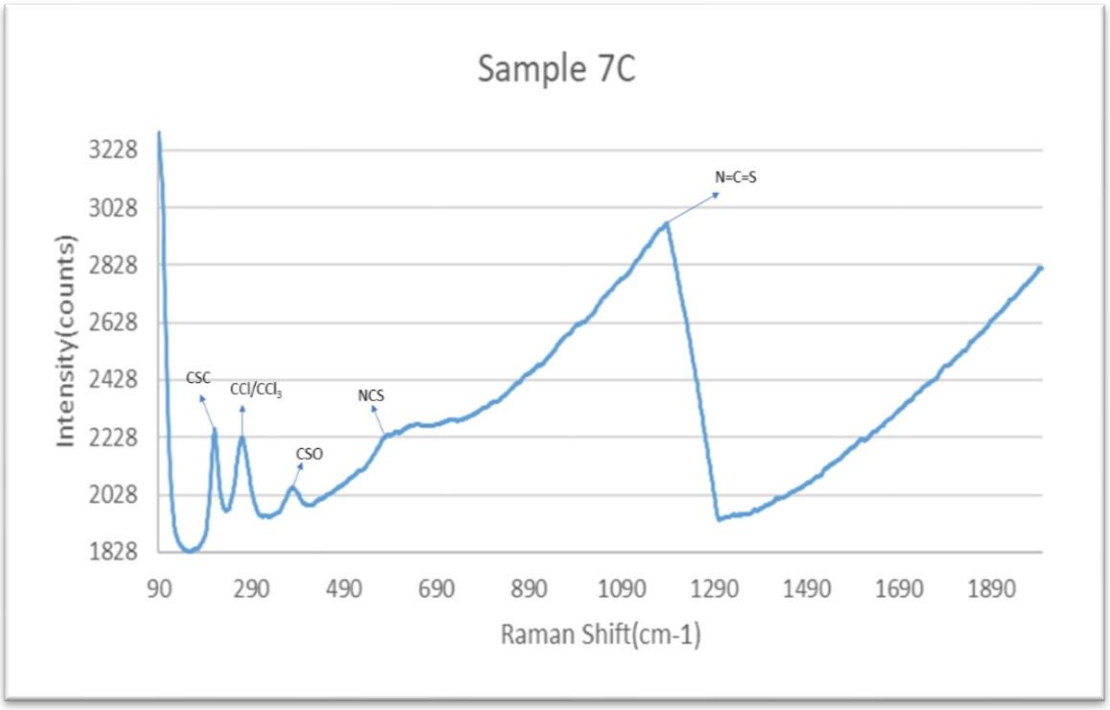

Figure 35. Raman analysis of samples from sample site 7.

Figure 35 shows the Raman spectrum for the samples from sample site 7. Samples 7B and 7C have spectrum, which have already been previously discussed containing compounds that are made up of mainly carbon, sulfur, nitrogen and chlorine. Sample 7A is the different spectrum for this sample site containing: aliphatic acid chlorides(Cl=C=O) at 423cm^{-1}, aliphatic chloroformates(CCl) at 491cm^{-1}, tertiary thioamides(NCS) at 584cm^{-1}, aliphatic sulfides and disulfides (C-S) at 676cm^{-1}, phosphorus to hydrogen bonding (P-H) at 1025cm^{-1}, isothiocyanates(N=C=S) at ~1188cm^{-1}, methyl sulphones (SO_2) at ~1290cm^{-1} and lastly aromatic acid salts (CO_2^-) at ~1550cm^{-1}.

The sharpest peak in sample 7A is the phosphorus to hydrogen bond, which has not been seen in other sample site containing phosphorus. Another new peak was at ~1550cm^{-1}, which has been identified as being aromatic acid salts. This is evidence that there is a corrosive environment and that carbon is helping with the deposition as aromaticity is usually from benzene ring made up of carbon.

pH and Conductivity

Sample Site	Sample	pH	Conductivity(μS)
7	A	7.55	254
	B	8.59	322
	C	7.57	423

Table 17. The pH and conductivity of samples from sample site 7.

Sample site 7 is slightly basic like sample site 6 as illustrated in **Table 17**. The conductivity is also very high like sample site 6. In fact, it is higher, the more basic the pH the higher the conductivity of the sample site. This is most likely because of the basic compounds, the formation of salts and presence of amine compounds as the Raman above has illustrated.

X-Ray Diffraction (XRD)

Sample 7A	Sample 7B	Sample 7C
Iron Oxide	Iron Silicate Oxide	Iron Oxide
Sodium Propanoate	Sodium Carbonate Sulfate	Iron Titanium Oxide
Sodium Phosphide	Magnesium Carbonate	Iron Sulfide
Sodium Zinc Silicate	Calcium Chlorate	Potassium Hydrogen Tartrate
Magnesium Sulfate	Calcium Carbonate	Sodium Chlorate
Calcium Hydroxide Phosphate	Calcium Silicate	Sodium Iron Oxide
Calcium Magnesium	Silicon Oxide	Magnesium Titanium Sulfate
Calcium Phosphate	Zinc Oxide	Magnesium Carbonate
Calcium Iron Oxide	Zinc Oxide Sulfate	Calcium Nitrate
Calcium Carbonate	Manganese Sulfate	Calcium Magnesium Silicate
Zinc Silicate	Titanium Oxide	Zinc Titanium Oxide
Zinc Sulfate	Barium Titanium Oxide	Zinc Oxide Sulfate
Aluminum Phosphate	Barium Bromide	Aluminum Oxide Carbide
Manganese Sulfide	Barium Manganese Silicate	Titanium Oxide
Manganese Oxide	Barium Oxide	Cerium Sulfide
Titanium Oxide	Barium Silicate	Ammonium Nitrate
Barium Sulfate	Barium Sulfide	Hydrogen Sulfate
Cerium Iron	Ammonium Thiocyanate	Heptadecylcyclohexane
Cerium Chlorate Hydrate	Urea	
Carbon Sulfide		

Table 18.XRD analysis of samples from sample site 7.

In **Table 18** all the samples contain at least one iron corrosion product from the steel structure. There is very little in terms of salts and mineral compounds. There is, however, a lot of zinc salts in the form of zinc sulphate.

There are a few compounds from the alloy but not as many as sample site 6, instead there are more heavier element corrosion products present. These are in the form of barium and cerium.

Sample 7A contains a carbon compound, which has come from the particulate matter on the underside of the bridge reacting with the sulfur oxides produced from car fumes. Sample 7B contains urea and ammonium thiocyanate, the urea is probably from birds and the ammonium thiocyanate has come from nitrogen oxides. Sample 7C has got an ion of sulfuric acid in the form of hydrogen sulphate and heptadecylcyclohexane, which is a long chain hydrocarbon.

3.2.4:Sample Site 8

Sample site 8 is located on the main road side of the security gate as shown in **Figure 14**.

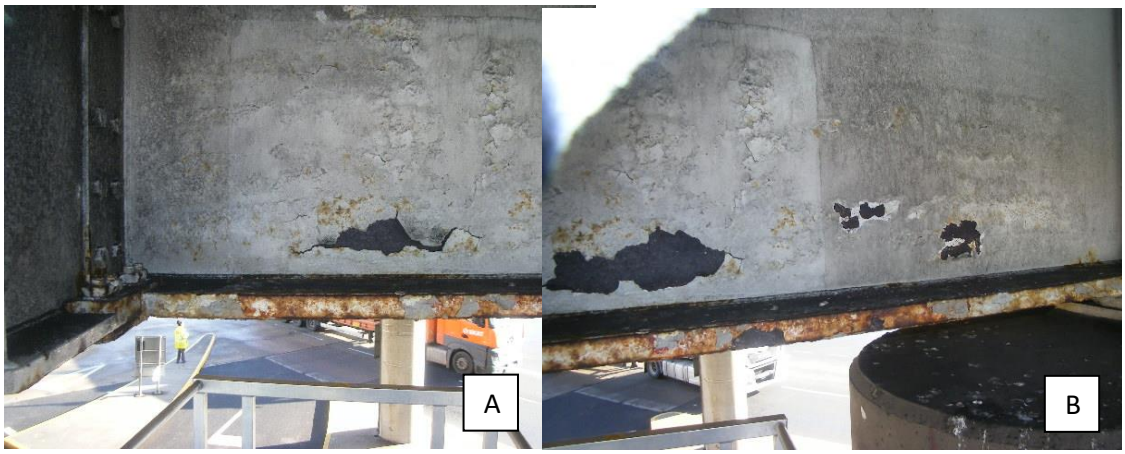

Figure 36. Before(A) and after(B) sampling of sample site 8.

The corrosion of sample site 8 is not severe like sample site 7, the coating is still intact and hanging from the metal. This would suggest that the types of corrosion are intergranular and filiform, with the possibility of it being cracking corrosion as the cracks are obvious in picture A and B of **Figure 36**. Uniform corrosion is also present happening to the metal underneath the coating.

Scanning Electron Microscope (SEM)

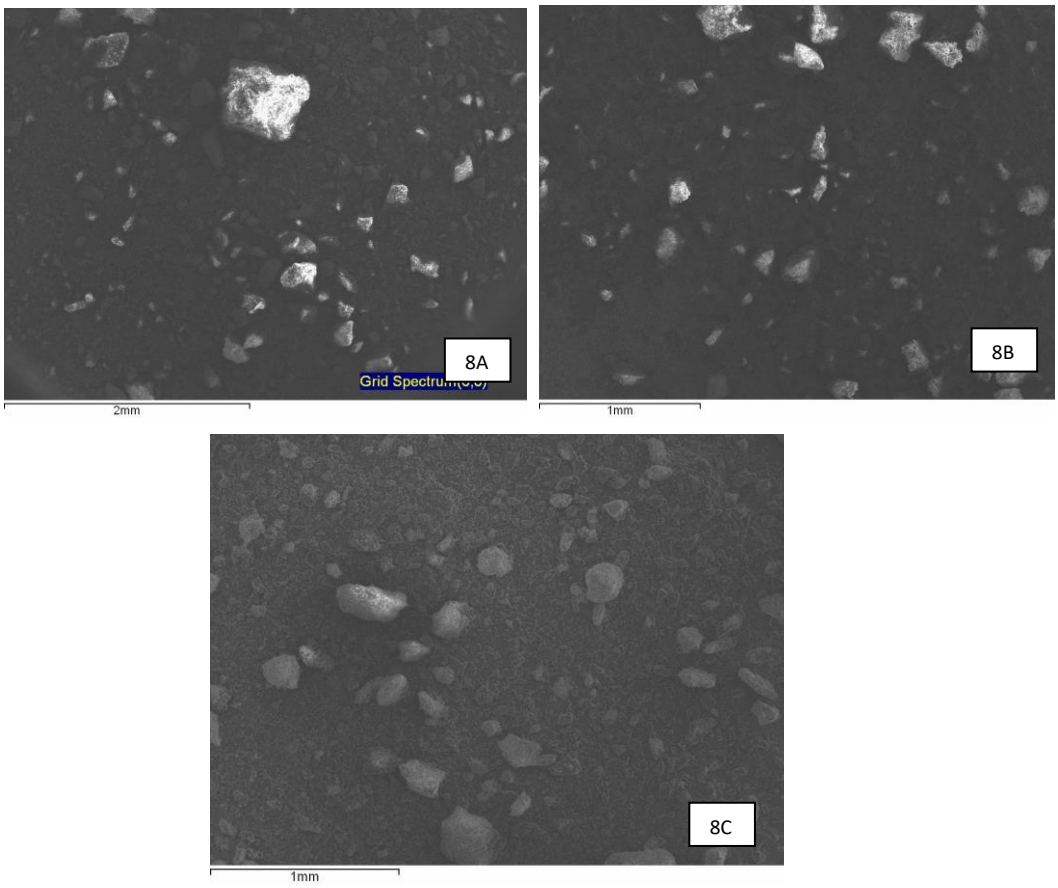

Figure 37. SEM analysis of samples from sample site 8.

Figure 37 shows the SEM images for sample site 8. Compounds detected by the EDX for sample site 8 where: chlorine, aluminium, carbon, silicon, calcium, sulfur, titanium, zinc, iron, cerium, sodium and magnesium. Sample 8A also contained barium, bromine, phosphorus and europium. Sample 8B additionally contained barium, phosphorus, rubidium, potassium and bromine. Sample 8C also contained potassium.

Raman

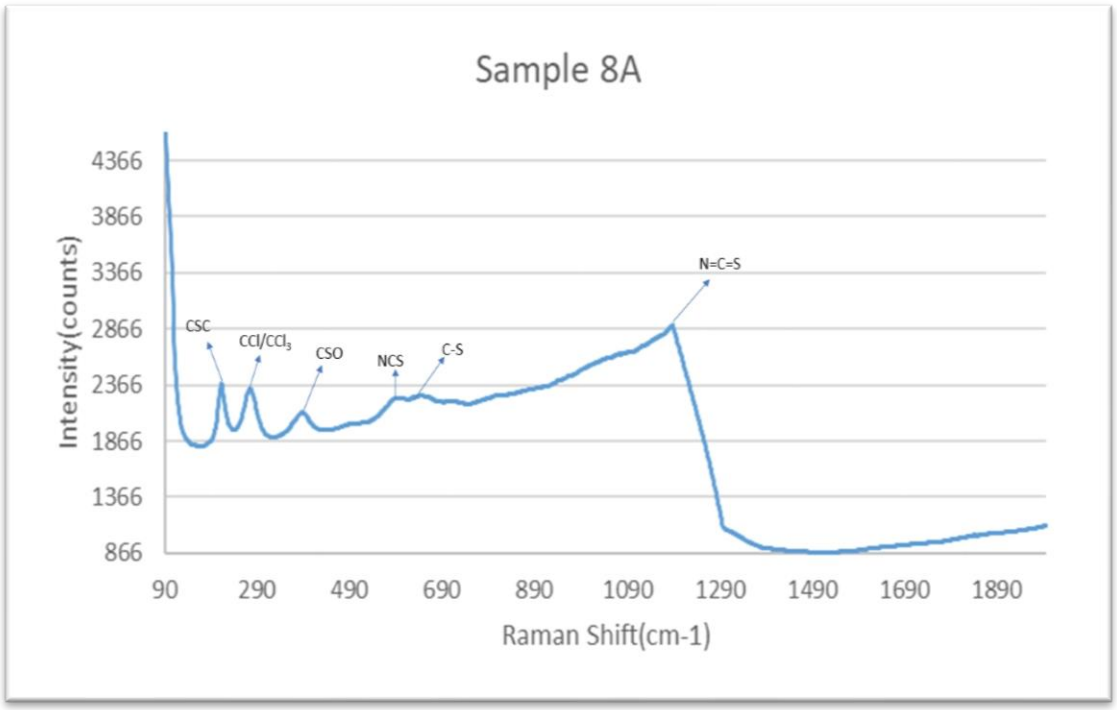
Sample 8A
Intensity(counts)
4366
3866
3366
2866
2366
1866
1366
866
CSC
CCl/CCl3
CSO
NCS
C-S
N=C=S
90
290
490
690
890
1090
1290
1490
1690
1890
Raman Shift(cm-1)

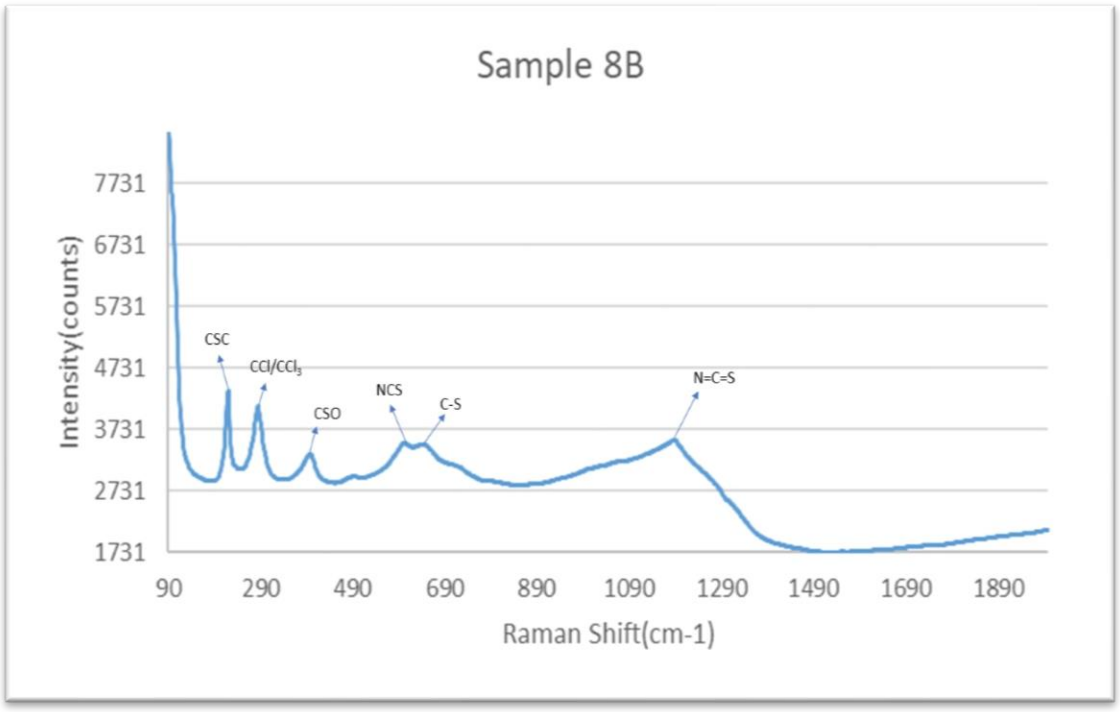
Sample 8B
Intensity(counts)
7731
6731
5731
4731
3731
2731
1731
CSC
CCl/CCl3
CSO
NCS
C-S
N=C=S
90
290
490
690
890
1090
1290
1490
1690
1890
Raman Shift(cm-1)

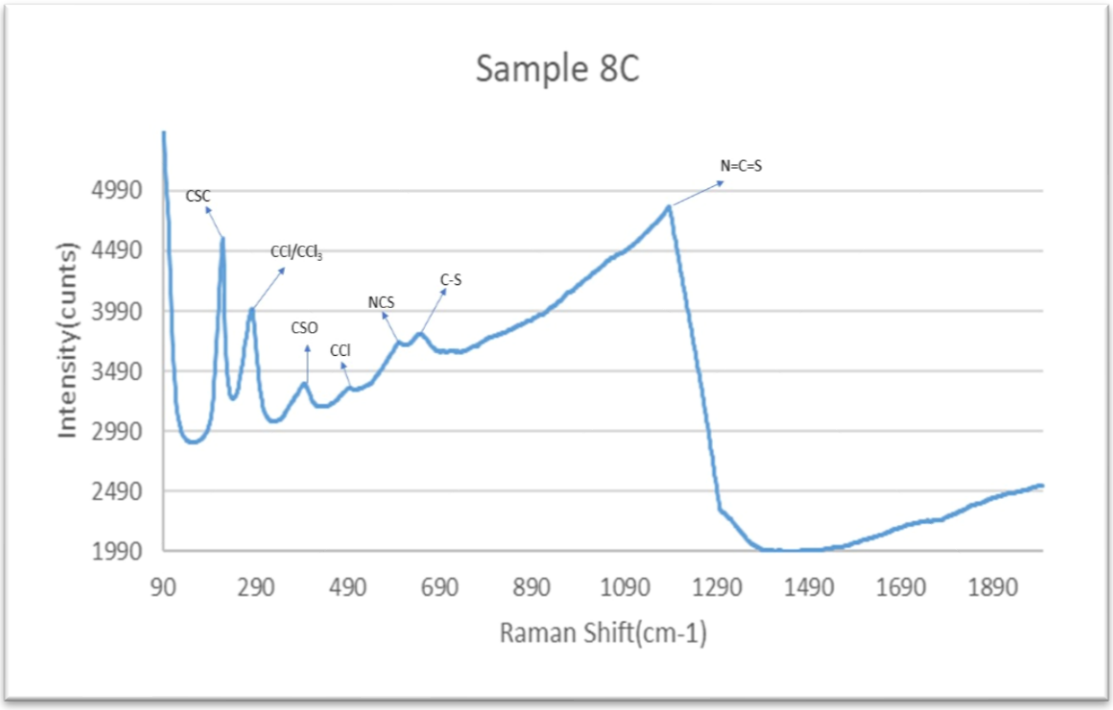

Figure 38. Raman analysis of samples from sample site 8.

All the samples for sample site 8 have been identified to have the same compounds present as shown in **Figure 38**. The only differences between the spectrum, is the presence of aliphatic chloroformates (CCl) at ~490cm^{-1} in sample 8C and that sample 8B has got a lot less fluorescence than the other two samples for sample site 8.

pH and Conductivity

Sample Site	Sample	pH	Conductivity(µS)
8	A	7.28	188
	B	7.26	382
	C	9.2	191

Table 19. the pH and conductivity of samples from sample site 8.

Table 19 shows this sample site is like samples sites 6 and 7 in being slightly basic (pH 7.3 to about pH 9). The samples do have a lower conductivity than the other high pH sample site in area 2 however, the conductivity is greater than that of any of the acidic sample sites.

X-Ray Diffraction (XRD)

Sample 8A	Sample 8B	Sample 8C
Iron Oxide	Iron Oxide	Iron Oxide
Iron Phosphide	Iron Zinc	Potassium Cyanide
Iron Titanium Oxide	Iron Oxide Hydroxide	Potassium Nitrate
Magnesium Silicate	Potassium Sulfate	Potassium Sulfate
Magnesium Zinc	Potassium Carbonate	Potassium Aluminum Nitrate
Calcium Phosphate	Sodium Carbonate	Potassium Magnesium Sulfate
Calcium Bromate	Magnesium Silicate	Potassium Aluminum Silicate
Calcium Carbonate	Magnesium Carbonate	Sodium Chlorate
Calcium Magnesium Carbonate	Silicon Sulfide	Magnesium Silicate
Calcium Carbonate	Silicon Oxide	Magnesium Carbonate
Zinc Sulfate	Zinc Oxide	Silicon Oxide
Zinc Hydroxide	Aluminum Phosphate	Zinc Sulfate
Aluminum Cerium	Titanium Oxide	Zinc Carbonate
Manganese Phosphate	Barium Titanium Oxide	Zinc Sulfide
Titanium Oxide	Barium Sulfate	Zinc Oxide
Titanium Silicide	Barium Sulfate	Aluminum Silicate
Barium Sulfate	Ammonium Chloride	Titanium Oxide
Barium Sulfide	Carbon Sulfide	Ammonium Nitrate
Cerium Zinc	Rubidium Chloride	Hydrogen Sulfate
Cerium Iron Nitride		

Table 20. XRD analysis of samples from sample site 8.

All the samples shown in **Table 20**, contain iron oxide with other iron products from the steel structure. Samples 8B and 8C contain a lot of salt products. Sample 8A has the lowest conductivity and contains the most mineral compounds out of the three samples. There are also heavy element compounds present in sample 8A. Sample 8B shows a high content of salt compounds with very little alloy corrosion products. Sample 8B as well as sample 8A contains heavy element compounds, together with a carbon compound from the build-up of particulates. Sample 8B indicates the presence of an ammonium compound. Sample 8C has the most salt and zinc salt compounds out of the three samples, while also containing sulfuric acid ions and ammonium salt from neutralising nitric acid. The rubidium in sample 8B most likely comes from fuel or lubricant.

3.2.5:Sample Site 9

Sample site 9 is close to sample site 8 near the main road as shown in **Figure 14**.

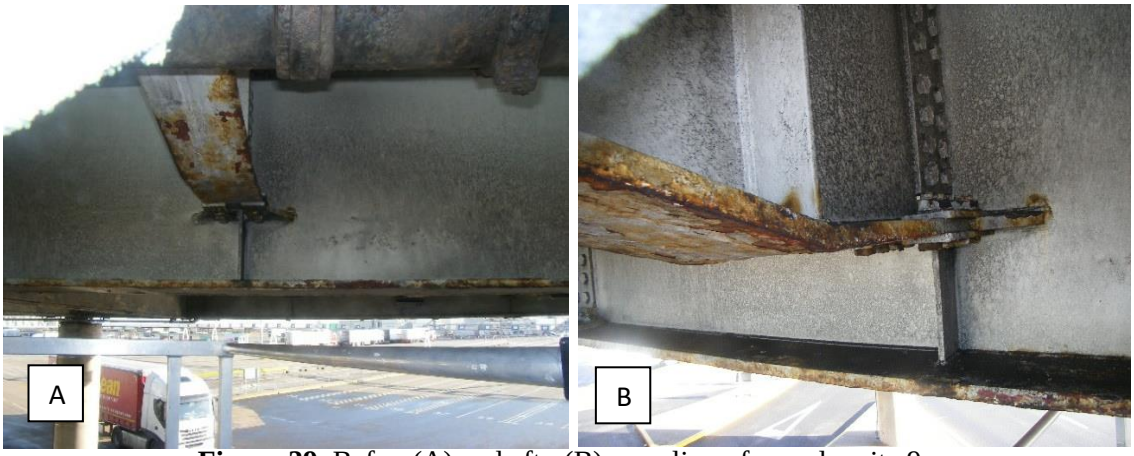

Figure 39. Before(A) and after(B) sampling of samples site 9.

The extent of corrosion at sample site 9 is not very severe, however, it just looks “filthy” from deposited pollution as seen in **Figure 39**. The types of corrosion observed at this site where: dezincification, intergranular and uniform corrosion. Dezincification leaves a coppery sheen as seen in picture A above, **Figure 39** A also displays the extent of the particulates deposited on the bridge by atmospheric pollution.

Scanning Electron Microscope (SEM)

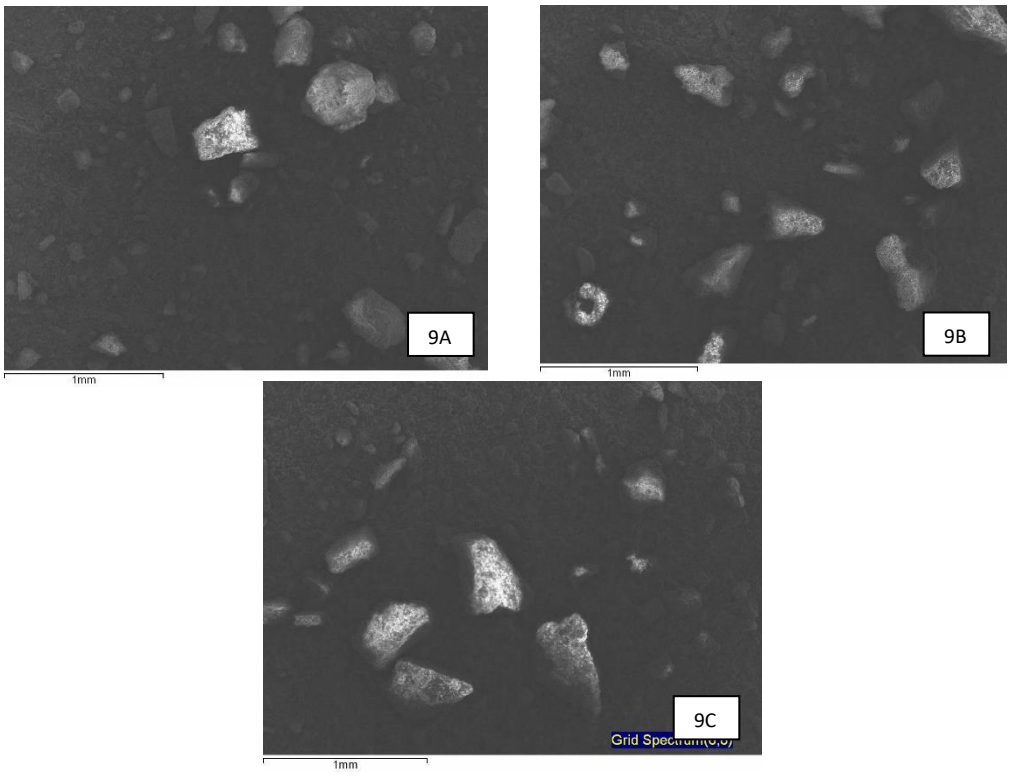

Figure 40. SEM analysis of samples from sample site 9.

The SEM images are shown in **Figure 40**, the following elements where detected: carbon, sulfur, titanium, manganese, chlorine, iron, phosphorus, calcium, zinc, aluminium, magnesium, sodium, silicon. Sample 9A also contained bromine, arsenic and barium. Sample 9B additionally contained cerium and barium, Sample 9C also contained cerium and potassium.

Raman

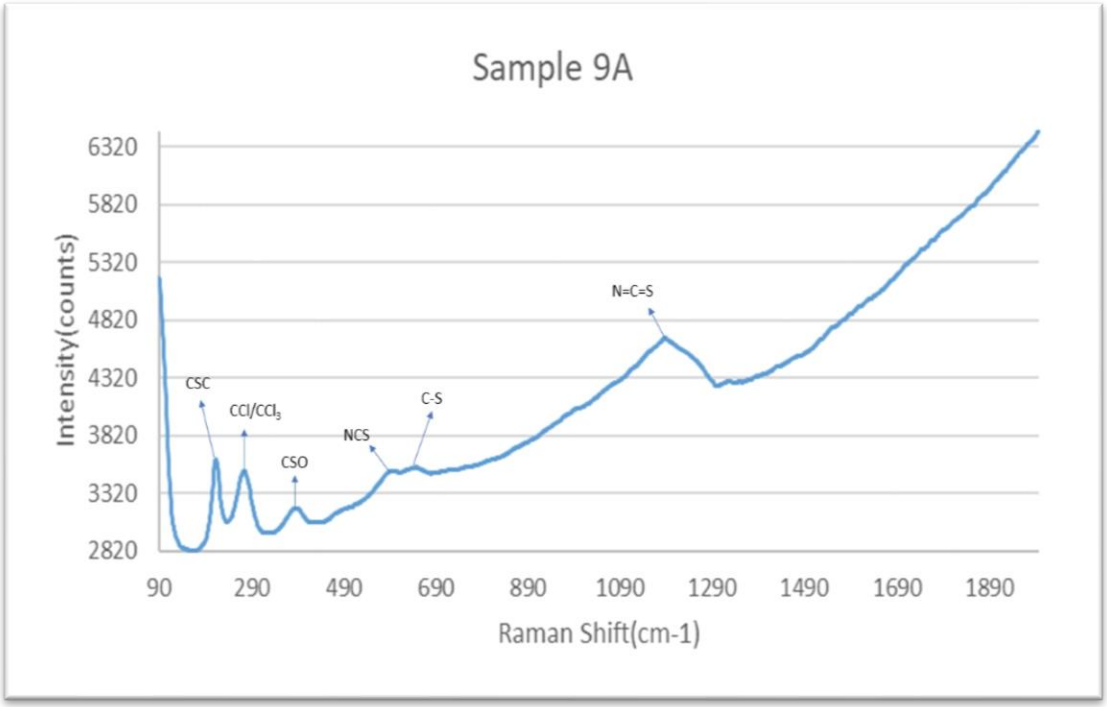
Sample 9A
Intensity(counts)
6320
5820
5320
4820
4320
3820
3320
2820
CSC
CCl/CCl3
CSO
NCS
C-S
N=C=S
90
290
490
690
890
1090
1290
1490
1690
1890
Raman Shift(cm-1)

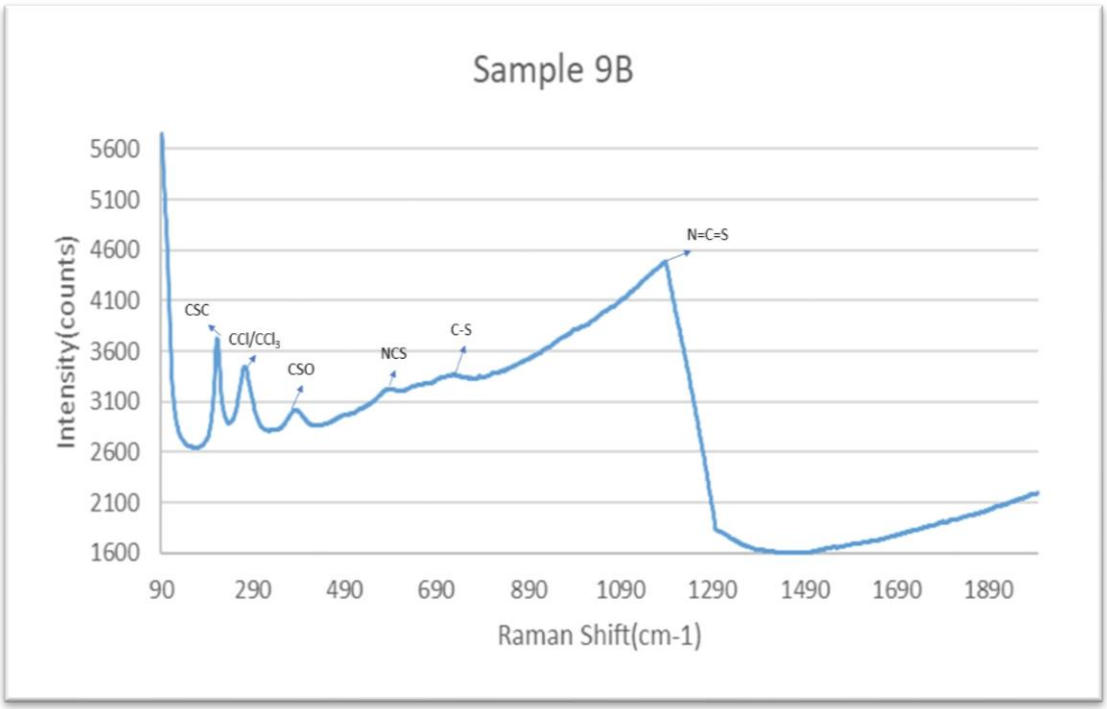
Sample 9B
Intensity(counts)
5600
5100
4600
4100
3600
3100
2600
2100
1600
CSC
CCl/CCl3
CSO
NCS
C-S
N=C=S
90
290
490
690
890
1090
1290
1490
1690
1890
Raman Shift(cm-1)

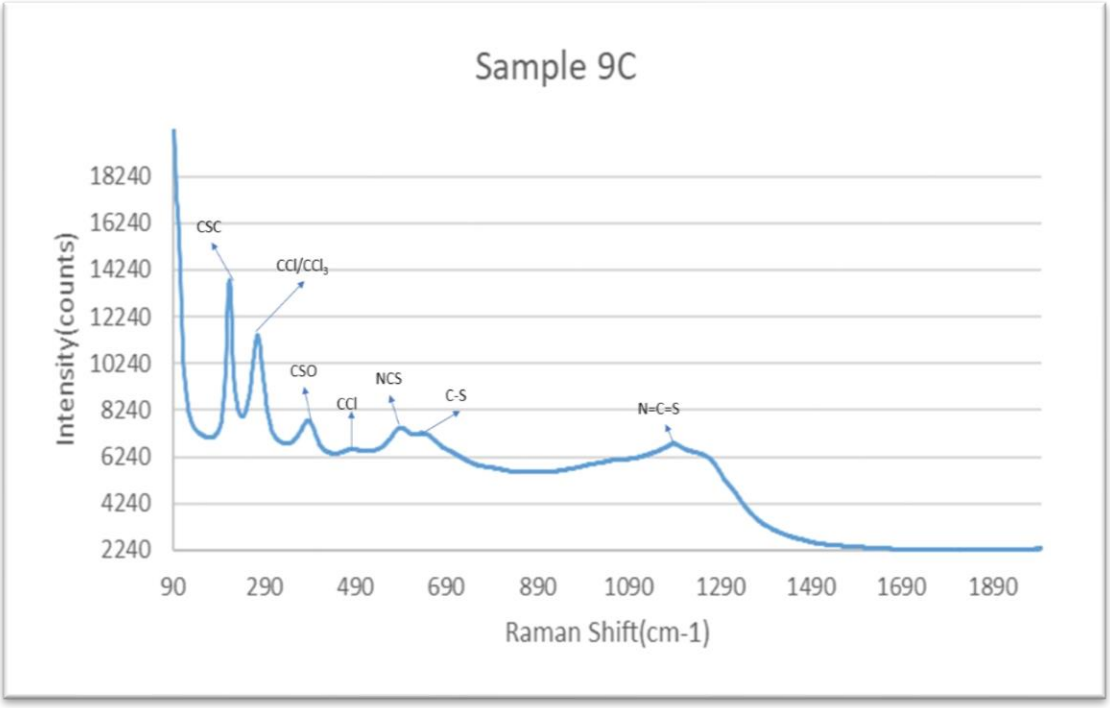

Figure 41. Raman analysis of samples from sample site 9.

The Raman spectra shown in **Figure 41**, are very similar to those recorded for sample site 8, where sample 9C contains the additional peak at ~490cm^{-1} for aliphatic chloroformates (CCl). Sample 9C demonstrated little fluorescence interference when compared to the other samples of sample site 9, which explains why that extra peak was able to be identified.

pH and Conductivity

Sample Site	Sample	pH	Conductivity(µS)
9	A	6.72	1338
	B	8.04	319
	C	9.24	556

Table 21. The pH and conductivity of samples from sample site 9.

Table 21 has a variation pH and conductivity for the samples at sample site 9. Sample 9A is acidic and has the highest conductivity out of all the samples. This might be explained from the place sample 9A was taken from. Sample 9A was taken from the lower shelf seen in picture B, in **Figure 39**, which is very clearly a different environment from the beam raised slightly above.

This also disproves that only the samples with a basic pH had the high conductivity, linking the conductivity with the corrosion rate suggests that the rate of corrosion in sample 9A is almost three times greater than its other samples.

X-Ray Diffraction (XRD)

Sample 9A	Sample 9B	Sample 9C
Iron tris(1,10-phenanthroline mono-N-oxide) perchlorate	Iron Oxide Hydrate	Iron Phosphate
Iron Aluminum Silicate	Iron Sulfate	Iron Titanium Oxide
Iron Sulfate	Iron Oxide	Iron Oxide Hydroxide
Sodium Sulfate	Magnesium Oxide	Iron Oxide
Magnesium Phosphate	Magnesium Sulfate	Iron Zinc
Calcium Sulfite	Calcium Silicate	Potassium Chlorate
Calcium Phosphate	Calcium Carbonate	Sodium Phosphate
Silicon Carbide	Calcium Nitride	Sodium Phosphide
Zinc Phosphate	Silicon Oxide	Calcium Carbonate
Zinc Sulfate Oxide	Zinc Hydroxide	Calcium Silicate
Zinc Silicate	Zinc Phosphate	Silicon Carbide
Manganese Arsenate	Aluminum Phosphate	Zinc Sulfate Hydroxide
Titanium Oxide	Aluminum Oxide	Zinc Oxide
Barium Chloride	Aluminum Manganese	Aluminum Iron Silicide
Barium Silicate	Manganese Oxide	Aluminum Oxide Hydroxide
Barium Titanium Oxide	Titanium Oxide	Manganese Oxide
Bromine Bromate	Barium Sulfate	Titanium Sulfide
Ammonium Nitrate	Barium Sulfide	Cerium Iron
Sulfuric Acid	Ammonium Chloride	
	Phosphorus Oxide	

Table 22. XRD analysis of samples from sample site 9.

From **Table 22** it can be seen that all samples contain iron corrosion products. There are more compounds present in sample 9C. The samples also contain salts and zinc salts. Sample 9A contains the most corrosion products that have heavy elements present, mainly barium compounds. In addition, sample 9A indicates the presence of ammonium salt and sulphates. Sample 9B contains much of the same with more alloy corrosion products than sample 9A, sample 9C is very similar in that respect. With sample 9B having more heavy element corrosion products than sample 9C. Sample 9C has the most corrosion products that come from the steel alloy.

The main difference is that sample 9A has no nitrogen compounds in any of the corrosion products detected by the XRD, despite having the peaks in the Raman spectra above. All of sample 9A's corrosion products are either oxides or from acidic reactants. This would explain the drastic difference in pH and possibly the difference in conductivity.

3.3:Area 3

3.3.1:Sample Site 10

Sample site 10 is located above ground level where the ramp joins the bridge as seen in **Figure 14**.

Figure 42. Before(A) and after(B) sampling from sample site 10.

As seen in **Figure 42** the corrosion at sample site 10 is not severe and is similar to what has been observed from other sample sites. There are obvious raised parts of the coating resulting in cracks in the paint as seen in picture A above. The types of corrosion that can be seen are: filiform, intergranular and uniform. The sample site is very discoloured from atmospheric pollution, the same as the other sample sites.

Scanning Electron Microscope (SEM)

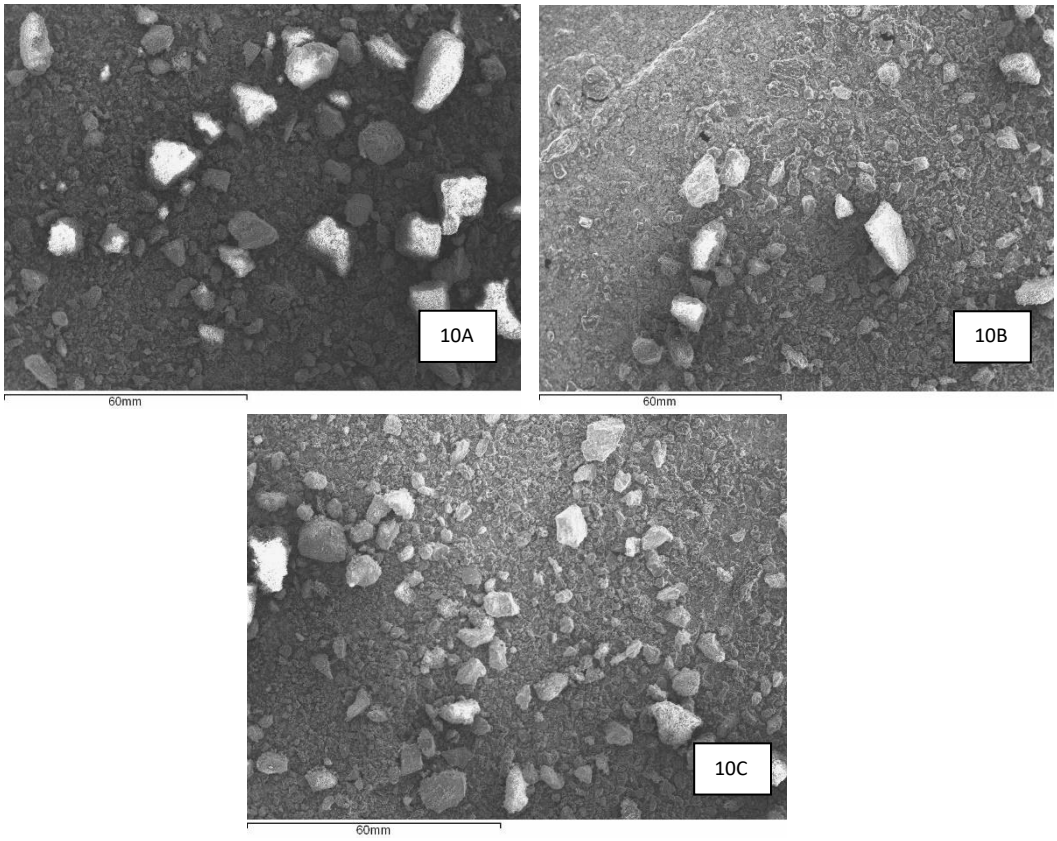

Figure 43. SEM analysis of samples from sample site 10.

The SEM images can be seen in **Figure 43**. The EDX detected the following elements that where seen in all the samples: chlorine, silicon, sulfur, manganese, cadmium, titanium, fluorine, calcium, sodium, zinc, iron, aluminium, carbon, potassium and magnesium. Samples 9A and 9B also contained phosphorus.

Raman

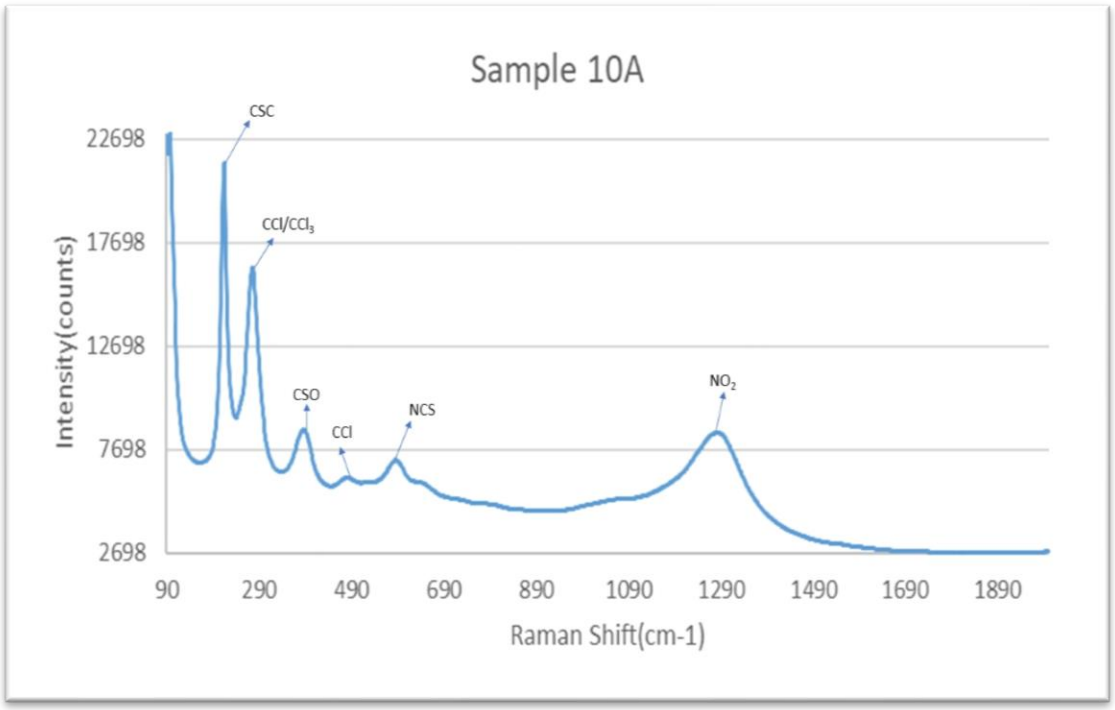
Sample 10A
CSC
CCl/CCl3
CSO
CCl
NCS
NO2
Intensity(counts)
22698
17698
12698
7698
2698
90
290
490
690
890
1090
1290
1490
1690
1890
Raman Shift(cm-1)

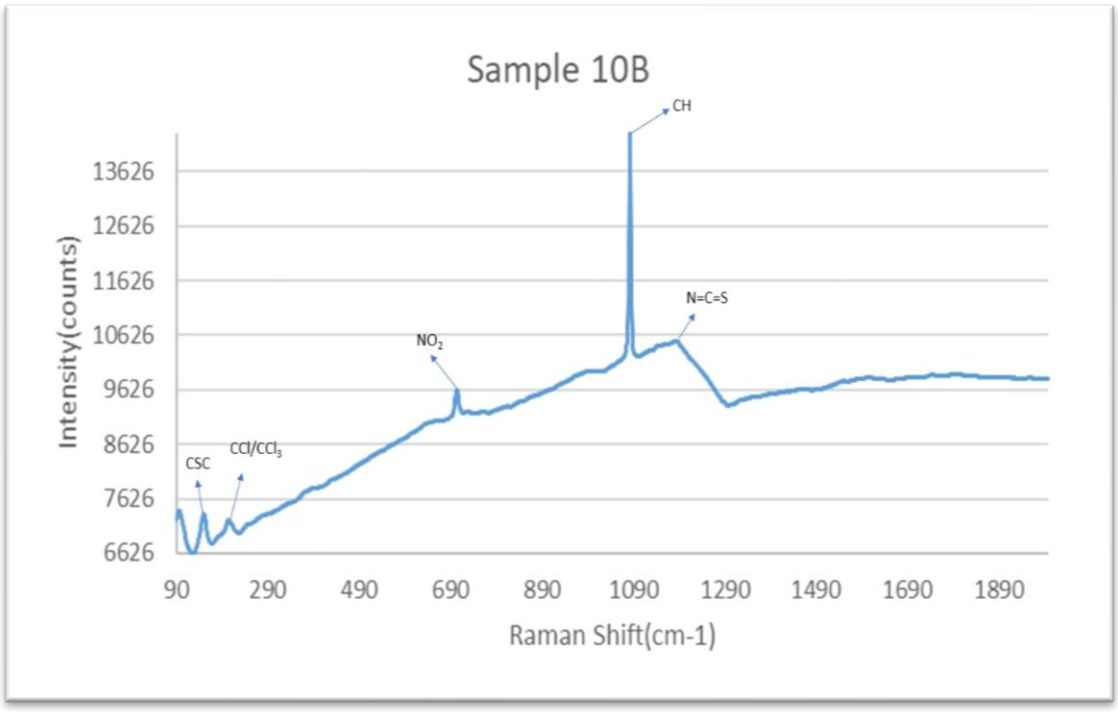
Sample 10B
CH
N=C=S
NO2
CCl/CCl3
CSC
Intensity(counts)
13626
12626
11626
10626
9626
8626
7626
6626
90
290
490
690
890
1090
1290
1490
1690
1890
Raman Shift(cm-1)

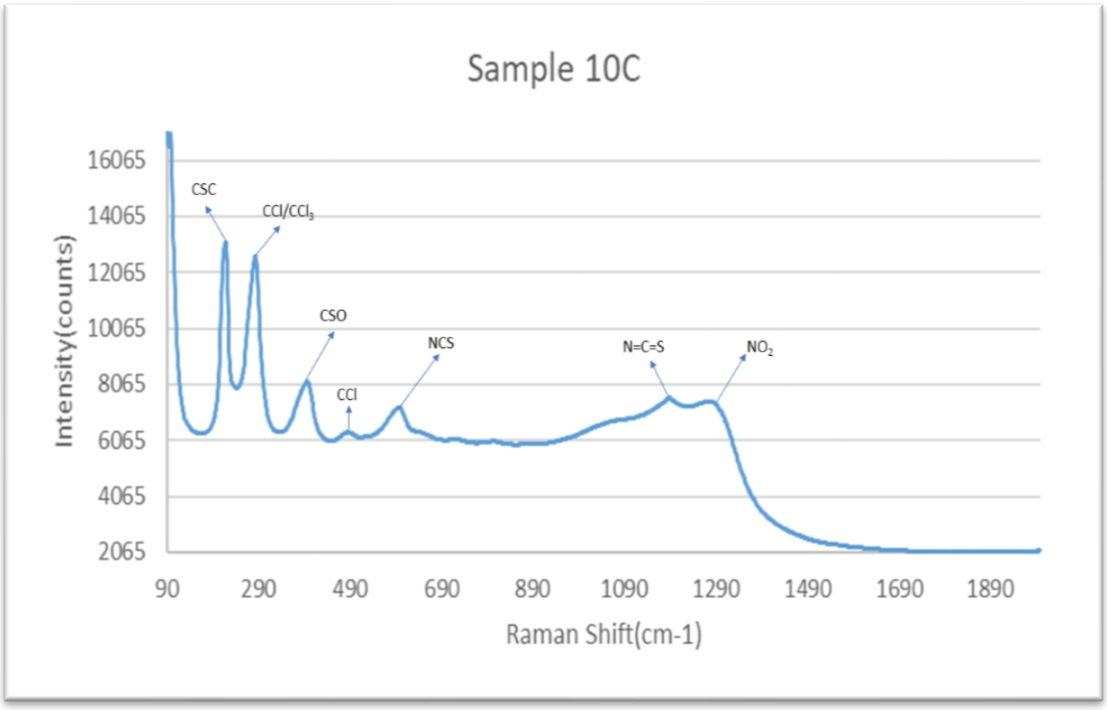

Figure 44. Raman analysis of samples from sample site 10.

Samples 10A and 10C have similar Raman spectra (**Figure 44**) with sample 10C having the additional peak at ~1188cm^{-1} of isothiocyanates (N=C=S) close to the peak at ~1270cm^{-1} nitroamines (NO_2). Both spectra have low fluorescence interference as seen in **Figure 44**.

Sample 10B is a very different spectrum, the differences from the other spectrums are: a peak at a ~700cm^{-1} identified as being nitrates (NO_2) and another peak at ~1000cm^{-1} mono-substituted and para-substituted benzene rings (CH).

pH and Conductivity

Sample Site	Sample	pH	Conductivity(µS)
10	A	9.85	427
	B	9.25	65
	C	9.85	201

Table 23. The pH and conductivity of samples from sample site 10.

All the samples from sample site 10 have a basic pH between 9-10. But there are differences in conductivity. Sample 9A and sample 9C have quite high conductivity when compared to sample 9B's low conductivity of 65µS.

X-Ray Diffraction (XRD)

Sample 10A	Sample 10B	Sample 10C
Iron Sulfide	Iron Phosphate	Iron Oxide
Iron Zinc	Iron Oxide	Iron Silicate
Iron Phosphate	Potassium Nitrate	Iron Oxide Hydroxide
Potassium Sulfate	Potassium Nitrite	Potassium Oxide
Sulfur Nitride	Potassium Aluminum Chloride	Potassium Nitrate
Magnesium Silicate	Potassium Sulfate	Potassium Carbonate
Magnesium Phosphate	Sodium Chlorate	Sodium Nitrate
Magnesium Fluoride Hydroxide	Sodium Chlorite	Sodium Potassium Cyanide
Calcium Carbonate	Sodium Iron Phosphate	Sodium Iron Oxide
Calcium Chloride	Magnesium Titanium Phosphate	Magnesium Carbide
Silicon Oxide	Calcium Silicate	Magnesium Carbonate
Zinc Oxide	Calcium Phosphide	Zinc Oxide
Zinc Hydroxide	Calcium Carbonate	Zinc Hydroxide
Aluminum Oxide	Silicon Carbide	Aluminum Carbide
Manganese Phosphate	Zinc Hydroxide	Manganese Carbide
Manganese Phosphide	Zinc Oxide Sulfate	Manganese Oxide
Titanium Sulfide	Manganese Phosphate	Titanium Fluoride
Titanium Oxide	Titanium Oxide	Titanium Oxide
Cadmium Sulfate	Cadmium Phosphide	Cadmium Nitrate
Cadmium Phosphate	Cadmium Sulfide	Ammonium Fluoride

Table 24. XRD analysis of samples from sample site 10.

All the samples have iron corrosion product as well as alloy corrosion products with sample 10B showing less compounds of both corrosion products. Instead sample 10B has the most mineral corrosion products. All samples contain salts and zinc salts. All samples also have heavier element corrosion products in the form of cadmium compounds, the exception being sample 10C that has an ammonium salt compound.

The loss of conductivity from sample 10B as seen above from **Table 24**, is associated with the mineral compounds present in the sample.

3.3.2:Sample Site 11

Sample site 11 has more corrosion than sample site 10 but is next to it as seen in **Figure 14**.

Figure 45. Before(A) and after(B) sampling of sample site 11.

The corrosion here is more severe than the other sample sites. The stained coating is just peeling away from the corroded metal, In **Figure 45A** there is some pitting in the exposed metal, the other types of corrosion are, filiform, intergranular and uniform. Pitting is a more serious type of corrosion as it burrows deep into the metal starting as a small hole to begin with.

Scanning Electron Microscope (SEM)

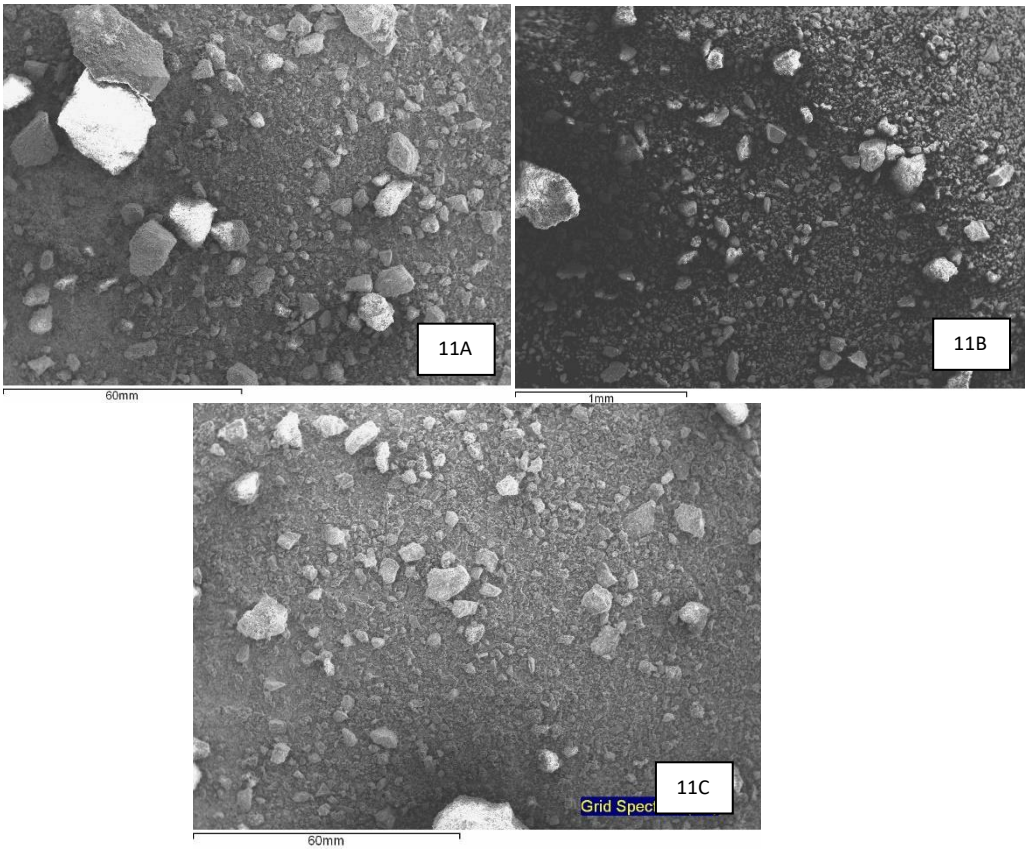

Figure 46. SEM analysis of samples from sample site 11.

All the samples in **Figure 46** contained the following elements: chlorine, sodium, calcium, titanium, iron, manganese, magnesium, zinc, silicon and sulfur. Sample 11A also contained fluorine, phosphorus and cadmium. Sample 11B additionally contains aluminium, potassium and cerium. Sample 11C also contained cadmium, fluorine, phosphorus, aluminium and potassium.

Raman

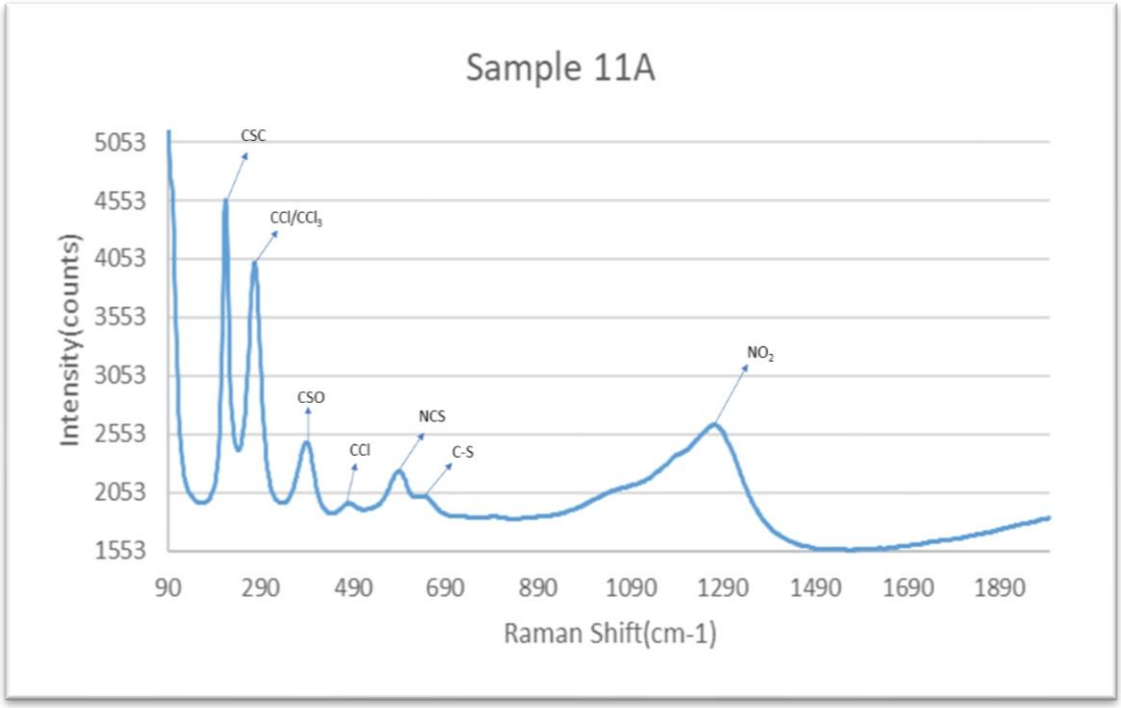
Sample 11A
Intensity(counts)
5053
4553
4053
3553
3053
2553
2053
1553
CSC
CCl/CCl3
CSO
CCl
NCS
C-S
NO2
90
290
490
690
890
1090
1290
1490
1690
1890
Raman Shift(cm-1)

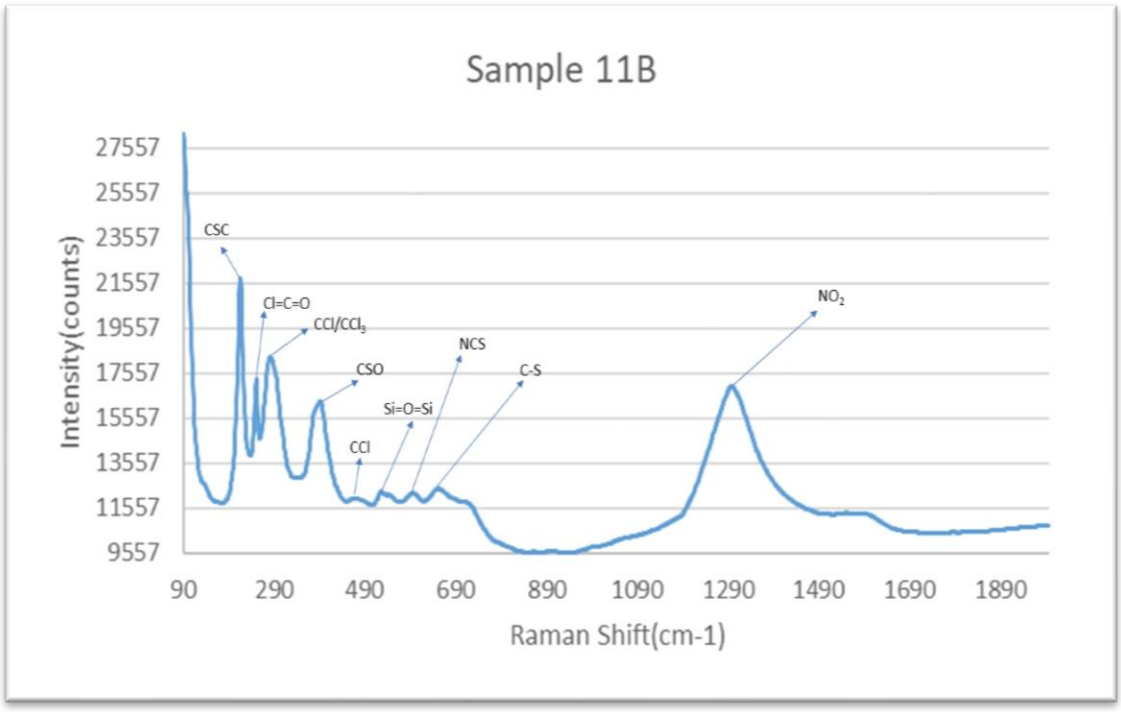
Sample 11B
Intensity(counts)
27557
25557
23557
21557
19557
17557
15557
13557
11557
9557
CSC
Cl=C=O
CCl/CCl3
CSO
CCl
Si=O=Si
NCS
C-S
NO2
90
290
490
690
890
1090
1290
1490
1690
1890
Raman Shift(cm-1)

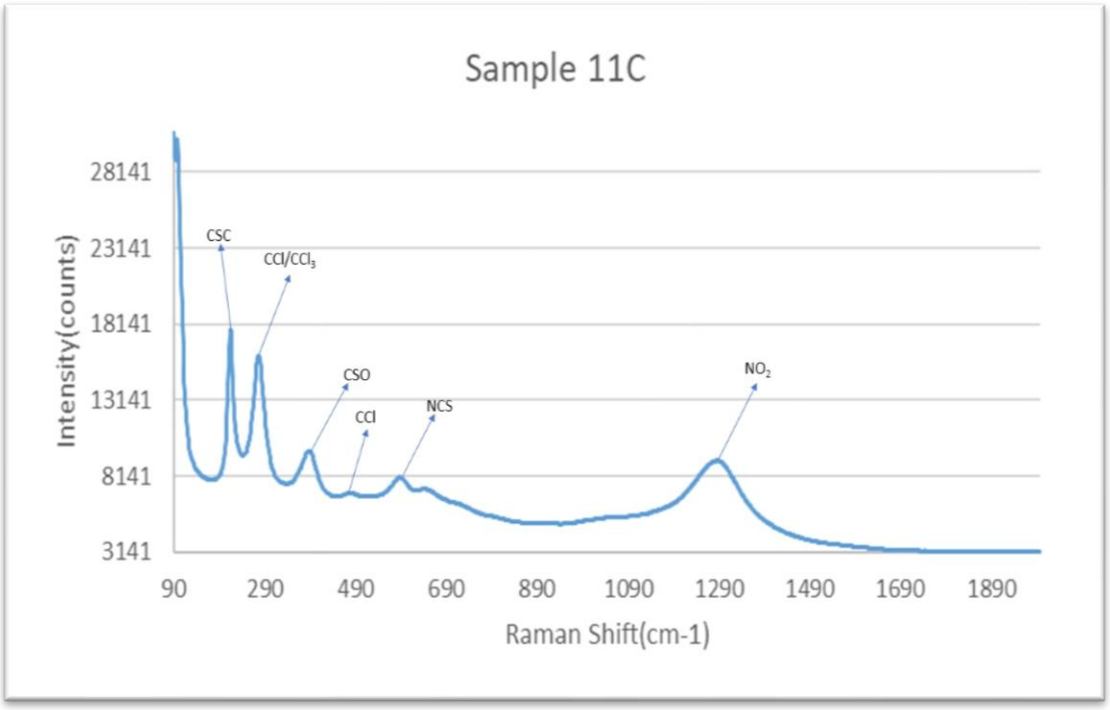

Figure 47. Raman analysis of samples from sample site 11.

The Raman spectra seen in **Figure 47**, are from the analysed samples taken from sample site 11, the spectra have low fluorescence interference. Spectrum for sample 11A and 11C are very similar with 11A containing an additional peak at ~650cm^{-1} of aliphatic sulfides and disulfides. Sample 11B contains more peaks than the other spectrum. The differences being: a peak at ~250cm^{-1} aliphatic acid chloride (Cl=C=O) and a peak at ~500cm^{-1}, which has been identified as silicon oxide (Si-O-Si).

pH and Conductivity

Sample Site	Sample	pH	Conductivity(µS)
11	A	6.58	766
	B	7.11	260
	C	7.26	388

Table 25. The pH and conductivity of samples from sample site 11.

Table 25 shows a neutral and slightly acidic sample site with high conductivity, the most conductive is Sample 11A, which is also the most acidic. This is very similar to sample 9A, which was very acidic and had a very high conductivity. This is different from area 1 which has acidic sample sites but poor conductivity.

X-Ray Diffraction (XRD)

Sample 11A	Sample 11B	Sample 11C
Iron Oxide Hydroxide	Potassium Calcium Phosphate	Iron Oxide Hydroxide
Iron Phosphate	Potassium Aluminum Silicate	Iron Phosphate
Iron Oxide	Magnesium Silicate	Iron Oxide
Iron Phosphide	Magnesium Zinc Phosphate	Potassium Sulfide
Magnesium Iron Silicate	Calcium Magnesium	Potassium Chlorate
Magnesium Carbonate	Calcium Silicate	Sodium Aluminum Silicate
Magnesium Silicate	Silicon Oxide	Sodium Magnesium Silicate
Calcium Phosphate Silicate	Aluminum Silicate	Sodium Chlorate
Calcium Carbonate	Aluminum Oxide	Magnesium Sulfate
Calcium Magnesium	Aluminum Silicon Carbide	Calcium Phosphate
Calcium Phosphate	Aluminum Potassium Silicate	Silicon Oxide
Zinc Sulfate Oxide	Aluminum Magnesium	Silicon Nitride
Zinc Manganese Oxide	Manganese Titanium	Zinc Manganese Oxide
Manganese Sulfide	Manganese Oxide	Aluminum Phosphate
Manganese Silicate	Titanium Oxide	Manganese Fluoride Phosphate
Titanium Oxide	Barium Iron Titanium Silicate	Titanium Oxide
Cadmium Cyanide	Barium Zinc Phosphate	Cadmium Phosphate
Cadmium Manganese Oxide	Cerium Silicide	Cadmium Phosphide
Cadmium Phosphate		Ammonium Fluoride
Ammonium Chloride		

Table 26. XRD analysis of samples from sample site 11.

In all the samples from sample site 11, corrosion products originating from the metals that make up the steel alloy where identified (**Table 26**). Sample 11B is the only sample that does not contain any iron corrosion products from the steel structure. Sample 11A does not have any sodium and potassium compounds compared to the other two samples from sample site 11. This is similar to sample 9A, which was also acidic with a high conductivity, it is possible that these salts reduce the conductivity.

3.4:Area 4

3.4.1:Sample Site 12

Sample site 12 is in a sheltered location form the sea but still gets run off from the bridge as shown in appendix 1 and **Figure 48** below.

Figure 48. Before(A) and after(B) sampling of sample site 12.

The corrosion at this sample site is not very severe and there is not a lot staining from atmospheric pollution when compared to the other sample sites. The types of corrosion that can be seen in **Figure 48** are: intergranular, filiform and uniform corrosion. Despite there being little to no staining, there is water run down from the top of the bridge, which is visible in picture A.

Scanning Electron Microscope (SEM)

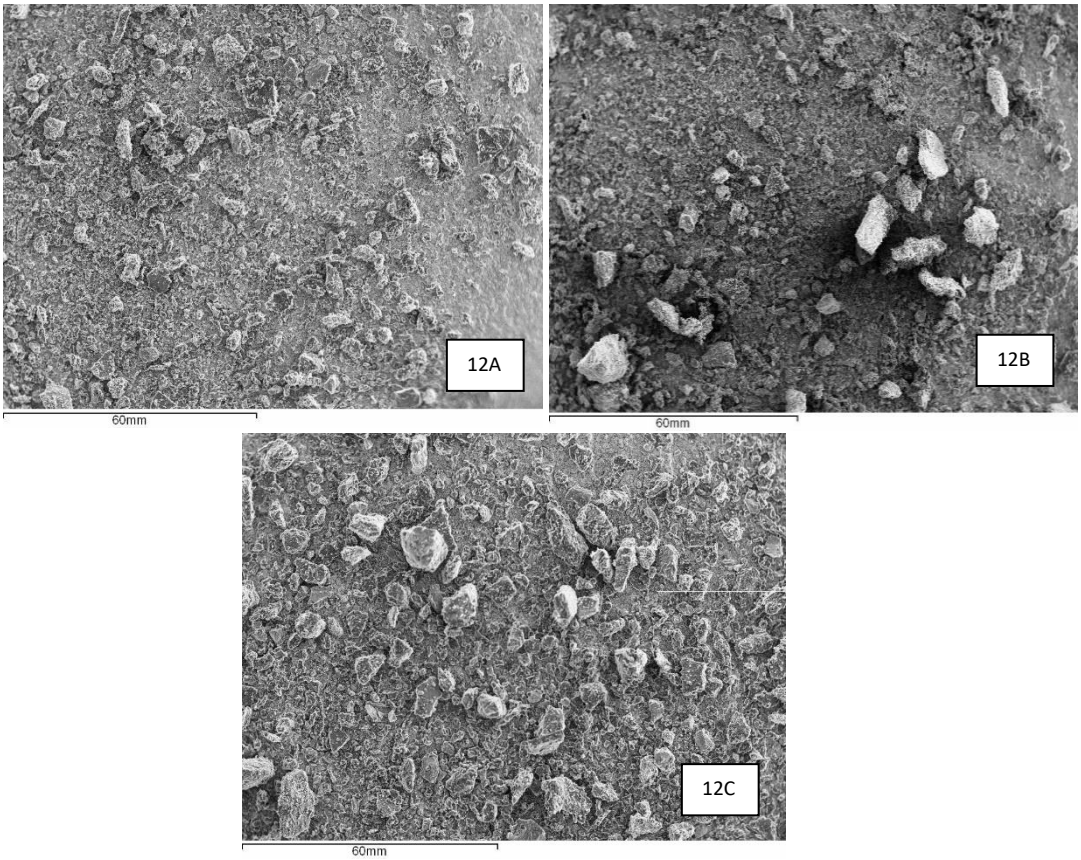

Figure 49. SEM analysis of samples from sample site 12.

Figure 49 shows the SEM images for sample site 12. The following elements where found in all the samples from samples site 10: carbon, iron, titanium, magnesium, silicon, sulfur, chlorine, fluorine, sodium, cadmium, calcium, zinc and phosphorus. Sample 12A also contained aluminium. Sample 12B additionally contained aluminium, manganese and copper.

Raman

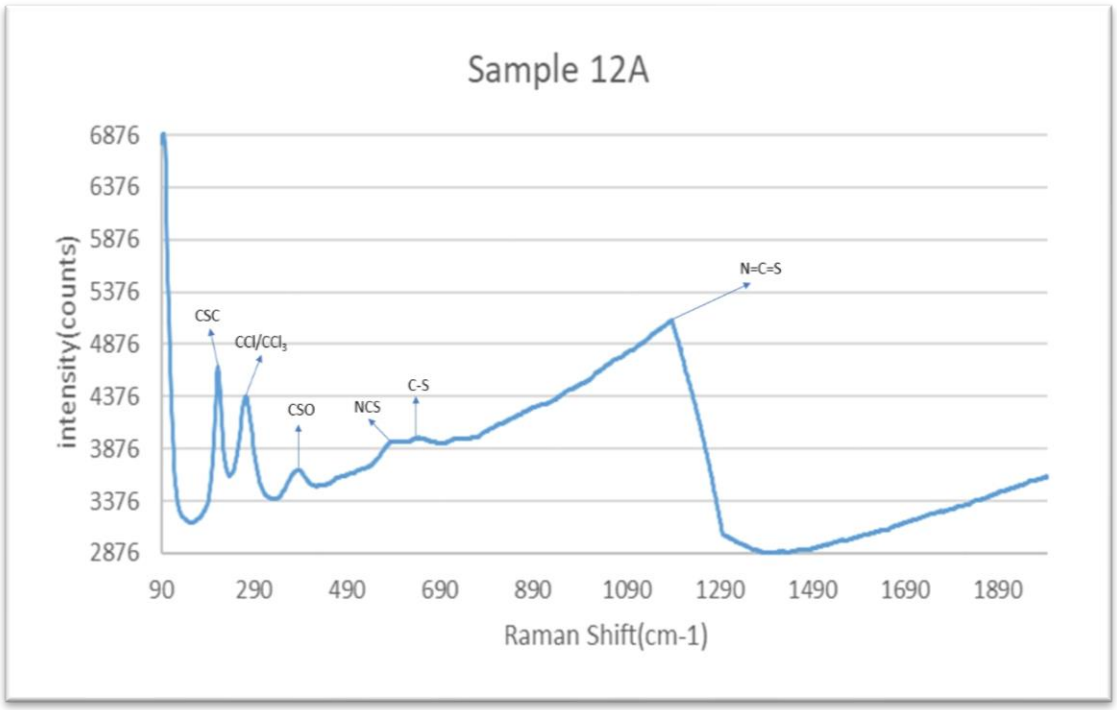
Sample 12A
intensity(counts)
6876
6376
5876
5376
4876
4376
3876
3376
2876
CSC
CCl/CCl3
CSO
NCS
C-S
N=C=S
90
290
490
690
890
1090
1290
1490
1690
1890
Raman Shift(cm-1)

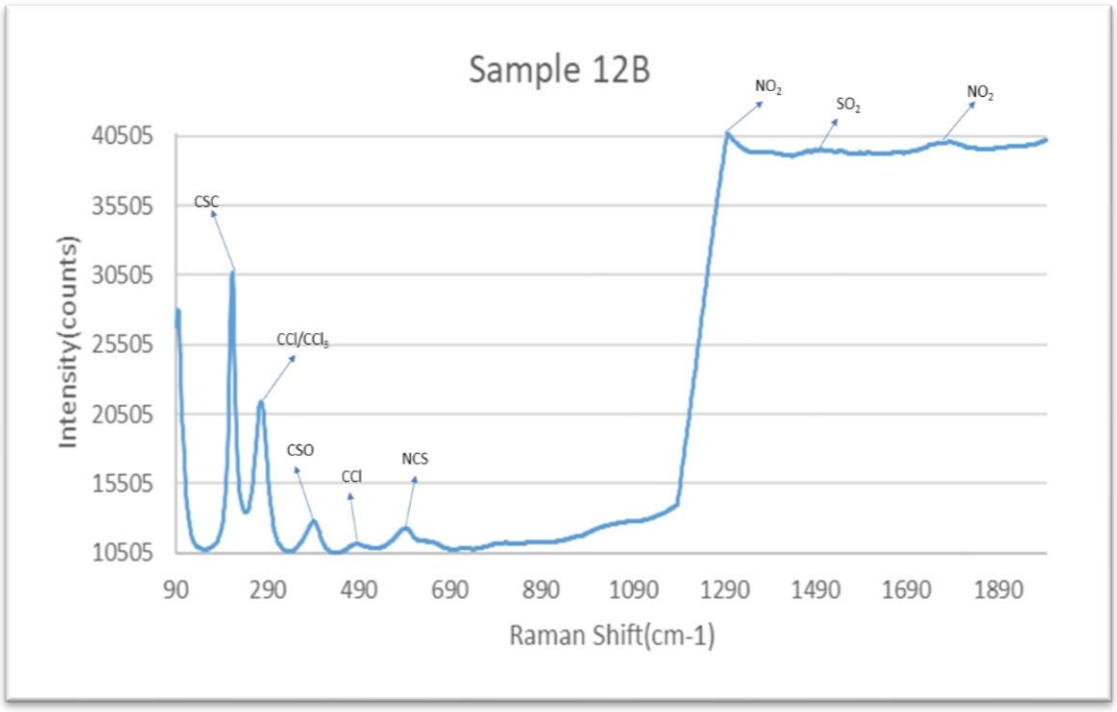
Sample 12B
Intensity(counts)
40505
35505
30505
25505
20505
15505
10505
CSC
CCl/CCl3
CSO
CCl
NCS
NO2
SO2
NO2
90
290
490
690
890
1090
1290
1490
1690
1890
Raman Shift(cm-1)

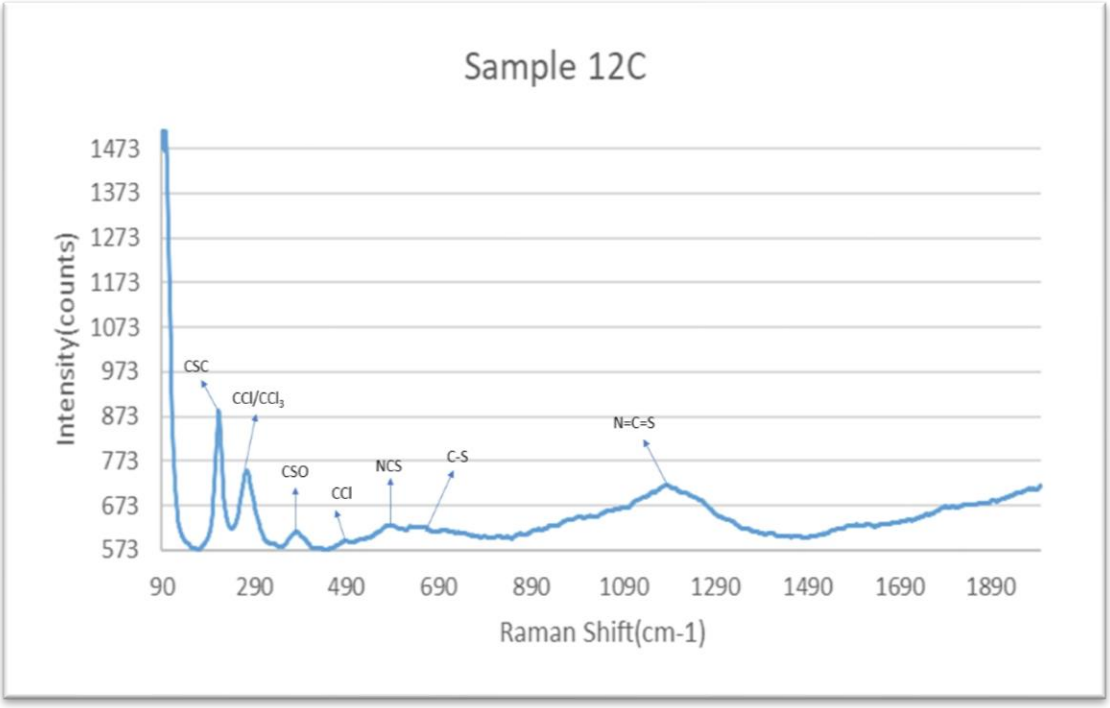

Figure 50. Raman analysis of samples from sample site 12.

The Raman spectra from sample site 12 shown in **Figure 50**, have similar characteristic peaks with low fluorescence interference. Sample 12B having the most differences at ~1290cm^{-1}, interpreted as nitroamimes (NO_2), at ~1355cm^{-1} methyl sulphones (SO_2) and at ~1502cm^{-1} aromatic nitro compounds (NO_2).

pH and Conductivity

Sample Site	Sample	pH	Conductivity(μS)
12	A	7.78	170
	B	7.66	260
	C	7.12	610

Table 27. The pH and conductivity of the samples from sample site 12.

Sample site 12 shows a pH between 7-7.8 as seen in **Table 27**, which is understandable from the lack of staining from atmospheric corrosion. The conductivity is still quite high, with the lower pH sample showing the highest conductivity similar to the acidic pH samples in the previous sample sites (excluding area 1 sample sites).

X-Ray Diffraction (XRD)

Sample 12A	Sample 12B	Sample 12C
Iron Oxide	Iron Titanium Oxide	Iron Sulfide
Iron Zinc	Sodium Iron Phosphate	Iron Zinc
Iron Oxide Hydroxide	Sodium Sulfide	Sodium Zinc Phosphate
Sulfur Fluoride	Sodium Carbonate	Sodium Phosphate
Sodium Ammine	Sodium Aluminum Oxide	Sodium Nitrite
Sodium Calcium Silicate	Magnesium Silicate	Calcium Iron Oxide
Magnesium Fluoride Silicate	Calcium Iron Oxide	Calcium Carbonate
Magnesium Phosphate Hydroxide	Calcium Carbonate	Silicon Oxide
Calcium Carbonate	Calcium Silicate	Zinc Silicate
Calcium Sulfite	Calcium Chlorite	Zinc Hydroxide
Silicon Phosphate	Calcium Phosphide	Zinc Phosphide
Silicon Oxide	Calcium Nitrate	Titanium Phosphide
Zinc Fluoride Nitride	Silicon Oxide	Titanium Sulfide
Zinc Fluoride	Zinc Sulfate	Titanium Oxide
Aluminum Oxide	Zinc Oxide	Titanium Fluoride
Titanium Nitride	Aluminum Iron	Cadmium Phosphide
Titanium Oxide	Aluminum Oxide	Cadmium Sulfate
Cadmium Nitrate	Manganese Oxide	Ammonium Chlorate
Ammonium Nitrate	Manganese Phosphate	
Nitrosyl Fluoride Phosphate	Copper Phosphate	

Table 28. XRD analysis of samples from sample site 12.

All samples from sample site 12 have iron corrosion product and alloy corrosion products from the steel structure (**Table 28**). Sample 12B has the most mineral compounds and the most salt compounds, with a copper compound. Sample 12A and 12C have similar XRD results containing metals, primer, cadmium and ammonium corrosion products. Sample 12C has less compounds and the least salts out of sample site 12.

3.4.1:Sample Site 13

Figure 51. Before(A) and after(B) sampling from sample site 13.

Sample site 13 was close to sample site 12 on the sheltered side of the bridge from the ocean as seen in **Figure 14.** In contrast to sample site 12, sample site 13 has a lot of staining from atmospheric corrosion as shown in **Figure 51**. The corrosion is still not very severe and the types of corrosion that can be seen are: filiform, intergranular and uniform corrosion.

Scanning Electron Microscope (SEM)

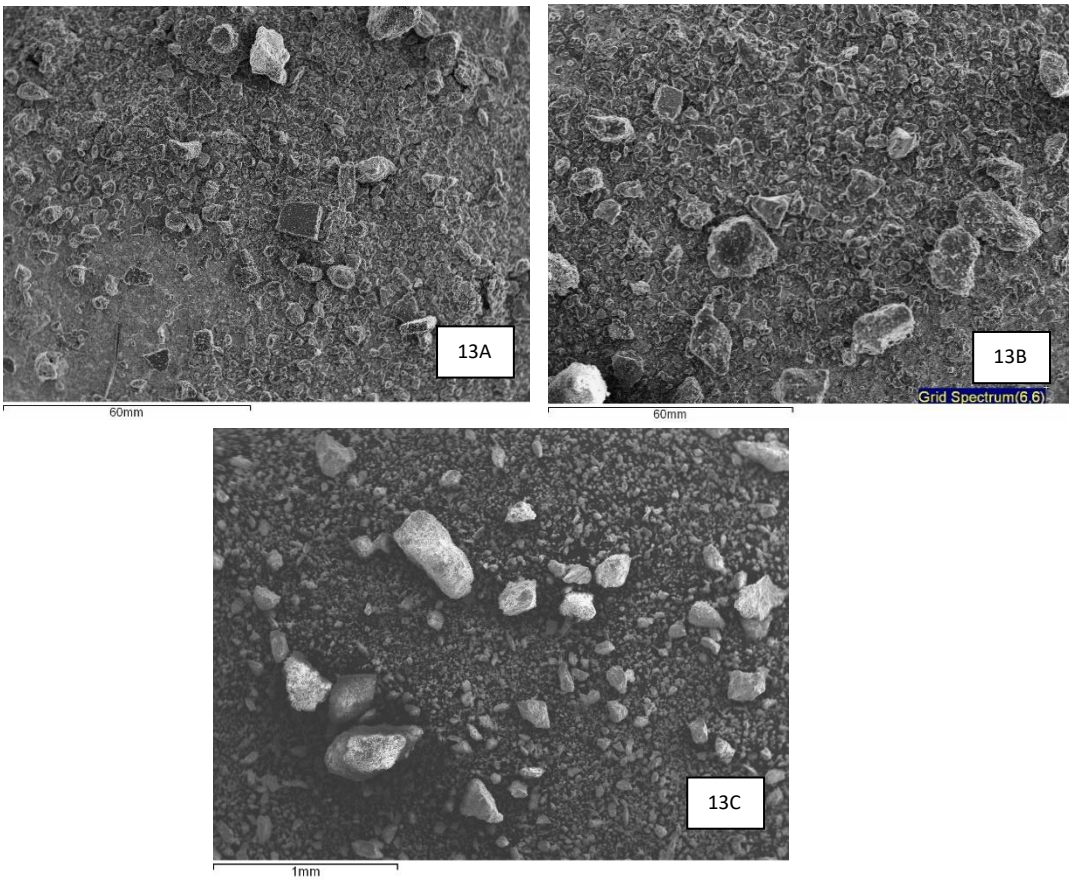

Figure 52. SEM analysis of samples from sample site 13.

Figure 52 shows the SEM images of sample site 13. The following elements where found in all the samples for sample site 13: carbon, iron, titanium, sodium, silicon, sulfur, calcium and chlorine. Sample site 13A and 13B also contained fluorine, and cadmium. Sample 13B additionally contained phosphorus. Sample 13C aluminium, potassium, manganese, cerium and barium.

Raman

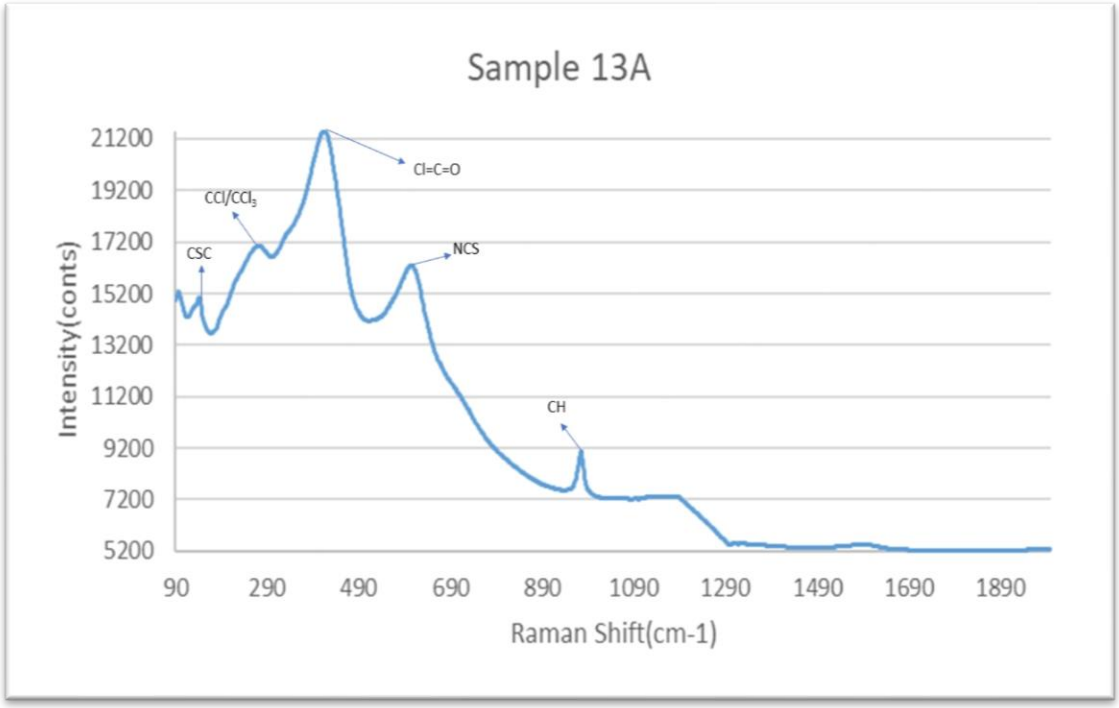
Sample 13A
Intensity(conts)
21200
19200
17200
15200
13200
11200
9200
7200
5200
90
290
490
690
890
1090
1290
1490
1690
1890
Raman Shift(cm-1)
Cl=C=O
CCl/CCl3
CSC
NCS
CH

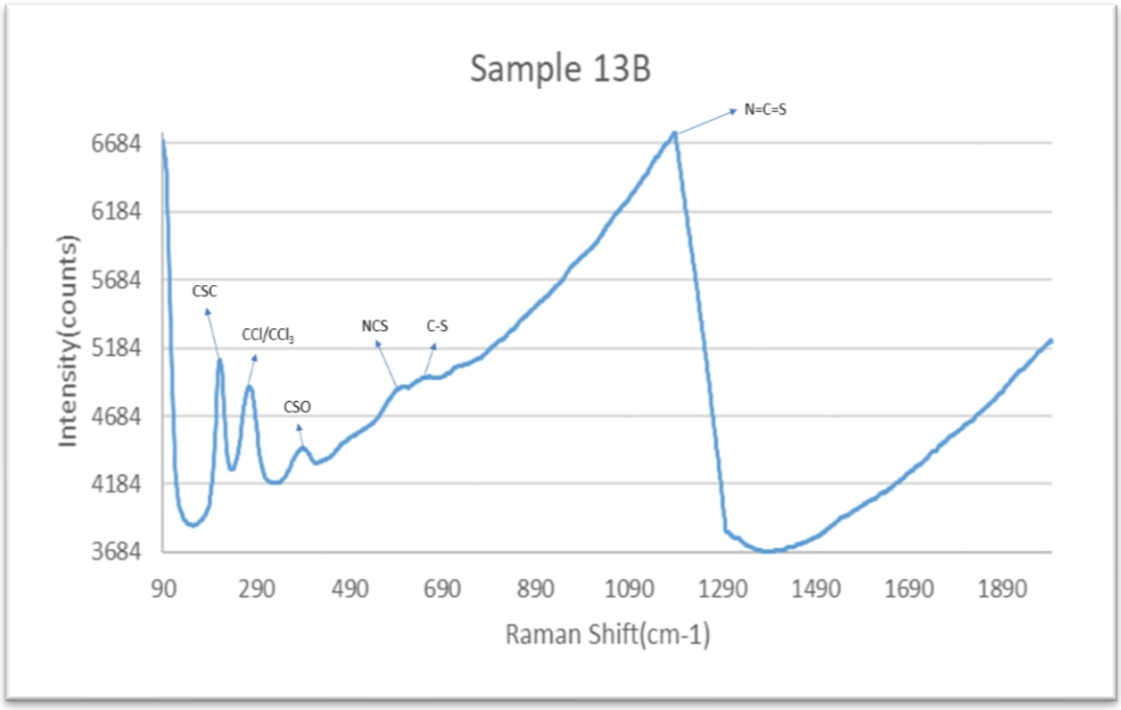
Sample 13B
Intensity(counts)
6684
6184
5684
5184
4684
4184
3684
90
290
490
690
890
1090
1290
1490
1690
1890
Raman Shift(cm-1)
N=C=S
CSC
CCl/CCl3
CSO
NCS
C-S

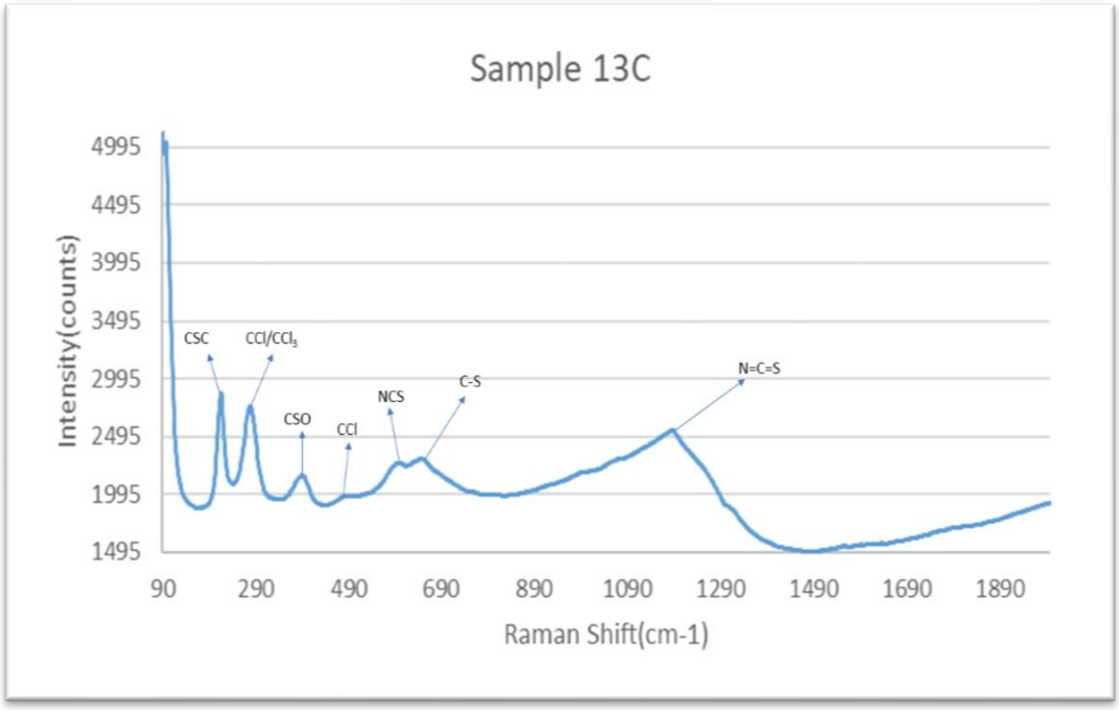

Figure 53. Raman analysis of samples from sample site 13.

Samples 13B and 13C have similar Raman spectra to the other sample sites (**Figure 53**). Sample 13A has a different spectrum but still contains commonly identified groups at ~210cm^{-1}, ~280cm^{-1}, ~380cm^{-1} and ~580cm^{-1}. The different peak from sample site 13A is at ~975cm^{-1} mono-substituted and para-substituted Benzene rings (CH).

pH and Conductivity

Sample Site	Sample	pH	Conductivity(µS)
13	A	7.43	93
	B	7.22	176
	C	7.18	329

Table 29. The pH and conductivity of samples from sample site 13.

This sample site also has a pH close to neutral as shown in **Table 29**, with the same trend of the lower the pH the greater the conductivity. However, the overall conductivity for sample site 13 is quite low compared to the other sample sites. This is expected as area 4 is sheltered from the ocean and slightly off the main road reducing direct pollution from cars and as a result reducing the presence of carbon particulates.

X-Ray Diffraction (XRD)

Sample 13A	Sample 13B	Sample 13C
Iron Titanium Oxide	Iron Oxide	Iron Carbonate
Iron Carbide	Iron Titanium Oxide	Iron Oxide
Iron Sulfate	Iron Oxide Hydroxide	Potassium Nitrite
Sulfur Oxide Fluoride	Sodium Sulfate	Potassium Sulfide
Sulfur Fluoride	Magnesium Silicate	Potassium Nitrate
Sodium Iron Sulfate	Magnesium Sulfate	Sodium Iron Sulfate
Sodium Oxide	Calcium Iron Oxide	Magnesium Silicate
Sodium Chlorate	Calcium Sulfate	Calcium Sulfate
Sodium Sulfate	Calcium Phosphide	Calcium Carbonate
Sodium Carbonate	Silicon Oxide	Silicon Oxide
Sodium Chlorate	Titanium Oxide	Zinc Oxide Sulfate
Calcium Sulfate	Titanium Nitride	Zinc Aluminum Oxide
Calcium Sulfite	Cadmium Phosphate Fluoride	Zinc Sulfide
Silicon Nitride	Cadmium Phosphide	Aluminum Cerium
Silicon Oxide	Cadmium Sulfide	Aluminum Oxide Carbide
Silicon Carbide	Ammonium Chloride	Titanium Nitride
Titanium Oxide	Ammonium Nitrate	Titanium Oxide
Cadmium Sulfide	Hydrazine Sulfate	Cerium Carbide
Ammonium Nitrate	Cyanuric acid	Ammonium Nitrate
4-Methoxy-phenol	Nitrosyl Sulfate	Hydrazine Sulfate

Table 30. XRD analysis of samples from sample site 13.

Table 30 shows that all samples from sample site 13 has no molybdenum and manganese corrosion products. The large number of mineral compounds recorded might have contributed to the neutral pH seen in **Table 29**. Sample site 13 contains more ammonium and heavier element corrosion product when compared to the other sites. There are still a fair amount of acids and salts present at sample site 13 but there is very little to no zinc salts, so the primer is not present where samples 13A and 13B were taken from.

3.5:Area 5

3.5.1:Sample Site 14

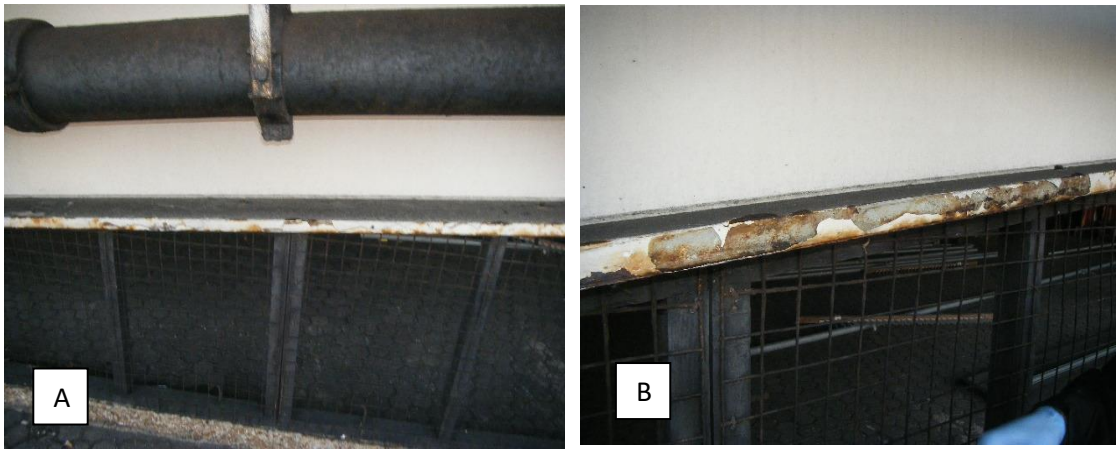

Figure 54. Before (A) and after (B) sampling for sample site 14.

Sample 14 is at ground level on the first ramp closest to the offices at the Port of Dover as seen in **Figure 14**. There is very little staining on this sample site which is at ground level close to the sea. There is not severe corrosion of the steel as seen in **Figure 54 B**, but the paint coating is just flaking off. The types of corrosion that can be identified are filiform and uniform corrosion. Filiform corrosion must occur for the paint to just be flaking off as seen in picture B and same of the metal underneath has been discoloured, as if it has started to corrode, proposing the presence of uniform corrosion.

Scanning Electron Microscope (SEM)

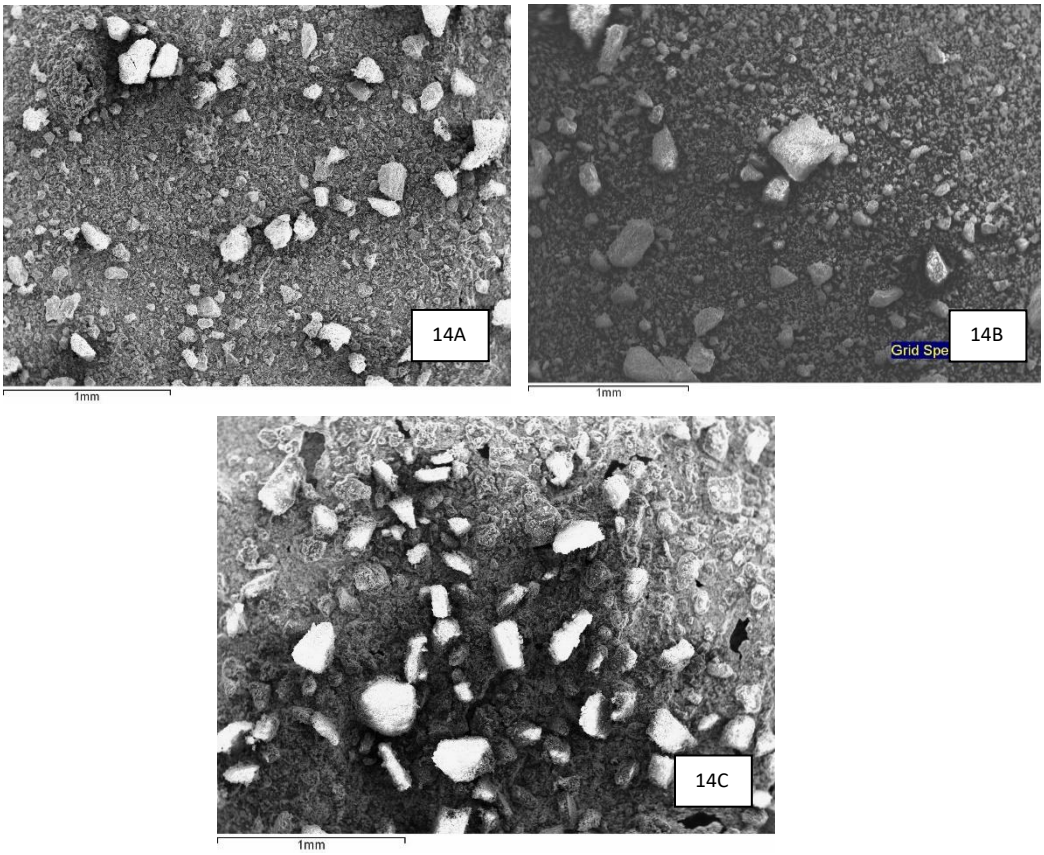

Figure 55. SEM analysis of sample site 14.

The SEM images are shown in **Figure 55** above. The elements detected in the samples for sample site 14: carbon, iron, zinc, chlorine, sodium, silicon, sulfur, calcium, titanium, cerium, aluminium and barium. Sample 14A additionally contained manganese and molybdenum. Sample 14B additionally contained potassium, manganese and neodymium. Sample 14C also contained rubidium.

Raman

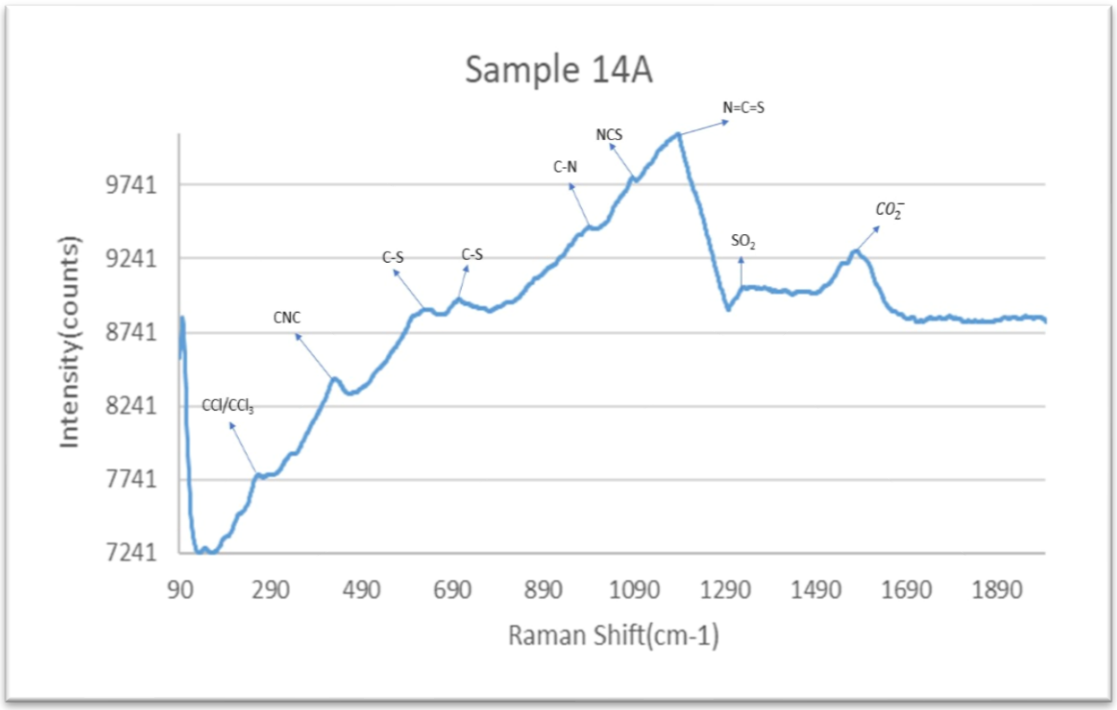
Sample 14A
Intensity(counts)
9741
9241
8741
8241
7741
7241
90
290
490
690
890
1090
1290
1490
1690
1890
Raman Shift(cm-1)
CCl/CCl3
CNC
C-S
C-S
C-N
NCS
N=C=S
SO2
CO2-

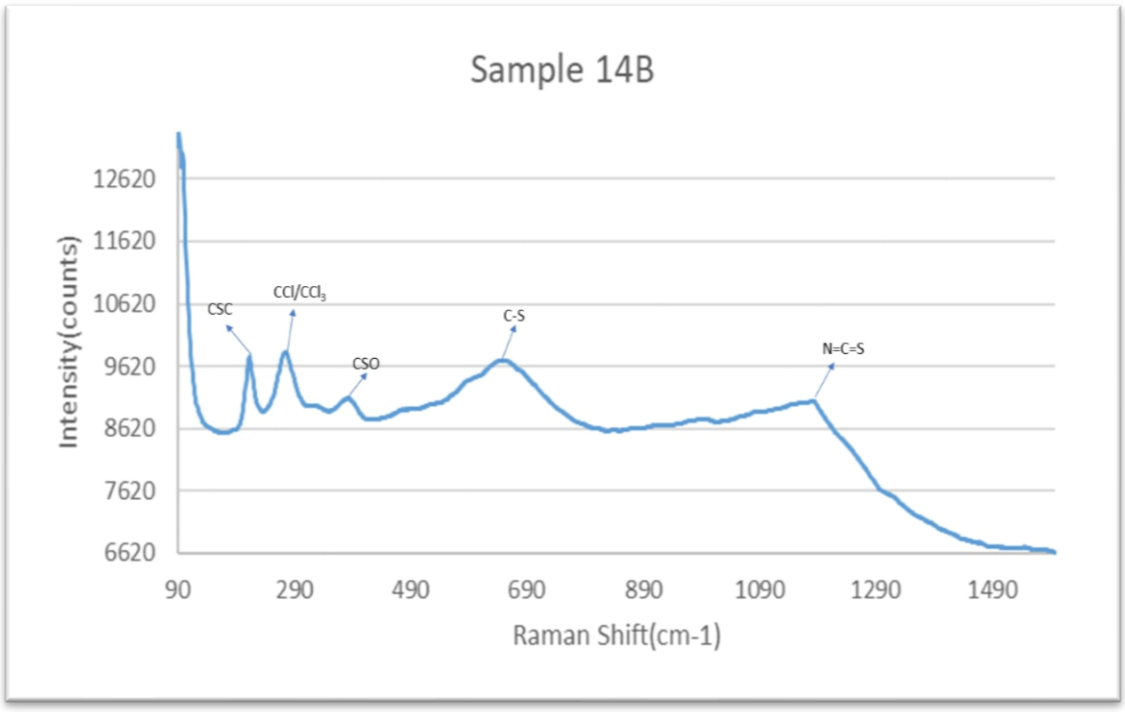
Sample 14B
Intensity(counts)
12620
11620
10620
9620
8620
7620
6620
90
290
490
690
890
1090
1290
1490
Raman Shift(cm-1)
CSC
CCl/CCl3
CSO
C-S
N=C=S

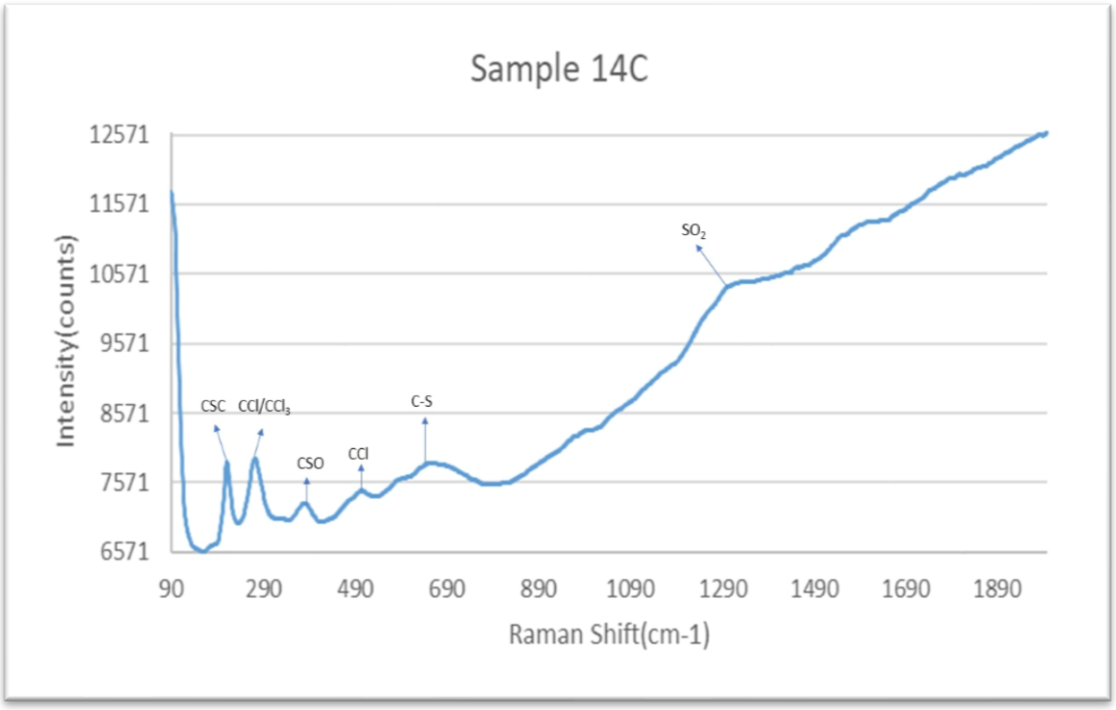

Figure 56. Raman analysis of samples form sample site 14.

Figure 56 shows the Raman spectra for sample site 14. Sample 14B and sample 14C show similar spectrum to other samples from the other sample sites. Sample 14A has a lot of fluorescence interference but some functional groups can be identified and associated with functional groups seen before. Sample 14A has peaks at 289, 432, 628, 704, 992, 1086, 1188, 1330 and 1551cm^{-1} representing the respective compounds: Carbon chlorides (CCl/CCl_3), secondary aliphatic amines (CNC), aliphatic sulfides and disulfides (C-S), mono and disulphonyl chlorides (C-S), saturated primary and secondary nitro compounds (C-N), alkyl isothiocyanates (NCS), isothiocyanates (N=C=S), methyl sulphones (SO_2) and lastly aromatic acid slats (CO_2^-), respectively.

pH and Conductivity

Sample Site	Sample	pH	Conductivity(µS)
14	A	8.6	220
	B	7.36	21
	C	8.08	98

Table 31. The pH and conductivity of samples from sample site 14.

The ground level sample site as seen in **Table 31**, has a basic pH and a low conductivity apart from sample 14A.

X-Ray Diffraction (XRD)

Sample 14A	Sample 14B	Sample 14C
Iron Oxide	Iron Zinc	Magnesium Silicate
Iron Zinc	Iron Oxide Hydroxide	Silicon Oxide
Calcium Silicate	Potassium Sulfide	Zinc Silicate
Calcium Chlorite	Sodium Sulfide	Titanium Oxide
Calcium Silicate Hydroxide	Sodium Hydroxide	Barium Oxide Hydrogen Peroxide
Silicon Oxide	Sodium Oxide	Cerium Silicate
Silicon Nitride	Silicon Oxide	Ammonium hydrogen adipate
Zinc Silicate	Zinc Oxide	Rubidium Copper Oxide
Aluminum Molybdenum	Zinc Sulfate	Rubidium Copper Chloride
Aluminum Oxide	Manganese Carbide	Rubidium Carbonate
Aluminum Manganese	Titanium Oxide	Rubidium Ozonide
Manganese Sulfate	Titanium Nitride	Rubidium Hydrogen Sulfate
Molybdenum Oxide	Barium Sulfide	p-Chloroaniline hydrochloride
Barium Silicide	Barium Cerium Oxide	
Barium Iron Oxide	Barium Copper Oxide	
Barium Sulfite	Barium Sulfite	
Cerium Chloride	Copper Sulfate	
Hydrazine Sulfate	Copper Chloride	
Polychloroprene	Hydrazine Sulfate	
p-Aminophenol		

Table 32. XRD analysis of samples from sample site 14.

Sample 14A has no salts and a lot of acidic corrosion products, sample 14B has the most salts and some alloy and metal corrosion products (**Table 32**). Sample 14C has one compound that is an alloy corrosion product and no iron corrosion products as seen in **Table 32**. Sample 14A's conductivity is higher than the other sample because it contains no salt compounds and more acidic corrosion products. Sample 14B and sample 14C have heavy element corrosion products. In fact, sample 14C is mostly comprised of heavy element corrosion products.

3.5.2:Sample Site 15

Sample site 15 is also at ground level on the other side of the ramp from samples site 14 as seen in **Figure 14**.

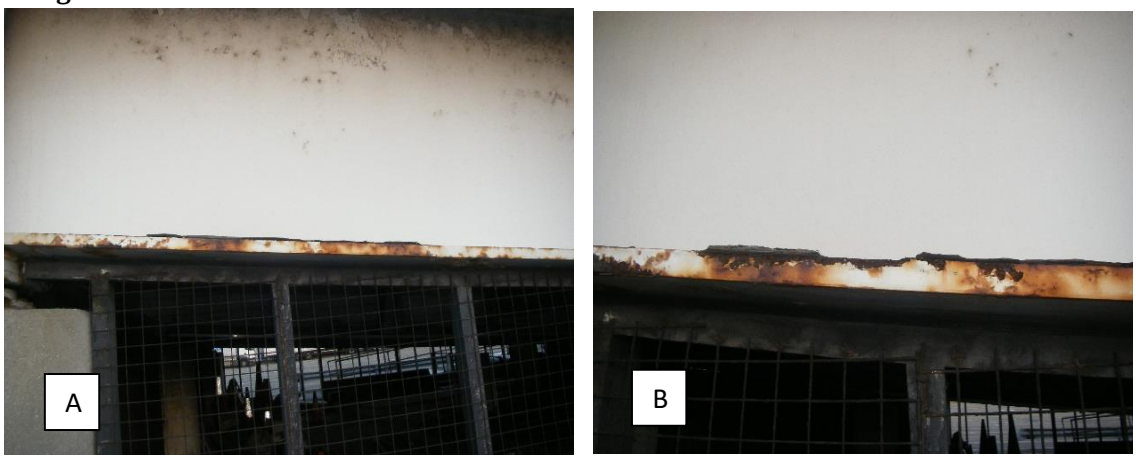

Figure 57. Before(A) and after(B) sampling at sample site 15.

Sample site 15 is far more stained than sample site 14, shown above in **Figure 57**, however, as seen in picture A above the corrosion is not very severe. The peeling coating on top of the ramp shelf is an intergranular corrosion, exfoliation where it separates the metal away from the structure in layers. Another type of corrosion observed is uniform corrosion of the metal underneath the coating.

Scanning Electron Microscope (SEM)

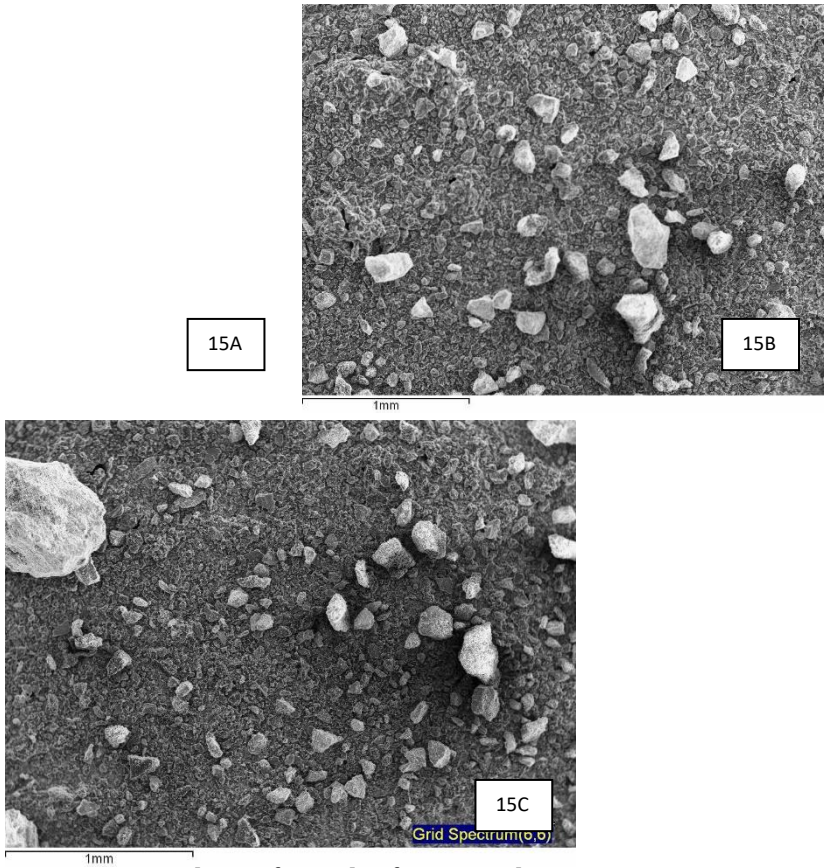

Figure 58. SEM analysis of samples from sample site 15.

The SEM images are shown above in **Figure 58**, the following elements where found in all the samples from sample site 15: carbon, titanium, iron, sodium, silicon, sulfur, zinc, chlorine, aluminium. Sample 15A also contains manganese, barium, potassium, calcium, magnesium and tungsten. Sample 15B additionally contains calcium, potassium and uranium. Sample 15C also contains magnesium.

Raman

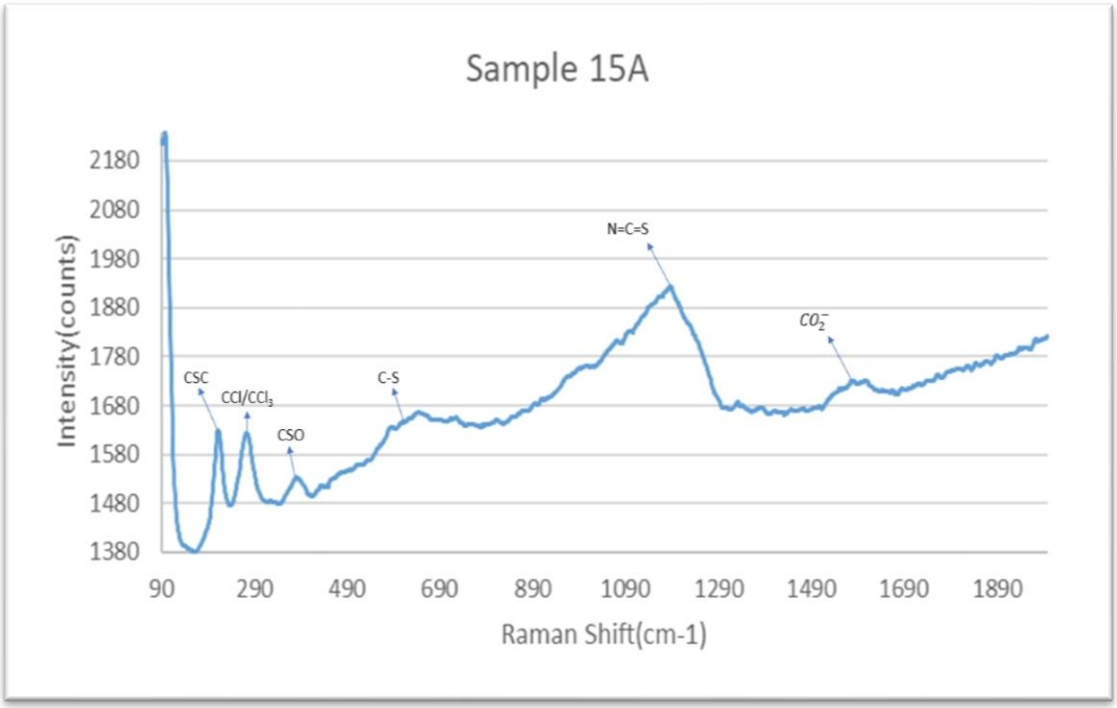
Sample 15A
Intensity(counts)
2180
2080
1980
1880
1780
1680
1580
1480
1380
CSC
CCl/CCl3
CSO
C-S
N=C=S
CO2-
90
290
490
690
890
1090
1290
1490
1690
1890
Raman Shift(cm-1)

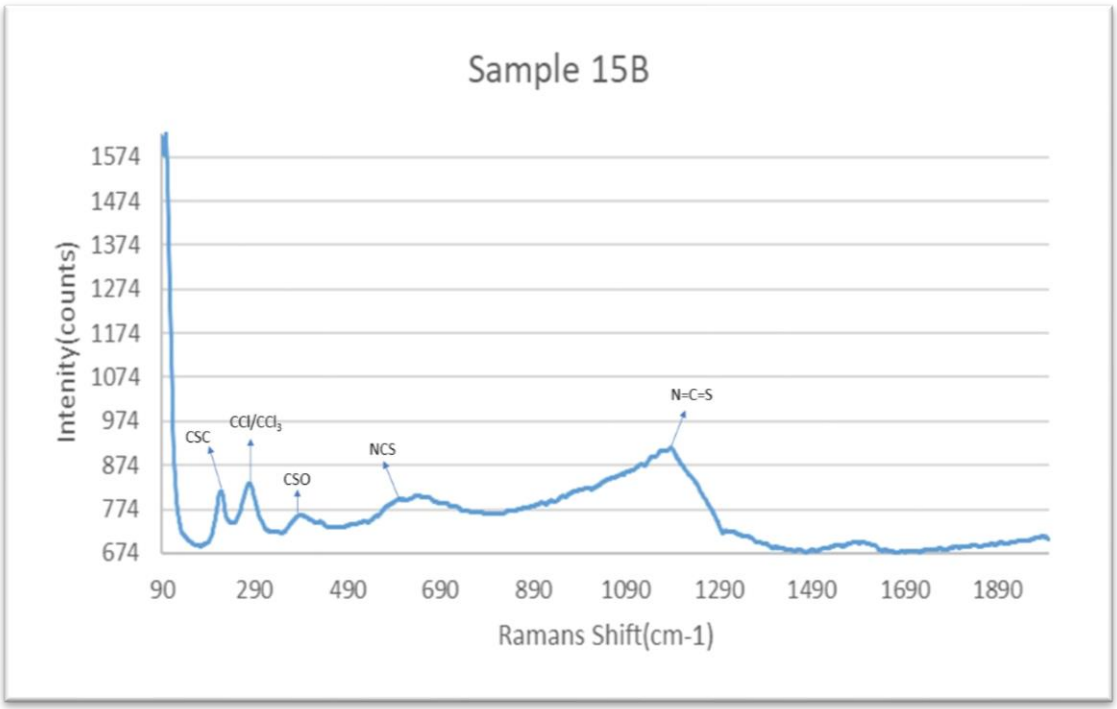
Sample 15B
Intenity(counts)
1574
1474
1374
1274
1174
1074
974
874
774
674
CSC
CCl/CCl3
CSO
NCS
N=C=S
90
290
490
690
890
1090
1290
1490
1690
1890
Ramans Shift(cm-1)

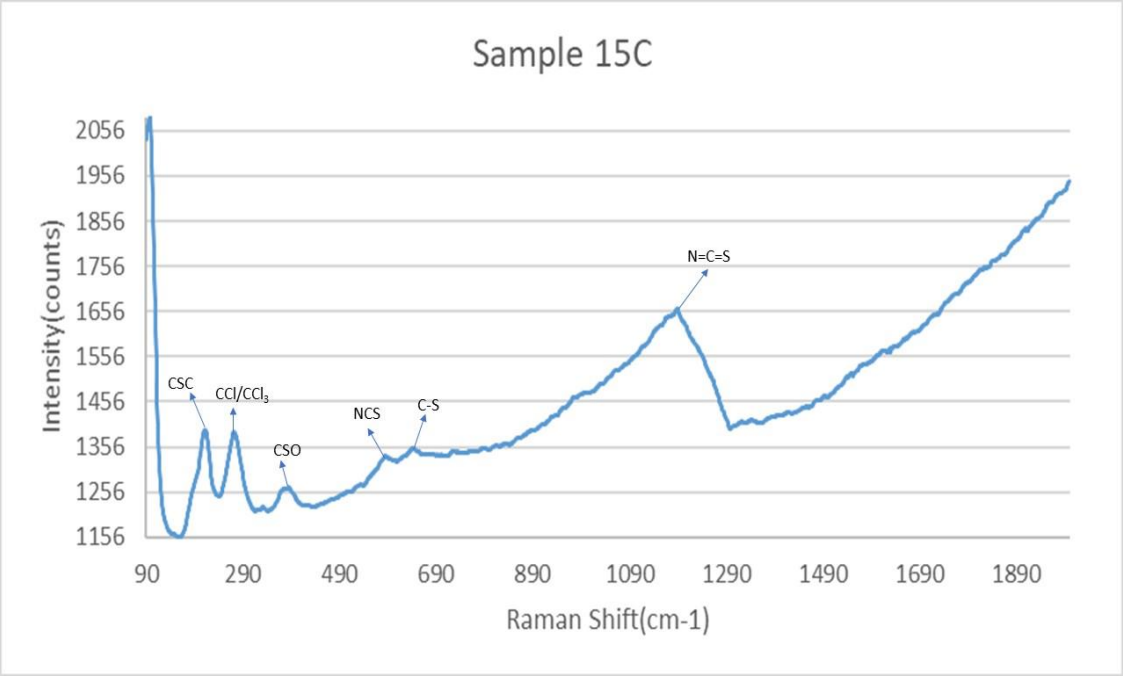

Figure 59. Raman analysis of samples from sample site 15.

Sample site 15 contains commonly identified compounds that are present in the other sample site, there are no drastic changes. Sample 15B has the least fluorescence interference compared to the other two samples from sample site 15 as seen in **Figure 59** above.

pH and Conductivity

Sample Site	Sample	pH	Conductivity(μS)
15	A	7.94	31
	B	7.56	59
	C	7.29	50

Table 33. The pH and conductivity of samples from sample site 15.

The pH is slightly basic at sample site 15, with the conductivity being very low when compared to other sample sites as displayed in **Table 33**. Sample site 15 must not be very acidic despite it being more stained than sample site 14.

X-Ray Diffraction (XRD)

Sample 15A	Sample 15B	Sample 15C
Iron Sulfate	Iron Sulfate	Iron Oxide Hydroxide
Potassium Nitrate	Potassium Sulfate	Iron Sulfate
Potassium Oxide	Potassium Aluminum Silicate	Iron Silicide
Magnesium Nitrate	Sodium Silicate	Iron Oxide
Magnesium Oxide	Sodium Iron Oxide	Iron Sulfide
Calcium Iron Oxide	Sodium Sulfate	Sodium Oxide
Calcium Carbonate	Sodium Iron Sulfate	Sodium Iron Sulfate
Silicon Carbide	Calcium Silicate	Sodium Oxide Chloride
Zinc Sulfate Oxide	Silicon Oxide	Sodium Carbide
Zinc Silicate	Zinc Oxide Sulfate	Magnesium Sulfate
Aluminum Oxide Hydroxide	Zinc Aluminum Sulfide	Magnesium Carbide
Aluminum Manganese	Zinc Oxide	Magnesium Nitride
Manganese Oxide	Zinc Hydroxide	Silicon Oxide
Titanium Nitride	Zinc Cyanide	Zinc Oxide Sulfate
Titanium Oxide	Titanium Oxide	Zinc Oxide
Barium Silicate	Uranium Silicon	Aluminum Silicate Oxide
Barium Sulfide	Uranium Oxide	Aluminum Oxide Carbide
Ammonium Chloride	Hydrazine Sulfate	Aluminum Oxide
Tungsten Oxide	L-Aspartic acid	Titanium Sulfide
Hydrazine Sulfate		Titanium Oxide

Table 34. XRD analysis of samples from sample site 15.

All the samples from sample site 15 contain a lot of salts and zinc salts, they also contain metal and alloy corrosion products which provides evidence that the steel structure is corroding, as shown in **Table 34**. Sample 15A and 15B contain heavy element corrosion products and acids, sample 15C has no heavy element corrosion products but instead the most salts and the most metal, alloy corrosion products. In all the samples from sample site 15 there are very little mineral corrosion compounds.

3.6:Area 6

3.6.1:Sample Site 16

Sample site 16 is slightly above ground on the ramp closest to the end of the bridge as seen in **Figure 14**.

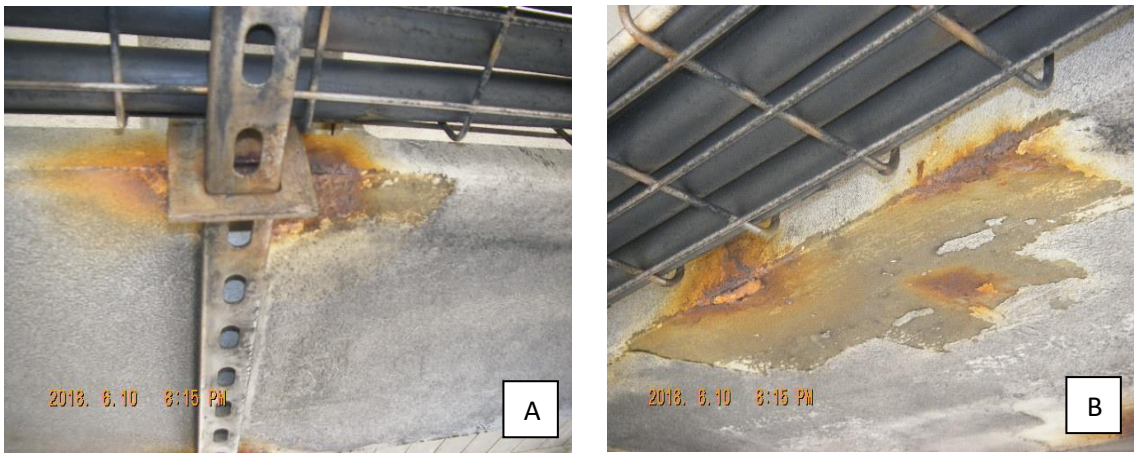

Figure 60. Before(A) and after(B) sampling of sample site 16.

Sample site 16 is located underneath the ramp that is part of the new bridge just above ground level and is slightly stained as observed in the pictures of **Figure 60**. The extent of corrosion is not very severe with some intergranular and exfoliation corrosion being seen in picture B above.

Scanning Electron Microscope (SEM)

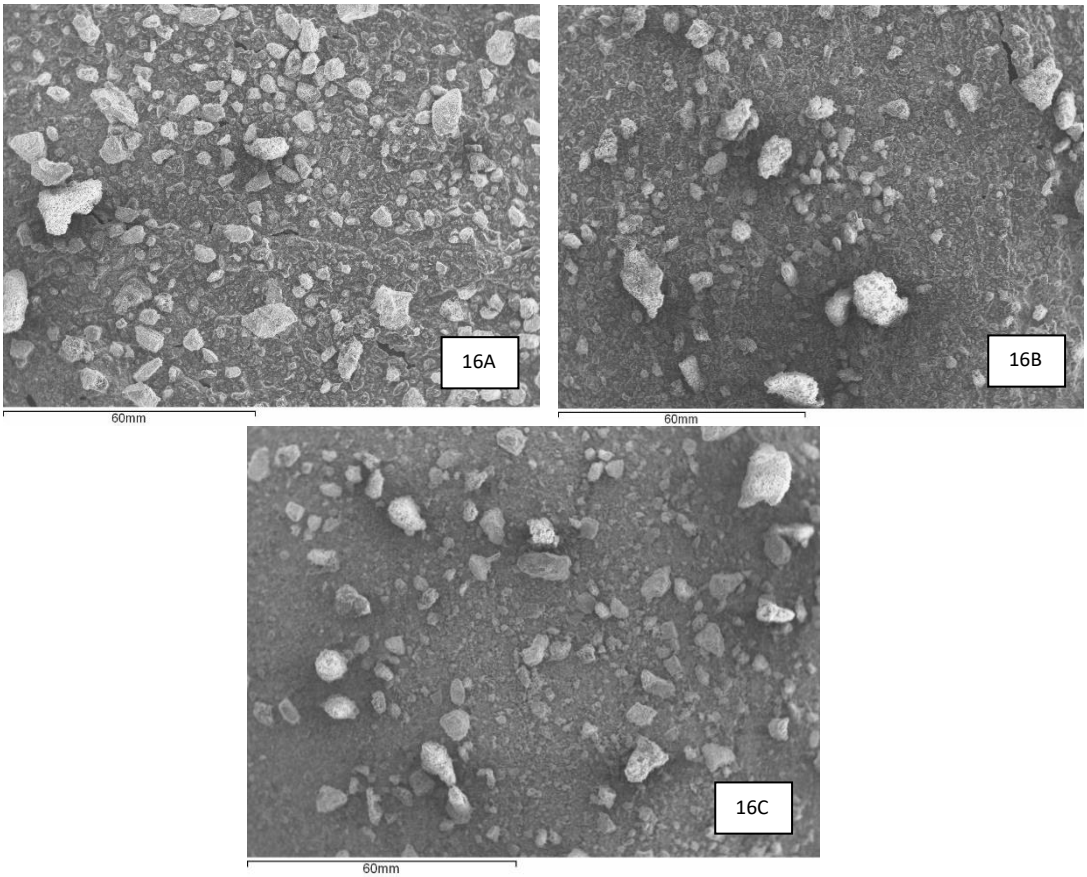

Figure 61. SEM analysis of samples from sample site 16.

The SEM images are as shown in **Figure 61**, the elements detected in all the samples from sample site 16 are; carbon, chlorine, iron, fluorine, zinc, silicon, sulfur, calcium, titanium, cadmium, aluminium. Sample 16A also contained sodium and sample 16B also contained potassium. Sample 16C additionally contained potassium, magnesium, sodium and phosphorus.

Raman

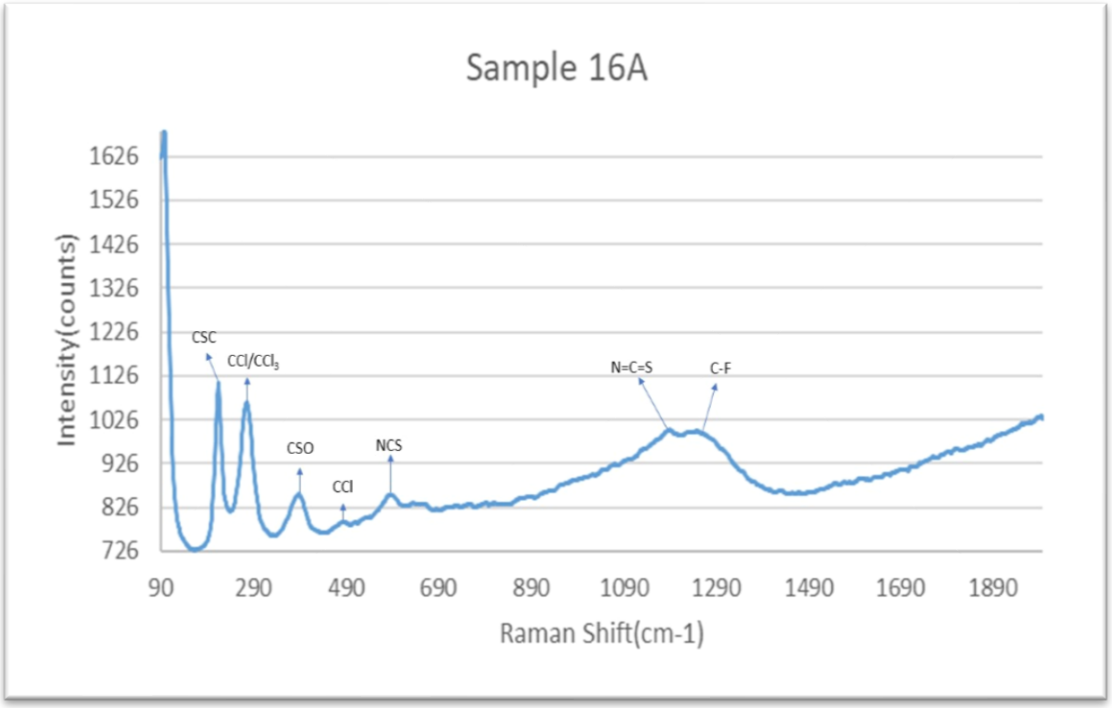
Sample 16A
Intensity(counts)
1626
1526
1426
1326
1226
1126
1026
926
826
726
CSC
CCl/CCl3
CSO
CCl
NCS
N=C=S
C-F
90
290
490
690
890
1090
1290
1490
1690
1890
Raman Shift(cm-1)

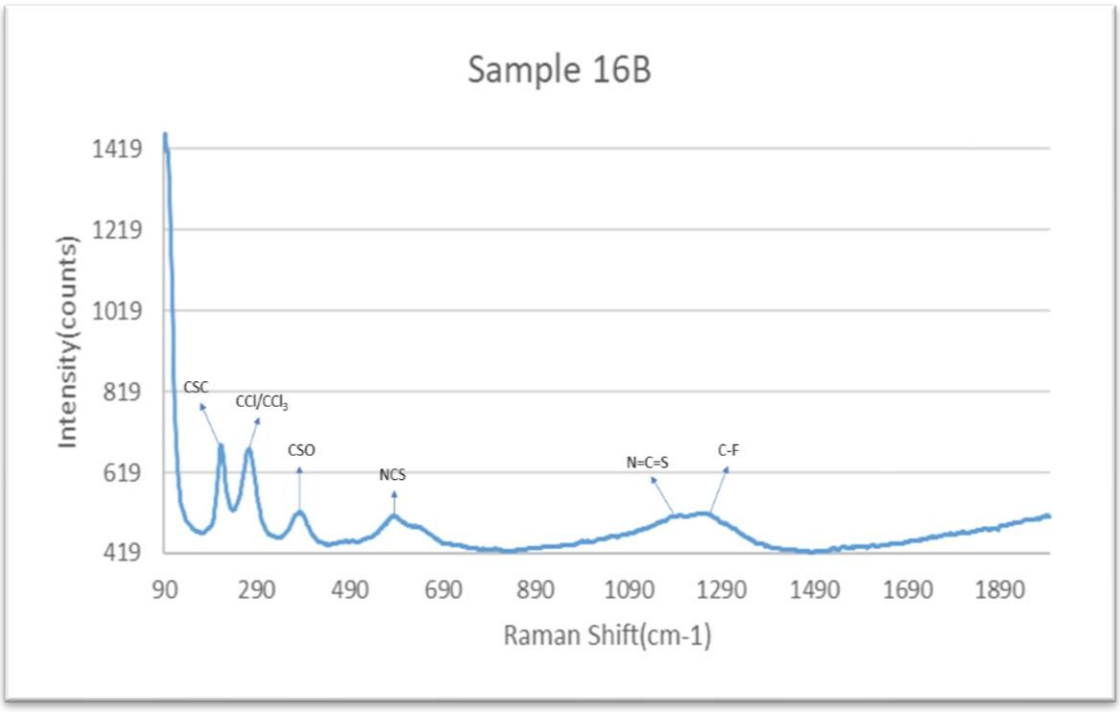
Sample 16B
Intensity(counts)
1419
1219
1019
819
619
419
CSC
CCl/CCl3
CSO
NCS
N=C=S
C-F
90
290
490
690
890
1090
1290
1490
1690
1890
Raman Shift(cm-1)

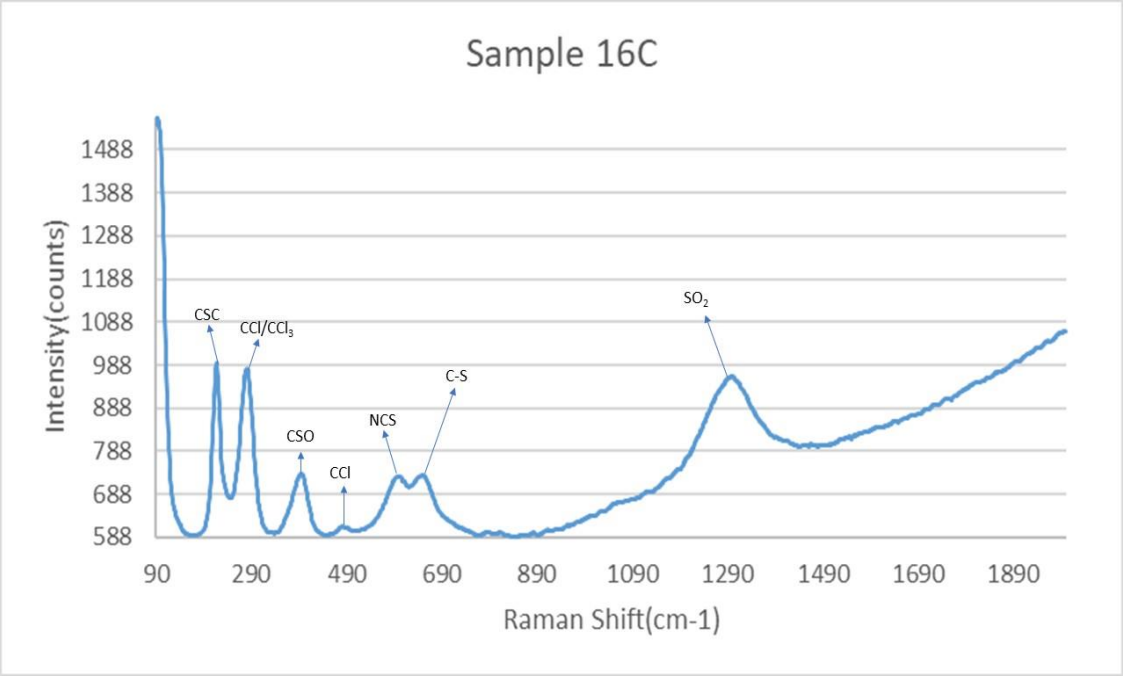

Figure 62. Raman analysis of samples from sample site 16.

Raman spectrum shown in **Figure 62**, have got low fluorescence interference, sample 16C is like spectra seen from other samples sites. Samples 16A and 16B contain a new identified compound, with the peak having a Raman Shift of ~1250cm^{-1} representing carbon fluoride (C-F) compounds. This is because all samples were analysed to have had fluorine in them but, sample 16C has higher fluorescence interference which allows the methyl sulphones (SO_2) to eclipse that possible peak.

pH and Conductivity

Sample Site	Sample	pH	Conductivity(µS)
16	A	7.52	53
	B	5.92	108
	C	8.78	338

Table 35. The pH and conductivity of samples from sample site 16.

Sample site 16 has a mixed pH with samples A and C being slightly basic and sample B being acidic, seen in **Table 35** above. The conductivity is low for sample A and reasonably high for samples B and C, with sample C having the highest conductivity. This breaks the theory of more acidic sample having a higher conductivity, excluding area 1 as it has only acidic samples and low conductivity.

X-Ray Diffraction (XRD)

Sample 16A	Sample 16B	Sample 16C
Iron Titanium Oxide	Iron Oxide	Iron Oxide
Iron Titanium Silicide	Iron Oxide Hydroxide	Iron Sulfate
Iron Sulfide	Potassium Nitrate	Potassium Nitrate
Sodium Iron Sulfate	Potassium Sulfide	Potassium Sulfide
Sodium Sulfide	Sulfur	Sodium Silicate
Calcium Carbonate	Calcium Sulfate	Sodium Iron Sulfate
Calcium Chloride	Calcium Nitrate	Magnesium Phosphate
Calcium Iron Oxide	Calcium Chloride	Calcium Silicate
Zinc Sulfate	Calcium Silicate	Calcium Phosphide
Zinc Hydroxide	Calcium Carbonate	Silicon Oxide
Zinc Cyanide	Aluminum Oxide	Aluminum Titanium Oxide
Zinc Oxide	Aluminum Silicate Hydroxide	Aluminum Phosphate
Aluminum Silicate	Titanium Silicide	Aluminum Oxide Carbide
Aluminum Iron	Titanium Chlorate	Aluminum Hydroxide
Aluminum Hydroxide	Titanium Oxide	Titanium Oxide
Titanium Oxide	Cadmium Sulfite	Cadmium Phosphate
Cadmium Nitrate	Cadmium Nitrate	Cadmium Sulfite
Ammonium Fluoride	Ammonium Chloride	Ammonium Chlorate
Ammonium Nitrate	Ammonium Nitrate	Thiodipropionic Acid
Ammonium Fluoride	Cyanuric acid	

Table 36. XRD analysis of samples from sample site 16.

All the samples in **Table 36**, contain iron and alloy corrosion products with only sample 16A containing zinc salts/corrosion products. Sample 16A also has the most iron and alloy corrosion products, in combination with the zinc corrosion products this must be the reason as to why it has the lowest conductivity out of the three samples. All the samples contain some heavy element corrosion products and ammonium compounds, with samples 16B and 16C containing acids in addition. The difference in conductivity can be due to sample 16B containing more mineral compounds which will not be acting as an insulator.

3.6.2:Sample Site 21

Sample site 21 is on the other side of the ramp to sample site 16, as seen in **Figure 14**.

Figure 63. Before(A) and after(B) sampling of sample site 21.

There is some staining of sample site 21 on the ramp of the new part of the bridge as seen in **Figure 63**. The corrosion is not severe and looks very similar to sample site 16. There is intergranular, exfoliation and uniform corrosion.

Scanning Electron Microscope (SEM)

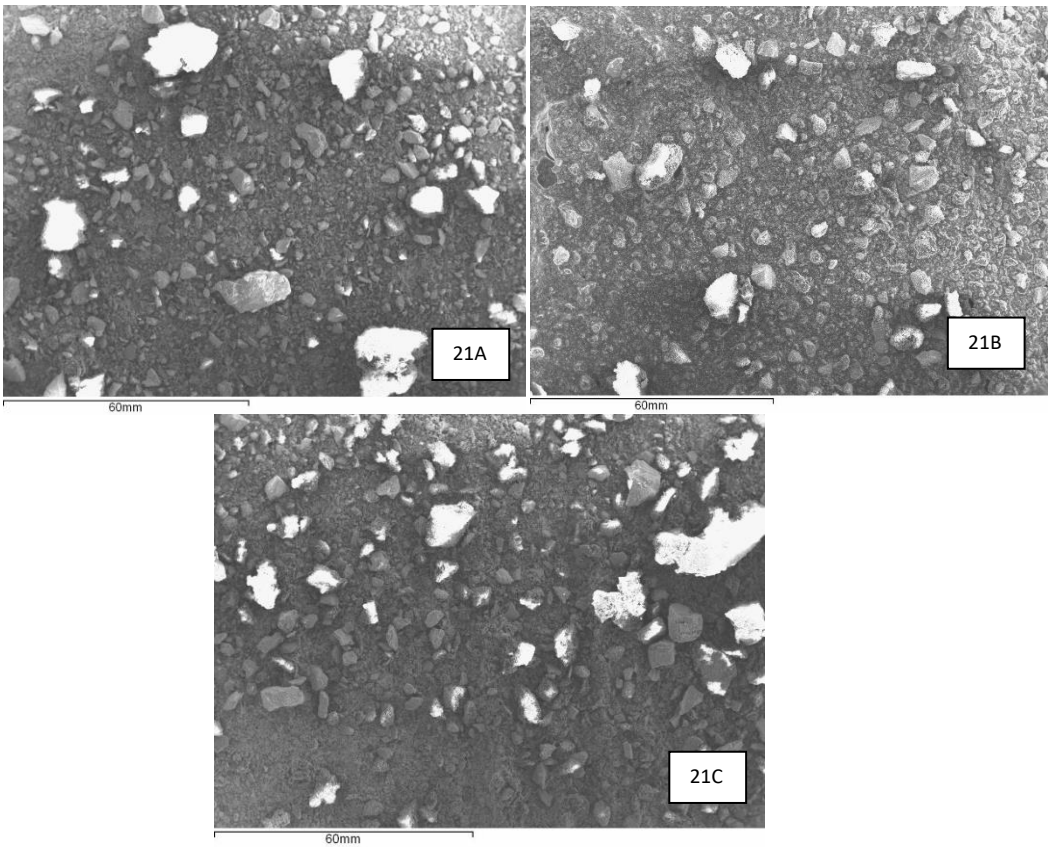

Figure 64. SEM analysis of samples form sample site 21.

The SEM images are show in **Figure 64**, the detected elements in all the samples for sample site 21 are; carbon, chlorine, iron, fluorine, manganese, silicon, cadmium, calcium, titanium, sodium, zinc, sulfur, magnesium, phosphorus and aluminium. Sample 21A also contained germanium.

Raman

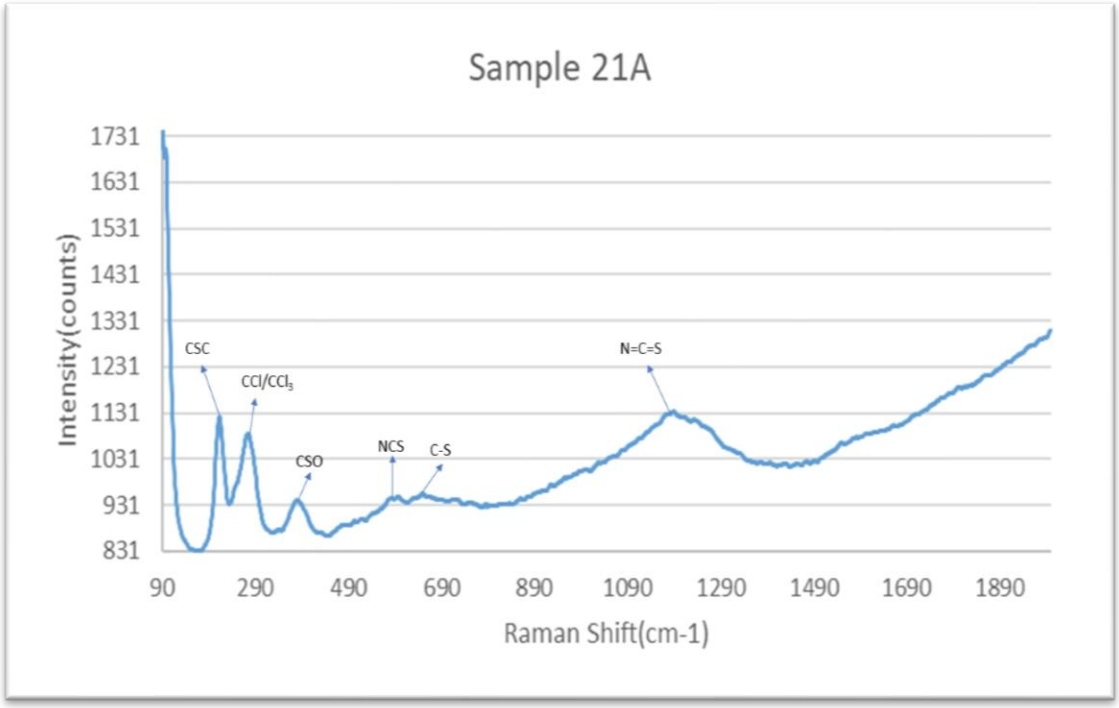
Sample 21A
Intensity(counts)
1731
1631
1531
1431
1331
1231
1131
1031
931
831
CSC
CCl/CCl3
CSO
NCS
C-S
N=C=S
90
290
490
690
890
1090
1290
1490
1690
1890
Raman Shift(cm-1)

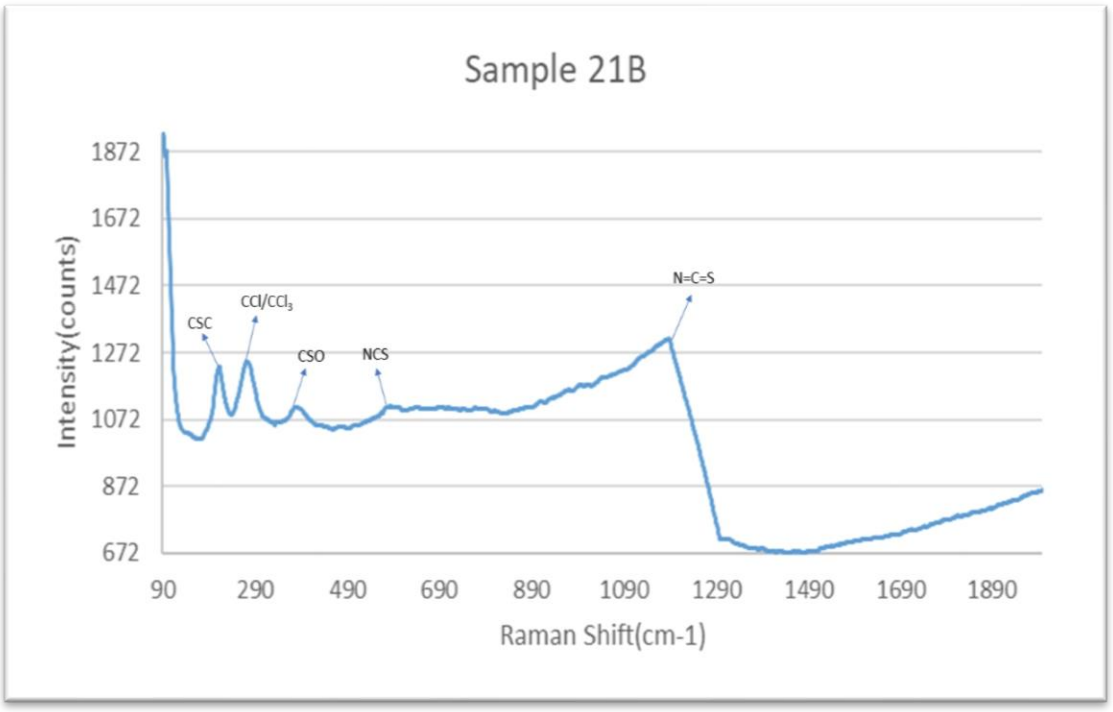
Sample 21B
Intensity(counts)
1872
1672
1472
1272
1072
872
672
CSC
CCl/CCl3
CSO
NCS
N=C=S
90
290
490
690
890
1090
1290
1490
1690
1890
Raman Shift(cm-1)

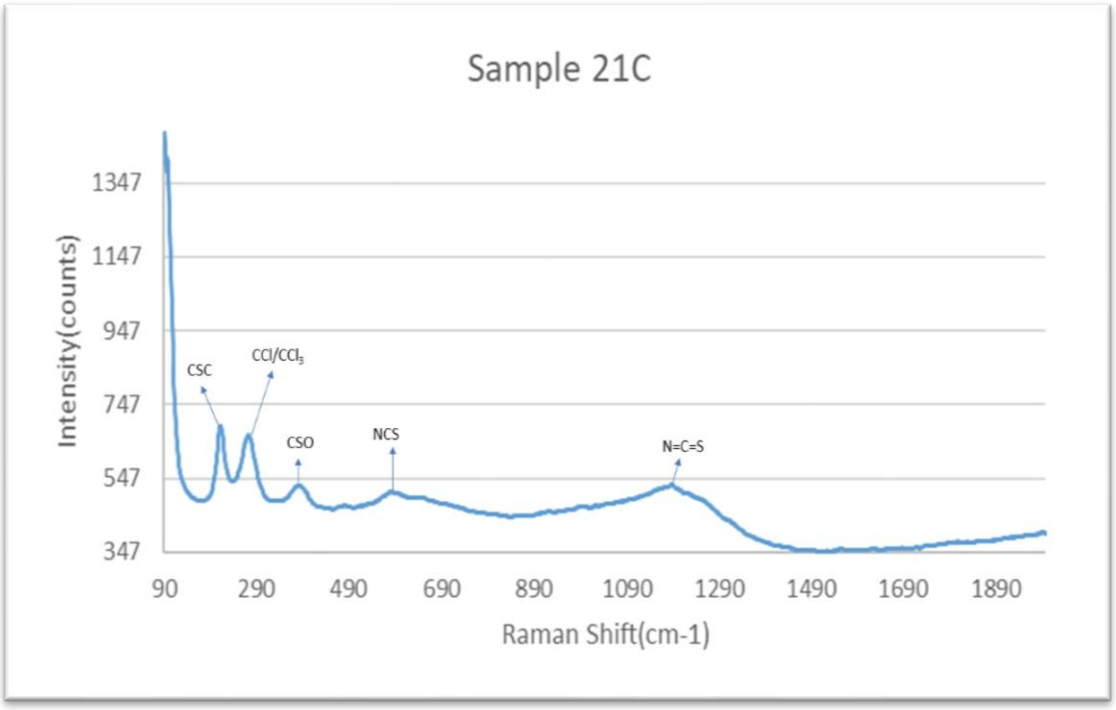

Figure 65. Raman analysis of samples from sample site 21.

The Raman spectrum in **Figure 65**, of samples from sample site 21 are similar that of other sample sites from before which have already identified the compounds relating to the peaks. There is however, a lot of noise in samples 21A and 21B.

pH and Conductivity

Sample Site	Sample	pH	Conductivity(μS)
21	A	6.9	100
	B	7.02	29
	C	6.92	26

Table 37. The pH and conductivity of samples from sample site 21.

Sample site 21 has a neutral/slightly acidic overall pH with poor conductivity similar to samples from area 1. Sample 21A has the highest conductivity of the samples and from having looked at previous samples, sample 21A has more acidic corrosion compounds and less salts.

X-Ray Diffraction (XRD)

Sample 21A	Sample 21B	Sample 21C
Iron Oxide	Iron Oxide Hydroxide	Iron Oxide
Iron Sulfate	Iron Silicate	Iron Sulfate
Iron Germanium Oxide	Iron Titanium Oxide	Sodium Carbonate
Iron Hydroxide Oxide	Sodium Sulfate	Magnesium Phosphate
Sodium Sulfate	Sodium Phosphate	Magnesium Fluoride
Sodium Carbonate	Magnesium Phosphate	Magnesium Zinc
Calcium Silicate	Magnesium Silicate	Magnesium Silicate
Calcium Carbonate	Magnesium Fluoride	Calcium Fluoride Silicate
Silicon Phosphate	Calcium Carbonate	Calcium Silicate
Zinc Oxide	Calcium Silicate	Silicon Oxide
Zinc Iron Phosphate	Calcium Sulfite	Zinc Phosphate
Zinc Oxide Sulfate	Calcium Phosphate	Aluminum Manganese
Aluminum Fluoride	Silicon Oxide	Aluminum Phosphate
Manganese Phosphate	Zinc Phosphate	Aluminum Oxide
Manganese Fluoride	Zinc Fluoride Nitride	Manganese Oxide
Manganese Germanium Oxide	Aluminum Silicate	Manganese Sulfate
Titanium Phosphate	Manganese Phosphate	Titanium Oxide
Titanium Oxide	Titanium Oxide	Cadmium Phosphate
Cadmium Phosphate	Cadmium Sulfate Oxide	Cadmium Nitrate
	Ammonium Chlorate	Ammonium Nitrate

Table 38. XRD analysis of samples from sample site 21.

All samples in **Table 38**, have iron and alloy corrosion products with sample 21A having the most of these compounds. Sample 21A also has the least salts but the most zinc and least mineral corrosion products. Having the least salts and most iron and alloy corrosion products is the reason as to why sample 21A has the highest conductivity. Samples 21B and 21C have similarly low conductivity which is due to having a lot of salt corrosion products.

3.7:Area 7

3.7.1:Sample Site 17

Sample site 17 is underneath the exit ramp of the new part of the bridge as seen in **Figure 14**.

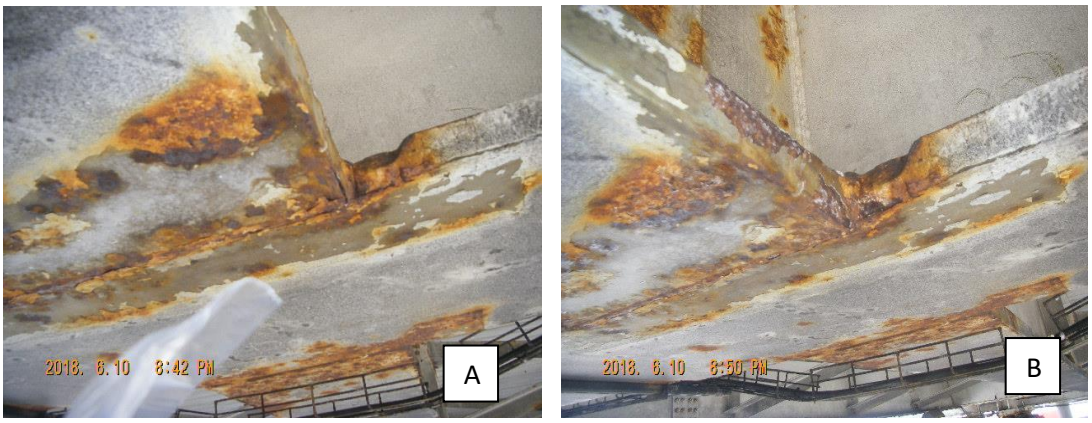

Figure 66. Before(A) and after(B) sampling for sample site 17.

Sample site 17 is stained along the underside of the bridge close to the exit ramp as seen in **Figure 66**. The extent of corrosion at this sample site is not severe and there is uniform, intergranular and exfoliation corrosion occurring in picture B.

Scanning Electron Microscope (SEM)

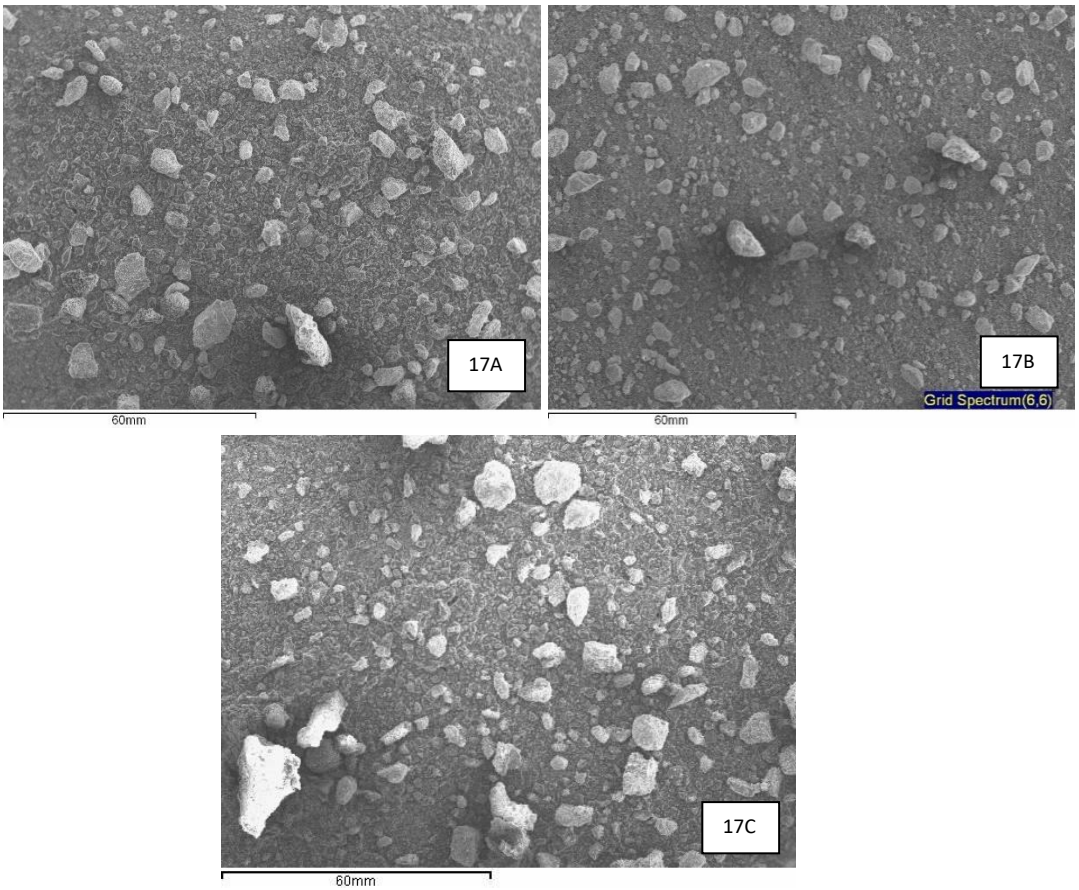

Figure 67. SEM analysis of samples from sample site 17.

The SEM images can be seen in **Figure 67**, the elements detected in all the samples from sample site 17 are; iron, titanium, chlorine, manganese, fluorine, carbon, cadmium, aluminium, silicon, calcium and sulfur. Sample 17A also contains calcium and magnesium. Sample 17C additionally contains calcium, sodium, magnesium and potassium.

Raman

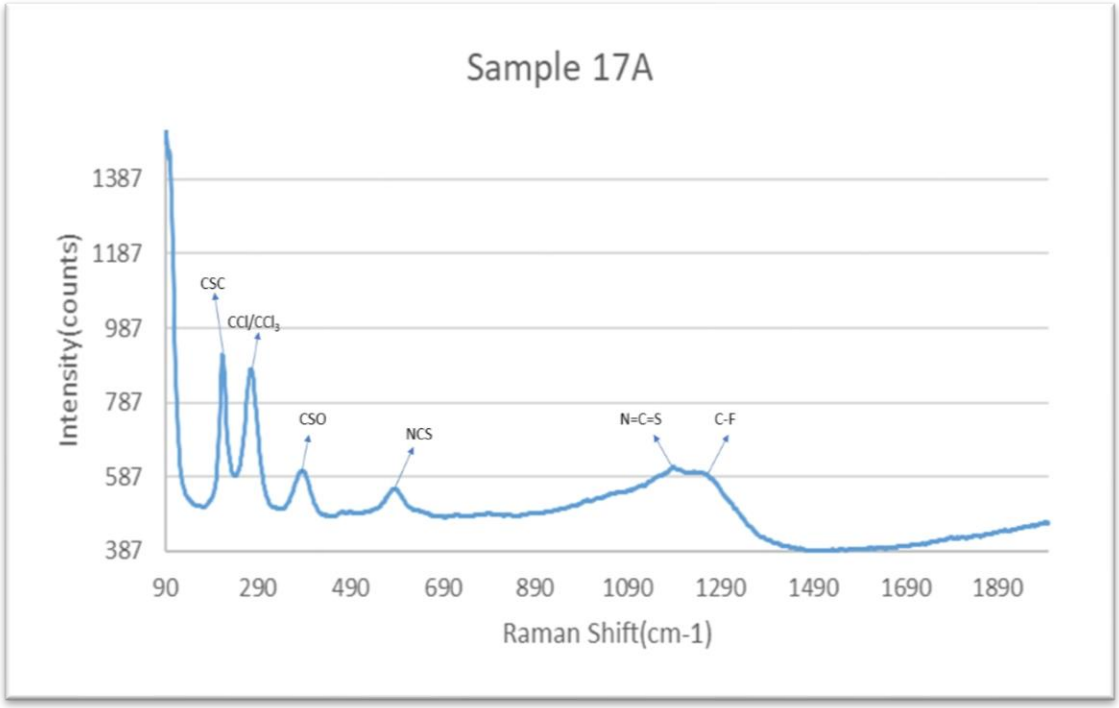
Sample 17A
Intensity(counts)
1387
1187
987
787
587
387
CSC
CCl/CCl3
CSO
NCS
N=C=S
C-F
90
290
490
690
890
1090
1290
1490
1690
1890
Raman Shift(cm-1)

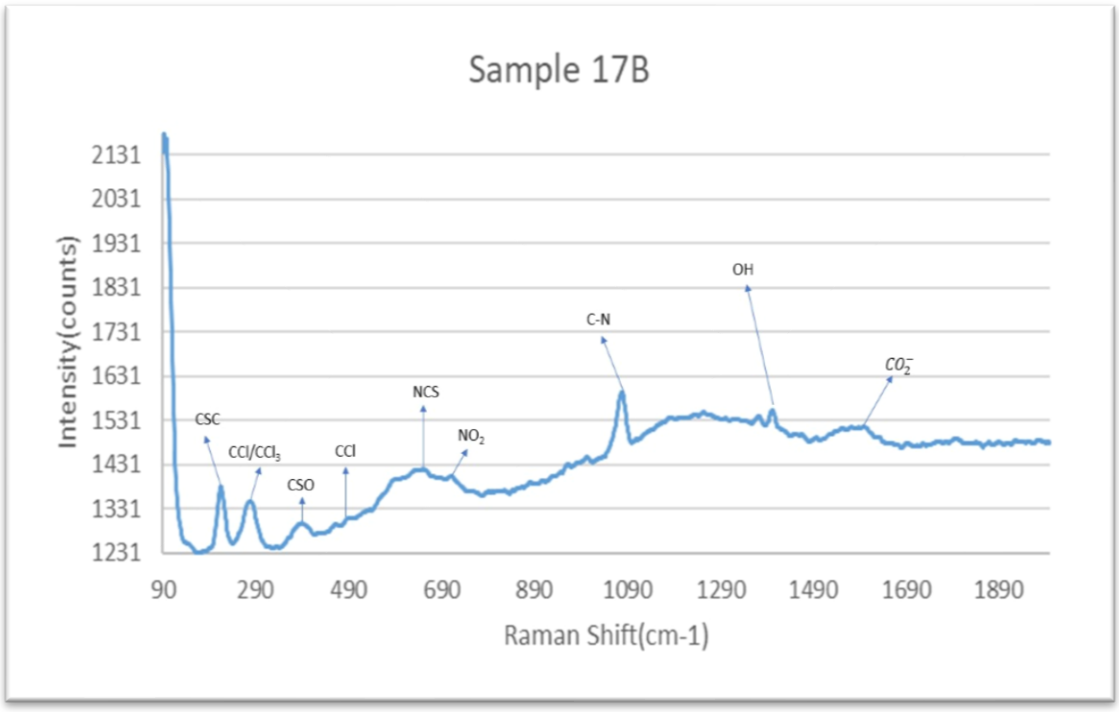
Sample 17B
Intensity(counts)
2131
2031
1931
1831
1731
1631
1531
1431
1331
1231
CSC
CCl/CCl3
CSO
CCl
NCS
NO2
C-N
OH
CO2-
90
290
490
690
890
1090
1290
1490
1690
1890
Raman Shift(cm-1)

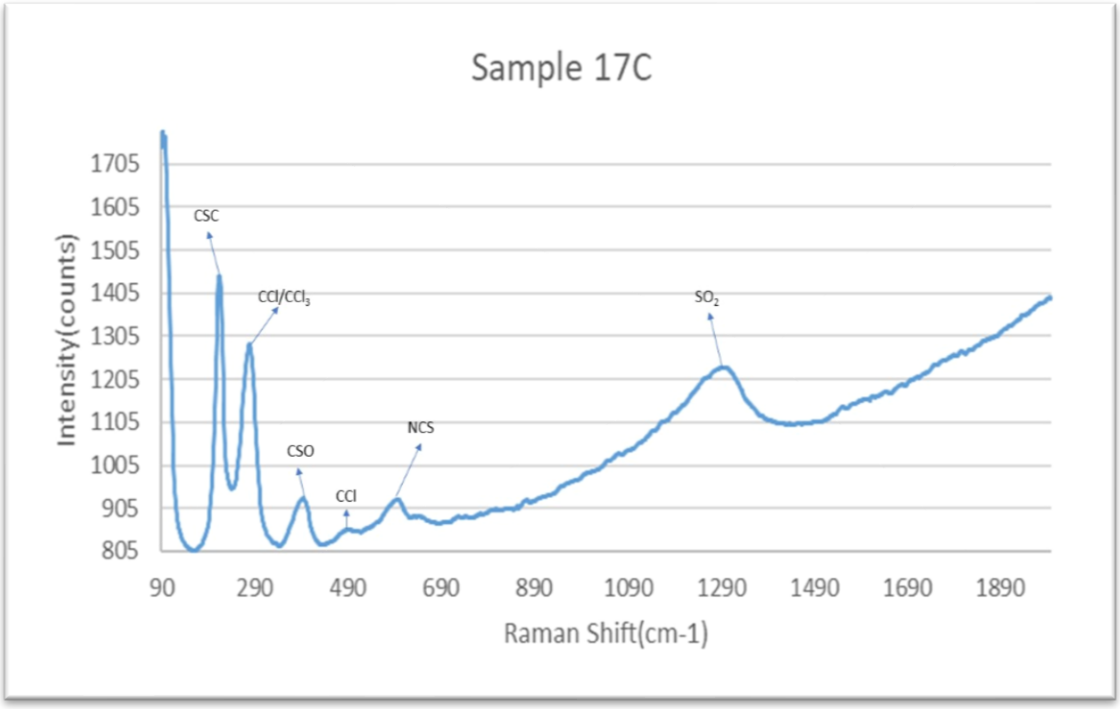

Figure 68. Raman analysis of samples from sample site 17.

All the spectra for the samples from sample site 17 are all different as illustrated in **Figure 68**. Sample 17A has an extra peak at ~1250cm^{-1} carbon fluoride compounds (C-F) next to the commonly identified peak at ~1188cm^{-1} isothiocyanates (N=C=S). Sample 17B has a lot of commonly identified peaks, the different peaks are at ~1078cm^{-1} sulphonyl fluorides (C-N) and ~1530cm^{-1} aromatic acid salts (CO_2^-). Sample 17C is made up of common peaks that have already been previously identified.

pH and Conductivity

Sample Site	Sample	pH	Conductivity(µS)
17	A	9.05	188
	B	9.03	195
	C	9.74	200

Table 39. The pH and conductivity of samples from sample site 17.

Table 39 shows sample site 17 has a basic pH with good conductivity. There is either lot of acid compounds present or a lack of salt corrosion products.

X-Ray Diffraction (XRD)

Sample 17A	Sample 17B	Sample 17C
Iron Sulfide	Iron Silicate	Iron Oxide Hydroxide
Iron Silicate	Iron Sulfate	Potassium Nitrate
Magnesium Silicate Hydroxide	Iron Oxide	Potassium Iron Silicate
Magnesium Silicate	Sulfur	Potassium Amide
Magnesium Titanium Sulfate	Silicon Carbide	Sodium Sulfate
Magnesium Fluoride	Silicon Oxide	Sodium Iron Sulfate
Calcium Carbonate	Aluminum Silicon Oxide	Magnesium Aluminum Silicate
Calcium Aluminum Silicate	Aluminum Silicate	Magnesium Silicide
Calcium Carbonate	Aluminum Manganese	Calcium Carbonate
Silicon Oxide	Aluminum Silicate Hydroxide	Calcium Chloride
Aluminum Oxide	Aluminum Fluoride	Silicon Oxide
Aluminum Silicate	Manganese Oxide	Silicon Carbide
Manganese Oxide	Manganese Fluoride	Manganese Oxide
Manganese Carbonate	Titanium Oxide	Titanium Oxide
Manganese Sulfate	Cadmium Oxide Chloride	Titanium Nitride
Titanium Oxide	Cadmium Sulfate	Ammonium Fluoride
Ammonium Chlorate	Ammonium Cadmium Fluoride	Ammonium Thiocyanate
Ammonium Nitrate	Ammonium Chloride	Hydrazine Sulfate
Ammonium Fluoride	Aniline hydrochloride	p-Aminophenol
Sulfamic Acid	Sulfonyl Amide	1,3,5-Trinitrobenzene

Table 40. XRD analysis of samples from sample site 17.

All the samples have iron and alloy metal corrosion products in **Table 40**. There are two examples of having a high conductivity, samples 17A and 17C both contain salt corrosion products, but they also contain acids. Sample 17A has sulfamic acid and sample 17C has trinitrobenzene. Sample 17B has a high conductivity because it has no salt corrosion products but does have a lot of neutral compounds.

3.7.2:Sample Site 18

Sample site 18 is one of the support pillars right next to sample site 17 as seen in **Figure 14**.

Figure 69. Before(A) and after(B) sampling at sample site 18.

Sample site 18, as seen in **Figure 69** above, is stained with a grey sheen on the underside of the metal plate this could be zinc patina which is an inert form of zinc coating, chemically known as zinc carbonate. The extent of corrosion is not that severe when compared to samples from the old part of the bridge. The types of corrosion that can be observed are intergranular, exfoliation and uniform corrosion.

Scanning Electron Microscope (SEM)

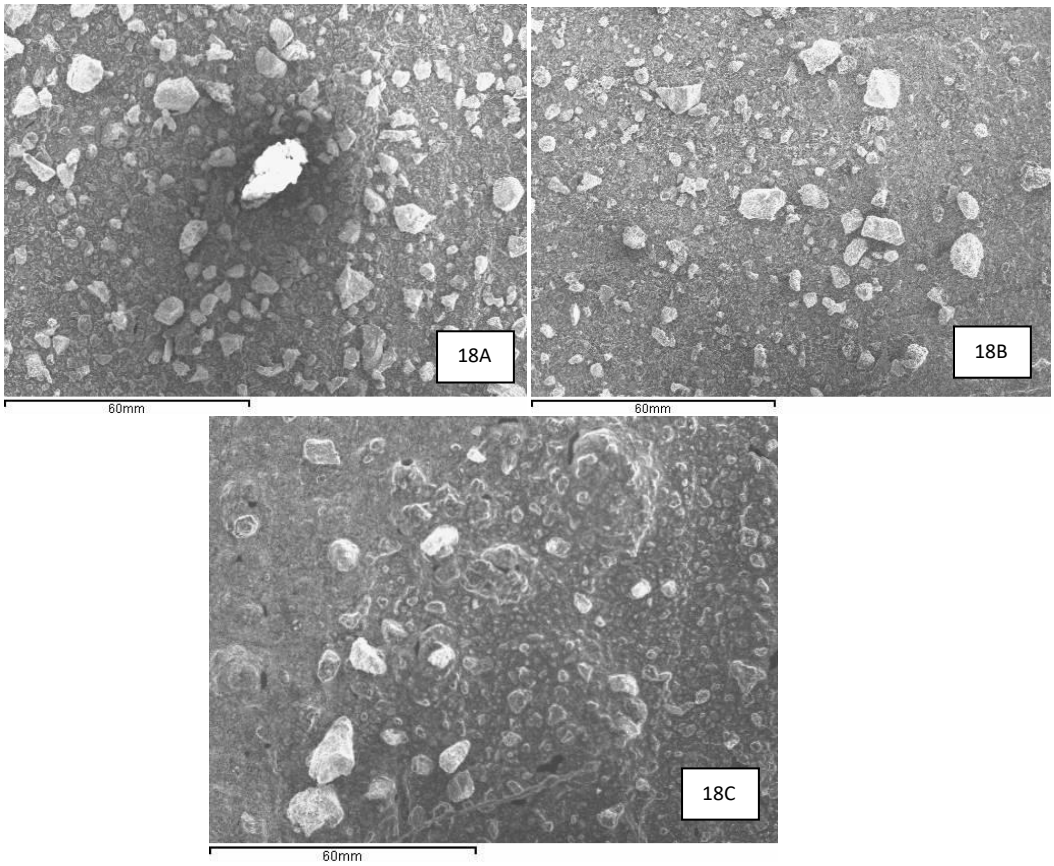

Figure 70. SEM analysis of samples from sample site 18.

The SEM images can be seen in **Figure 70**. All the samples for sample site 18, contain the elements: chlorine, iron, carbon, fluorine, sodium, silicon, cadmium, manganese, magnesium, zinc, calcium, aluminium, titanium and sulfur. Samples 15A and 15C additionally contain potassium.

Raman

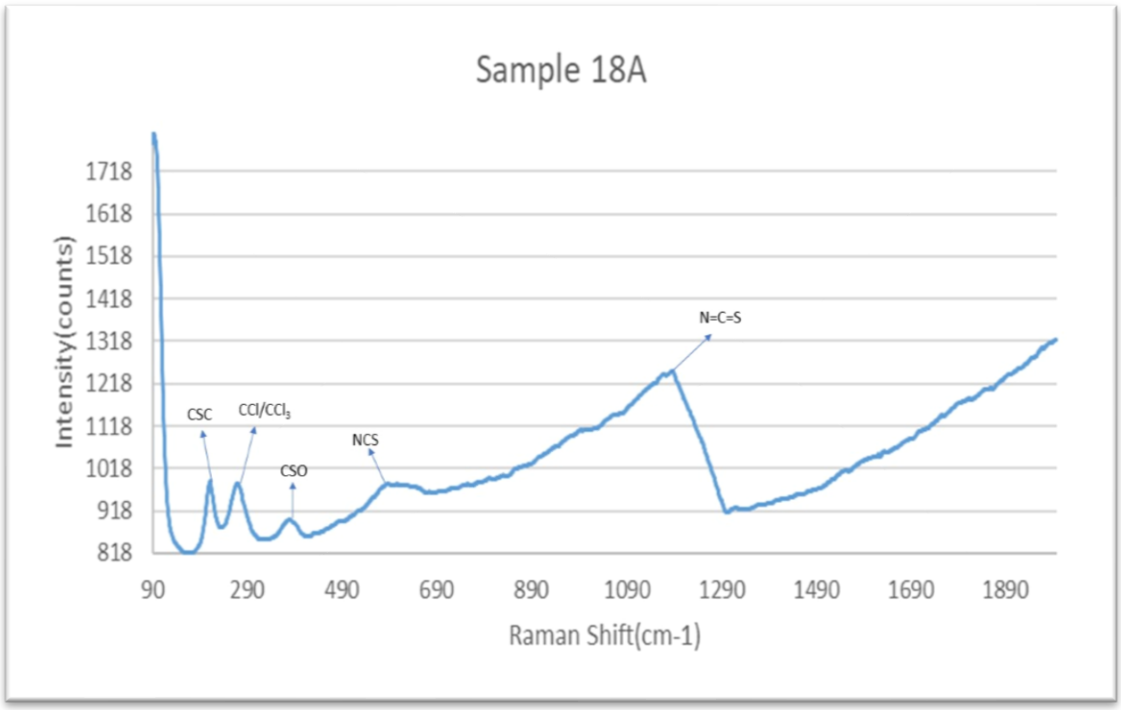
Sample 18A
Intensity(counts)
1718
1618
1518
1418
1318
1218
1118
1018
918
818
CSC
CCl/CCl3
CSO
NCS
N=C=S
90
290
490
690
890
1090
1290
1490
1690
1890
Raman Shift(cm-1)

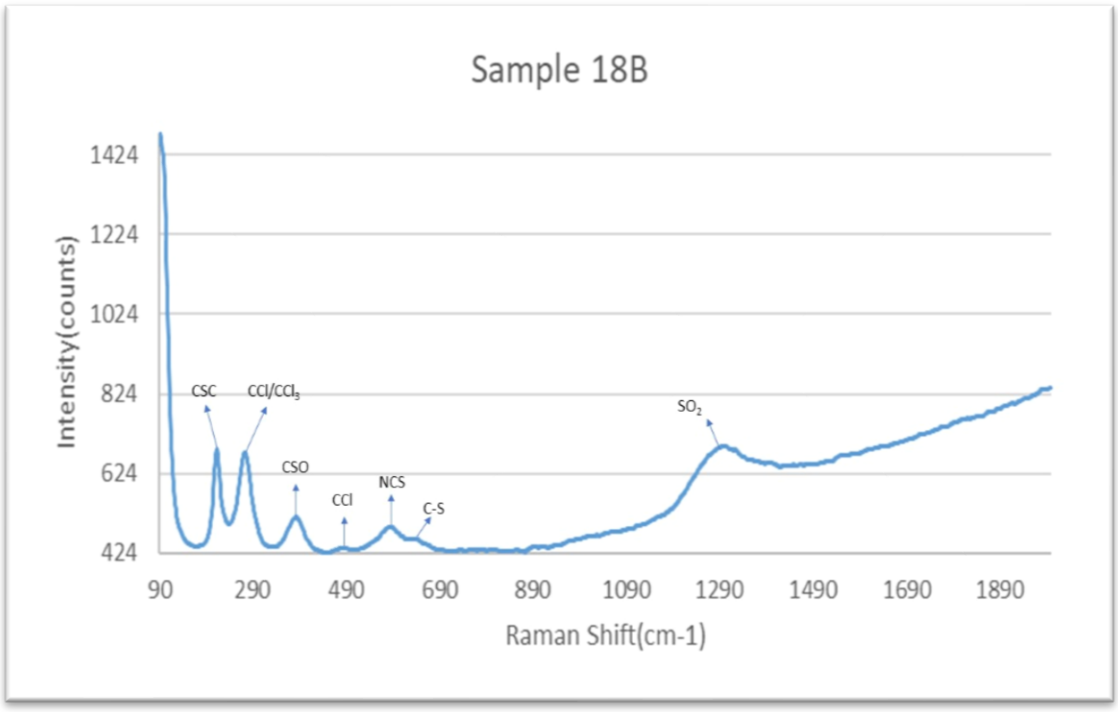
Sample 18B
Intensity(counts)
1424
1224
1024
824
624
424
CSC
CCl/CCl3
CSO
CCl
NCS
C-S
SO2
90
290
490
690
890
1090
1290
1490
1690
1890
Raman Shift(cm-1)

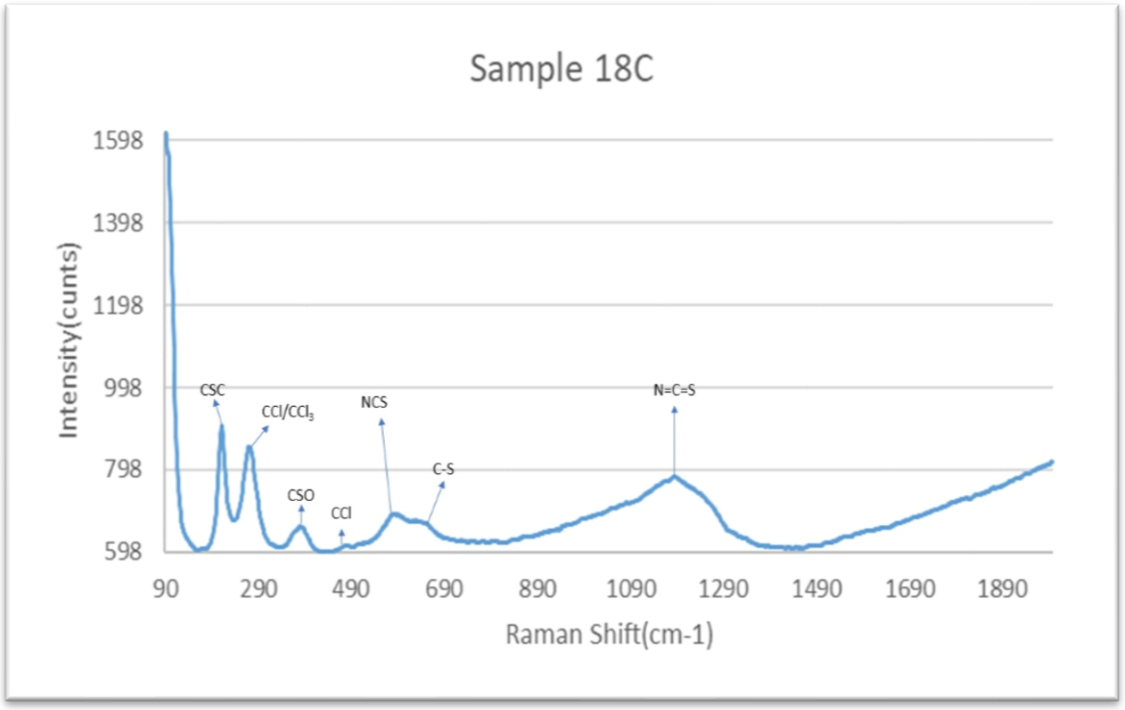

Figure 71. Raman analysis of samples from sample site 18.

The Raman analysis of sample site 18 has already been identified previously in other sample sites. Sample 18A has the worst fluorescence interference out of the samples for sample site 18, the evidence can be seen in **Figure 71**.

pH and Conductivity

Sample Site	Sample	pH	Conductivity(µS)
18	A	8.03	302
	B	8.27	68
	C	7.43	207

Table 41. The pH and Conductivity of samples from sample site 18.

Sample site 18 is a slightly basic sample site overall, with samples A and C having good conductivity. Sample B has very poor conductivity this could be due to a large presence of salts and mineral corrosion products. Samples A and C will have more acidic compounds and less salt corrosion products.

X-Ray Diffraction (XRD)

Sample 18A	Sample 18B	Sample 18C
Iron Oxide	Iron Oxide	Iron Titanium Sulfate
Iron Sulfate	Iron Oxide Hydroxide	Iron Oxide
Potassium Aluminum Silicate	Sodium Hydrogen Sulfate	Iron Sulfide
Potassium Nitrate	Sodium Nitrate	Potassium Magnesium Nitride
Sodium Zinc Silicate	Magnesium Manganese Silicate	Potassium Sulfate
Magnesium Sulfate	Magnesium Iron Silicate	Sulfur Chloride Nitride
Magnesium Fluoride	Calcium Sulfate	Sodium Zinc Sulfate
Magnesium Silicate	Calcium Silicate	Magnesium Titanium Oxide
Magnesium Iron Silicate	Silicon Oxide	Silicon Nitride
Calcium Aluminum Silicate	Zinc Hydroxide	Zinc Oxide
Zinc Hydroxide	Zinc Sulfate	Aluminum Silicate
Zinc Sulfate	Aluminum Oxide	Aluminum Iron Silicate
Aluminum Silicate	Aluminum Hydroxide	Aluminum Manganese
Aluminum Manganese	Aluminum Manganese	Cadmium Sulfate
Manganese Sulfate	Manganese Sulfate	Sulfamic Acid
Titanium Oxide	Titanium Oxide	3,4-Dihydroxy-benzaldehyde
Titanium Nitride	Cadmium Sulfate	D-Sorbitol
3-Chloropropionic acid	Cadmium Manganese Oxide	
2,4,6-Trichlorophenoxy acetic acid	Ammonium Aluminum Hydrogen Chlorate	
	L-Aspartic acid	

Table 42. XRD analysis of samples from sample site 18.

All the samples seen in **Table 42**, contain iron and alloy metal corrosion products. Both samples 18A and 18C have more acidic compounds but both samples also contain a lot of salt corrosion products, sample 18C has less than 18A. The main difference between these two samples is that 18A has no mineral corrosion products, whereas sample 18C has silicon and a neutral compound mix of sulfur chlorine and nitrogen. Sample 18B has an acidic compound of aspartic acid but also contains a lot of salt, mineral and heavy element corrosion products that are likely hindering conductivity.

3.8:Area 8

3.8.1:Sample Site 19

Sample site 19 is located behind the ramps above ground level in the middle of the bridge as seen in **Figure 14**.

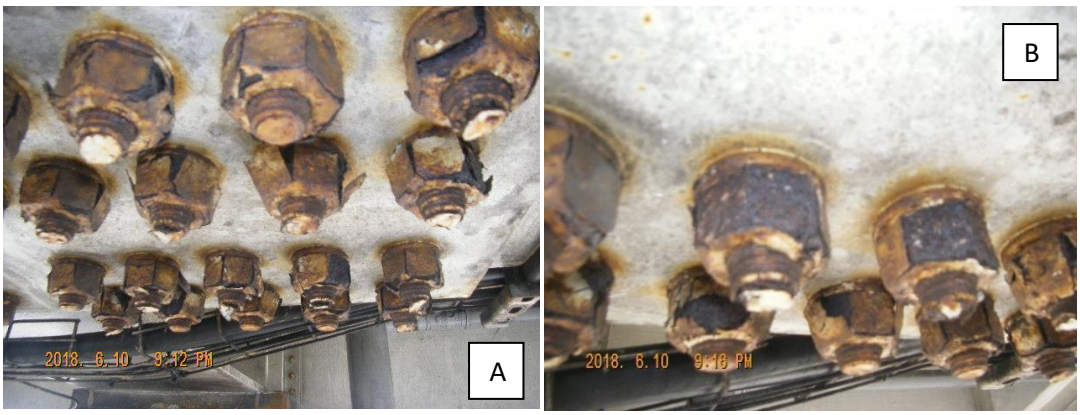

Figure 72. Before(A) and after(B) sampling of sample site 19.

Sample site 19 has severe corrosion on the bolts, as can be seen above in **Figure 72**, the coating is just flaking off the bolts. The metal plate is fine in terms of corrosion, it has the zinc patina's grey sheen to it. The types of corrosion displayed on the bolts are intergranular, filiform and uniform corrosion.

Scanning Electron Microscope (SEM)

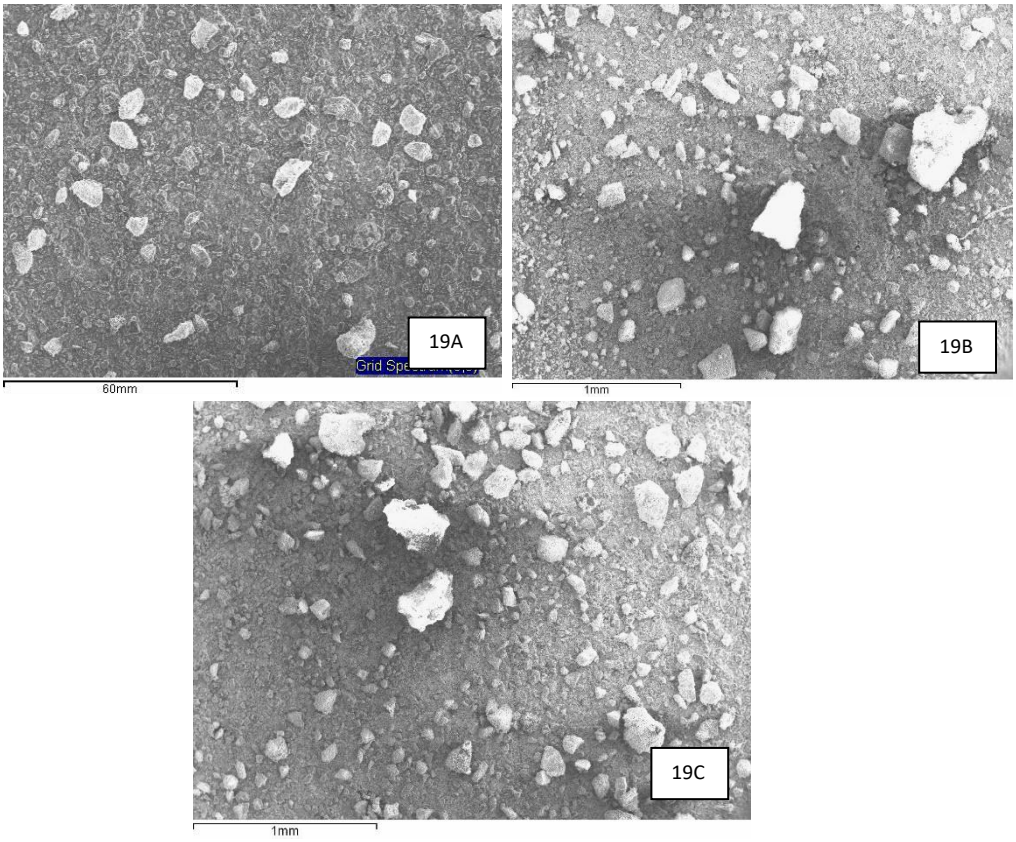

Figure 73. SEM analysis of samples from sample site 19.

The SEM images for site 19 can be seen in **Figure 73**. The elements detected in all the are: chlorine, carbon, iron, sodium, zinc, silicon, manganese, titanium, sulfur, calcium and aluminium. Sample 19A also contains fluorine, cadmium and phosphorus. Sample 19B additionally contains phosphorus, magnesium and barium.

Raman

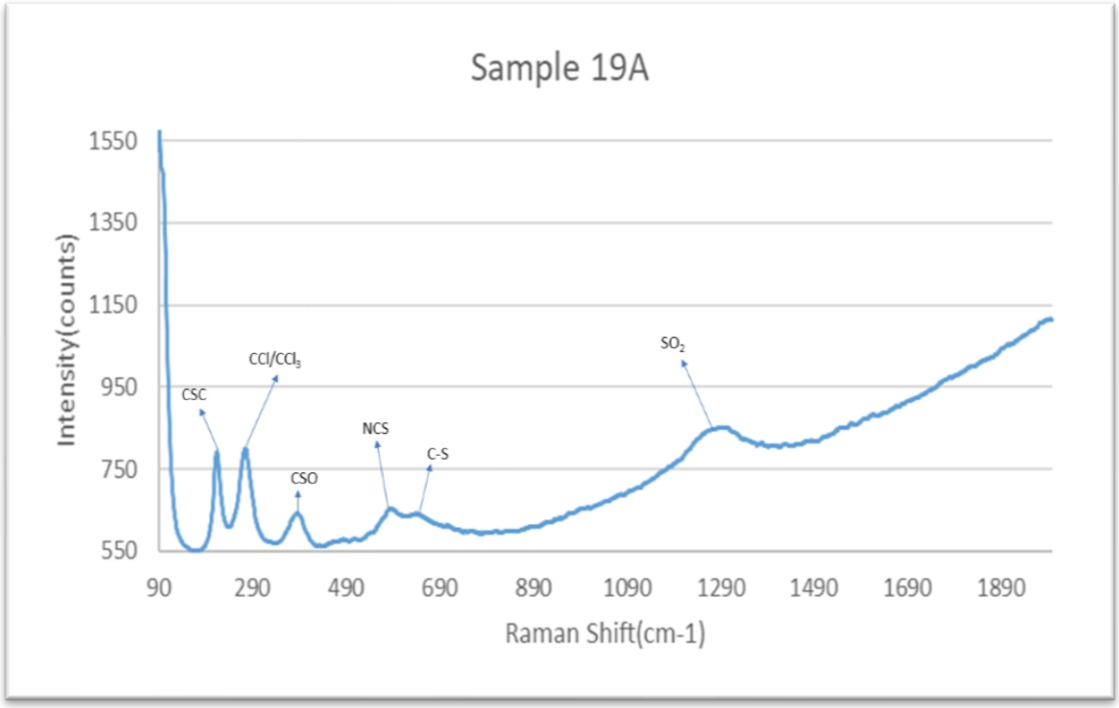
Sample 19A
Intensity(counts)
1550
1350
1150
950
750
550
CSC
CCl/CCl3
CSO
NCS
C-S
SO2
90
290
490
690
890
1090
1290
1490
1690
1890
Raman Shift(cm-1)

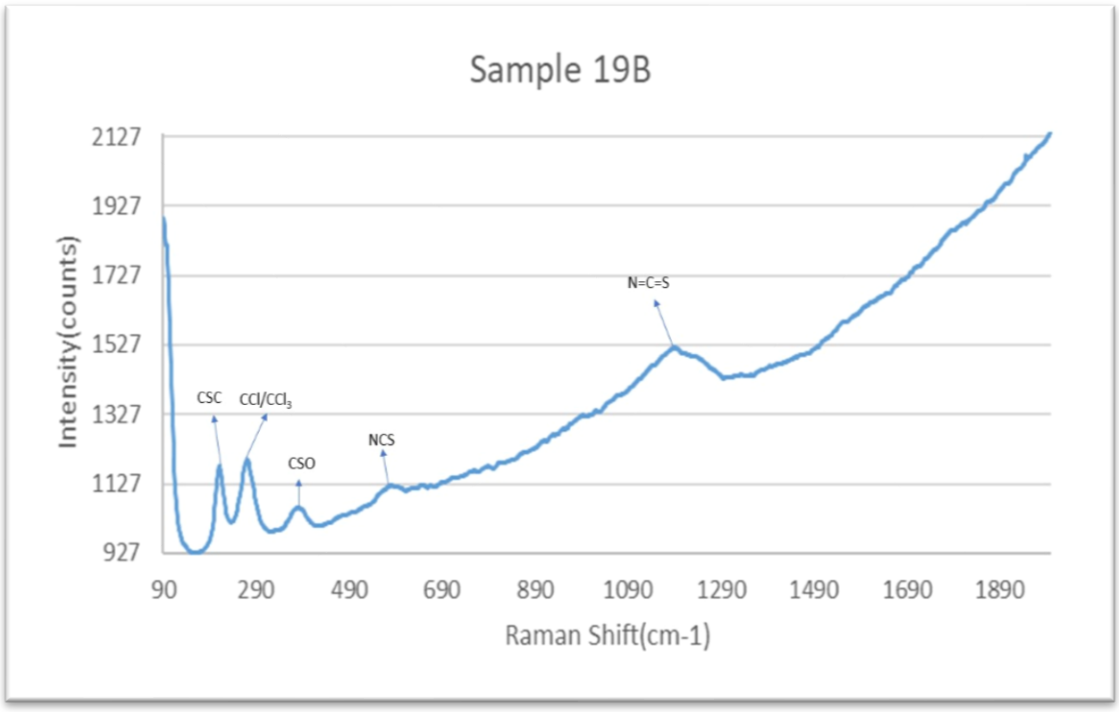
Sample 19B
Intensity(counts)
2127
1927
1727
1527
1327
1127
927
CSC
CCl/CCl3
CSO
NCS
N=C=S
90
290
490
690
890
1090
1290
1490
1690
1890
Raman Shift(cm-1)

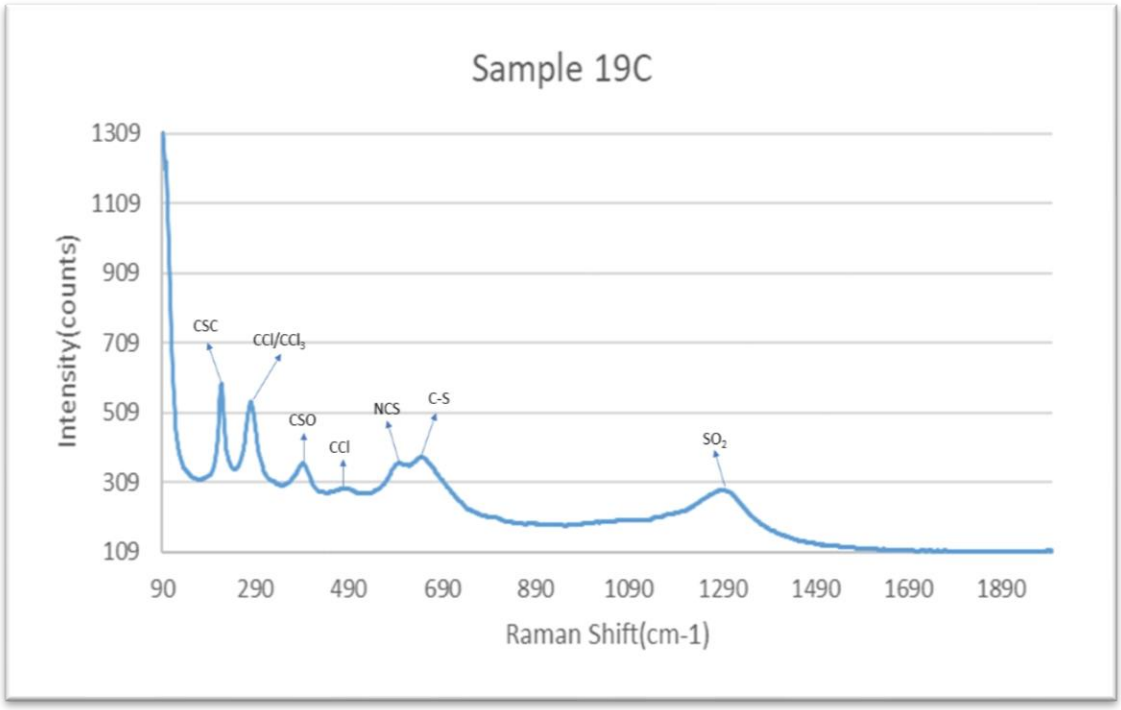

Figure 74. Raman analysis of samples from sample site 19.

The Raman spectra for site 19 are seen in **Figure 74**. The samples contain peaks that have already been identified in previous samples. Sample 19C having very little fluorescent interference and 19A having a little but, sample 19B has a lot of interference.

pH and Conductivity

Sample Site	Sample	pH	Conductivity(µS)
19	A	8.69	194
	B	7.73	324
	C	7.34	269

Table 43. The pH and conductivity of samples from sample site 19.

The pH of sample site 19 is overall slightly basic with good conductivity. Sample 19B having the highest value as seen in **Table 43**. Samples B and C have a neutral pH and a higher conductivity when compared t the more basic sample A.

X-Ray Diffraction (XRD)

Sample 19A	Sample 19B	Sample 19C
Iron Oxide Hydroxide	Iron Oxide Hydroxide	Iron Titanium Oxide
Iron Sulfate	Iron Phosphate	Iron Silicate Oxide
Iron Oxide	Iron Oxide Hydrate	Sodium Sulfide
Iron Phosphate	Sodium Sulfite	Sodium propanoate
Iron Carbonate	Sodium Sulfate	Calcium Sulfite
Sodium Zinc Silicate	Sodium Iron Sulfate	Calcium Chlorate
Sodium Carbonate	Sodium Phosphate	Silicon Oxide
Sodium Hydrogen Sulfate	Sodium Carbonate Hydrate	Zinc Aluminum Sulfide
Calcium Carbonate	Magnesium Silicate	Zinc Oxide Sulfate
Calcium Sulfate	Calcium Silicate	Zinc Carbonate
Calcium Silicate	Silicon Oxide	Aluminum Oxide
Calcium Zinc	Zinc Titanium Oxide	Aluminum Silicate
Silicon Oxide	Zinc Sulfate	Manganese Silicate
Manganese Oxide	Aluminum Oxide	Manganese Sulfate
Manganese Phosphate	Aluminum Silicate	Titanium Oxide
Manganese Oxide Hydroxide	Titanium Oxide	Titanium Nitride
Titanium Oxide	Barium Oxide	Ammonium Oxide Chlorate Hydroxylamine
Cadmium Phosphate	Ammonium Thiocyanate	Fumaric acid
Cadmium Phosphide	Ammonium Chloride	Piperazine adipate
Sulfamic Acid	1,3,5-Tribromobenzene	Glyoxime

Table 44. XRD analysis of samples from sample site 19.

All the XRD results in **Table 44**, have iron and alloy metal corrosion products, acids and salts. Sample 19A has more mineral compounds than the other samples, it also contains more metal and heavy element corrosion products. Sample 19B has the most salt compounds and least in terms of mineral and alloy metal corrosion products. The acidic compound in sample 19B is tribromobenzene. Sample 19C has a good number of mineral compounds and metal corrosion products. This sample contains several organic compounds as well as ammonium oxide chlorate hydroxylamine which is ammonium chlorate as hydroxyl amine is an intermediate compound. The high conductivity in sample 19B can be associated with the fact it has less metal and heavy element corrosion products.

3.8.2:Sample Site 20

Sample site 20 is located right next to sample site 19 on the new part of the bridge, illustrated in **Figure 14**.

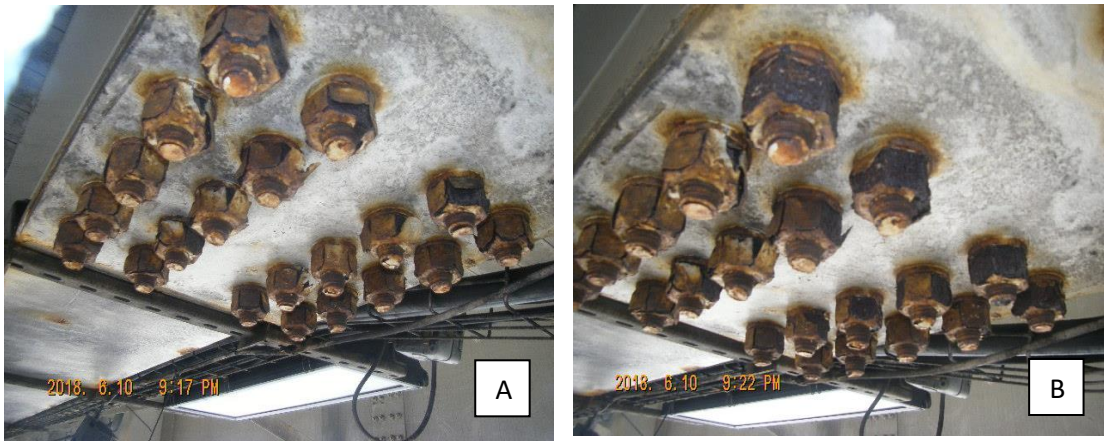

Figure 75. Before(A) and after(B) sampling of sample site 20.

Sample site 20 (**Figure 75**), is very similar to sample site 19, the corrosion on the bolts is reasonable severe but the metal plat itself is just stained in particulates. The types of corrosion are the same, intergranular, filiform and uniform corrosion.

Scanning Electron Microscope (SEM)

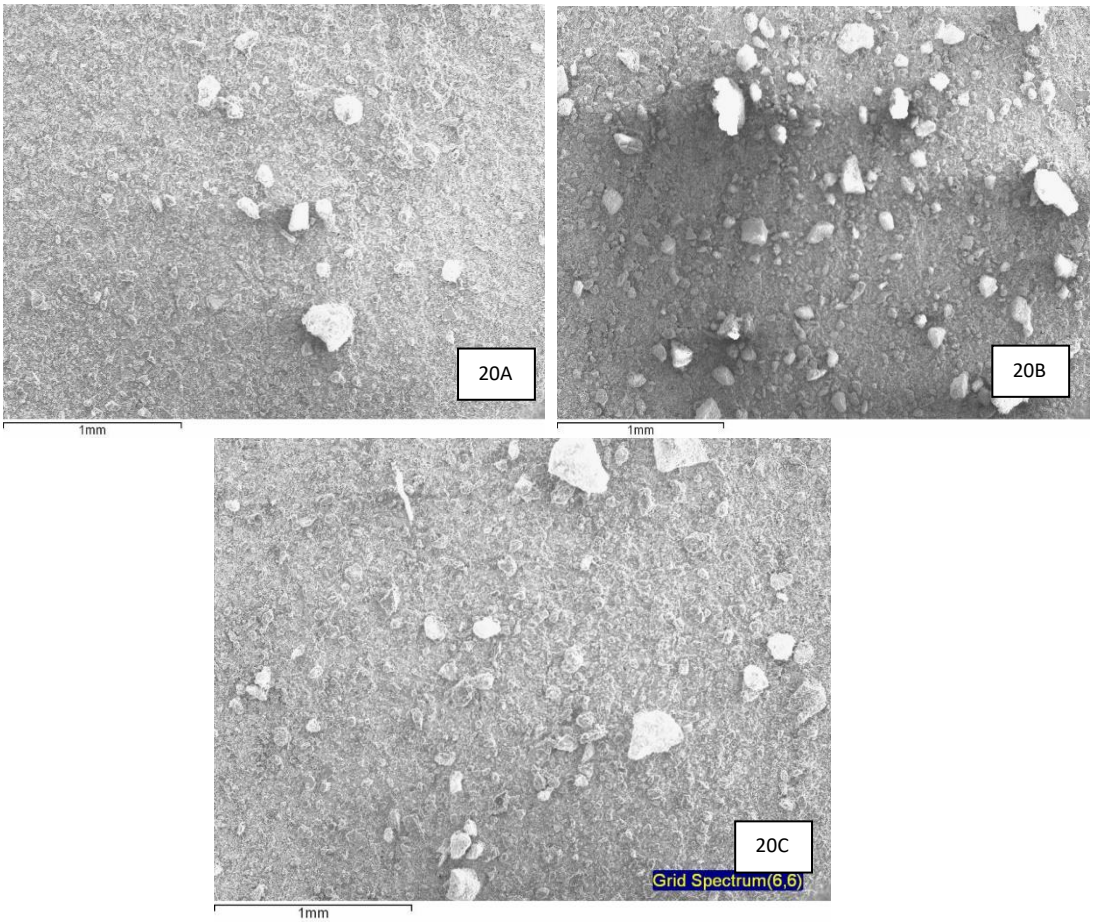

Figure 76. SEM analysis of samples from sample site 20.

The SEM images from site 20 can be seen in **Figure 76**. The samples from sample site 20, all contained the following elements: iron, carbon, silicon, sodium, chlorine, zinc, aluminium, manganese, titanium, calcium and sulfur. Sample 20A also contained magnesium and barium. Sample 20B additionally contained copper, bromine and rubidium. Sample 20C also contained bromine, magnesium, cerium and copper.

Raman

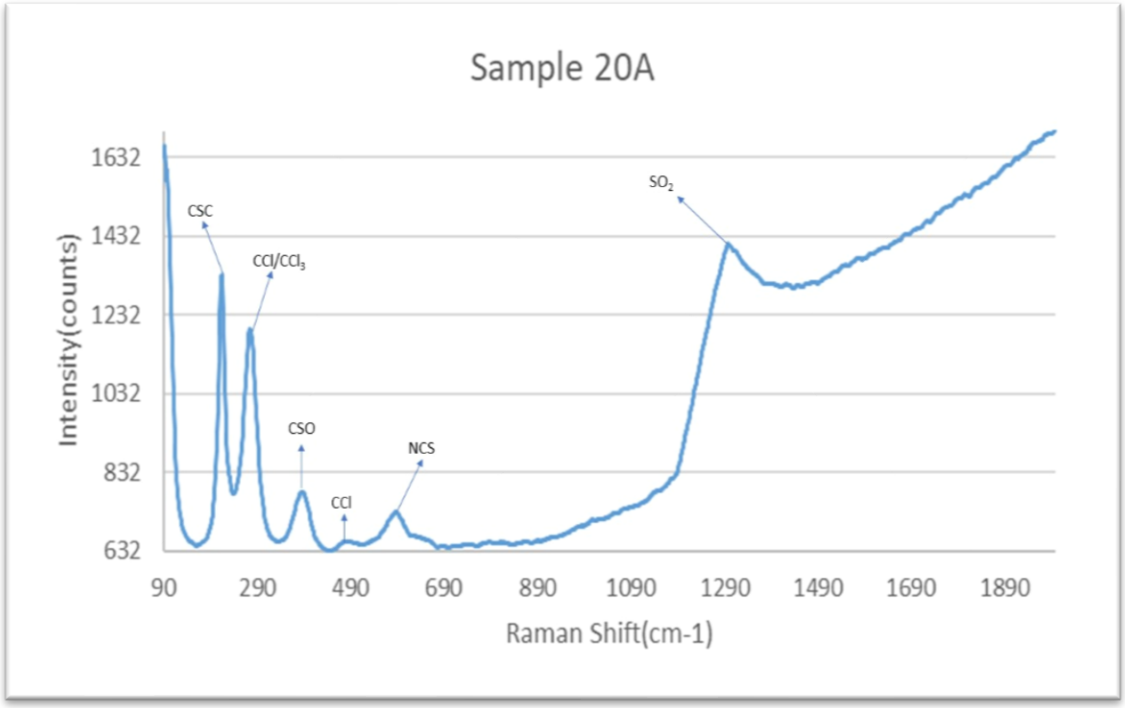
Sample 20A
Intensity(counts)
1632
1432
1232
1032
832
632
CSC
CCl/CCl3
CSO
CCl
NCS
SO2
90
290
490
690
890
1090
1290
1490
1690
1890
Raman Shift(cm-1)

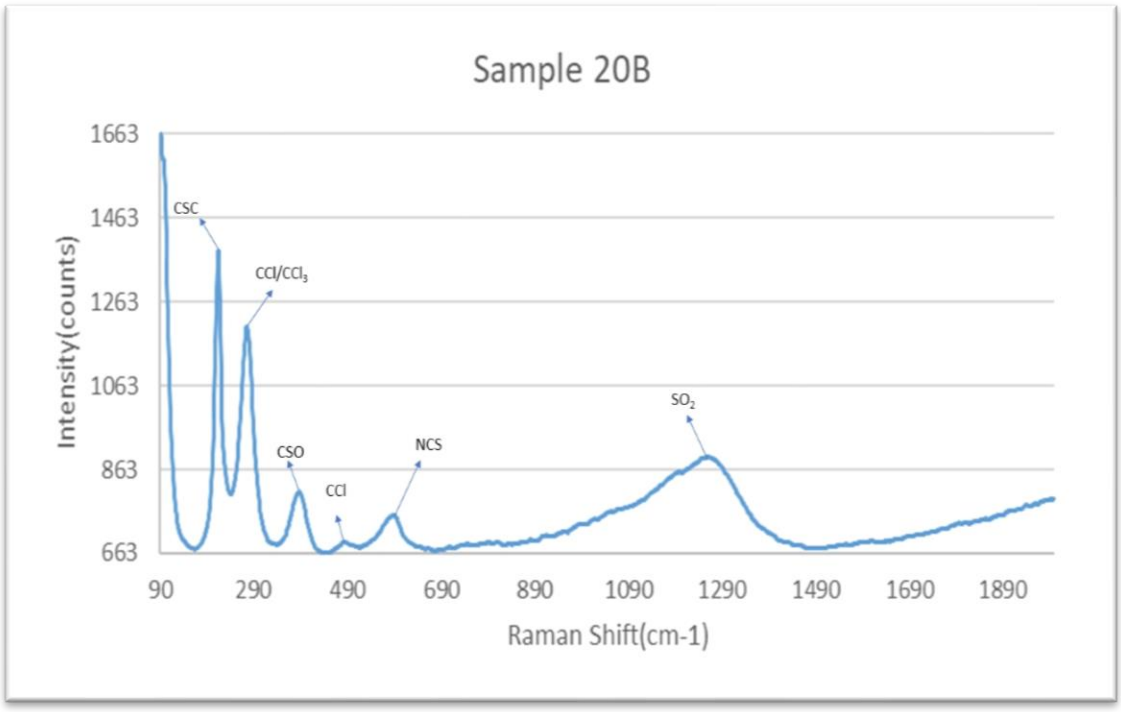
Sample 20B
Intensity(counts)
1663
1463
1263
1063
863
663
CSC
CCl/CCl3
CSO
CCl
NCS
SO2
90
290
490
690
890
1090
1290
1490
1690
1890
Raman Shift(cm-1)

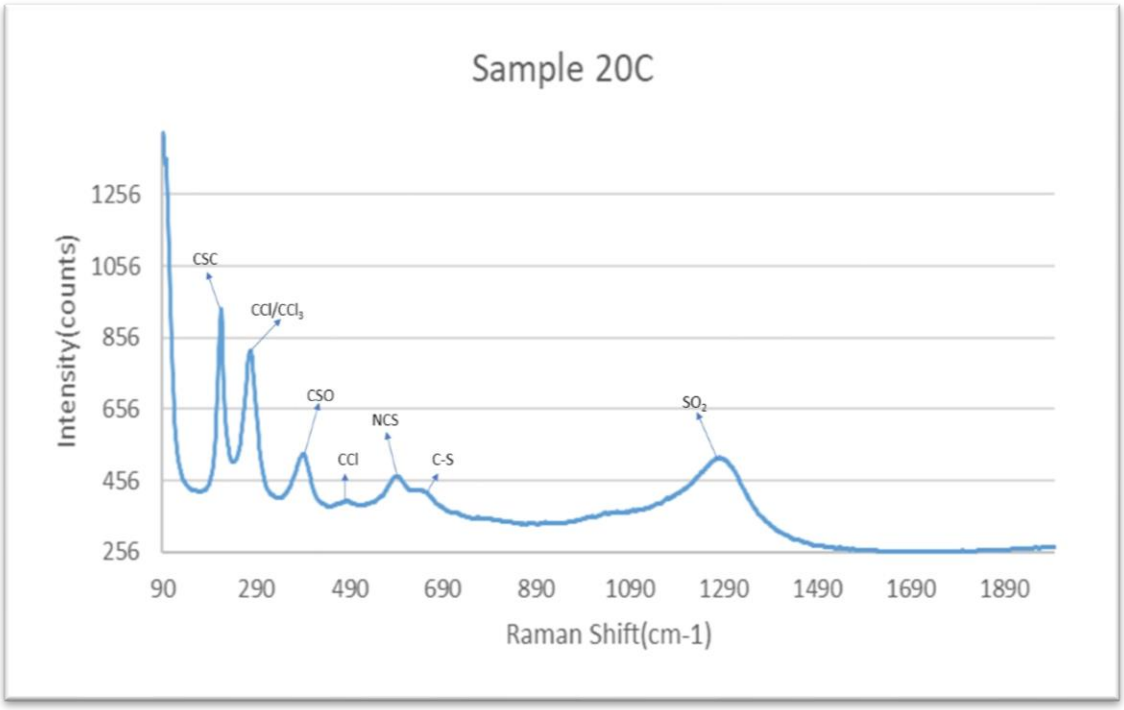

Figure 77. Raman analysis of samples from sample site 20.

All the Raman spectra for sample site 20 shown in **Figure 77**, have already been identified in previous samples. Samples 20B and 20C have very little fluorescence interference when compared to sample 20A.

pH and Conductivity

Sample Site	Sample	pH	Conductivity(μS)
20	A	7.55	420
	B	6.63	200
	C	6.76	330

Table 45. The pH and conductivity of samples from sample site 20.

Sample site 20 is overall slightly acidic in pH, with good conductivity. The conductivity is slightly higher than the other sample sites of the new bridge, the difference is that the pH is acidic instead of basic, which suggests that there will be more acidic compounds in the XRD (**Table 46**) and less salts.

X-Ray Diffraction (XRD)

Sample 20A	Sample 20B	Sample 20C
Iron Oxide Hydroxide	Iron Oxide	Iron Sulfate
Iron Oxide	Iron Sulfate	Sodium Sulfate
Iron Zinc Oxide	Sodium Thiocarbonate Hydrate	Magnesium Silicate
Sodium Sulfate	Sodium Sulfate	Calcium Silicate
Magnesium Sulfate	Sodium Nitrate	Calcium Magnesium Silicate
Calcium Aluminum Silicate	Sodium Zinc Silicate	Calcium Carbonate
Calcium Manganese Oxide	Calcium Silicate	Calcium Sulfate
Calcium Chloride	Calcium Sulfate	Calcium Chlorate
Silicon Oxide	Calcium Silicate	Silicon Oxide
Zinc Sulfate	Silicon Oxide	Zinc Hydroxide
Zinc Hydroxide	Zinc Hydroxide	Zinc Sulfide
Aluminum Oxide	Zinc Sulfate	Zinc Manganese Oxide
Aluminum Manganese	Aluminum Manganese	Aluminum Manganese
Manganese Silicate	Manganese Oxide	Manganese Bromide
Titanium Oxide	Titanium Oxide	Titanium Oxide
Barium Oxide	Copper Iron Oxide	Copper Sulfide
Barium Carbonate	Ammonium Bromide	Ammonium Thiocyanate
Barium Silicate	Rubidium Carbonate	1,3,5-Trinitrobenzene
Ammonium Nitrate	Rubidium Silicate	5-Bromo-2-chloronicotinic acid
Ammonium Chloride	p-Dichlorobromobenzene	

Table 46. XRD analysis of samples from sample site 20.

From the XRD analysis it was concluded that all of the samples in **Table 46** contain iron and alloy metal corrosion products, as well as heavy element compounds. Sample 20A has little in terms of salts and zinc salts but, it does have barium and ammonium corrosion compounds. Sample 20B has the most salt compounds out of the three samples, explaining why its conductivity is low. Sample 20C has the most mineral compounds but also two acids present, proposing that it shows higher conductivity than sample 20B.

Chapter 4:Summary and Discussion

Linking back to the objectives in chapter 1.1, the severity of corrosion described in the results section was identified by the naked eye and characterised using the types of corrosion and loss of metal. The loss of metal can be determined after the sampling. This is particularly true regarding samples from area 1 as this area was the easiest to remove large chunks of corroded metal without any tools. Types of corrosion are an important part in determining the severity of corrosion as some types of corrosion – pitting and stress cracking corrosion – are far more structurally undermining than others and can lead to more rapid failure [8][9]. The map of severity of corrosion is presented in Appendix 1. This map demonstrates that there are no areas with severe corrosion proposing that there are no signs of imminent structural failure. The bridge is corroded and particularly the old parts of the bridge shows signs of a large amount of corrosion products and metal exfoliation. Sample areas 1 and 8 where worse than the others. Area 1, being over a car park and part of the old bridge, it was the easiest area to get samples from. Sample area 8 had serious corrosion around the bolts and is part of the new bridge. This was the main part of the site that had severe corrosion.

As part of the objectives an air monitor (series 500 portable air monitor), was hired to measure the air quality in the Port of Dover in areas selected with the most sever corrosion and one ground level sampling area for comparison. The air monitor had three sensors, one for ozone, one for volatile organic compounds (VOC) and one for sulfur dioxide (SO_2). Unfortunately, due to instrument complications no readings where successfully taken of the air quality in the Port of Dover. The other environmental reading that was measured is pH.

There are many variables that affect corrosion, finding a clear trend is very difficult. In **Figure 79** the pH was compared to the conductivity for each sample site.

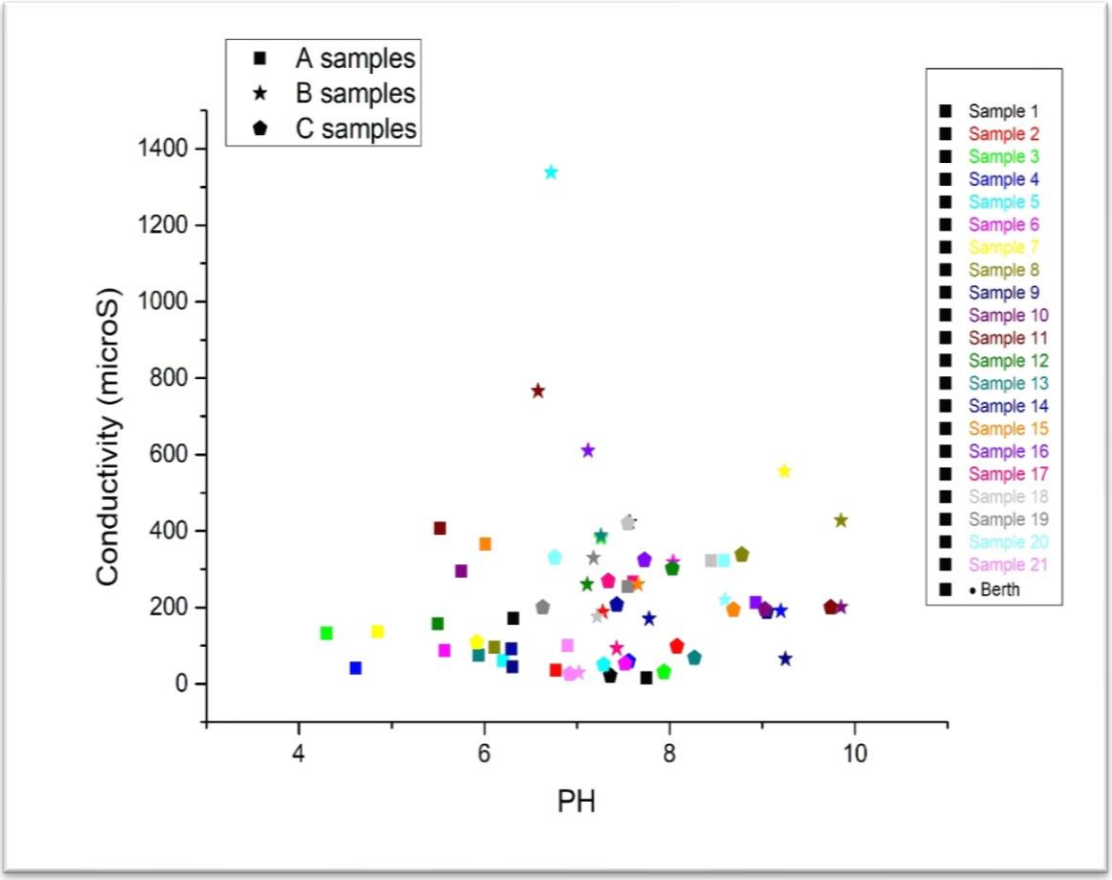

Figure 78. The pH against conductivity for all samples.

As can be seen in **Figure 78**, sample area 1 was quite acidic in general, with samples from the second sample area also having high acidity. The difference is the conductivity with respect to the two areas. The more alkaline samples with high conductivity readings are found in areas of the new part of the elevated bridge. The main differences between the samples from areas 1,2 and samples from the new part of the bridge (sample areas 6,7 and 8 as seen in **Figure 14**) is that: area 1 and 2 are in very high-density traffic zones, area 1 is a car park next to a major road, area 2 is the security gate next to the busiest road of the port and next to the workshop. The new part of the bridge is close to this very busy road, but it is right at the end, so it does not get aa much traffic as the old part of the bridge. This is due to the traffic siphoning off into their respective lanes for the ferry's and port services.

The new part of the bridge is also closer to the sea than the old part of the bridge. This shows when comparing the corrosion products in different areas. All the samples from the new part of the bridge contain ammonia compounds but most of the old part of bridge does not have these compounds.

Appendix 2 shows the variation of pH across the bridge, in the sample areas to give an overview perspective. pH's effect on the rate of corrosion is linked to the conductivity, which is a key component in the rate of degradation. Understanding how pH affects corrosion rate, requires an understanding of the relationship between pH and the corrosion potential, E_c. The current expression for this relationship is (dEc/dpH). However, Hoar and Havenhand found that the slope of the overpotential and logarithm rate for iron in acidic solution was similar to that of a Tafel's line slope. Tomashov carried out the corrosion potential experiment by plotting a series of η (overpotential) – ί (density) relationships for cathodic and anodic polarisations. The intersection of the net cathodic and net anodic currents gave the corrosion potential [75].

Time has played an important factor int eh corrosion rate. The map of severity in Appendix 1 shows that the old part of the bridge has the more severe areas of corrosion. Lastly there is runoff from the top of the bridge that will greatly affect corrosion and the old part of the bridge is again where all the traffic must cross. Showing that the traffic density is different when comparing the old to the new part of the elevated road. Linking back to the objectives **Table 47** below shows a selection of the corrosion products from each sample area.

Area	Severity of Corrosion	Main corrosion products
1 (old part of the bridge)	severe	Iron Oxide, Zinc Sulfate, Barium Chloride, Iron Sulfate, Iron Phosphate
2 (old part of the bridge)	mild	Iron hydroxide, Iron oxide, Magnesium Iron Silicate, Ammonium Nitrate, Octachlorodibenzofuran
3 (old part of the bridge)	mild	Iron Sulfate, Calcium Silicate, Zinc Oxide, Iron Oxide, Calcium Chloride, Titanium Oxide, Cadmium Phosphate, Potassium Aluminum Silicate
4 (old part of the bridge)	severe	Zinc Fluoride, Iron Titanium Oxide, Iron Hydroxide, Iron Sulfide, Copper Phosphate, Cyanuric acid
5 (old part of the bridge)	mild	Polychloroprene, Iron Oxide, Zinc Sulfate, Rubidium Copper Chloride, L-Aspartic acid
6 (new part of the bridge)	mild	Cyanuric acid, Sodium Iron Sulfate Thiodipropionic Acid, Manganese Sulfate
7 (new part of the bridge)	mild	1,3,5-Trinitrobenzene, 2,4,6-Trichlorophenoxy acetic acid, Sulfamic Acid
8 (new part of the bridge)	mild	1,3,5-Tribromobenzene, Barium Carbonate, 1,3,5-Trinitrobenzene

Table 47. Summary of severity and corrosion products from each sample area.

Table 47 contains a quick summary of the important and unique corrosion products found in the sample areas. The corrosion products where picked because they are particular to that sample. As expected, there are some compounds that are consistent in all the samples, which contain the main elements: iron, zinc, aluminium, titanium, molybdenum, manganese, magnesium, calcium, silicon, sulfur, sodium, chlorine and carbon. Therefore, **Table 47** focuses on the compounds that are more unique to their respective areas and are not containing these elements.

The iron, aluminium, titanium, molybdenum and manganese are all part of the alloy that make up steel in the bridge and are elements that are present in all samples. Another element, cadmium is also part of the alloy but in the old part of the bridge there is very little to no cadmium. This may be because over time the old part of the bridge will have had the cadmium in the alloy leached in the corrosion process, or had none, or less cadmium in the steel alloy [20][21]. The main source of cadmium in the samples comes from the new part of the bridge. Another metal that is present in **Table 47** is copper, which may come from cables or pipes.

The calcium and silicon originate from the silica chalk cliffs of Dover. The sulfur and nitrogen come from the nitrous oxides and sulfur oxides produced by vehicles. This is also known as atmospheric pollution. Sodium and chlorine both come from sodium chloride, which is present in sea salt, lastly carbon is found in many places; hydrocarbons from unburned fuel, carbon oxides and carbon particulates from car exhaust fumes.

The heavier elements, barium and rubidium compounds (**Table 47**). Barium is used as a catalyst in a catalytic converter producing barium nitrate, and also used in steel production to reduce NO_x emissions. Rubidium has less applications and so it is difficult to speculate it's origin. Area 5, sample 14C is a ground level sample on the first ramp (**Figure 14**) displays a high presence of rubidium compounds. Area 5 also contains polychloroprene, which is a long chain chlorine containing unsaturated hydrocarbon. This polymer is also referred to a neoprene and is a rubber, which can be derived from car tires [82]. This is specific to this area as it is at ground level.

Ammonium nitrate like phosphate could be coming from fertilisers from farms on the cliffs above, this is the only explanation as to why this compound is present in the corrosion products. The cyanuric and sulfamic acid are both for cleaning, cyanuric acid is typically used in pools and sulfamic acid is a cleaning agent [76][77]. Aspartic acid is used in water treatment products and petroleum production. This compound could have come from any water treatment at the port or residue from vehicle runoff in unburned petrol [81]. Thiodipropionic acid is used in coatings and paints, so it has come from the original coating system [78]. 2,4,6-Trichlorophenoxy acetic acid has got three chlorine leaving groups, influencing the pH and possibly aiding in adsorption of corrosion products.

1,3,5-Trinitrobenzene and 1,3,5-Tribromobenzene may come from benzene that is present in exhaust fumes from vehicles passing through the port. The benzene would have to react with nitrogen dioxide to form 1,3,5-Trinitrobenzene, and bromine to form 1,3,5-Tribromobenzene. Bromine is a good leaving group and could have come from the sea [79]. Both area 7 and 8 are close to the ocean and are directly under the main road to the ferry terminals, making both organic compounds viable in these areas.

How do corrosion compounds affect corrosion? Firstly, there are all kinds of corrosion products. The question that will aid in the understanding of how they affect corrosion is; are they soluble in water? This is because the corrosion process depends on the ion transfer in an aqueous medium, mainly the diffusion of oxygen to form hydroxide ions. The corrosion products in the results have been colour coded to represent the various types of corrosion products:

- Red – iron corrosion products
- Blue – salts
- Purple – zinc salts/corrosion products
- Yellow – aluminium and titanium corrosion products as they could have been part of the alloy or old coating system, it was however determined after research that titanium is part of the alloy complex as it is not used in coating systems. The compound aluminium manganese in sample 9B shows that it is part of the alloy make up.
- Green – manganese and molybdenum as they where known to be part of the alloy make up.
- Black – the positioning of the uncoloured determines what it is in the tables above. Between the salts and alloy metals are the uncoloured minerals that have come most likely from the dover cliffs.

  The other black compounds underneath the alloy corrosion products are a range of organics (acids, hydrocarbons), heavy element compounds (barium, rubidium), other metals (copper, cadmium) and anything else that was uncommonly detected (ammonium corrosion products).

As mentioned in the coating theory some corrosion products can protect the metal underneath and this is utilised in the coating industry. These compounds are insoluble in water and reduce the diffusion of oxygen. Zinc patina otherwise known as zinc carbonate is very unreactive and provides an excellent protective layer [33][34]. However, soluble corrosion products can influence the corrosion rate. An example of this is that in the thin water film, corrosion products can hold a high concentration of iron (Fe) ions in their pores and similarly with chlorine (Cl). In the case of the chloride ions it is explained by the flow of ions from the anode on the metal surface and the cathode reaction on the surface of the corrosion products in the medium, providing conductivity [83].

In terms of solubility many ionic compounds will be soluble in water, including salts, some metal compounds and minerals. Organic compounds are generally not soluble in water as it is a polar solvent and most organic compounds are non-polar.

Linking back to the types of corrosion as seen in the objectives, there is a lot of filiform corrosion, which is a type of crevice corrosion as seen in the results. Typically, this corrosion comes about from micro cracks formed from intergranular corrosion. These types of corrosion are in almost every sample as seen in the results, with the crevice corrosion trapping corrosion products, allowing for more conductivity to take place. This in turn increases the rate of corrosion.

Analysing the Raman spectra in the results, consist entirely of carbon-based compounds. This provides evidence for the theory that the black particulates covering the surface of the bridge are carbon compounds. When studying **Table 47**, with all the hydrocarbon compounds, there is more evidence that it was aiding the adsorption and retention of corrosion products on the surface of the bridge.

Chapter 5:Conclusion

To conclude, the severity of corrosion on the elevated road is not at a critical point where structural failure will occur, but there is corrosion occurring all over the bridge. A mapped version of severity across the bridge at the Port of Dover can be seen in Appendix 1. Where the overview provided utilizes the initial visual analysis of the bridge, and the visual analysis of the sample sites. There is no clear trend in the corrosion products obtained from the analysis of the samples from the old and new part of the bridge, despite the consistency of several compounds. This shows that there are many factors at the Port of Dover affecting the corrosion mechanism and the corrosion products reflect what area of the port the sample sites are located. There is a trend which can be seen in the images for each sample. A clear discoloring and particulate deposition, with the bolts and nuts displaying the worse for wear. The coating and metal peeling away with ease from the bolts. Crevice and uniform corrosion being the most common types of corrosion identified.

Despite being unable to carry out the air monitoring the analysis of the sample using SEM/EDX and XRD have made it possible to determine where the pollutants and corrosive agents are coming from in the Port. With the majority coming from car fumes and unburned petrol.
The main causes of corrosion in this case are: the atmospheric pollution from the heavy traffic and ships, the runoff from the top of the elevated bridge, the humidity and the sea spray. The black particulates are from the car exhausts carbon oxides, which is forming a layer over every surface on the port. This thin layer of carbon particulates is aiding the deposition of harmful corrosion ions, sulfur and chlorine. The carbon is also helping to retain corrosion products, which creates a more aggressive and localized environment allowing for more serious forms of corrosion to occur.

The deposition of heavier elements were also found in the samples via SEM/EDX and XRD. This can be seen in the XRD patterns with the heavier elements being found in rust samples along with acids, ammonia and hydrocarbons. The heavier elements did not show up as much on the SEM/EDX as they did in the XRD, apart from barium and bromine being the most consistent. The SEM/EDX was an excellent technique for providing the elemental make up of each sample showing the elements involved. Raman was used for organic analysis and provided excellent information with almost all the identified compounds being carbon based, additionally these compounds also contained sulfur, fluorine, nitrogen, chlorine and oxygen. Showing that the carbon on the bridge is adsorbing corrosive elements, the most common elements being chlorine and sulfur in a marine industrial port. The oxygen adsorption allows for more diffusion in the reaction and produces more OH^- ions, increasing the rate of the corrosion reaction.

The rate of degradation across the board can be related to the basic pH associated with the environment or the steel alloy. In the results the basic pH samples have a closer average in terms of conductivity. The acidic samples are more varied in terms of conductivity. This is happening to the bridge that is closer to the sea, area 2 is an exception as sample 5 was sheltered from the sea and sample 9 has a slightly acidic sample A with a high conductivity. The rest of the samples have a basic pH and good conductivity. This area is also in one of the most heavily trafficked areas of the port. The new part of the bridge is highly basic and has some acidic areas, but the conductivity is steady and not very high as seen in **Figure 78**.

The elevated sample areas have a greater conductivity basic pH when compared to the sample areas at ground level. There is no clear difference between the ground level and raised sample sites. However, looking at the images of the samples and the varied differences in conductivity and pH between these areas, there is evidence to suggest that the elevated sample areas are corroding at a faster rate.

Conclusively there is a lot of evidence backing the pollution from the heavy traffic being the major cause of the corrosion in the port. There are other elements that have aided this such as the sea spray, which is known for having adverse effects in the degradation of metal structures. Additionally, having seen the Raman data, the carbon particulates on the bridge are able to adsorb corrosive agents and oxygen allowing for an increased diffusion rate.

In order to consider these conditions and reduce any further corrosion, the appropriate protective coating should be selected for a very highly polluted marine/industrial environment.

A duplex system is described as a sacrificial metal applied as the initial coating, possibly done using galvanization would be an ideal situation. Then to have a paint system added on top of the initial layer of sacrificial metal. This system is not feasible of course due to cost and traffic implication in the Port. Instead the recommendation is that, after removing the current rust on the bridge a new paint system should be applied using the arc thermally spraying technique. The paint system recommended is the zinc epoxy/polyurethane paint system. This is a multilayered system using zinc phosphate as the primer before using a zinc epoxy rich layer, until the intermediate layer. Here a mixture of epoxy and micaceous iron oxide is used for further corrosion protection, possibly another layer of epoxy before the addition of the top layer, which is a poly urethane coat to prevent UV light form providing energy to the corrosion reaction.

This paint coating is for the most corrosive of environments and is the most suitable for the Port of Dover. This does not however consider the carbon particulate matter. As a countermeasure for the particulate matter that is produced in the port, a maintenance system should be put in place to reduce buildup of the particulates and, hence, the formation of corrosion products. Cleaning the elevated bridge regularly will aid the prevention of corrosion. The timeline seen below in **Figure 79**, in the future work, illustrates the buildup of corrosion before and after a wash.

Chapter 6:Future Work

There are many directions that can be taken at the end of this project as possible future work. The most obvious research project would be the effect of the particulates has on the deposition of corrosion products, and its knock-on effect on the rate of corrosion. The other direction that this project could be taken is on the environmental side, where extensive environmental monitoring could be done and then looked at to see how to reduce the emissions. Monitoring the rate of particulate deposition with the washing of the bridge structure is another possible future research topic. However, this was not in the scope of this project.

The effect of the particulate matter on corrosion would be a very useful project as it could be used in urban and industrial areas all over the world that have heavy traffic and an issue with particulate matter. Other future projects could also involve:

- Linking traffic density to corrosion rate/particulate formation.
- Cost of washing the bridge versus allowing particulate formation.
- Removing corrosion from the bridge and repainting.
- Future directions regarding coatings/protection from corrosion.
- Steel alloys for future extensions or other buildings within the port.

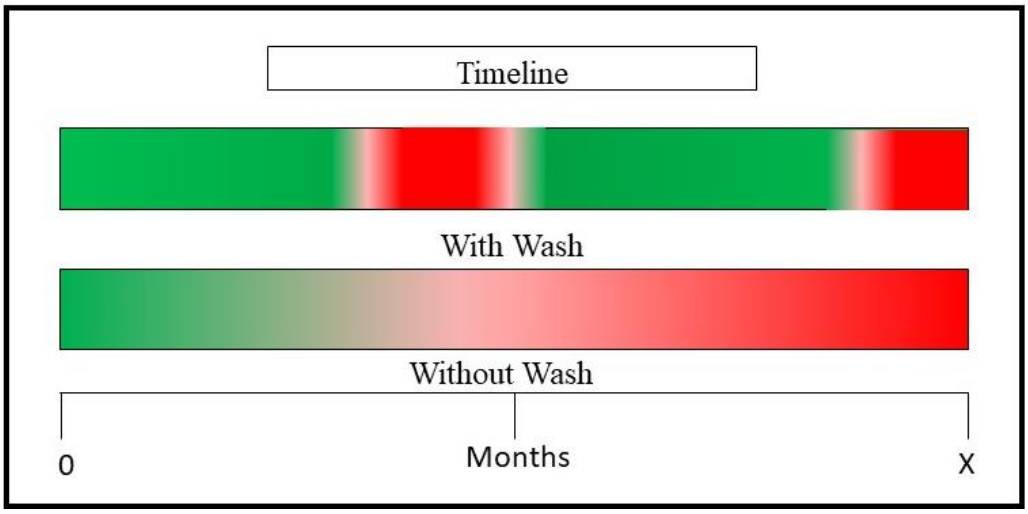

Figure 79. Example timeline of the elevated bridge being washed and without being washed.

Figure 79 is an example of a timeline in which particulate matter forms allowing for more deposition. The key for this figure is green for when there is no particulate matter and red for when there is. This figure is to illistrate the benefit of washing the bridge on a regular basis.

References

[1] Koch, G., Varney, J., Thompson, N., Moghissi, O., Gould, M. and Payer, J. (2016). *International Measures of Prevention, Application, and Economics of Corrosion Technologies Study*. [online] Available at: http://impact.nace.org/documents/Nace-International-Report.pdf [Accessed 28 Aug. 2018].

[2] Trethewey, K. and Chamberlain, J. (1995). *Corrosion for Science and Engineering*. 2nd ed. Essex: Longman.

[3] Paipai, E. (1999). Report SR 554. *Guidelines for Port Environmental Managment*. [online] Available at: http://eprints.hrwallingford.co.uk/843/1/SR554.pdf [Accessed 28 Aug. 2018].

[4] CHAPTER 1. (n.d.). *Introduction to Corrosion and its Prevention*. [online] Available at: http://shodhganga.inflibnet.ac.in/bitstream/10603/79572/10/10_chapter%201.pdf [Accessed 28 Aug. 2018].

[5] Syed, S. (2016). ATMOSPHERIC CORROSION OF MATERIALS. *Emirates Journal for Engineering Research*, [online] 11(1), pp.1-24. Available at: https://www.researchgate.net/profile/Sabir_Syed2/publication/228357453_Atmospheric_corrosion_of_materials/links/53fec0590cf283c3583be465/Atmospheric-corrosion-of-materials.pdf [Accessed 28 Aug. 2018].

[6] A.Shaw, B. and G.Kelly, R. (2006). What is Corrosion?. *The Electrochemical Society*, [online] pp.24-26. Available at: https://www.electrochem.org/dl/interface/spr/spr06/spr06_p24-26.pdf [Accessed 30 Aug. 2018].

[7] Introduction and Overview of Electrochemical Corrosion. (2000). *Fundamentals of Electrochemical Corrosion*. [online] Available at: https://www.asminternational.org/documents/10192/3466254/ACFA9DE.pdf/dcf8d808-336a-4636-aadf-80b7e2092398 [Accessed 30 Aug. 2018].

[8] Bardal, E. (2004). Different Forms of Corrosion Classified on the Basis of Appearence. *Corrosion and Protection*, [online] pp.89-191. Available at: https://link.springer.com/chapter/10.1007%2F978-1-85233-845-9_7#citeas [Accessed 30 Aug. 2018].

[9] Coastal Netting Systems. (n.d.). *Engineered Netting Systems - Steel Pole Manufacturers*. [online] Available at: http://www.polymercompositesinc.com/instructionpdf/STRYK5388PERFORMANCETECHNICALBULLETIN.pdf [Accessed 30 Aug. 2018].

[10] Nimo, B. and Hinds, G. (2003). Beginners Guide to Corrosion. [online] Available at: https://www.pipekala.com/Content/images/pages/daneshname/corrosion2.pdf [Accessed 30 Aug. 2018].

[11] Stansbury, E. and Buchanan, R. (2000). *Fundamentals of electrochemical corrosion*. Materials Park, Ohio: ASM International, pp.271-332. [ONLINE] Available at: http://dl.iran-mavad.com/pdf95/Fundamentals%20of%20Electrochemical%20Corrosion_iran-mavad.com.pdf [Accessed 20 Aug. 2018].

[12] Callister, W. and Rethwisch, D. (2013). *Materials science and engineering*. Wiley, pp.76-107. [ONLINE] Available at: http://www.mse.berkeley.edu/groups/morris/MSE205/Extras/defects.pdf [Accessed 30 Aug. 2018].

[13] Zhang, X. (2011). *Galvanic Corrosion*. Ontario: Wiley, pp.123-143. [ONLINE] Available at: file:///C:/Users/Kieran%20Scobbie/Downloads/Galvaniccorrosion.pdf [Accessed 30 Aug. 2018].

[14] Bimetallic Corrosion. (1982). *Guide to Good Practice in Corrosion Control*. [online] Available at: http://www.npl.co.uk/upload/pdf/bimetallic_20071105114556.pdf [Accessed 30 Aug. 2018].

[15] Gerasimov, V. and Rozenfeld, I. (1957). Thermogalvanic Corrosion. *Russian Chemical Bulletin*, 6(1), pp.29-31.

[16] Salam, A. and Makhlouf, H. (2015). Intelligent Stannate-Based Coatings of Self-Healing Functionality for Magnesium Alloys. *Intelligent Coatings for Corrosion Control*, pp.537-555.

[17] Rashidi, N., Alavi-Soltani, S. and Asmatulu, R. (2007). Crevice Corrosion Theory, Mechanisms and Prevention Methods. *Proceedings of the 3rd Annual GRASP Symposium*, [online] pp.215-216. Available at: https://soar.wichita.edu/bitstream/handle/10057/917/grasp%20216.pdf?sequence=1 [Accessed 30 Aug. 2018].

[18] Gowda, S. (2016). MULTI-SCALE EFFECTS OF CORROSION ON STEEL STRUCTURES. [online] Available at: https://etd.ohiolink.edu/!etd.send_file?accession=akron1469007207&disposition=inline [Accessed 30 Aug. 2018].

[19] Frankel, G. (1998). Pitting Corrosion of Metals A Review of the Critical Factors. *Journal of the Electrochemical Society*, [online] 145(6), pp.2186-2198. Available at: https://pdfs.semanticscholar.org/85ee/a0856f78d89a54ce34539c0f857dae54d43a.pdf [Accessed 30 Aug. 2018].

[20] Han, Z., He, Y., Lin, H. and Zhao, H. (2000). Dealloying characterizations of Cu-Al alloy in marine environment. *JOURNAL OF MATERIALS SCIENCE LETTERS*, [online] 19, pp.393-395. Available at: https://link.springer.com/content/pdf/10.1023/A:1006782519836.pdf [Accessed 30 Aug. 2018].

[21] Zhang, Y. (2009). Dezincification and Brass Lead Leaching in Premise Plumbing Systems: Effects of Alloy, Physical Conditions and Water Chemistry. [online] Available at: https://vtechworks.lib.vt.edu/bitstream/handle/10919/36280/Zhang_Y_T_2009.pdf?sequence=1 [Accessed 30 Aug. 2018].

[22] Birbilis, N. and Hinton, B. (2011). Corrosion and Corrosion protection of Aluminium. *Fundamentals of Aluminium Metallurgy*, pp.574-604.

[23] Frayne, C. (2010). Environmental Modification for Cooling, Heating and Potable Water Systems. *Materials Science and Materials Engineering*, 4, pp.2930-2970.

[24] Ganz, S. (2012). Cavitation: Causes, Effects, Mitigation and Application. [online] Available at: https://pdfs.semanticscholar.org/5518/7741e98014397b8a9b3de2645fc30513d4a3.pdf [Accessed 30 Aug. 2018].

[25] Schijve, J. (2001). *Fatigue of structures and materials*. Boston, MA: Kluwer Academic, pp.363-380. [Online] Available at: https://archive.org/details/springer_10.1007-0-306-48396-3 [Accessed 30 Aug. 2018].

[26] Stress Corrosion Cracking. (1982). *Guides to Good Practice in Corrosion Control*. [online] Available at: http://www.npl.co.uk/upload/pdf/stress.pdf [Accessed 30 Aug. 2018].

[27] Larossa, N., Akid, R. and Ainsworth, R. (2017). Corrosion-fatigue: a review of damage tolerance models. *International Materials Reviews*, [online] pp.283-308. Available at: https://www.tandfonline.com/doi/pdf/10.1080/09506608.2017.1375644?needAccess=true [Accessed 30 Aug. 2018].

[28] Natesan, M., Selvaraj, S., Manickam, T. and Venkatachari, G. (2008). Corrosion behavior of metals and alloys in marine-industrial environment. *Science and Technology of Advanced Materials*, [online] 9(4). Available at: https://www.ncbi.nlm.nih.gov/pmc/articles/PMC5099644/ [Accessed 30 Aug. 2018].

[29] Knotkova, D. and Kreislova, K. (2007). Corrosivity of atmospheres – derivation and use of information. *Transactions on State of the Art in Science and Engineering*, [online] 28, pp.73-105. Available at: https://www.witpress.com/Secure/elibrary/papers/9781845640323/9781845640323003FU1.pdf [Accessed 30 Aug. 2018].

[30] Steelconstruction.info. (2018). *Standard corrosion protection systems for buildings*. [online] Available at: https://www.steelconstruction.info/Standard_corrosion_protection_systems_for_buildings [Accessed 30 Aug. 2018].

[31] Iso 12944 8 1998 en paints and varnishes corrosion. (n.d.). [online] Available at: https://pdfentity.co/downloads/iso_12944_1.pdf [Accessed 30 Aug. 2018].

[32] Coating for the Protection of Structural Steelwork. (1982). *Guides to Good Practice in Corrosion Control*. [online] Available at: http://www.npl.co.uk/upload/pdf/steelwork.pdf [Accessed 30 Aug. 2018].

[33] A Comparative Analysis of Process and Performance Characteristics. (n.d.). *ZINC COATINGS*. [online] Available at: https://galvanizeit.org/uploads/publications/Zinc_Coatings.pdf [Accessed 30 Aug. 2018].

[34] In the Atmosphere, Soil, Water, Concrete, and More. (2010). *Performance of Hot-Dip Galvanized Steel Products*. [online] Available at: https://galvanizeit.org/uploads/publications/Performance_of_Galvanized_Steel_Products.pdf [Accessed 30 Aug. 2018].

[35] Thermally Sprayed Metal Coatings. (n.d.). *The Steel Construction Institute*. [online] Available at: http://file:///C:/Users/Kieran%20Scobbie/Downloads/GN_8-04-secure%20(1).pdf [Accessed 30 Aug. 2018].

[36] Hot Dip Galvanizing and Corrosion Categories. (n.d.). *Nordic Glavanizers*. [online] Available at: http://www.nordicgalvanizers.com/Frontpage%20links/documents/Corrcat_000.pdf [Accessed 30 Aug. 2018].

[37] Paints and varnishes -- Corrosion protection of steel structures by protective paint systems -- Part 2: Classification of environments. (2011). *ISO 12944-2:2017*, [online] (2). Available at: https://www.iso.org/standard/64834.html [Accessed 30 Aug. 2018].

[38] Hot-Dip Galvanising for Corrosion Protection a specifiers guide. (2012). *American Galvanizers Association*. [online] Available at: https://galvanizeit.org/uploads/publications/Galvanized_Steel_Specifiers_Guide.pdf [Accessed 30 Aug. 2018].

[39] HOT DIP GALVANIZED COATING PROCEDURE. (2008). *SANG CHAREON HOT DIP GALVANIZE COMPANY LIMITED*. [online] Available at: http://www.sangchareongroup.com/images/brochure/Brochure.pdf [Accessed 30 Aug. 2018].

[40] THE GALVANIZING PROCESS. (n.d.). *ACME*. [online] Available at: http://www.acmegalv.com/pdfs/THE-GALV-PROCESS.pdf [Accessed 30 Aug. 2018].

[41] Hot-Dip Galvanizing For Corrosion Protection of Steel Products. (n.d.). *AZZ Galvanizing*. [online] Available at: https://www.azz.com/sites/default/files/AZZ%20Galvanzing%20Overview.PDF [Accessed 30 Aug. 2018].

[42] Metal-spray.co.nz. (2018). *Coatings Guide for Thermal Spray Corrosion Protection*. [online] Available at: http://www.metal-spray.co.nz/technical/coating-guide/ [Accessed 30 Aug. 2018].

[43] Galvanizers Association. (2018). *Galvanizing Process Hot Dip Steel Galvanising Process UK Ireland*. [online] Available at: https://www.galvanizing.org.uk/galvanizing-process/ [Accessed 30 Aug. 2018].

[44] Malone, J. (1992). Painting Hot Dipped Galvanised steel. *Materials Performance*, [online] 31(5), pp.39-42. Available at: https://galvanizeit.org/uploads/publications/Painting_Galvanized_Steel_Malone.pdf [Accessed 30 Aug. 2018].

[45] Malek, M., Saad, N., Abas, S. and Shah, N. (2013). Thermal Arc Spray Overview. *Materials Science and Engineering*, 46.

[46] Slip and Creep of Thermal Spray Coatings. (2014). *Federal Highway Administration*. [online] Available at: https://www.fhwa.dot.gov/publications/research/infrastructure/structures/bridge/14083/14083.pdf [Accessed 30 Aug. 2018].

[47] Mandeno, W. (2012). THERMAL METAL SPRAY: SUCCESSES, FAILURES AND LESSONS LEARNED. *Opus International Consultants*. [online] Available at: http://www.metal-spray.co.nz/files/3214/4364/6911/CP12_Paper_Mandeno.pdf [Accessed 30 Aug. 2018].

[48] Corrosion protection of steel bridges. (2015). *Corus Construction & Industrial*. [online] Available at: http://resource.npl.co.uk/docs/science_technology/materials/life_management_of_materials/publications/online_guides/pdf/protection_of_steel_bridges.pdf [Accessed 30 Aug. 2018].

[49] Devasahayam, S. (2006). Towards improving wet-adhesion in a metal oxide-polymer coating system. *Journal of Applied Polymer Science*. [online] Available at: https://onlinelibrary.wiley.com/doi/pdf/10.1002/app.22759 [Accessed 30 Aug. 2018].

[50] Painting over Hot-Dipped Galvanised Steel. (2012). *Duplex Systems*. [online] Available at: http://daamgalvanizing.com/wp-content/uploads/2015/12/Paint_Over_Galvanized_Steel_Duplex_Systems2012.pdf [Accessed 30 Aug. 2018].

[51] Davison, B. and Owens, G. (1992). *Steel Designers' Manual: The Steel Construction Institute*. Oxford: Wiley, pp.1041-1042. [Online] Available at: https://books.google.co.uk/books?id=mb-60WSlb5sC&pg=PA1041&lpg=PA1041&dq=One-pack+chemical+resistant+paints+(e.g.+acrylated+rubbers+or+vinyls)&source=bl&ots=bi1TASmNm-&sig=WW6L0uGT2-q8Se1HZcttRnsvXvk&hl=en&sa=X&ved=0ahUKEwjV2d73t7XcAhUJPFAKHXqzAxYQ6AEILDAB#v=onepage&q=One-pack%20chemical%20resistant%20paints%20(e.g.%20acrylated%20rubbers%20or%20vinyls)&f=false [Accessed 30 Aug. 2018].

[52] Tang, Y., Cao, J., Qu, S., Quan, L., Zhao, X. and Zuo, Y. (2018). Degradation of a High Build Epoxy Primer/Polyurethane Composite Coatings under Cyclic Wet–dry Conditions. *International Journal of Electrochemical Science*, [online] 13, pp.3874 – 3887. Available at: http://www.electrochemsci.org/papers/vol13/130403874.pdf [Accessed 30 Aug. 2018].

[53] SELECTION OF PAINT SYSTEM. (2018). *Material Selection*. [online] Available at: https://www.bca.gov.sg/Professionals/Iquas/gpgs/Painting/PMaterialSelect.pdf [Accessed 30 Aug. 2018].

[54] Wang, H., Wang, Y., Liu, D., Sun, Z. and Wang, H. (2014). Effects of Additives on Weather-Resistance Properties of Polyurethane Films Exposed to Ultraviolet Radiation and Ozone Atmosphere. *Journal of Nanomaterials*. [online] Available at: https://www.hindawi.com/journals/jnm/2014/487343/ [Accessed 30 Aug. 2018].

[55] Rashvand, M., Ranjbar, Z. and Rastegar, S. (2011). Nano zinc oxide as a UV-stabilizer for aromatic polyurethane coatings. *Progress in Organic Coatings*, 71(4), pp.362-368.

[56] Singh, R., Tomer, N. and Bhadraiah, S. (2001). Photo-oxidation studies on polyurethane coating: effect of additives on yellowing of polyurethane. *Polymer Degradation and Stability*, 73(3), pp.443-446.

[57] Nichols, M. and Gerlock, J. (2000). Rates of photooxidation induced crosslinking and chain scission in thermoset polymer coatings II. Effect of hindered amine light stabilizer and ultraviolet light absorber additives. *Polymer Degradation and Stability*, 69(2), pp.197-207.

[58] Craig, B. (n.d.). Selection Guidelines for Corrosion Resistant Alloys in the Oil and Gas Industry. [online] Available at: http://www.stainless-steel-world.net/pdf/10073.pdf [Accessed 30 Aug. 2018].

[59] Craig, B. and Smith, L. (2011). Corrosion Resistant Alloys (CRAs) in the oil and gas industry – selection guidelines update. *Nickel Institue*, [online] 3. Available at: https://www.nickelinstitute.org/~/media/Files/TechnicalLiterature/CorrosionResistantAlloysintheOilandGasIndustrySelectionGuidelinesUpdate_10073.ashx?la=en [Accessed 30 Aug. 2018].

[60] Hechler, O. and Collin, P. (n.d.). On the use of duplex stainless steels in bridge construction. [online] Available at: http://www.stalbyggnadsinstitutet.se/uploads/source/files/Artiklar/On%20the%20use%20of%20duplex%20stainless%20steels%20in%20bridge%20construction.pdf [Accessed 30 Aug. 2018].

[61] An Introduction to Super-Duplex Stainless Steels. (n.d.). *Corrotherm International*. [online] Available at: https://www.corrotherm.co.uk/hubfs/resources/corrotherm-introduction-super-duplex-stainless-steels.pdf [Accessed 30 Aug. 2018].

[62] Solid Solution Hardening & Strength. (2010). *Technical Tidbits*, [online] (16). Available at: https://materion.com/-/media/files/alloy/newsletters/technical-tidbits/issue-no-16-solid-solution-hardening--strength.pdf [Accessed 30 Aug. 2018].

[63] Pantazopoulos, G. and Vazdirvanidis, A. (2014). Identification of corrosion and damage mechanisms by using scanning electron microscopy and energy-dispersive X-ray microanalysis: contribution to failure analysis case histories. *Materials Science and Engineering*, 55.

[64] Wahab, M. (2018). *Proceedings of the 7th International Conference on Fracture Fatigue and Wear*. Belgium: Springer, pp.32-753.[Online] Available at: https://books.google.co.uk/books?id=TQ9kDwAAQBAJ&pg=PA40&lpg=PA40&dq=Pantazopoulos+G+2011+Damage+assessment+using+fractography+as+failure+evaluation:+applications+in+industrial+metalworking+machinery.+J.+Fail+Anal.+and+Preven.+11+588-594&source=bl&ots=IWZHKvdXTB&sig=tnN3P_A06mDDPAOxzvAnU2oIslU&hl=en&sa=X&ved=2ahUKEwipjrLsy__cAhUPbVAKHUpdDfIQ6AEwAnoECAgQAQ#v=onepage&q=SEM&f=false [Accesssed 31 Aug. 2018].

[65] Introduction to Energy Dispersive X-ray Spectrometry (EDS). (n.d.). [online] Available at: https://cfamm.ucr.edu/documents/eds-intro.pdf [Accessed 30 Aug. 2018].

[66] CORROSION & SCALE APPLICATION. (n.d.). *Proto Manufacturing*. [online] Available at: http://www.protoxrd.com/assets/corrosion.pdf [Accessed 30 Aug. 2018].

[67] Antunes, R., Costa, I. and Araújo de Faria, D. (2003). Characterization of Corrosion Products Formed on Steels in the First Months of Atmospheric Exposure. *Materials Research*, [online] 6(3), pp.403-408. Available at: http://citeseerx.ist.psu.edu/viewdoc/download;jsessionid=75E229CBB16D9BB3606EC5BBDEFC0B47?doi=10.1.1.632.1367&rep=rep1&type=pdf [Accessed 30 Aug. 2018].

[68] Antunes, R., Ichikawa, R., Martinez, L. and Costa, I. (2014). Characterization of Corrosion Products on Carbon Steel Exposed to Natural Weathering and to Accelerated Corrosion Tests. *International Journal of Corrosion*. [online] Available at: https://www.hindawi.com/journals/ijc/2014/419570/ [Accessed 30 Aug. 2018].

[69] Malinovschi, V., Ducu, C., Aldea, N. and Fulger, M. (2006). Study of carbon steel corrosion layer by X-ray diffraction and absorption methods. *Journal of Nuclear Materials*, 352(1-3), pp.107-115.

[70] Ida, T. (2013). Bragg's law. *Crystal Structure Analysis*. [online] Available at: http://www.crl.nitech.ac.jp/~ida/education/structureanalysis/1/1e.pdf [Accessed 30 Sep. 2018].

[71] Li, Z. and Peng, J. (2017). Raman Spectroscopy and Electrochemical Analysis of the Corrosion Behaviour of Reinforcing Steel in the Presence of TEE as an Inhibitor. *International Journal of Electrochemical Science*, [online] 12, pp.8177 – 8187. Available at: http://www.electrochemsci.org/papers/vol12/120908177.pdf [Accessed 30 Aug. 2018].

[72] Fishman, D., Ohana, L. and Foucks, N. (2016). Corrosion Characterization: Use of Raman Spectroscopy for Failure Analysis. *J Fail. Anal. and Preven*, [online] pp.1067-1070. Available at: https://link.springer.com/content/pdf/10.1007%2Fs11668-016-0183-1.pdf [Accessed 30 Aug. 2018].

[73] Criado, M., Martínez-Ramirez, S., Fajardo, S., Gómez, P. and Bastidas, J. (2013). Corrosion rate and corrosion product characterisation using Raman spectroscopy for steel embedded in chloride polluted fly ash mortar. *Materials and Corrosion*, [online] 64(5), pp.372-380. Available at: https://onlinelibrary.wiley.com/doi/pdf/10.1002/maco.201206714 [Accessed 30 Aug. 2018].

[74] Janssen, S., Raulf, M. and Sommer, D. (2007). Characterization of Polymers and Corrosion Products by Raman Spectroscopy. [online] Available at: https://link.springer.com/content/pdf/10.1007%2Fs00501-006-0267-4.pdf [Accessed 30 Aug. 2018].

[75] Ammar, I. and Riad, S. (1958). Effect of pH on Corrosion Potentials. *The Journal of Physical Chemsitry*,[online] 62(2), pp.150-154. Available at: https://pubs.acs.org/doi/pdf/10.1021/j150560a004 [Accessed 14 Nov. 2018].

[76] Pubchem.ncbi.nlm.nih.gov. (n.d.). *Sulfamic acid*. [online] Available at: https://pubchem.ncbi.nlm.nih.gov/compound/sulfamic_acid#section=Uses [Accessed 14 Nov. 2018].

[77] Pubchem.ncbi.nlm.nih.gov. (n.d.). *Cyanuric acid*. [online] Available at: https://pubchem.ncbi.nlm.nih.gov/compound/cyanuric_acid#section=Use-and-Manufacturing [Accessed 14 Nov. 2018].

[78] Pubchem.ncbi.nlm.nih.gov. (n.d.). *Thiodipropionic acid*. [online] Available at: https://pubchem.ncbi.nlm.nih.gov/compound/3_3_-Thiodipropionic_acid#section=Cellular-Locations [Accessed 15 Nov. 2018].

[79] Wajima, T. (2014). Removal of Bromide from Desalinated Water Using Hydrotalcite. *International Journal of Environmental Science and Development*, [online] 5(2), pp.202-206. Available at: https://pdfs.semanticscholar.org/2529/1c7a53266526594597a3cab05b254c364cd4.pdf [Accessed 15 Nov. 2018].

[80] Pubchem.ncbi.nlm.nih.gov. (n.d.). *Octachlorodibenzofuran*. [online] Available at: https://pubchem.ncbi.nlm.nih.gov/compound/octachlorodibenzofuran [Accessed 15 Nov. 2018].

[81] Pubchem.ncbi.nlm.nih.gov. (n.d.). *Aspartic acid*. [online] Available at: https://pubchem.ncbi.nlm.nih.gov/compound/L-aspartic_acid#section=Use-and-Manufacturing [Accessed 18 Nov. 2018].

[82] Elastomer Engineering. (n.d.). *CR - Polychloroprene (Neoprene®) - Elastomer Engineering*. [online] Available at: http://www.elastomer.co.uk/materials/polychloroprene-cr-neoprene/ [Accessed 18 Nov. 2018].

[83] Gullman, J. (1991). Factors Influencing the Corrosion Rate of Metal Objects. *arkeologiska forskningslaboratoriet stockholms universitet*, [online] (5), pp.189-193. Available at: http://www.academia.edu/6992580/Factors_Influencing_the_Corrosion_Rate_of_Metal_Objects [Accessed 19 Nov. 2018].

[84] Blog.phenom-world.com. (n.d.). *EDX analysis with a scanning electron microscope (SEM): how does it work?*. [online] Available at: http://blog.phenom-world.com/edx-analysis-scanning-electron-microscope-sem [Accessed 30 Nov. 2018].

[85] Introduction to Energy Dispersive X-ray Spectrometry (EDS). (n.d.). [online] pp.1-12. Available at: https://cfamm.ucr.edu/documents/eds-intro.pdf [Accessed 1 Dec. 2018].

[86] Tanney, R. (2017). *Zeolite-A as a Remediation Technique for Soil Contaminated with Lead*. Doctor of Philosophy (PhD). University of Kent.

[87] Sas.upenn.edu. (2018). *The Raman Spectrophotometer*. [online] Available at: https://www.sas.upenn.edu/~crulli/TheRamanSpectrophotometer.html [Accessed 14 Dec. 2018].

[88] Raman Spectroscopy Basics. (n.d.). [ebook] Priceton Instruments, pp.1-5. Available at: http://web.pdx.edu/~larosaa/Applied_Optics_464-564/Projects_Optics/Raman_Spectrocopy/Raman_Spectroscopy_Basics_PRINCETON-INSTRUMENTS.pdf [Accessed 14 Dec. 2018].

[89] Pignon, J. (2005). Diesel Engines: Design and Emissions. *Platinum Metals Review*, 3(49), p.119.

[90] Hobbs, L. (2006). Gibbs Free Energy, Anodic Corrosion & the EMF Series. *Materials Laboratory*. [online] Available at: https://ocw.mit.edu/courses/materials-science-and-engineering/3-014-materials-laboratory-fall-2006/labs/w3_b2.pdf [Accessed 12 Apr. 2019].

Appendix 1


The X's are sample sites.
Colour Key:
Yellow – Corrosion.
Orange – Severe Corrosion.
Red – Extreme Corrosion.
The types of corrosion according to severity:
Yellow
Orange
Pitting corrosion
Intergranular corrosion
Filiform (Crevice) corrosion
Uniform corrosion
Exfolation (Intergranular) corrosion
Dezincification corrosion
Red
Stress Cracking corrosion
1
2
3
4
5
6
7
8
9
10
11
12
13
14
15
16
17
18
19
20
21

Appendix 2

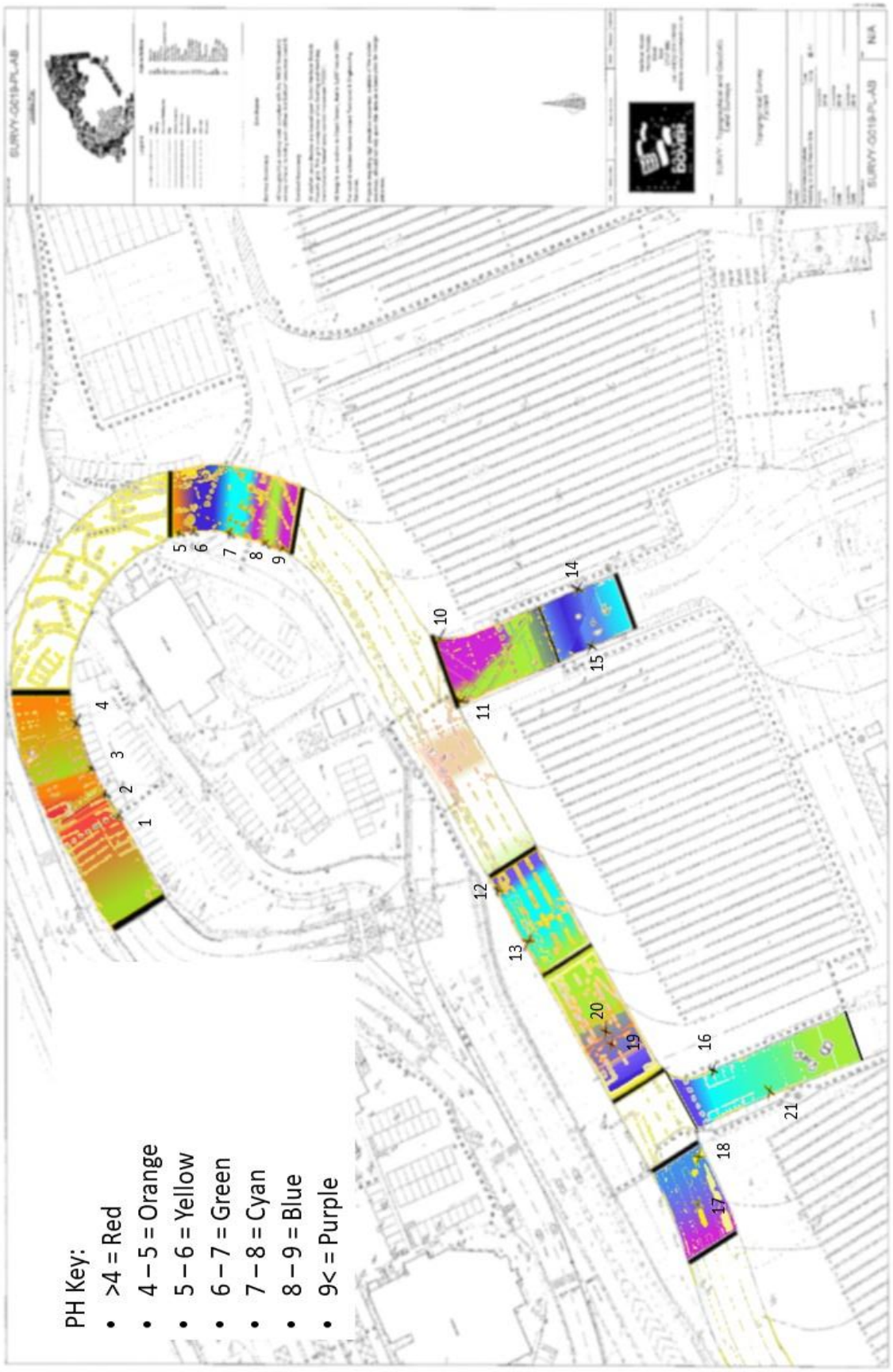
PH Key:
>4 = Red
4 – 5 = Orange
5 – 6 = Yellow
6 – 7 = Green
7 – 8 = Cyan
8 – 9 = Blue
9< = Purple
1
2
3
4
5
6
7
8
9
10
11
12
13
14
15
16
17
18
19
20
21